ACS SYMPOSIUM SERIES [illegible]

Separations for the Nuclear Fuel Cycle in the 21st Century

EDITED BY
Gregg J. Lumetta, Kenneth L. Nash, Sue B. Clark,
and Judah I. Friese

Downloaded by 89.163.35.42 on August 9, 2012 | http://pubs.acs.org
Publication Date: June 9, 2006 | doi: 10.1021/bk-2006-0933.fw001

Separations for the Nuclear Fuel Cycle in the 21st Century

In Separations for the Nuclear Fuel Cycle in the 21st Century; Lumetta, G., et al.;
ACS Symposium Series; American Chemical Society: Washington, DC, 2006.

Downloaded by 89.163.35.42 on August 9, 2012 | http://pubs.acs.org
Publication Date: June 9, 2006 | doi: 10.1021/bk-2006-0933.fw001

ACS SYMPOSIUM SERIES **933**

Separations for the Nuclear Fuel Cycle in the 21st Century

Gregg J. Lumetta, Editor
Pacific Northwest National Laboratory

Kenneth L. Nash, Editor
Washington State University

Sue B. Clark, Editor
Washington State University

Judah I. Friese, Editor
Pacific Northwest National Laboratory

Sponsored by the
ACS Divisions of Industrial and Engineering Chemistry, Inc. and Nuclear Chemistry and Technology

American Chemical Society, Washington, DC

Downloaded by 89.163.35.42 on August 9, 2012 | http://pubs.acs.org
Publication Date: June 9, 2006 | doi: 10.1021/bk-2006-0933.fw001

Library of Congress Cataloging-in-Publication Data

Separations for the nuclear fuel cycle in the 21st century / Gregg J. Lumetta, editor ... [et al.] ; sponsored by the ACS Divisions of Industrial and Engineering Chemistry, Inc. and Nuclear Chemistry and Technology.

p. cm.—(ACS symposium series ; 933)

"Developed from a symposium sponsored by the ACS Divisions of Industrial and Engineering Chemistry, Inc. and Nuclear Chemistry and Technology at the 227th ACS National Meeting, Anaheim, California, March 28–April 1, 2004"—Pref.

Includes bibliographical references and index.

ISBN *978–0–8412–3931–9 (alk. paper)

1. Nuclear f fuels—Congresses. 2. Reactor fuel reprocessing—Congresses. 3. Separation (Technology)—Congresses.

I. Lumetta, Gregg J., 1960– II. American Chemical Society. Divisions of Industrial and Engineering Chemistry, Inc. and Nuclear Chemistry and Technology. III. American Chemical Society. Meeting (227th : 2004 : Anaheim, California) IV. Series.

TK9360.S435 2006
621.48'335—dc22 2005057229

The paper used in this publication meets the minimum requirements of American National Standard for Information Sciences—Permanence of Paper for Printed Library Materials, ANSI Z39.48–1984.

Copyright © 2006 American Chemical Society

ISBN-10: 0–8412–3931–2

Distributed by Oxford University Press

All Rights Reserved. Reprographic copying beyond that permitted by Sections 107 or 108 of the U.S. Copyright Act is allowed for internal use only, provided that a per-chapter fee of $33.00 plus $0.75 per page is paid to the Copyright Clearance Center, Inc., 222 Rosewood Drive, Danvers, MA 01923, USA. Republication or reproduction for sale of pages in this book is permitted only under license from ACS. Direct these and other permission requests to ACS Copyright Office, Publications Division, 1155 16th Street, N.W., Washington, DC 20036.

The citation of trade names and/or names of manufacturers in this publication is not to be construed as an endorsement or as approval by ACS of the commercial products or services referenced herein; nor should the mere reference herein to any drawing, specification, chemical process, or other data be regarded as a license or as a conveyance of any right or permission to the holder, reader, or any other person or corporation, to manufacture, reproduce, use, or sell any patented invention or copyrighted work that may in any way be related thereto. Registered names, trademarks, etc., used in this publication, even without specific indication thereof, are not to be considered unprotected by law.

PRINTED IN THE UNITED STATES OF AMERICA

Downloaded by 89.163.35.42 on August 9, 2012 | http://pubs.acs.org
Publication Date: June 9, 2006 | doi: 10.1021/bk-2006-0933.fw001

Downloaded by 89.163.35.42 on August 9, 2012 | http://pubs.acs.org
Publication Date: June 9, 2006 | doi: 10.1021/bk-2006-0933.fw001

Foreword

The ACS Symposium Series was first published in 1974 to provide a mechanism for publishing symposia quickly in book form. The purpose of the series is to publish timely, comprehensive books developed from ACS sponsored symposia based on current scientific research. Occasionally, books are developed from symposia sponsored by other organizations when the topic is of keen interest to the chemistry audience.

Before agreeing to publish a book, the proposed table of contents is reviewed for appropriate and comprehensive coverage and for interest to the audience. Some papers may be excluded to better focus the book; others may be added to provide comprehensiveness. When appropriate, overview or introductory chapters are added. Drafts of chapters are peer-reviewed prior to final acceptance or rejection, and manuscripts are prepared in camera-ready format.

As a rule, only original research papers and original review papers are included in the volumes. Verbatim reproductions of previously published papers are not accepted.

ACS Books Department

In Separations for the Nuclear Fuel Cycle in the 21st Century; Lumetta, G., et al.;
ACS Symposium Series; American Chemical Society: Washington, DC, 2006.

Preface

Energy will be a critical issue in the 21st century. It can be anticipated that one of the great challenges in this century will be ensuring that the energy supplies required to raise the global standard of living will be available in the face of the threat of global climate change and decreasing availability of "clean" fossil fuels. Although not a panacea, fission-based nuclear power should play a key role in meeting this challenge. Nuclear power based on the fissioning of uranium and plutonium produces virtually no greenhouse gas emissions and sufficient nuclear fuel is available to support humankind's energy needs for decades at present consumption levels. However, for fission-based nuclear power to contribute significantly to future energy supplies, it will be essential to maintain the improvements that have been made in plant operational efficiency in the past decades, to license geological repositories for waste isolation, and to consider again the issue of recycling of spent nuclear fuels. Recycling spent fuels has the potential to both ensure adequate supplies of nuclear fuel long into the future and to reduce the long-term radiotoxicity of the wastes.

This book is the outcome of a symposium titled *Separations for the Nuclear Fuel Cycle* that was held at the 227th American Chemical Society (ACS) National Meeting in Anaheim, California, March 30–April 1, 2004. The focus of this symposium was on assessing the current state of the art in nuclear separations science and technology as well as on identifying directions research and development should take to enable nuclear separations to meet 21st Century demands for waste minimization, environment protection, safety, and security. The subject matter of this book has been organized into five topical areas: (1) current trends and direction to the future, (2) aqueous processing, (3) emerging separations systems, (4) actinide–lanthanide separations, and (5) solution–solid interactions. This collection of chapters provides a snapshot of the current state of nuclear separations chemistry and can be used to help guide future directions in this critical technological field.

Downloaded by 89.163.35.42 on August 9, 2012 | http://pubs.acs.org
Publication Date: June 9, 2006 | doi: 10.1021/bk-2006-0933.pr001

Acknowledgments

We gratefully acknowledge the Separations Science and Technology Subdivision of the ACS Division of Industrial and Engineering Chemistry, Inc. and the ACS Division of Nuclear Chemistry and Technology for sponsoring this symposium. We thank all of the participants of this symposium as well as the authors and reviewers of the manuscripts published in this book for their cooperation and valuable contributions. Finally, we thank the ACS Books Department for their encouragement and support in the publication of this book.

Downloaded by 89.163.35.42 on August 9, 2012 | http://pubs.acs.org
Publication Date: June 9, 2006 | doi: 10.1021/bk-2006-0933.pr001

Gregg J. Lumetta
Pacific Northwest National Laboratory
P.O. Box 999, Mail Stop MSIN P7–22
Richland, WA 99352
gregg.lumetta@pnl.gov (email)

Kenneth L. Nash
Washington State University
P.O. Box 644630
Pullman, WA 99164–4630
knash@mail.wsu.edu (email)

Sue B. Clark
Washington State University
P.O. Box 644630
Pullman, WA 99164–4630
s_clark@mail.wsu.edu (email)

Judah I. Friese
Pacific Northwest National Laboratory
P.O. Box 999, Mail Stop MSIN P5–50
Richland, WA 99352
judah.friese@pnl.gov (email)

Downloaded by 89.163.35.42 on August 9, 2012 | http://pubs.acs.org
Publication Date: June 9, 2006 | doi: 10.1021/bk-2006-0933.ch001

Chapter 1

Significance of the Nuclear Fuel Cycle in the 21^{st} Century

Kenneth L. Nash[1,*], Gregg J. Lumetta[2], Sue B. Clark[1], and Judah Friese[2]

[1]Chemistry Department, Washington State University, P.O. Box 644630, Pullman, WA 99164–4630
[2]Pacific Northwest National Laboratory, P.O. Box 999, Richland, WA 99352

Summary

The combined effects of increasing industrialization around the world, the threat of global climate change, and decreasing availability of "clean" fossil fuels will make the development of alternative energy sources more important in the coming decades. For fission-based nuclear power to contribute significantly to future energy supplies, it will be essential to maintain the improvements that have been made in plant operational efficiency, to license geological repositories for waste disposal, and to consider again the issue of recycling of spent nuclear fuels to recover its fuel value and to reduce the long-term radiotoxicity of the wastes. In this chapter, we present an overview of the nuclear fuel cycle from spent fuel recycling through the repository performance in the context of its importance to energy production in the 21^{st} Century.

In Separations for the Nuclear Fuel Cycle in the 21st Century; Lumetta, G., et al.;
ACS Symposium Series; American Chemical Society: Washington, DC, 2006.

Energy Demand and Geopolitical Situation

At the beginning of the 21st Century, the world faces an unprecedented combination of energy and environment related challenges. At the same time that countries with large populations and underdeveloped infrastructure are engaging in a rapid modernization (industrialization) of their economies, we are becoming increasingly aware of the negative impacts of reinjecting fossil carbon into the environment as we consume fossil fuels to sustain the global economy. The transformation of poor economies into more modern versions is desirable for the stability of the world, as the poverty associated with underdevelopment is at the root of many social ills.

However, increased demand for fossil fuels will simultansouely have the effect of increasing the rate of release of CO_2 into the atmosphere and diminishing supplies of fossil carbon at an increasingly rapid rate. Though definitive conclusions cannot be drawn because the entire ecosystem is far too complex to reliably model, there are increasing indications that global climate change could result in severe environmental degradation, which in turn might result in significant social upheaval. To sustain development of modern societies capable of supporting a growing population, nuclear power based on fission combined with effective energy conservation may be the most rational approach to avoiding the impacts of a runaway greenhouse atmosphere. To further complicate the picture, it is likely that at some point in the future fossil carbon will become more valuable as a chemical feedstock than it is as a source of energy.

Hoffert and coworkers (1) analyzed the global energy situation in a featured paper in *Science* entitled "Advance Technology Paths to Global Climate Stability: Energy for a Greenhouse Planet". They reported that:

Current global power consumption:	is 12 TW (10^{12} Watts)
	is 85% fossil fueled
Atmospheric CO_2:	was 275 ppm in 1900
	is 370 ppm in 2000
	will be 550 ppm in 2100

They conclude that we will need 15 TW of emission free power by 2050 to stabilize atmospheric CO_2 at 550 ppm. These authors further indicate that fission based nuclear power is the only presently developed technology that could deliver this performance. They further suggest that known terrestrial reserves of uranium are inadequate to sustain this level of power production if we utilize only the fissile ^{235}U that is present. They conclude that it is imperative that development begin immediately on a serious international effort to close the nuclear fuel cycle and to breed additional fissile plutonium.

Downloaded by 89.163.35.42 on August 9, 2012 | http://pubs.acs.org
Publication Date: June 9, 2006 | doi: 10.1021/bk-2006-0933.ch001

In recent years, a number of books have been published that consider the possible impacts of the combined effects of population growth, continued fossil fuel consumption, and increased industrialization. On the Editor's Page of the March 15, 2004 edition of *Chemical and Engineering News*, Rudy M. Baum reviewed "Out of Gas: The End of the Age of Oil" by David Goodstein and Frank J. Gilloon. Baum characterized the book as "a simultaneously brilliant polemic and a clear examination of the chemistry and physics of global energy issues." He notes that the book opens with an apocalyptic vision from the authors:

> "The world will soon start to run out of conventionally produced, cheap oil. If we manage to overcome that shock by shifting the burden to coal or natural gas, life may go on more or less as it has been until we run out of all fossil fuels by the end of the century. And by the time we have burned up that fuel, we may well have rendered the planet unfit for human life. Even if human life does go on, civilization as we know it will not survive unless we can find a way to live without fossil fuels."

Downloaded by 89.163.35.42 on August 9, 2012 | http://pubs.acs.org
Publication Date: June 9, 2006 | doi: 10.1021/bk-2006-0933.ch001

In the following week's edition, Chemical and Engineering News, March 22, 2004, Baum continued on the Editor's page with "A Challenge We Must Meet II" making the following observations...

> "Nuclear energy will be an essential component of any strategy for weaning humanity from fossil fuels. While fissile uranium-235 is also a limited resource, breeder reactor technologies exist for converting ^{238}U to fissile plutonium-239 and thorium-232 to fissile ^{233}U. Breeder reactors can extend the supply of the earth's fissile material several hundred fold, enough to last at least several centuries."

He continues ....

> "(Problems of spent reactor fuel and ^{239}Pu) ...do not compare to the economic and environmental crises that our continued dependence on fossil fuels is guaranteed to engender."

As will be discussed below, there are no energy production technologies that do not include some cost. Accepting the assumption of limited fossil fuel resources and the environmental dangers of global warming through the greenhouse effect, it can reasonably be argued that the path forward will demand that we explore all possible avenues for energy production for both electricity and transportation fuels, and increase emphasis on efficient usage of the power we produce. With the planet's population presently approaching 6.5 billion and projected doubling of that number in the next century, energy, water, food production and environmental quality will become paramount issues.

Environmental Impact of Energy Production

Although it is essential that sufficient energy be made available to raise the standard of living of the world's populace, it is equally important that the production of that energy does not result in a concomitant decline in living standards due to environmental degradation. For this reason, future energy decisions must take into account the environmental impacts of energy technologies deployed. All forms of energy production impact the environment in some manner. Direct comparison of the environmental impacts of different energy sources can be somewhat problematic, but the application of life cycle assessments can be used to compare different energy production methods on a common basis (2,3). Life cycle assessments are based on a "cradle-to-grave" approach to analyzing environmental impacts. For that reason, they examine extraction of raw materials, production of system components, the actual energy production technology, and waste disposal. They typically do not account for factors that are difficult to quantify such as land utilization and impacts to visual landscapes.

Gagnon et al. recently published a comparison of life cycle assessments performed on a number of different electricity generation options (4). Figure 1 summarizes the results of that study. The figure presents results for four key environmental factors including greenhouse gas emissions, acid rain potential as represented by SO_2 emissions, land use requirements (a parameter often not considered in life cycle analyses), and the energy payback ratio (that is, how much energy is produced divided by the energy invested for its production).

Based on the Gagnon study, run-of-the river hydropower by far has the best performance in terms of greenhouse gas emissions. Nuclear power is comparable with wind, solar power, and hydropower with a reservoir. Not surprisingly, all the fossil-fuel based options compare poorly in the category of greenhouse gas emissions. Similarly, run-of-the river hydropower has the least impact in terms of SO_2 emissions, with fossil-fueled power production being the most impactful. Nuclear power is nearly comparable to run-of-the river hydropower in this respect.

Nuclear energy has the least impact in terms of land use, although the analysis by Gagnon et al. did not include land use associated with long-term waste disposal which would be expected to adversely affect the land use assessment for the nuclear option.

Downloaded by 89.163.35.42 on August 9, 2012 | http://pubs.acs.org
Publication Date: June 9, 2006 | doi: 10.1021/bk-2006-0933.ch001

Hydropower options have the best payback in terms of the amount of energy produced versus the amount expended. Wind energy also has a large energy payback ratio. Nuclear power fares well in comparison to the other energy production options examined.

It should be pointed out that in the case of the "renewable" energy sources (i.e., solar, wind, and run-of-the river hydropower), the life cycle assessments results reported by Gagnon et al. can be viewed as incomplete, as was pointed out by those authors. The life cycle assessments did not take into account the reliability of the individual power sources. The reliability of these power sources are low because the driving force is not always present at a level necessary for efficient electricity production. In other words, the sun does not always shine on the photovoltaic cells, the wind does not always adequately turn the wind turbines, and river flows can be highly variable (the maintenance of a reservoir eliminates this unreliablility for hydropower, but at the expense of submerged landscapes).(a) For these reasons, the popular renewable energy technologies cannot always provide power on demand. Thus, solar and wind power generating stations typically do not stand alone and must be backed up by more conventional technologies so that the electric power grid system remains balanced (4,5). If powered by fossil fuels, this backup generating capacity could be running at less than peak efficiency. Consideration of this backup generating capacity should be factored into the overall environmental impact of wind and solar technology and run-of the river hydropower.

On the other hand, the back-end of the nuclear fuel cycle is often neglected in life cycle assessments because of the uncertainties associated with ultimate waste disposition. The environmental impacts associated with ultimate waste disposition might be decreased if the currently-planned disposal of irradiated fuel were replaced by a plan involving fuel reprocessing, and might be decreased even more by implementing partitioning and transmutation (P&T) technologies. Much of the subject matter of this book is particularly relevant to partitioning science and technology.

Based on published life cycle assessments, it can be concluded that the environmental impacts of nuclear energy are miniscule when compared with

Downloaded by 89.163.35.42 on August 9, 2012 | http://pubs.acs.org
Publication Date: June 9, 2006 | doi: 10.1021/bk-2006-0933.ch001

(a) Gagnon et al. (4) also consider nuclear power to have low flexibility and thus requires backup power generation. Presumably this is due to the necessity for nuclear plants to occasionally go off line for refueling operations. We question the conclusion that this would have significant environmental impact because the backup for such outages can just as easily be provided by a separate nuclear power plant as from another more polluting power source.

Downloaded by 89.163.35.42 on August 9, 2012 | http://pubs.acs.org
Publication Date: June 9, 2006 | doi: 10.1021/bk-2006-0933.ch001

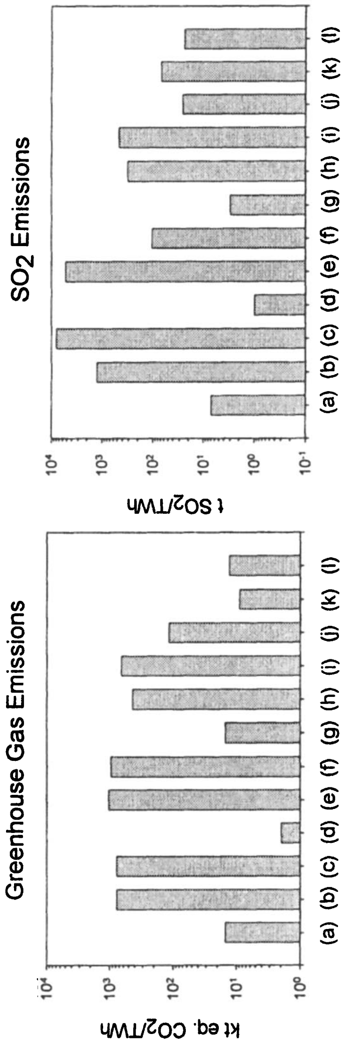

Downloaded by 89.163.35.42 on August 9, 2012 | http://pubs.acs.org
Publication Date: June 9, 2006 | doi: 10.1021/bk-2006-0933.ch001

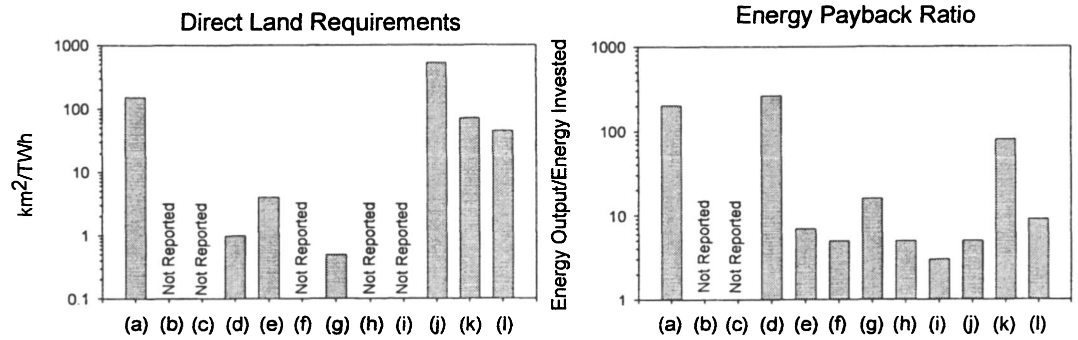

Figure 1. Summary of Environmental Factors for Various Electricity Generating Options Based on Life Cycle Assessment; adapted from reference 4; a) Hydro w/ Reservoir, b) Diesel (0.25% S), c) Heavy Oil (1.5%S) w/o SO_2 Scrubbing, d) Hydro Run-of-River, e) Coal (1% S) without SO_2 Scrubbing, f) Coal (2%S) w/ SO_2 Scrubbing, g) Nuclear, h) Natural Gas, i) Fuel Cell (H_2 from gas reforming), j) Biomass Plantation, k) Wind, l) Solar PV.

those of coal, oil and even natural gas-fired turbines if the link of carbon dioxide to global warming is accepted. Nuclear power also compares vary favorably with solar and wind power, and in contrast to these technologies, nuclear plants can be configured to provide continuous on-demand power (no matter what the weather).

Role of Nuclear Power

The world-wide production of electricity by nuclear fission is, at present, nearly 351 gigawatts electric (Gw_e), generated from 438 operating nuclear reactors and accounting for about 16% of electricity production worldwide. The spent fuel from power production reactors is about 1.0-1.5% transuranium (TRU) actinides 3.5-4.0% fission products, 95% still slightly enriched uranium upon discharge from the reactor. There are three choices for the management of the spent fuel: a) recycle to recover valuable components (reprocessing with or without actinide partitioning and transmutation), b) “permanent” geologic disposal as waste (single pass fuel cycle), or c) long-term monitoring after stabilization for surface or near-surface storage. World–wide, both byproduct recycle and monitoring of spent fuel in storage are done. Option b is the present official policy for dealing with spent fuel from commercial reactors in the U.S. It must also be noted that the need for a geologic repository does not disappear in option a. A geologic repository will still be essential for the sequestration of radioactive wastes from reprocessing from the surrounding environment.

Unfortunately, after more than 30 years of continuous investigation, no repositories for permanent geologic disposal of either spent reactor fuels or vitrified reprocessing wastes have been licensed. Clearly, safe disposal of either spent fuel or the high-level waste (HLW) generated during reprocessing of spent fuel is a matter of great environmental concern (6). Waste disposal and the increased risk of proliferation of nuclear weapons are the two major issues standing in the way of further implementation of this otherwise environmentally friendly technology. Furthermore, a recent analysis projecting how fission-based nuclear power could favorably impact greenhouse gas emissions emphasizes the need for breeding additional fuel to satisfy a projected long-term shortage or fuel for fission reactors (1). Meeting this demand can only be accomplished by closing the loop on spent fuel reprocessing.

Overall, the major factors that must be addressed for the expansion of fission-based nuclear power from the present level to its full potential include the following:

1) safety and efficiency of energy production must be maintained,
2) a strategy (or strategies) for the final disposal of the radioactive byproducts of fission must be developed,

Downloaded by 89.163.35.42 on August 9, 2012 | http://pubs.acs.org
Publication Date: June 9, 2006 | doi: 10.1021/bk-2006-0933.ch001

3) mistrust by the general public (and in many cases elected officials and stockholders) for the technology must be overcome, and
4) the comparatively high initial installation costs for nuclear power plants must be reduced.

Ultimately, it will become necessary to convert fertile ^{238}U and/or ^{232}Th to fissile ^{239}Pu and ^{233}U if nuclear power is to assume an increasing role. Before this will happen, it will be necessary to overcome:

5) the comparatively low price and relative abundance of natural uranium,
6) concerns about the proliferation of nuclear weapons,

and to develop

7) a next generation reprocessing capability that responds to 21st Century demands for protection of the environment.

Some of these factors could yield to increased education of the public to reduce misunderstandings (Item 3); some have already been greatly improved (Item 1) and require only preservation of the gains that have been made; some while not definitively "solved" have perhaps yielded a bit to decades of investigation (Item 2); some will simply have to await a correction from natural market factors (Item 5) and technological improvements (Item 4). The issue of weapons proliferation can be most efficaciously addressed by political means, i.e., international agreements with serious monitoring, consequences for violators and vigilance for those who seek to expand the availability of nuclear materials for weapons. The proliferation of nuclear weapons can also be hindered by transmutation, which results in either the destruction of fissile materials or their conversion into materials less suitable for the production of efficient fission weapons (for example, changing isotopic mixture of Pu through successive neutron capture). Besides environment protection, the next generation reprocessing capability envisioned in item 7 will also have to be proliferation proof.

Having garnered substantial experience during the past 50 years with nuclear science and technology, humanity may be poised for an acceptable expansion of this segment of our energy production capacity. In the following sections, some aspects of the current state of affairs in nuclear energy production are discussed.

Management of Irradiated Fuel

Spent fuel freshly discharged from a reactor is intensely radioactive and generates substantial heat. Over a period of a few decades, most of the penetrating radiation decays to comparatively low levels, though the spent fuels retain sufficient heat and penetrating radiation to have an impact on geological

Downloaded by 89.163.35.42 on August 9, 2012 | http://pubs.acs.org
Publication Date: June 9, 2006 | doi: 10.1021/bk-2006-0933.ch001

systems. From 30-300 years, the long-lived fission products ^{137}Cs and ^{90}Sr dominate the radiation dose. From 300-10,000 years, the radiation dose is dominated by plutonium and americium isotopes. From 10,000-250,000 years plutonium isotopes are dominant while ^{237}Np, ^{129}I, and ^{99}Tc are the most important beyond 250,000 years. The latter three species are particularly troublesome from a regulatory perspective, as they exist in generally soluble forms under environmental conditions.

At present, half of the world's spent nuclear fuel is managed in a "once-through cycle." The other half is reprocessed to recycle U and Pu. Though a great deal of research has been done, no country has as yet committed to further partition and transmute long-lived radioactive byproducts (fission products and minor actinides). Deep geological repositories are universally considered the preferred option for the long-term isolation of either spent fuel or reprocessing residues from the biosphere. It is widely believed that such a repository, properly sited and constructed, can effectively accomplish the necessary sequestration for either spent fuel or high level reprocessing wastes. However, two issues associated with the operational characteristics of a geologic repository remain troubling, at least from a licensing standpoint:

- A repository is designed to insure that the radioactive materials be retained within its boundaries until most of the radioactivity has decayed away. Though more than 99% of the radioactivity derived from fission products decays away within about 300 years, some fission products and most of the actinides persist for millennia. If spent fuel is directly disposed as waste, it becomes necessary to make predictions of repository performance at least 250,000 years into the future. Making accurate prediction of the behavior of engineered systems in this timeframe is problematic at best. The behavior of selected geologic systems can be estimated with somewhat greater accuracy, but it is not possible to predict the impact of all possible events. We also have minimal experience (direct or indirect) with the long-term effects of radiolysis on the stability of geomedia.
- In addition to the radiation emitted by the spent fuel, it remains thermally hot for an extended period as well. Research and modeling conducted on repository performance appears to indicate that elevated temperatures within the repository environment can have a deleterious effect on repository performance, particularly those features moderated by groundwater influx.

Current policy in the U.S. is for direct disposal of spent fuel in the Yucca Mountain repository, which is scheduled to be licensed to accept spent fuel in 2012. A nearly 50 year inventory of spent fuel is presently in temporary storage at reactor sites around the U.S. The current design of the Yucca Mountain repository demands spacing of the waste cannisters such that the temperature

Downloaded by 89.163.35.42 on August 9, 2012 | http://pubs.acs.org
Publication Date: June 9, 2006 | doi: 10.1021/bk-2006-0933.ch001

remain below the boiling point of water at the repository boundary. Within this design criterion, it is expected that the repository will be at capacity within six years after it is licensed to accept spent fuel in permanent disposal (a legislated limit – the actual physical capacity may exceed this limit by a factor of two). With this repository configuration, one or more additional repositories will be needed to accommodate the demands for spent fuel disposal, even if no new reactors are developed and deployed. If additional generating capacity is created, the need for additional geologic storage becomes more urgent.

The already-low risk of disposing of spent fuel in a geologic repository can be reduced by reprocessing the fuel so that the bulk of the plutonium is not sent to the repository. It can be reduced even further by P&T. Reprocessing to recycle U and Pu reduces the volume of wastes by a factor of roughly 20, as only minor actinides and fission products will require geologic dispositioning. Recycle of Pu and U has only a comparatively slight impact on the short term heat effects but reduces long-term radioactivity of the wastes in the 80,000-250,000 year timeframe by reducing the amount of Pu isotopes in the wastes. Partitioning to isolate minor actinides and long-lived fission products from the short-lived fission products and disposal of only the long-lived species in a geologic repository further reduces the volume and significantly reduces the heat load on the repository (assuming the short-lived species are otherwise handled). This option has little effect on reducing the long-term radiotoxicity of the wastes. The added step of transmutation of minor actinides and long-lived fission products relieves most of the burden of long-term radiotoxicity.

Each stage of treatment provides either a true reduction in the various hazards, or an increase in the accuracy of long-term predictions. Homogeneous feed streams emerging from a cycle including partitioning would enable the use of waste forms specifically designed to accommodate the class of waste being sequestered (as opposed to demanding that one waste form be compatible with the large part of the periodic table present in wastes as is required in the absence of partitioning). The long-term stability of such tailored waste forms would be easier to assure based on analogies with natural systems.

A worldwide interest in implementing P & T technologies (to markedly reduce the quantities of long-lived transuranics requiring disposal in a repository) emerged in the early 1980's, a result of cleanup efforts at weapons production facilities like Hanford. Successful application of this approach to radioactive waste management could substantially reduce the needed geologic repository capacity. The trade-offs are that a P & T approach to radioactive waste management requires more manipulation of fissile materials (and so increased opportunities for their diversion to illicit purposes) and could increase the volumes of some categories of radioactive wastes. However, even if the cost of P & T exceeds the value of the energy gained from actinide transmutation, the added safety margin for the repository and the possibility of avoiding the construction of additional repositories could justify the expense.

Downloaded by 89.163.35.42 on August 9, 2012 | http://pubs.acs.org
Publication Date: June 9, 2006 | doi: 10.1021/bk-2006-0933.ch001

It should be noted that that there are different degrees of difficulty associated with different processing options. Spent fuel freshly discharged from the reactor (or allowed only a short cool-down interval) is the most demanding because of the radiation, thermal heat, and diversity of materials to be separated. Long-term storage of these materials prior to reprocessing reduces these problems, as heat and the most intense radiation decline at a moderate rate and the sheer numbers of isotopes also declines as they decay. In plants designed to recycle purified materials that have not been irradiated (for example, decommissioned weapons), the radiation effects are significantly diminished and heat loads are minimal thus the processes are less damaging of materials and reagents. For tank wastes like those found in the DOE complex in the U.S., their already long-term storage implies that most of the fission product radioactivity has decayed and heat loads are significantly reduced (though not eliminated). But for such materials, chemical diversity remains and challenging solid-liquid separations are needed prior to any processing. It should also be noted that the energy value (as represented by actinide content) of these reprocessing residues is too low for them to be considered a valuable asset for energy production. Their dispositioning to permanent storage is a matter of environment preservation/restoration.

Downloaded by 89.163.35.42 on August 9, 2012 | http://pubs.acs.org
Publication Date: June 9, 2006 | doi: 10.1021/bk-2006-0933.ch001

Future Nuclear Separations: Key Attributes

During the first 50 years of the reprocessing of spent nuclear fuels to recover plutonium for nuclear weapons or for recycle, the predominant method for industrial scale applications has been solvent extraction based on the use of tributyl phosphate (TBP). Solvent extraction offers the great ability to develop processes for continuous operation and high throughput. The TBP-based PUREX process, developed to replace less efficient coprecipitation ($BiPO_4/LaF_3$) or solvent extraction (REDOX, BUTEX) processes, selectively separates U and Pu from the complex and highly radioactive mixture that results as irradiated fuel elements are dissolved in nitric acid. It rejects most fission products and all actinides other than Pu and U. In conventional PUREX processing, the so-called minor actinides (Np, Am, Cm) are routed to the waste stream with the fission products. Though this strategy allows for the most expeditious isolation of U and Pu, employing this approach has created challenging waste disposal problems. The ability to readily separate pure Pu samples from PUREX processing also raises weapons proliferation concerns.

A change of philosophy that developed during the past several decades has led to a substantial increase in research on new methods to recover the minor actinides in the waste stream. This emphasis has had an international flavor, involving independent research activities focusing principally on solvent extraction-based processes for isolation of minor actinides from fission products;

this is commonly termed "partitioning". Partitioning of actinides can be employed to varied levels of recovery to either improve the integrity of repository-disposed wastes or to employ advanced reactor or accelerator based transmutation of the long-lived actinide isotopes into shorter-lived fission products. The strategy of partitioning with or without transmutation can significantly reduce the burden of establishing the integrity of a geological repository for an unrealistically long period of time.

The various hydrometallurgical processes that have been developed for reprocessing and partitioning are described as follows:

- *PUREX/TBP (7) – The only currently used industrial-scale process for actinide recovery from spent fuel has been used for 50 years. The extractant is inexpensive and its chemistry well-understood, but it degrades significantly, doesn't extract Am,Cm and introduces phosphate into waste streams.*

- *TRUEX/CMPO (89) – Various options for the application of this and other bifunctional extractant systems have been demonstrated to the pilot-plant scale, extracts Am, Cm, and lanthanides, is directly compatible with TBP/PUREX, but the degradation products are more difficult to deal with than those of the PUREX process and the extractant is expensive. Less complex CMPO reagents have been developed that require instead special diluents.*

- *Diamex/DMDBTDMA (9) – To simplify waste management, the French reprocessing establishment has focused during the past two decades on the development of extractants capable of recovering Am and Cm, while avoiding the application of organophosphorus reagents. These reagents have received a significant degree of testing through the pilot scale, are completely incinerable, their degradation products not deleterious, but they suffer somewhat from a greater tendency toward third phase formation and a comparatively steep acid dependence on the extraction side (requiring that feed stocks be adjusted to a rather narrow range of [HNO_3]). Because they are weaker extractants than the phosphine oxides (such as CMPO), they must be employed at moderately high concentrations to achieve acceptable extratction behavior. The French sysem also employs a highly branched hydrocarbon diluent (with a comparatively low flash point) to reduce the possibility of third phase formation.*

- *TRPO (10) – In China, a process for extraction of Am and Cm has been developed based on the application of trialkylphosphine oxide extractants.*

Downloaded by 89.163.35.42 on August 9, 2012 | http://pubs.acs.org
Publication Date: June 9, 2006 | doi: 10.1021/bk-2006-0933.ch001

Extraction efficiency is good within a relatively narrow range of acidity and the extractant is inexpensive, but the feed (dissolved fuel) must be diluted and nitric acid concentration reduced prior to conducting the extraction. Testing has proceeded through the pilot scale.

- *DIDPA (11) – In Japan, a process for Am/Cm extraction analogous to the Swedish CTH process has been developed based on the acidic extractant diisodecylphosphoric acid. Like the TRPO process, the DIDPA process requires that acidity and nitrate content of the feed solution must be reduced prior to extraction. A possible Ln-An separation (based on the use of aminopolycarboxylate complexants) has also been demonstrated and the process has been tested at the small scale pilot level.*

- *Soft Donor Reagents (12) – For transmutation of minor actinides, it will be necessary to control the amount of lanthanide fission product in the fuel element/target for Am/Cm transmutation. With some minor exceptions, this separation is most efficiently accomplished through the use of ligand donor atoms containing S or N donor atoms (or chloride ions as in the TRAMEX process (13)). Some examples of potential reagents are known, but no large-scale testing has been done. Hydrolytic and radiolytic stability of the reagents has proven to be the most important limitation in their development. As a result, no fully acceptable aqueous processes or reagents are presently available, though significant effort continues.*

Downloaded by 89.163.35.42 on August 9, 2012 | http://pubs.acs.org
Publication Date: June 9, 2006 | doi: 10.1021/bk-2006-0933.ch001

Pyrochemical and electrometallurgical processes could in principle form the basis of separation processes that may generate smaller volumes of waste byproducts (though there are significant waste disposal issues that remain unresolved in this approach). The deployment of pyroelectrometallurgical methods are significantly challenging in different ways. Two pyro-processes that have undergone significant development work are the Dimitrovgrad Dry Process (DDP) and the Integral Fast Reactor (IFR) program. Future developments of fast spectrum reactors for actinide transmutation might ultimately prove the most significant driver for the development of pyro processing. There are significant materials handling issues that must be addressed before such processes can have a significant impact on the fuel cycle, as the molten salt solutions are moderately corrosive to many materials, and far higher temperature operations are essential than are needed for aqueous methods.

During 60 years of spent fuel reprocessing, a considerable volume of waste byproduct solutions has been accumulated in a number of locations around the world. In the U.S., these materials are primarily from weapons plutonium production and so date to the earliest days of nuclear power/weapons programs.

The materials in storage in above ground vaults or subsurface liquid retention tanks represent a diverse mixture of materials in challenging combinations. They have also been subjected to decades of storage at elevated temperatures and in the presence of high levels of radiation. This existing waste legacy must be treated to protect the local environment and, given time constraints for cleanup, will most likely be processed using aqueous technologies. Because the actinides contained in these wastes are not likely to be recovered for reuse, a considerable economy can be derived through the application of combined processes.

Conclusions: Future Directions for the Nuclear Fuel Cycle

In a recent publication entitled "Chemical Separations in Nuclear Waste Management", Choppin et al. (14) made a number of salient observations regarding future directions for the nuclear fuel cycle:

- Separations of useful materials from spent fuel will become increasingly desirable in coming decades
- Any new separations technologies must minimize wastes
- Improved efficiency in partitioning processes is needed
- Waste considerations must be integrated into process development (rather than as an afterthought as has been done in the past)
- Environmental consequences of reprocessing must be considered
- Partitioning and transmutation should be considered as an alternative to repository disposition of spent fuel or reprocessing wastes[1]
- Surplus weapons plutonium should be incorporated in MOX fuel for consumption in light water reactors
- The idea of a single waste form should be abandoned; rather, waste forms should be tailored to maximize retention of individual wastes streams in the repository
- International cooperation is essential
- Weapons proliferation must also be considered if spent fuel is recycled

Though industrial-scale reprocessing of spent power reactor fuel is not practiced in the US, it is elsewhere in the world. Aqueous-based technologies will likely continue to dominate the field for at least the next 20 years, but

Downloaded by 89.163.35.42 on August 9, 2012 | http://pubs.acs.org
Publication Date: June 9, 2006 | doi: 10.1021/bk-2006-0933.ch001

---

[1] It must be noted that partitioning and transmutation do not eliminate the need for a geologic repository. P&T does reduce the timeframe for isolation, reduce the radiotoxicity and heat load of the waste package, and decrease the volume of material requiring this most expensive form of disposal.

opportunities exist for further improvements. Some emerging science has the potential to impact the progress of this science and technology significantly. A few examples include:

- Ionic liquids as solvents or media for electrometallurgcal separations
- Supercritical fluids for the dissolution of spent fuel matrices
- Micelle-based separations (i.e., non-conventional aqueous processes)
- Solid sorbents with high-throughput capabilities/physical stability
- Non aqueous concepts (pyrometallurgy, volatility)

Continuing analyses of the economic incentives for reprocessing, partitioning and recycle of the useful components of spent nuclear fuels have not supported deployment of partitioning strategies at present. However, these analyses do not appear to adequately take into account future financial consequences of energy dependence (particularly in the developed world), global competition for resources, global climate change or the great uncertainty associated with licensing a repository (or the expense of constructing multiple repositories) that are associated with the direct disposal of spent fuel. Energy supplies are certain to be stressed as the world's population continues to grow and the pace of international industrialization continues to increase.

In this context, new programs have been developed in the U.S. considering more carefully the pathway to the future for nuclear energy. The Advanced Fuel Cycle Initiative (AFCI) is supporting research examining the science and technology of the nuclear fuel cycle as it will need to be if nuclear power is to contribute more significantly to the future of global energy production (and to reduce our dependence on fossil energy sources). The Generation IV program is exploring the most productive designs for future power production or byproduct transmutation reactor concepts. This effort is connected to the AFCI in that AFCI supports both development of readily deployable technologies for separations today and for separations appropriate to future reactor designs. These programs emphasize international cooperation as a means to successful implimentation. The well-conceived and operated French fuel cycle program (and it's extension to include European partners in research activities) provides important guidance for future directions in these programs.

Because of the current geopolitical situation, the spectre of proliferation of nuclear weapons also hangs over the future of nuclear energy. It is essential that the proliferation of nuclear weapons be controlled. Without serious international controls on fissile materials, it is highly likely that nuclear weapons will be used somewhere on earth in the future. The fissile materials present in spent nuclear fuel are inherently protected by the considerable radiation field of the fission product radioactivity, hence spent fuel is considered to be a proliferation-resistant waste form. Of course, the relative effectiveness of this deterrent rapidly

Downloaded by 89.163.35.42 on August 9, 2012 | http://pubs.acs.org
Publication Date: June 9, 2006 | doi: 10.1021/bk-2006-0933.ch001

decreases as the radioactivity of the short-lived fission product decays away. Actinide reprocessing and partitioning carries with it some increased risk of the diversion of the separated materials to weapons purposes. However, the partitioning and transmutation option has the virtue of significantly reducing the amounts of fissile materials, the ultimate non-proliferation strategy

Finally, but perhaps most importantly, nuclear power is a complex technology demanding a well-educated work force. In the U.S., the peak of educational opportunities in nuclear science, engineering and radiochemistry was passed in the late 1970's. The intervening decades have seen an approximately three fold degeneration in the numbers of Ph.D.-granting institutions in the U.S. with specialization in radiochemistry. Nuclear engineering education has suffered a similar, though not quite so precipitous, decline during this interval. It is essential that such expertise be maintained so that future options in nuclear fuels reprocessing can be preserved. This decline is not unique to the U.S. As noted by Choppin et al., (14) it is a global crisis.

Downloaded by 89.163.35.42 on August 9, 2012 | http://pubs.acs.org
Publication Date: June 9, 2006 | doi: 10.1021/bk-2006-0933.ch001

References

1. Hoffert, M. I., Caldeira, K., Benford, G., Criswell, D. R., Green, C., Herzog, H., Jain, A. K., Kheshgi, H. S., Lackner, K. S., Lewis, J. S., Lightfoot, H. D., Manheimer, W., Mankins, J. C., Mauel, M. E., Perkins, L. J., Schlesinger, M. E., Volk, T., and Wigley, T. M. L. (2002). *Science* **298**: 981-987.
2. Rebitzer, G.; Ekvall, T.; Frischknect, R.; Hunkeler, D.; Norris, G.; Rydberg, T.; Schmidt, W. -P.; Suh, S.; Weidema, B. P.; Pennington, D. W. *Environ. International* **2004,** *30*, 701.
3. Pennington, D. W.; Potting, J.; Finnveden, G.; Lindeijer, E.; Jolliet, O.; Rydberg, T.; Rebitzer, G. *Environ. International* **2004,** *30*, 721.
4. Gagnon, L.; Bélanger, C.; Uchiyama, Y. *Energy Policy* **2002,** *30*, 1267.
5. EMPAInc. 2002. "Wind Energy Economics in the State of Washington," http://www.tsaugust.org/images/Wind%20Energy%20Economics%20in%20the%20State%20of%20Washington%20From%20Schleede%20for%20web%20site.pdf.
6. Baetsle, L. H. (1992). IAEA bulletin: 32-34.
7. Musikas, C.; Schulz, W. W. In *Principles and Practices of Solvent Extraction*; Rydberg, J.; Musikas, C.; Choppin, G. R., Eds.; Marcel Dekker: New York, 1992; Chapter 11.
8. Horwitz, E. P.; Kalina, D. G.; Diamond, H.; Vandegrift, G. F.; Schulz, W. W. *Solvent Extr. Ion Exch.* **1985**, *3*, 75.
9. Cuillerdier, C.; Musikas, C.; Hoel, P.; Nigond, L.; Vitart, X. *Sep. Sci. Technol.* **1991**, *26*, 1229.

10. Jianchen, W.; Chongli, S. *Solvent Extr. Ion Exch.* **2001**, *19*, 231.
11. Morita, Y.; Glatz, J.-P.; Kubota, M.; Koch, L.; Pagliosa, G.; Roemer, K.; Nicholl, A. *Solvent Extr. Ion Exch.* **1996**, *14*, 385.
12. Nash., K. L. *Solvent Extr. Ion Exch.* **1993**, *11*, 729-768.
13. Baybarz, R. D., B. S. Weaver and H. B. Kuiser (1963). Nucl. Sci. Eng. **17**: 457-462.
14. *Chemical Separations in Nuclear Waste Management.* G. R. Choppin, M. K. Khankhasayev, and H. S. Plendl (Eds.). Columbus, Ohio, Battelle Press (DOE/EM-0591) 96 pp.

Downloaded by 89.163.35.42 on August 9, 2012 | http://pubs.acs.org
Publication Date: June 9, 2006 | doi: 10.1021/bk-2006-0933.ch001

Downloaded by COLUMBIA UNIV on August 9, 2012 | http://pubs.acs.org
Publication Date: June 9, 2006 | doi: 10.1021/bk-2006-0933.ch002

Chapter 2

Twenty-First Century Approaches to Actinide Partitioning

Kenneth L. Nash

Chemistry Department, Washington State University, P.O. Box 644630, Pullman, WA 99164–4630

Summary

In the earliest days of the nuclear fuel cycle, the objective was production of plutonium for weapons and closed loop operations were essential. With the advent of the application of nuclear power for energy production, the need for and desirability of recycling the valuable components of spent nuclear fuel came to be an economic or political decision. Consideration of closed loop recycling of power reactor fuels was abandoned in the U.S. in the 1970's because of nuclear weapons proliferation concerns, though spent fuel reprocessing continued elsewhere. At the dawn of the 21st Century, concerns about the adequacy of global energy supplies and waste management issues have renewed discussions about reprocessing of spent nuclear fuels. The Advanced Fuel Cycle Initiative and Generation IV (reactor development) programs have commenced within the past several years to assess future directions for the nuclear fuel cycle. This report discusses the present status of research on this subject in light of how such plants must operate in an age of environmental consciousness.

In Separations for the Nuclear Fuel Cycle in the 21st Century; Lumetta, G., et al.;
ACS Symposium Series; American Chemical Society: Washington, DC, 2006.

Introduction

At present, half of the world's spent nuclear fuel is produced in a "once-through cycle". The other half is reprocessed to recycle uranium and plutonium as thermal reactor fuel. Several countries are considering further options for partitioning of spent fuel, principally as a means of improving waste management. The final resting place for either unprocessed spent fuel or the high level wastes from reprocessing will be a deep geological repository. The repository will rely on natural and engineered barriers to isolate the radioactive materials from the biosphere. However, without transmutation radioactivity levels in spent fuel remain above the natural background of uranium ore for several hundred thousand years. It is a daunting challenge to assess the integrity of the local environment surrounding a geologic repository over a span of time that exceeds that of human civilization. At the same time, public acceptance of such repositories is an essential element of any plan to sustain or expand nuclear power as a viable energy option for the future.

Developing a viable solution to the issue of radioactive waste management becomes even more essential if one considers the rapid pace of industrialization around the world. Modernization and electrification in large countries like China and India will place unprecedented stress on global energy supplies in the coming decades. The potential impact of global climate instability and a possible runaway greenhouse effect (1) on civilization raise the option of fission-based nuclear energy production to the level of a global priority. If such growth is to take place, the recycle of fissile uranium and plutonium in spent nuclear fuel and even the purposeful breeding of additional fissile plutonium or uranium become more important (2).

The treatment of spent nuclear fuel can in principle be pursued at several levels. The simplest option of separating uranium and plutonium from spent fuel (reprocessing) for recycle to thermal reactors will decrease the mass of the spent fuel by more than 95% and eliminate the long term radiotoxicity of plutonium isotopes from the performance envelope of the repository. This limited form of spent fuel treatment is practiced in France, the United Kingdon, Japan, and Russia. The materials remaining in the residues of spent fuel reprocessing include the trans-plutonium actinides, neptunium, and all of the fission products. Most of the fission product radioactivity decays away within about 5 years after removal from the reactor, but long–lived species like ^{137,135}Cs, ^{90}Sr, ^{99}Tc, and ^{129}I contribute significantly to the long-term radiotoxicity of the reprocessing residues. From 300 to 10,000 years for such materials, the dose is dominated by americium isotopes $^{241,\,243}$Am. Beyond 10,000 years, ^{237}Np, ^{99}Tc, and ^{129}I are the

Downloaded by COLUMBIA UNIV on August 9, 2012 | http://pubs.acs.org
Publication Date: June 9, 2006 | doi: 10.1021/bk-2006-0933.ch002

most important species. Increased recycle of plutonium in MOX fuels will increase the percentage of transuranic elements in spent fuel.

Exercise of the partitioning and transmutation (P&T) option for spent fuel management seeks to convert long-lived nuclides into short-lived radioactive (and ultimately stable) species. France leads an effort in the European Union to determine whether this option will be pursued in the future within their existing program for recycling uranium and plutonium. Successful application of this approach to radioactive waste management would lead to the effective elimination of radiotoxicity of the most of the wastes within less than 1,000 years and substantially reduce the requirement for geologic repository capacity and ot the time during which repository performance must be established. The isotopic mix of plutonium shifts toward higher atomic masses as it is recycled, making it far less attractive for nuclear weapons diversion. Within the P & T option, tailoring waste glass to contain a narrower mix of fission byproducts, rather than the broad spectrum of materials in a single waste form required of less extensive partitioning, becomes possible.

The trade-offs (aside from expense) are that a P&T approach to radioactive waste management demands increased safeguards to minimize opportunities for proliferation of nuclear weapons and will increase the volumes of other wastes. Transmutation of Am/Cm, Np, Tc, I also requires the development of fast-neutron spectrum reactors or accelerator transmutation facilities. The Generation IV reactor development program includes consideration of fast spectrum reactors for transmutation applications. It could be argued that even if the cost of P & T exceeds the gain in energy from actinide incineration, the added safety margin for the repository could justify the expense. If the P & T option makes it possible to avoid the construction of additional geological repositories, the cost benefit becomes clear.

The nearly 60 years of industrial-scale experience that has been accumulated world-wide on aqueous-based processing of nuclear fuels clearly qualifies these methods as the best approach to actinide recycle during at least the next 20 years. Dry (i.e., non aqueous) processes like pyrometallurgy or volatility-based separations may ultimately prove to be more efficient methods for actinide recycle and transmutation. Significant further development is needed to fully mature these technologies, particularly as regards materials of construction. In this report, ongoing research seeking new approaches to processing of nuclear fuels will be outlined emphasizing wet processing options. Important features of dry processing options and more unconventional materials will also be discussed.

Downloaded by COLUMBIA UNIV on August 9, 2012 | http://pubs.acs.org
Publication Date: June 9, 2006 | doi: 10.1021/bk-2006-0933.ch002

Pu and U Recovery Processes with Substantial Industrial Experience

There are several coprecipitation and solvent extraction procedures that have been utilized to separate and recover actinides from different solutions including the solutions resulting from dissolution of spent fuel. Among the coprecipitation reagents, lanthanum fluoride and bismuth phosphate were widely used in earlier times. Coprecipitation on bismuth phosphate was the first process used for plant scale separation of Pu from dissolver solutions. Among the solvent extraction processes, REDOX, BUTEX, TLA and PUREX processes have been demonstrated at the production scale, mainly for the separation of uranium and plutonium from fission products and minor actinides. Only the PUREX process is still in operation for actinide recovery from spent nuclear fuel today. Various efforts underway around the world seek to further improve the efficiency of this workhorse process.

PUREX process

The PUREX (plutonium uranium recovery by extraction) process uses tributyl phosphate (TBP, Fig. 1) dissolved in an inert aliphatic hydrocarbon diluent as the extractant for uranium and plutonium from dissolver solution (3-6). Normally a solution of 20-30% TBP in *n*-dodecane, odorless kerosene, or another normal (or branched) paraffinic hydrocarbon (or mixture of hydrocarbons) of low flammability is employed. This process was first developed at the Oak Ridge National Laboratory (7). It has been employed at the industrial scale for nearly 50 years and remains the cornerstone of nuclear fuel reprocessing for both defense and power reactor fuels around the world. One of the major advantages of this process is that it selectively extracts $Pu(NO_3)_4$ and $UO_2(NO_3)_2$ from dissolved spent nuclear fuels from solutions of moderate nitric acid concentrations, requires no addition of any salts and is plagued by few co-extracted impurities. The extractant is readily purified by aqueous scrubbing/column procedures or vacuum distillation and the most common diluent (odorless kerosene) is relatively non-flammable and non-toxic. The principal disadvantage of PUREX is in the area of proliferation resistance, as this process enables the ready preparation of a pure plutonium product. The features of this technology have been widely described in the open literature.

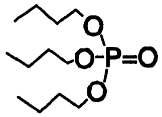

Figure 1. Tributyl phosphate

In PUREX, both tetravalent and hexavalent actinides are readily extracted into the organic phase from 2-3 M nitric acid , whereas trivalent and pentavalent actinides are weakly extracted from this medium. Unless additional reagents are employed to control its oxidation state, neptunium will always be present in part in the more extractable Np(IV) and Np(VI) oxidation state hence there is often "leakage" of neptunium into undesirable process streams in a PUREX plant (8).

In Separations for the Nuclear Fuel Cycle in the 21st Century; Lumetta, G., et al.;
ACS Symposium Series; American Chemical Society: Washington, DC, 2006.

Downloaded by COLUMBIA UNIV on August 9, 2012 | http://pubs.acs.org
Publication Date: June 9, 2006 | doi: 10.1021/bk-2006-0933.ch002

In the waste management strategy based on TBP extraction called UREX+ Codecontamination flowsheet, the oxidation state of Np is adjusted to the tetravalent state with acetohydroxamic acid to enable its coextraction with U and Pu. (9)

The practical steps involved in the PUREX flow sheet include adjusting [HNO_3] to 2-3 M and plutonium valency to IV, most commonly with H_2O_2 or HNO_2. In the first cycle, U(VI) and Pu(IV) are co-extracted into the TBP phase leaving behind the fission products, trivalent actinides and Np(V) in the aqueous raffinate. To separate Pu from U, Pu(IV) is reduced to Pu(III) using ferrous sulfamate, U(IV), or hydroxylamine; U(VI) is subsequently stripped with very dilute nitric acid solution; final cleanup of remaining traces of U(VI) occurs during extractant reconditioning with Na_2CO_3.

A second uranium and plutonium extraction cycle follows for both the aqueous phases separately after feed adjustments to improve recovery. Final purification of plutonium is done in modern PUREX plants using additional TBP solvent extraction steps. Historically, pure Pu has been prepared using anion exchange chromatography, as follows: the feed is adjusted to 7.1 M HNO_3 and the plutonium anionic species $Pu(NO_3)_6^{2-}$ is adsorbed strongly onto the column; remaining contaminants like U, Zr-Nb, Ru and Fe are not adsorbed. After adequate washings, plutonium is eluted from the anion exchange resin with 0.5 M nitric acid.

THOREX process

In the 1960s and 70s, significant interest developed in the thorium fuel cycle as a potential supplement to limited uranium reserves. The slightly harder neutron spectrum of heavy water and gas-cooled reactors make such reactors reasonable centerpieces of a uranium-thorium breeder reactor cycle. However, it has been shown that thorium can be used practically in any type of existing reactor. Stewart et al. (10) described a thorium-uranium breeder fuel cycle designed around the now-decommissioned Fort St. Vrain gas cooled reactor. Molten salt reactors also have a favorable neutron spectrum for this fuel cycle. These initiatives have been virtually brought to a halt due to the comparative abundance (at present) of available uranium, and to the important radiolytic complications of this cycle as discussed below). Research on the Th-U breeder reactor cycle continues in India, where the comparative abundance of thorium mineral deposits and unavailability of U minerals drives interest (11).

The initial ^{233}U to operate this fuel cycle must be produced in a ^{235}U-fueled reactor, or with an initial ^{235}U or ^{239}Pu charge surrounded by a ^{232}Th breeding blanket. Two fundamental limitations of the U-Th fuel cycle are the creation of ^{228}Th ($t_{1/2}$ = 1.912 yr, 5.42 MeV α) and ^{232}U ($t_{1/2}$ = 68.9 yr, 5.32 MeV α) and their daughters as byproducts, and the creation of ^{233}Pa ($t_{1/2}$ = 27 d, 0.3 MeV γ, 0.6 MeV β^-) as parent of the desired ^{233}U product. The buildup of isotopic contaminants during successive irradiations of recycled ^{233}U-Th fuels can greatly

Downloaded by COLUMBIA UNIV on August 9, 2012 | http://pubs.acs.org
Publication Date: June 9, 2006 | doi: 10.1021/bk-2006-0933.ch002

affect the handling procedures used in fuel-element refabrication. The fuel cycle has been advocated as nonproliferating because of the presence of the ^{232}U isotope and the energetic γ activity of its ^{208}Tl and ^{212}Bi daughters (12). Another significant advantage of this fuel cycle is the reduced production of long-lived transuranic actinides.

The separation of thorium from uranium is most typically accomplished using the same basic chemistry that drives the PUREX process, i.e., extraction of Th(IV) and U(VI) from nitric acid solutions into TBP solutions with aliphatic hydrocarbon diluents. The use of an acid-deficient feed (0.15 M) induces high decontamination while injection of HNO_3 at the fourth extraction stage provides high salting strength and insures quantitative uranium and thorium extraction. The introduction of $Al(NO_3)_3$ (13) or $Be(NO_3)_2$ (14) as salting out reagent has been demonstrated as desirable, because thorium is extracted by TBP less effectively than Pu(IV) or U(VI). Stripping of thorium is most often accomplished using dilute nitric or sulfuric acid (under conditions wherein a bit of omplexing strength is helpful). With limitations in the availability of uranium reserves, concerns about plutonium proliferation, the Generation IV program which includes development activities on fast-spectrum reactor designs, and the general threat of global climate change, it is becoming increasingly likely that this fuel cycle will again receive attention in the coming decades.

Downloaded by COLUMBIA UNIV on August 9, 2012 | http://pubs.acs.org
Publication Date: June 9, 2006 | doi: 10.1021/bk-2006-0933.ch002

Actinide Separation Processes at the Design and Pilot Stages

Addressing the problem of minor actinide (Am, Cm, Np) recycle is a many-faceted challenge and none of the processes noted above can be used to isolate these species in an efficient manner, i.e., without excessive creation of wastes. During the last two decades, concerted and mission-oriented research conducted around the world has identified a number of promising systems for actinide separations using solvent extraction, extraction chromatography, supported liquid membrane, magnetically assisted chemical separations or pyroprocessing. Plant scale demonstrations have yet to occur for any of these processes, as the considerable capital investment must be weighed against the benefits. In the following discussion, the performance of the extraction systems that have been developed for trivalent actinide partitioning will be compared.

Octyl(phenyl)-N,N-di-isobutylcarbamoylmethylphosphine oxide

To overcome the inability of TBP to extract transplutonium actinides, a class of bifunctional extractants was suggested initially by Siddall (15). Interest was revived in this class of compounds by Schulz as a viable waste management strategy in the late 1970's (16). During the following decade, an effort led by Horwitz at Argonne National Lab resulted in the development and pilot scale demonstration of carbamoylmethyl phosphine oxide extractants (Fig 2.) and the

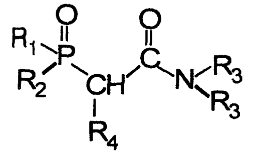

Figure 2. Carbamoyl methyl phosphine oxide.

TRUEX process (17,18). Two papers describe the synthesis and purification (19) and the spectral properties of the carbamoylmethyl phosphine oxides in detail (20). The extraction behavior of mainly trivalent actinides, lanthanides and a few other metal ions has been studied with all the reagents synthesized in this class. Actinide extraction properties and phase compatibility varied significantly with the nature of the substituents on the carbamoylmethylphosphine oxide core. Of the compounds investigated, octyl(phenyl)N,N-diisobutylcarbamoylmethyl phosphine oxide (OΦDiBCMPO or CMPO) was found to possess the best combination of properties for actinide extraction in a PUREX-compatible diluent system. The CMPO type compounds have received the greatest attention of all potential actinide-partitioning reagents developed over the past 20 years and as a result represent the best-understood hydrometallurgical reagents for total actinide partitioning from wastes. Fundamental features of this system have been reviewed previously (17,18)

The now well-known TRUEX Process for the recovery of all the actinides from various types of highly acidic nuclear waste solutions is based on CMPO as the principal extractant. The TRUEX process solvent is 0.2-0.25 M CMPO + 1.0-1.4 M TBP in paraffinic hydrocarbon (linear or branched, though the process has been demonstrated in chlorinated diluents as well). TBP hinders third phase formation, contributes to better acid dependencies for D_{Am}, improves phase compatibility, and reduces hydrolytic and radiolytic degradation of CMPO. The ability to efficiently extract tri-, tetra-, and hexavalent actinides from solutions of moderate acid concentration and with good selectivity over most fission products (except lanthanides) is a key feature of this extractant. From an engineering perspective, the more-or-less constant D values of Pu(IV), U(VI) and Am(III) between about 1 and 6 M HNO_3 is important, as it allows efficient extraction of actinides from wastes or dissolved fuels with little or no need to adjust the acidity of the feed solution. This particular feature of TRUEX distinguishes this extraction system from other methods for TRU isolation.

Russian researchers have independently developed a TRU extraction process based on a somewhat simpler (thus, less expensive) derivative of CMPO (diphenyl-N,N-di-*n*-butyl CMPO - DΦDBuCMPO) employing a fluoroether diluent (Fluoropol-732) (21). This process behaves similarly to the TRUEX process in terms of its efficiency for actinide extraction, shows little tendency toward third phase formation, and avoids the interferences caused by degradation of TBP. It has been tested in centrifugal contactors and found to recover actinides with greater than 99.5% efficiency. The corrosive nature of aqueous effluents derived from degraded solvent (i.e., containing HF) is a potential

Downloaded by COLUMBIA UNIV on August 9, 2012 | http://pubs.acs.org
Publication Date: June 9, 2006 | doi: 10.1021/bk-2006-0933.ch002

Downloaded by COLUMBIA UNIV on August 9, 2012 | http://pubs.acs.org
Publication Date: June 9, 2006 | doi: 10.1021/bk-2006-0933.ch002

drawback for this process. This variation on this version of TRUEX processing has been incorporated within the Universal Extraction (UNEX) process (22-25).

At Japan's Power Reactor and Nuclear Fuel Development Corporation (JNC), batch and counter-current runs with real high-active raffinate from FBR spent fuel reprocessing have been carried out without adjusting acidity, using 0.2 M CMPO + 1.2 M TBP in *n*-dodecane. The rare earths were extracted along with actinides and some fraction of ruthenium. The D_f for actinides was greater than 10^3. Oxalic acid was added in the feed and scrubbing solutions to improve ruthenium decontamination and effectively lower the D values of zirconium and molybdenum (26). In another communication from the same laboratory, Ozawa et al. (27) suggested improvements in the TRUEX process flow sheet, specifically, increasing the acidity of the feed to about 5 M to improve Ru decontamination in the actinide fraction, and using salt free reagents like hydrazine oxalate, hydrazine carbonate and tetramethylammonium hydroxide for stripping and cleanup steps to obtain a final raffinate that is α-inactive and salt-free. The TRUEX process has been extensively tested on different classes of radioactive wastes and spent fuel raffinates in India as well.

Trialkylphosphine oxide (TRPO)

Trialkylphosphine oxide, a mixture of seven alkyl phosphine oxides (Fig. 3), R being heptyl and octyl alone and a mixture of hexyl, heptyl and octyl groups[1], has been tested in China at the Institute for Nuclear Energy and Technology (Tsinghua University) (28). Tests were continued in collaborative efforts with the European Institute for Transuranium Elements (Karsruhe, Germany) for the extraction of actinides, lanthanides and other fission products from HNO_3 and HLW solutions (29-31). From studies in HNO_3 medium with 30% TRPO in *n*-dodecane as the extractant, it was observed that D_{Am} was smaller than 1 at 3 M and about 10 only at 1 M HNO_3. To achieve an acceptable D_f for Am, the acidity of HLW (typically 3-6 M) must be reduced to less than 1 M. Neptunium extraction is accomplished after electrolytic reduction to Np(IV) in HNO_3 and in simulated HAW solutions. During all of the experiments with concentrated wastes initially in 3 M HNO_3, the waste was diluted 10 times and the acidity then adjusted to between 0.7 and 1.0 M. Under such conditions, the recovery of U, Np, Pu, Am and Cm from HAW using a 7-stage mixer-settler was highly efficient. Centrifugal contactor using a battery of 12 centrifgal contactors with actual diluted HLW has given $D_{f\ \mathrm{actinides}}$ between 10^3 to 10^5. The actinides have in all cases been stripped with 5 M HNO_3 (Am, Cm, rare earths), 0.5 M oxalic acid (Np, Pu) and 5% Na_2CO_3 (U).

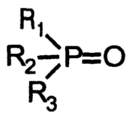

Figure 3. Trialkyl phosphine oxides.

---

[1] Zhu and Song (1992) report approximate composition of 10% hexyl; 50% heptyl and 40% octyl

Diisodecylphosphoric acid (DIDPA)

At the Japan Atomic Energy Research Institute, separation of metal ions from the HLW solutions has been classified into four groups: transuranium elements, Tc-platinum group metals, Sr-Cs, and other elements. For the separation of TRU elements, a mixture of 0.5 M DIDPA (Fig. 4) + 0.1 M TBP in *n*-dodecane has been proposed with the acidity of the HLW reduced to 0.5 M (32, 33). Neptunium is reduced from Np(V) to Np(IV) using H_2O_2 and then co-extracted with Pu(IV). Batch as well as counter-current tests using a 16-stage miniature mixer-settler with conditioned synthetic HLW have given very high extraction of actinides including neptunium. During stripping, batch studies with diethylenetriaminepentaacetic acid (DTPA) as a stripping agent gave an Am/rare earths separation factor of greater than 10. In this process, reduction of acidity to about 0.5 M is accomplished using formic acid. At such low acidity molybdenum and zirconium precipitate out, carrying about 93% of the plutonium. Filtration units are needed to get a clean HLW solution.

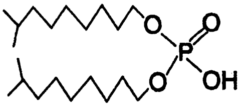

Figure 4. Diisodecyl phosphoric acid

N,N'-Dimethyl-N,N'-dibutyltetradecylmalonamide (DMDBTDMA)

One drawback of using organophosphorus extractants is the solid residue that results upon their incineration at the end of their useful life. French researchers have championed the CHON (carbon, hydrogen, oxygen, nitrogen) principle of extractant design (avoiding the use of S or P containing reagents as possible) to minimize the generation of wastes from extractant destruction. This approach to extractant design has generated a large amount of interesting research on a diverse group of reagents. Bidentate diamide extractants have proven to be good reagents for trivalent actinides and lanthanides partitioning from PUREX raffinates.

Among the numerous diamides synthesized and employed for extraction of actinides from nitric acid solutions (34-38), N,N'-dimethyl-N,N'-dibutyl-2-tetradecyl malonamide (DMDBTDMA, Fig 5) has shown the greatest promise. This diamide dissolves in *n*-dodecane, does not give a third phase when in contact with 3-4 M HNO_3, and a 1 M solution gives a D_{Am} of about 10 at 3 M HNO_3. A steep dependence on [HNO_3] makes stripping simpler than is seen for CMPO. More recently, the tetradecyl backbone substituent has been replaced by a hexoxyethyl (ether) group to improve phase compatibility characteristics. Batch studies, mixer-settler and centrifugal contactor runs with synthetic as well as actual high-active wastes have given good results for the recovery of actinides. Radiation and hydrolytic stability of the reagent is comparable to that of CMPO. A further advantage of this class of reagents is the

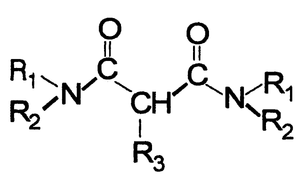

Figure 5. Malonamide.

Downloaded by COLUMBIA UNIV on August 9, 2012 | http://pubs.acs.org
Publication Date: June 9, 2006 | doi: 10.1021/bk-2006-0933.ch002

comparatively benign nature of the degradation products of the primary extractant on process operations. The DIAMEX Process, based on the use of these diamide extractants, has undergone extensive testing, and appears poised for application pending the outcome of France's decision on the advisability of actinide partitioning as a waste management strategy.

Following the CHON strategy, JAERI researchers have investigated in recent years the extraction properties of amide extractants based on diglycolic acid. Foremost among the extractants being investigated is tetraoctyldiglycolamide (TODGA). This reagent exhibits a considerable affinity for trivalent lanthanides and actinides, extracting them significantly more strongly than hexavalent actinides, and with a comparable strength to that of tetravalent actinide cations. Some features of TODGA's extraction performance suggest that supramolecular organization of solute species in the organic phase has a major impact on actinide extraction. This extractant has been suggested as the cornerstone reagent for the ARTIST Process for actinide partitioning in Japan (39).

Downloaded by COLUMBIA UNIV on August 9, 2012 | http://pubs.acs.org
Publication Date: June 9, 2006 | doi: 10.1021/bk-2006-0933.ch002

Trivalent Actinide/Lanthanide Group Separation

In the PUREX process, as in most new processes being developed for actinide partitioning from HLW, the stripped fraction containing the trivalent actinides (Am and Cm) also contains the trivalent lanthanides. If all actinides are to be recycled for transmutation, it is essential to separate americium and curium from trivalent lanthanides to avoid the strong absorption of thermalized neutrons by the lanthanides. Separation of trivalent actinides as a group from the lanthanides has been a topic of great interest since the time of discovery of the transplutonium elements. Because the solution chemistry of trivalent lanthanides and actinides are nearly identical in every other respect, extractants or complexing agents containing donor atoms softer than O or F^-, in particular, N, S, Cl, are essential to efficient group separations (40). A number of techniques and reagents have been developed to achieve separation of trivalent actinides and lanthanides. Among these, a few important existing methods and those being newly developed are discussed below.

TRAMEX process

Solution of concentrated LiCl containing small amounts of HCl to inhibit hydrolysis of the metal ions in contact with a tertiary amine solution in kerosene or diethyl benzene is the basis of the TRAMEX Process for plant scale separation of trivalent actinides from fission product lanthanides (41). In this process, the feed solution is 11 M LiCl (0.02 M HCl) containing trivalent actinides and the fission products. The organic phase employed is 0.6 M

Alamine 336 (a mixture of tertiary C_6-C_8 alkyl amines) in diethyl benzene. The scrubbing solution is 11 M LiCl (0.02 M HCl). Trivalent actinides are extracted into the organic phase while the trivalent lanthanide fission products remain in the raffinate. The actinides are subsequently stripped from the organic phase with 5 M HCl. In a single extraction contact, trivalent actinides (Am, Cm, Bk, Cf, Es and Fm) as a group have a separation factor of about 100 from the trivalent lanthanides (Ce, Nd, Eu, Tb, Ho and Tm). The order of extraction for the actinides is reported to be Cf > Fm > Es > Bk > Am > Cm. Waste disposal considerations ultimately hinder wide application of this process.

TALSPEAK process

The chemistry of the TALSPEAK process has been discussed extensively in prior reports (42). This process has been shown to achieve trivalent actinide–lanthanide group separations of greater than 10. The separation is based principally on the relative affinity of aminopolycarboxylic acid complexants for trivalent actinides over lanthanides. Though not deployed as such for accomplishing lanthanide-trivalent actinide separations at process scale, the critical reagent in TALSPEAK, diethylene-triamine-N,N,N',N",N"-pentaacetic acid (DTPA, Fig. 6), has repeatedly been employed in the conceptual development of actinide - lanthanide hydrometallurgical separation processes. In the DIDPA and SETFICS processes, the separation of 4f and 5f elements is accomplished in a reverse-TALSPEAK stripping with 0.05 M DTPA. In the context of modern process design, the aminopolycarboxylates are acceptable reagents, as they are composed of only C, H, O, and N, and hence are fully incinerable. At the same time, application of aminopolycarboxylates in process chemistry during the Cold War created significant complications in subsurface waste storage tanks at Hanford. Any plans for their application in actinide partitioning in the 21^{st} Century would demand a plan for their distruction as a part of waste management. These are not suitable reagents for direct disposal to process waste tanks, particularly in the tanks are made alkaline.

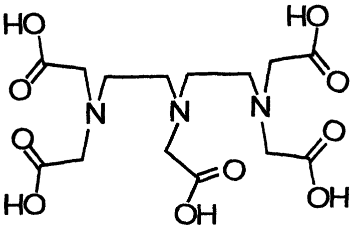

Figure 6. Diethylenetriamine-N,N,N',N",N"-pentaacetic acid

Employing soft-donor extractants

Though Musikas (43) indicated the potential for effective separation of trivalent actinides from lanthanides using thiophosphoric acid extractants ($(RO)_2PS_2H$), the instability of such extractants towards hydrolysis hindered their utility. However, dithiophosphinic acids (R_2PS_2H), represented by the commercially available extractant Cyanex-301 (Fig. 7), are less susceptible to hydrolysis (44). In a counter-current fractional process having three extraction and two scrubbing stages, more than 99.99% of americium can be separated

Downloaded by COLUMBIA UNIV on August 9, 2012 | http://pubs.acs.org
Publication Date: June 9, 2006 | doi: 10.1021/bk-2006-0933.ch002

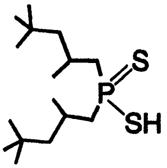

Figure 7. Bis(2,4,4-trimethylpentyl) dithiophosphinic acid, Cyanex 301.

from a trace amount of europium with less than 0.1% extraction of the latter (45-48). Polyaza ligands of appropriate geometries have also received significant attention and have some unique properties (49, 50). French researchers have demonstrated actinide/lanthanide separation processes based on each of these classes of extractants (SANEX processes). Ultimately, the susceptibility of both thiophosphinic acid and the polyaza ligands to degradation in contact with nitric acid solutions containing radioactive materials significantly has limited their potential for deployment. Work continues on efforts to increase the stability of these classes of reagents (without erasing their separation potential). Furthermore, the thiophosphinic acid reagents do not conform to the present reigning philosophy of only using CHON reagents.

Downloaded by COLUMBIA UNIV on August 9, 2012 | http://pubs.acs.org
Publication Date: June 9, 2006 | doi: 10.1021/bk-2006-0933.ch002

Other Potential Options for Advanced Processing

Past practices in aqueous processing have led to the creation of some challenging environmental restoration problems, particularly in the U.S. and Russia. One side effect of this situation is the search for "unconventional" options for a next generation of actinide processing technologies. Several options have received significant attention and perhaps could eventually provide useful alternatives to conventional processes.

Pyrochemical processes

The most substantially developed alternative approaches to the task of spent fuel reprocessing are those based on the application of molten metals and/or molten salts. Electrometallurgical processing schemes have some substantial advantages in certain respects, though materials compatibility remains an issue. Pyrochemical processing involves the conduct of "dry" chemical reactions at high temperature in which the reactions occur in solid, liquid and gas phases. Oxidation-reduction, volatilization (of halide or metal), slagging (melt refining, molten salt extraction, carbide slagging), liquid metal (melt refining, liquid metal extraction, liquation, precipitation), and electrolytic processes are the most common types. Molten salts have some properties which make them attractive for nuclear applications: (i) they are less subject to radiolytic degradation than aqueous media due to their ionic liquid structure, (ii) criticality concerns and problems are reduced due to the absence of neutron moderating elements and organic solvents. These properties in particular make it possible to process materials that produce high radiation loadings, for example, fuels containing high concentrations of fissile materials after a short cooling time period. In addition, it is possible to reduce the number of chemical conversion steps compared to that needed for aqueous processes. Pyroprocessing of nuclear materials have been reviewed by Willit et al. (51).

Today, molten alkali and alkaline-earth chlorides have been most extensively studied for plutonium conversion and separation. Three processes are in use throughout the world at significant scale-up (52): (i) DOR process (Direct Oxide Reduction) in which PuO_2 is reduced by calcium in Ca-based chloride salt, (ii) MSE process (Molten Salt Extraction) for ^{241}Am removal from weapon-grade plutonium by $MgCl_2$ in alkali chloride salt, (iii) ER process (ElectroRefining) for high plutonium purification using molten alkali and/or alkali-earth chloride electrolyte. From the former Soviet Union emerged a concept of vibropacked fuel fabrication for fast reactors and pyroelectrochemical reprocessing based on electrolysis of oxide fuel in molten alkali chlorides. After being applied to UOX fuel, the DDP process (Dimitrovgrad Dry Process) has been adapted today for MOX fuel reprocessing and weapon-grade plutonium conversion into plutonium oxide for civilian use in Russian fast reactors (53,54).

In the Integral Fast Reactor (IFR) fuel cycle, after the spent core fuel is discharged, the fuel is chopped and placed in an anode basket. The anode basket containing the chopped fuel is put into an electrorefiner containing molten LiCl-KCl electrolyte and a liquid cadmium pool under inert atmosphere. $CdCl_2$ is added in the electrolyte to oxidize electropositive fission-product metals (alkali, alkaline earths and a large fraction of the rare earth metals) to their chlorides. The amount of oxidizing agent to be added is adjusted to maintain 2 mol % actinide chlorides in the salt phase. The basket is made anodic and: (i) nearly pure uranium is electro-transported to a solid mandrel cathode, (ii) transuranium elements and some uranium are transferred by electro-transport to a liquid cadmium cathode. Noble metal fission products remain in an unoxidized form and are removed from the basket with the cladding hulls, although some portion falls into the cadmium pool at the bottom of the electrolyser. Electropositive fission products remain in the salt and build up during the successive reprocessing batches and progressively modify the electrochemical and physical properties of the electrolyte. Periodic treatment is thus required to remove them and recycle the electrolyte. The molten metal-salt extraction (using Li-Cd alloys) has been proposed for reduction and removal of TRUs from the electrolyte salt and for TRU reoxidation back into the salt to start the next electrorefining campaign. Moreover, the use of UCl_3 as oxidant makes it possible to avoid the introduction of cadmium in the electrorefiner and thus the lower cadmium pool can be eliminated. This approach avoids the deposition of cadmium and makes easier the removal of solids that accumulate at the bottom of the electrolyser. Pyrometallurgical operations in general also suffer the throughput limitations imposed by batch operations.

Downloaded by COLUMBIA UNIV on August 9, 2012 | http://pubs.acs.org
Publication Date: June 9, 2006 | doi: 10.1021/bk-2006-0933.ch002

Volatility-based Separations

The comparative ease with which hexavalent uranium and plutonium can be sublimed (UF_6 is a solid ar room temperature, but readily sublimes at 64°C) creates an opportunity to accomplish the separation of the elements from the bulk of fisson products with high efficiency under the appropriate circumstances. Among fission products, only Te, Tc, and I form volatile fluorides and so represent the principle fission product contaminants likely to be present in a volatilized effluent from spent fuel dissolution by this method. Oxidized Np, but not trivalent Am or Cm will follow U and Pu in a volatility-based process. The volatility of UF_6 has been particularly important in the development of nuclear technology, as every isotope enrichment technique used for the preparation of reactor fuels (or highly enriched U for weapons production) relies in some fashion on the volatility of UF_6.

A conceptual flowsheet for a fluoride volatility process for spent fuel processing has been suggested (55). Conditions must be maintained strictly dry and redox conditions under control for an actinide volatility process to be operational, as UF_6 is readily hydrolyzed to UO_2F_2 or reduced to the far less volatile species UF_4 (or PuF_4). Though considerable operational experience has been acquired in isotope enrichment, the highly corrosive nature of volatile fluorides demands that special materials of constricuction be used in plant-scale operations. Other volatile species (for example various β-diketone complexants) have received some attention, but so far have proven inadequate for process development. The potential economies of scale (i.e., small footprint plants) and clear selectivity of fluoride volatility processes are the principle advantages of this approach. The corrosiveness of the volatile fluorides and the need to handle radioactive gases are the potential impediments to large-scale development of processes of this type. The small footprint of such a process might also present weapons proliferations concerns, as an illicit separations plant might be more readily concealed than a process based on nitric acid dissolution of fuel and aqueous processing. Separations based on the use of supercritical fluids share some of these imitations (see below).

Aqueous Biphasic Extraction

One method that has been investigated and might have some utility for selected separations are those based on aqueous biphasic systems. The combination of hydrophilic organic species like polyethylene glycols with selected classes of salt solutions can produce two-phase systems (56). The key characteristic of these systems is that the immiscible phases are both largely aqueous in nature. Myasoedov and Chmutova (57) have reported conditions for the separation of transplutonium elements from uranium, thorium and lanthanides. The aqueous biphase itself does not extract actinides strongly, but Arsenazo III (2,7-bis(2,2'-arsonophenylazo)-1,8-dihydroxynaphthalene-3,6-

Downloaded by COLUMBIA UNIV on August 9, 2012 | http://pubs.acs.org
Publication Date: June 9, 2006 | doi: 10.1021/bk-2006-0933.ch002

disulfonic acid) is a highly effective carrier for these metal ions. Overall, while the aqueous biphasic extraction approach brings forward some interesting features, the high salt concentrations needed to generate the biphase work against its utility for large-scale separations. Polyethylene glycols remain useful compounds when employed as phase modifiers in conventional solvent extraction.

Actinides in room-temperature ionic liquids (RTILs)

Room temperature ionic liquids (RTILs) were discovered by Hurley and Wier (58), who found that a mixture of $AlCl_3$ and ethylpyridinium bromide (EPB) in a 2:1 molar ratio melted at −40°C and that this liquid is suitable for the electrodeposition of aluminum metal at room temperature. The present generation of RTILs (59-61) are salts made of organic cations, such as: (i) N-alkyl quaternary ammonium, R_4N^+, (ii) N-alkyl pyridinium, (iii) N-alkylisoquinolinium, (iv) 1-N-alkyl-3-methylimidazolium, (v) N-alkyl quaternary phosphonium, R_4P^+, associated with various anions, e.g. halides (Cl^-, Br^-), haloaluminates (chloro or bromo), chlorocuprate ($CuCl_2^-$), tetraalkylborides (R_4B^-), NO_3^-, $CF_3CO_2^-$, BF_4^-, PF_6^-, $N(SO_2CF_3)_2^-$. With the anions BF_4^-, PF_6^-, $N(SO_2CF_3)_2^-$, the RTILs are most often hydrophobic and can be used, for example, for the development of liquid-liquid extraction separation processes (61). Studies of RTIL's as alternative solvents for solvent extraction have given indications of greater per-stage extraction efficiency, but a significant tendency toward irreversible reactions (62, 63). Rogers and coworkers have published several important papers in this field (64-68) including a review paper (61). For more information on the properties of these materials, see reviews by Hussey (60) and Welton (69).

Supercritical fluid extraction of actinides

The rationale for the use of SFE of metal ions as an alternative to conventional liquid-liquid extraction (LLE) was mainly to minimize the generation of the secondary organic waste often encountered in LLE processes. Carbon dioxide was chosen as the most appropriate supercritical fluid because: (i) the values of the critical point were appropriate for a SFE application: P_c = 72.9 atm, T = 304.2 K, ρ_c = 0.47 g·mL^{-1}, (ii) CO_2 can be considered a green solvent for the environment, (iii) (aside from asphyxiation hazards) CO_2 is harmless to workers, (iv) CO_2 is almost inert with respect to radiolysis, (v) CO_2 is inexpensive. Moreover, the high diffusivity of sc-CO_2 means that rapid extraction of the metal ions from their sources can be expected. Since 1991, about eighty reports related to the SFE of metal ions have been published, most of them related to actinides. The most studied actinide ion is U(VI), with about 50 papers. This field was recently reviewed by Darr and Poliakoff (70) and by Wai (71). Current research results establish the potential for the use of supercritical CO_2 media for the dissolution of actinide oxide fuel matrices (72), though the prospect of extension of sc-CO_2 to the task of the main option for

Downloaded by COLUMBIA UNIV on August 9, 2012 | http://pubs.acs.org
Publication Date: June 9, 2006 | doi: 10.1021/bk-2006-0933.ch002

spent-fuel reprocessing might ultimately be limited by the potential hazards of manipulating highly radioactive solutions at elevated temperature and pressure.

Conclusions

Actinide partitioning if and when incorporated at the back-end of the nuclear fuel cycle will considerably reduce the long-term radiological risks and thereby increase the safety of the disposal of nuclear wastes in a geologic repository. Whether actinides are recycled to a reactor (or accelerator) for transmutation or disposed of in a repository, a significant reduction in the hazard associated with the wastes (with transmutation) or the cost (without transmutation) can be achieved through the deployment of actinide partitioning technologies. Though there is no universal consensus on the desirability of actinide partitioning for radioactive waste disposal, continuing research around the world offers an ever-increasing number of potentially viable options for accomplishing partitioning based on solvent extraction, extraction chromatography, supported liquid membranes, or magnetically assisted chemical separations. The continued development of more options relying on the proven technology of solvent extraction may assist immeasurably in securing the public acceptability of nuclear power as the most viable strategy for combating global warming. The long term prospects of dry processes and unconventional materials have further potential to dramatically impact spent fuel processing options.

Downloaded by COLUMBIA UNIV on August 9, 2012 | http://pubs.acs.org
Publication Date: June 9, 2006 | doi: 10.1021/bk-2006-0933.ch002

References

1. Goodstein, D. *Out of Gas: The end of the age of oil,* W. W. Norton and Company, New York **2004** is representative of a significant literature on this subject.
2. Hoffert, M. I.; Caldeira, K.; Benford, G.; Criswell, D. R.; Green, C.; Herzog, H.; Jain, A. K.; Kheshgi, H. S.; Lackner, K. S.; Lewis, J. S.; Lightfoot, H. D.; Manheimer, W.; Mankins, J. C.; Mauel, M. E.; Perkins, L. J.; Schlesinger, M. E.; Volk, T.; Wigley, T. M. L. *Science* **2002** *298*, 981-987.
3. Cooper, U. R.; Walling Jr., M. T. in *Proc. 2nd Int. Conf. Peaceful Uses of Atomic Energy, Geneva,* **1958**, *Vol. 17*: pp. 291-373.
4. Mc Kay, H. A. C. in *Proc., Ist Int. Conf. Peaceful uses of Atomic Energy, Geneva,* **1955**, Vol. 7: pp. 314-317.

5. Mathieson, W. A.; Nicholson, C. A. **1968**, *PUREX Chemical Flow Sheet-Processing of Aluminium clad Uranium Fuels*, Hanford Works, Report ARH-214 DEL.
6. Koch, G.; Baumgartner, F.; Goldacker, H.; Ochsenfeld, W.; Schmieder, M. **1977**, A solvent extraction flowsheet for a large-scale LWR fuel reprocessing plant, Kernforschungszentrum Karlsruhe, Report KFK-2557.
7. Flanary, J. R. *Reactor Sci. Technol.* **1954** *4*, 9-36.
8. Drake, V. A. **1990** in *Science and Technology of Tributyl Phosphate, Volume III.* W. W. Schulz, L. L. Burger,; J. D. Navratil (Eds.). Boca Raton, Florida, CRC Press: pp. 123-145.
9. Bakel, A. J.; Aase, S. B.; Arafat, H.; Bowers, D.; Byrnes, J. P.; Clark, M. A.; Emery, J. W.; Falkenberg, J. R.; Gelis, A. V.; Periera, C.; Hafenrichter, L.; Laidler, J. J.; Regalbuto, M. C.; Tsai, Y.; Quigley, K. J.; Vander Pol, M. H.; Vandegrift, G. F. *Lab-scale demonstration of the UREX+ process.* Abstracts of Papers, 227th ACS National Meeting, Anaheim, CA, United States, March 28-April 1, 2004 (2004), IEC-109.
10. Stewart, H. B.; Dahlberg, R. C.; Goeddel, W. V.; Trauger, D. B.; Kasten, P. R.; Lotts, A. L. **1971** *Utilization of the thorium cycle in the HTGR [High-Temperature Gas-Cooled Reactor]*, Gulf General Atomics, Inc., San Diego, CA, USA., U. S. At. Energy Comm.
11. Lung, M.; Gremm, O. *Nuclear Engineering and Design* **1998** *180*, 133-146.
12. Ragheb, M. M. H.; Maynard, C. W. *Atomkernenergie/Kerntechnik* **1980** *35*, 122-124.
13. Oliver, J. R. **1958** *THOREX process: third uranium cycle studies*, *U.S. Atomic Energy Comm.* **ORNL-2473**: 15 pp.
14. Farrell, M. S.; Orrock, B. J.; Temple, R. B. **1962** *The reprocessing of beryllium-based reactor fuels. A chemical feasibility study of a modified THOREX process for the recovery of the uranium and thorium*, U. S. Atomic Energy Commission Report AAEC/TM-146, 12 pp.
15. Siddall, T. H., Jr. *J. Inorg. Nucl. Chem.* **1963** *25*, 883-892.
16. Schulz, W. W.; McIsaac, L. D. **1975** *Removal of actinides from Nuclear fuel reprocessing waste solutions with bidentate organophosphorus extractants*, Atlantic Richfield Hanford Co., Richland, Washington, ARH-SA-217
17. Schulz, W. W.; Horwitz, E. P. *Sep. Sci. Technol.* **1988** *23*, 1191-1210.
18. Horwitz, E. P.; Schulz, W. W. **1990** *The TRUEX process: A vital tool for disposal of U.S. defense Nuclear waste, New separation chemistry for Radioactive waste and other specific applications,* sponsored by the

Downloaded by COLUMBIA UNIV on August 9, 2012 | http://pubs.acs.org
Publication Date: June 9, 2006 | doi: 10.1021/bk-2006-0933.ch002

Commission of the European Communities and the Italian Commission for Nuclear and alternative Energy sources, Rome, Italy, May 16-18.

19. Gatrone, R. C.; Kaplan, L.; Horwitz, E. P. *Solvent Extr. Ion Exch.* **1987** *5,* 1075-1116.
20. Gatrone, R. C.; Rickert, P. G. *Solvent Extr. Ion Exch.* **1987** *5,* 1117-1139.
21. Myasoedov, B. F.; Chmutova, M. K.; Smirnov, I. V.; Shadrin, A. U. **1993.** in *Global '93: Future Nuclear Systems: Emerging Fuel Cycles and Waste Disposal Options,* American Nuclear Society, LaGrange Park, IL: pp. 581-587.
22. Todd, T. A.; Law, J. D.; Herbst, R. S.; Peterman, D. R. Decontamination of acidic radioactive waste using the universal extraction (UNEX) process. American Institute of Chemical Engineers, [Spring National Meeting], New Orleans, LA, United States, Mar. 30-Apr. 3, 2003 (2003), 2349-2355.
23. Herbst, R. S.; Law, J. D.; Todd, T. A.; Romanovskiy, V. N.; Smirnov, I. V.; Babain, V. A.; Esimantovskiy, V. N.; Zaitsev, B. N. *Sep. Science Technol.* **2003** *38(12 & 13),* 2685-2708.
24. Herbst, R. S.; Law, J. D.; Todd, T. A.; Romanovskiy, V. N.; Babain, V. A.; Esimantovskiy, V. M.; Smirnov, I. V.; Zaitsev, B. N. *Solvent Extr. Ion Exch.* **2002** *20(4 & 5),* 429-445.
25. Romanovskiy, V. N.; Smirnov, I. V.; Babain, V. A.; Todd, T. A.; Herbst, R. S.; Law, J. D.; Brewer, K. N. *Solvent Extr. Ion Exch.* **2001** *19,* 1-21.
26. Ozawa, M.; Nemoto, S.; Togashi, A.; Kawata, T.; Onishi, K. *Solvent Extr. Ion Exch.* **1992** *10*, 829-846.
27. Ozawa, M.; Koma, Y.; Nomura, K.; Tanaka, Y. *J. Alloys Compd.* **1998** *271-273,* 538-543.
28. Zhu, Y.; Jiao, R.; Wang, S.; Fan, S.; Liu, B.; Zheng, H.; Zhou S.; Chen, S. **1983**. An extractant (TRPO) for the removal and recovery of actinides from high level radioactive liquid waste. ISEC'83, Denver, Colorado USA.
29. Zhu, Y.; Song; C., Eds. **1992.** *Recovery of Neptunium, Plutonium and Americium from high active waste.* in *Transuranium Elements: A half Century.,* Morss, Lester R.; Fuger, J. (Eds) American Chemical Society, Washington D.C.: pp. 318-30.
30. Zhu, Y.; Jiao, R. *Nucl. Technol.* **1994** *108*: 361-369.
31. Glatz, J. P., Song; C., Koch; L., H.; Bokelund H.; He, X. M. **1995**. *Hot tests of the TRPO process for the removal of TRU elements from HLLW.* in *International Conference on Evaluation of Emerging Nuclear fuel cycle systems Global' 95*, Versailles, France.
32. Morita, Y.; Kubota, M. *J. Nucl. Sci. Technol.* **1987** *24*: 227-232.
33. Morita, Y.; Kubota, M. *Solvent Extr. Ion Exch.***1988** *6*: 233-246.
34. Musikas, C. *Inorg. Chim. Acta* **1987** *140*: 197-206.

Downloaded by COLUMBIA UNIV on August 9, 2012 | http://pubs.acs.org
Publication Date: June 9, 2006 | doi: 10.1021/bk-2006-0933.ch002

35. Cuillerdier, C.; Musikas, C.; Hoel, P.; Nigond, L.; Vitart, X. *Sep. Sci. Technol.* **1991** *26*: 1229-1244.

36. Cuillerdier, C.; Musikas, C.; Hoel, P.; Nigond, L. *Sep. Sci. Technol.* **1993** *28*: 155-175.

37. Nigond, L.; Musikas, C.; Cuillerdier, C. *Solvent Extr. Ion Exch.* **1994** *12*, 261-296.

38. Nigond, L.; Musikas, C.; Cuillerdier, C. *Solvent Extr. Ion Exch.* **1994** *12*: 297-323.

39. Sugo, Y.; Sasaki, Y.; Tachimori, S. *Radiochimica Acta* **2002** *90(3)*, 161-165.

40. Nash; K. L. **1994**. *Separation Chemistry for Lanthanides and Trivalent Actinides* in *Handbook on the Physics and Chemistry of Rare Earths, Chapter 121*. K. A. Gschneidner, Jr.; L. Eyring; G. R. Choppin and G. H. Lander. **18:** pp. 197-235.

41. Baybarz, R. D.; Weaver, B. S.; Kuiser, H. B. *Nucl. Sci. Eng.* **1963** *17*, 457-462.

42. Weaver, B.; Kappelmann, F. A. *J. Inorg. Nucl. Chem.* **1968** *30*, 263-72.

43. Musikas, C. **1985**. in *Actinide/Lanthanide Separations*. G. R. Choppin; J. D. Navaratil; W. W. Schulz (Eds.). Honolulu, HI, World Scientific, Singapore: pp. 19-30.

44. Sole, K. C.; Hiskey, J. B.; Ferguson, T. L. *Solvent Extr. Ion Exch.* **1993** *11*, 783-796.

45. Zhu, Y. *Radiochim. Acta* **1995** *68*, 95-98.

46. Zhu, Y.; Chen, J.; Jiao, R. *Solvent Extr. Ion Exch.* **1996** *14*, 61-68.

47. Chen, J.; Jiao, R.; Zhu, Y. *Radiochim. Acta* **1997** *76*, 129-130.

48. Hill, C.; Madic, C.; Baron, P.; Ozawa, M.; Tanaka, X. *J. Alloys Compd.* **1998** *271-273*: 159-162.

49. Kolarik, Z.; Mullich, U.; Gassner, F. *Solvent Extr. Ion Exch.* **1999** *17*, 1155-1170.

50. Watanabe, M.; Mirvaliev, R.; Tachimori, S.; Takeshita, K.; Nakano, Y.; Morikawa, K.; Mori, R. *Chemistry Letters* **2002** *12*, 1230-1231.

51. Willit, J. L.; Miller, W. E.; Battles, J. E. *J. Nucl. Mater.* **1992** *195*, 229-249.

52. Moser, W. S.; Navratil, J. D. **1983** *Review of Major Plutonium Pyrochemical Technology*, Rocky Flats Plant Report RFP-3686.

53. Bychkov, A. V.; Vavilov, S. K.; Porodnov, P. T.; Skiba, O. V. **1995**. *Experience on Spent Oxide Fuel Reprocessing in Molten Chlorides*. Abstracts of the Molten Salt in Nuclear Technologies Seminar, Dimitrovgrad, Russia.

54. Skiba, O. V.; Ivanov, V. B. **1995**. *State and Prospects of the Fuel Cycle Development Using Pyroelectrochemical Processes in Molten Salts.*

Downloaded by COLUMBIA UNIV on August 9, 2012 | http://pubs.acs.org
Publication Date: June 9, 2006 | doi: 10.1021/bk-2006-0933.ch002

Abstracts of the Molten Salt in Nuclear Technologies Seminar, Dimitrovgrad, Russia.

55. Choppin, G. R. **2002** in Chemical Separations in Nuclear Waste Management: The State of the Art and a Look to the Future (DOE/EM-0591, G. R. Choppin, M. K. Khankhasayev, H. S. Plendl, Eds., Battelle Press, Columbus, Ohio, pp. 49-56.
56. Rogers, R. D.; Bond, A. H.; Bauer, C. B. *Sep. Sci. Technol.* **1993** *28,* 1091.
57. Myasoedov, B. F.; Chmutova, M. K. **1995** in *Separations of f-Elements*. K. L. Nash; G. R. Choppin (Eds.). New York, Plenum Press: pp. 11-29.
58. Hurley, F. H.; Wier, T. P. J. *J. Electrochem. Soc.* **1951** *98,* 203-206.
59. Hussey, C. L. *Advances in Molten Salt Chemistry* **1983** *5,* 185-230.
60. Carpio, R. A.; King, L. A.; Lindstrom, R. E.; Nardi, J. C.; Hussey, C. L. *J. Electrochem. Soc.* **1979** *126,* 1644-1650.
61. Visser, A. E.; Holbrey, J. D.; Rogers, R. D. **2002**. in *Proceedings of the International Solvent Extraction Conference, ISEC 2002*. K. C. Sole; P. M. Cole; J. S. Preston;; D. J. Robinson (Eds.). Capetown, South Africa, South African Institute of Mining and Metallurgy, Johannesburg, Published by Chris van Rensburg Publications (Pty) Ltd: pp. 474-480.
62. Jensen, M. P.; Bond, A. H. *Radiochim. Acta* **2002** *90,* 205-209.
63. Jensen, M. P.; Neuefeind, J.; Beitz, J, V.; Skanthakumar, S.; Soderholm, L. *J. Am. Chem. Soc.* **2003** *125*, 15466-15473.
64. Visser, A. E.; Swatloski, R. P.; Reichert, W. M.; Griffin, S. T.; Rogers, R. D. *Ind. Eng. Chem. Res.* **2000** *39*, 3596-3604.
65. Visser, A. E.; Swatloski, R. P.; Rogers, R. D. *Green Chemistry* (Feb.) **2000**: 1-4.
66. Visser, A. E.; Swatloski, R. P.; Griffin, S. T.; Hartman, D. H.; Rogers, R. D. *Sep. Sci. Technol.* **2001** *36(5&6),* 785-804.
67. Visser, A. E.; Swatloski, R. P.; Reichert, W. M.; Mayton, R.: Sheff, S.; Wierzbicki, A.; Davis, J. H. J.; Rogers, R. D. *Chem. Comm.* **2001** 135-6.
68. Visser, A. E.; M. P. Jensen; I. Laszak; K. L. Nash; G. R. Choppin; R. D. Rogers. "Uranyl Coordination Environment in Hydrophobic Ionic Liquids: An In Situ Investigation." *Inorg. Chem.* **2003** *42,* 2197-2199.
69. Welton, T. *Chem. Rev.* **1999** *99,* 2071-2083.
70. Darr, J. A.; Poliakoff, M. *Chem. Revs.* **1999** *99*, 495-541.
71. Wai, C. M. **2002**. in *Supercritical Fluid Technology in Materials Science and Engineeering. Syntheses, Properties and Applications*. V.-P. Sun (Eds.). New York-Basel, Marcel Dekker, Inc.: pp. pp. 351-386.
72. Wai, C. M.; Waller, B. E. *Ind. Eng. Chem. Res.* **2000** *39*, 4837-4841.

Downloaded by COLUMBIA UNIV on August 9, 2012 | http://pubs.acs.org
Publication Date: June 9, 2006 | doi: 10.1021/bk-2006-0933.ch002

Downloaded by NORTH CAROLINA STATE UNIV on August 10, 2012 | http://pubs.acs.org
Publication Date: June 9, 2006 | doi: 10.1021/bk-2006-0933.ch003

Chapter 3

Advanced Separation Technologies for Processing Spent Nuclear Fuel and the Potential Benefits to a Geologic Repository

T. A. Todd[1] and R. A. Wigeland[2]

[1]**Idaho National Laboratory, P.O. Box 1625, MS 3860, Idaho Falls, ID 83415–3860**
[2]**Argonne National Laboratory, 9700 South Cass Avenue, Argonne, IL 60439**

The United States Department of Energy's Advanced Fuel Cycle Initiative (AFCI) is developing advanced separation technologies to process spent light water reactor fuel. The purpose of these separation processes is to remove the bulk of the mass of spent nuclear fuel (uranium) and the primary heat generating elements, which limit the amount of material that can be placed in a given amount of repository space. The thermal load to the repository is a function of both short-term heat generating elements, such as the fission products cesium and strontium, and long-term heat generating elements, such as plutonium and americium. For example, calculations of the proposed repository at Yucca Mountain indicate that 99 to 99.9 % removal of these four elements would allow a substantial increase in drift loading in the repository, as much as 50 times greater than for direct disposal of spent fuel. The current AFCI program includes investigation of strategies for the separation of uranium, for low-level waste disposal, and/or for separation and recycle of transuranic elements. Cesium and strontium would be separated for storage (approximately 200-300 years) to allow time for their decay, and would then be disposed as low-level waste. Group separation of actinides, such as neptunium, plutonium, americium and curium, and lanthanides, are also being studied, with interm storage of at least some of the actinides in the repository. These materials would be retrieved at a later date for transmutation in thermal or fast reactors.

In Separations for the Nuclear Fuel Cycle in the 21st Century; Lumetta, G., et al.;
ACS Symposium Series; American Chemical Society: Washington, DC, 2006.

Introduction

The Advanced Fuel Cycle Initiative is developing advanced separation technologies for spent nuclear fuel treatment for potential implementation in a nuclear fuel cycle in the United States (1). One of the primary goals of the program is to develop technologies to reduce the environmental impact and the cost of spent nuclear fuel disposal. Near-term benefits of chemical separations include more effective use of repository space due to the reduction of volume (and mass) as well as reduction of the thermal load from the waste (2). Subsequent transmutation of the recovered actinide elements, along with continued reprocessing, provides for the destruction of plutonium and minor actinides, resulting in reduced long-term radiotoxicity of the waste materials in the repository. Further separation of cesium and strontium would allow a substantial increase in the utilization of repository space, opening up more options for solving the issue of long-term waste disposal. Implementation of such strategies will allow the eventual transition from the current once-through use of nuclear materials to a sustainable Generation IV nuclear energy system.

The enabling technologies for reducing the volume (and mass) of the high-level waste resulting from spent fuel, as well as managing the heat generating isotopes, are chemical separation processes. These processes include both aqueous-based processes and electrometallurgical-based processes; however, the current focus of the AFCI program for processing the existing stockpile of spent light water reactor fuel is on aqueous-based technologies. Spent light water reactor fuel is approximately 95% uranium (by mass); therefore, initial separation of the uranium from the spent nuclear fuel can greatly reduce the size and complexity of subsequent processes. If the uranium separation process produces a uranium product that is non-transuranic (TRU), the uranium could likely meet low-level waste disposal criteria. The separated uranium could also be utilized in the production of new nuclear fuel, if desired. At this time, the AFCI program has successfully developed and demonstrated the Uranium Extraction (UREX) solvent extraction process, which effectively removes uranium and technetium (in separate streams) from spent nuclear fuel dissolved in nitric acid. The UREX process was specifically designed to not extract plutonium, leaving it mixed with the other actinide and fission products for proliferation resistance.

Simultaneous separation of the primary short-term heat generators, cesium and strontium (and their very short-lived decay products barium and yttrium), from the UREX raffinate, can be achieved utilizing another solvent extraction technology. Simultaneous extraction of cesium and strontium reduces overall process complexity and allows for a single product form to be produced that facilitates separate storage. The AFCI program has developed and is testing two different processes for the separation of cesium and strontium.

Downloaded by NORTH CAROLINA STATE UNIV on August 10, 2012 | http://pubs.acs.org
Publication Date: June 9, 2006 | doi: 10.1021/bk-2006-0933.ch003

Currently, the proposed initial phase of spent nuclear fuel processing in the United States includes the separation of the TRU's (Np, Pu, Am, Cm) as a single group from dissolved spent nuclear fuel, to provide enhanced proliferation resisitance. These TRU elements may also be separated in various combinations along with some or all of the lanthanides. The TRU (and lanthanide, if applicable) fraction would be stored in the repository on an interim basis, until appropriate thermal or fast reactors would be available for transmutation. Subsequent phases of a U.S. spent fuel processing program would likely include separation of plutonium and neptunium, from the other TRU elements, which can be transmuted in either a thermal or fast reactor, as well as separation of americium and curium from lanthanides, for burning in fast reactors. This paper will describe the separation technologies under development for the separation of uranium and technetium, cesium and strontium, and group TRU/lanthanide separation. The potential effects that these separation processes would have on a geologic repository is then discussed.

Downloaded by NORTH CAROLINA STATE UNIV on August 10, 2012 | http://pubs.acs.org
Publication Date: June 9, 2006 | doi: 10.1021/bk-2006-0933.ch003

Uranium/Technetium Extraction

Uranium and technetium are separated from the dissolved spent fuel solution by one of two selective solvent extraction processes, employing the well-known extractant tri-*n*-butyl phosphate (TBP), shown in Figure 1, in a normal paraffin hydrocarbon (NPH) diluent. The first process, called the Uranium Extraction (UREX) process, uses acetohydroxamic acid (AHA) to reduce plutonium in the acidic feed solution to the trivalent state, and to form inextractable complexes of plutonium and neptunium, preventing TBP from extracting them (3). Both uranium and technetium are extracted into the TBP-bearing solvent along with other minor extractible species, which are subsequently scrubbed from the solvent. Technetium is stripped from the solvent using 10 M nitric acid. The technetium strip product is then scrubbed of uranium in a uranium re-extraction section to prevent uranium from leaving with the technetium product. Uranium is subsequently stripped using 0.01 M nitric acid, and the resulting uranyl nitrite stream denitrated. Depending on the residual level of TRU elements, the solid uranium product might be disposed as low level waste. The uranium product could also be utilized in the fabrication of new nuclear fuels. Plutonium and other TRU's remain with the fission products and may be incorporated in the process waste.

The UREX process has been studied extensively for the past few years, including two flowsheet demonstration tests in small-scale centrifugal contactors using spent light water reactor fuel (4,5). Results of the demonstration tests were very promising, and indicate that the process may be a viable technology for treating spent nuclear fuel. Some areas for further development have been identified, primarily related to the extraction and stripping of technetium. Also, the feed solution to the UREX process requires low acid concentration (~0.8 M), which enhances the complexation of plutonium and neptunium, as well as increases the extraction of technetium (as pertechnetate ion). However, the low acid concentration in this feed solution may pose some challenges in the kinetics and efficiency of the spent fuel dissolution process, and potentially form polymerized zirconium complexes. Further work in this area is warranted.

The second potential process for uranium separation is referred to as the co-decontamination process, as both uranium and plutonium are simultaneously extracted from the dissolved spent nuclear fuel (6). In this process, the valence of neptunium is adjusted from (V) to (VI) using a strong oxidant, such as chromate, to enhance neptunium extraction. Uranium, technetium, plutonium and neptunium are all extracted into a TBP/NPH solvent. Most other extracted species are subsequently scrubbed from the solvent using a high-nitric acid scrub. Extracted zirconium will not scrub out of the solvent in a high-acid scrub, therefore an additional low nitric acid (~0.6 M) scrub is utilized to remove zirconium from the solvent. Plutonium and neptunium are stripped from the solvent in dilute nitric acid containing AHA. This strip product must be scrubbed with a sufficient concentration of nitric acid to re-extract any uranium or technetium in the plutonium/neptunium strip product. Following the Pu/Np strip, uranium and technetium are stripped in 0.01 M nitric acid. Technetium is removed from the uranium product by an ion exchange column.

The primary difference between the codecontamination process and the UREX process is that plutonium and neptunium are separated from the other TRU's and fission products in the codecontamination process. This separation is advantageous if the plutonium and neptunium are to be recycled for transmutation. The codecontamination process also requires a relatively high nitric acid concentration in the feed (~ 3 M), which may improve spent fuel dissolution efficiency and dissolver solution stability. A potential disadvantage of the coextraction process is that in some proposals for the initial phase of spent fuel processing, the separated plutonium and neptunium would be mixed back into the TRU and lanthanide stream for interm storage, since the presence of separated plutonium raises some concerns (real or perceived) regarding proliferation. This material would have to be separated again prior to reuse in a reactor.

The codecontamination process was successfully tested using a surrogate spent nuclear fuel feed in a hot cell facility at Oak Ridge National Laboratory and later using actual spent nuclear fuel at Argonne National Laboratory (6,7).

Cesium/Strontium Extraction

Two technologies are under development for the concurrent separation of cesium and strontium from the raffinate resulting from the UREX or

Downloaded by NORTH CAROLINA STATE UNIV on August 10, 2012 | http://pubs.acs.org
Publication Date: June 9, 2006 | doi: 10.1021/bk-2006-0933.ch003

codecontamination process. The first process utilizes chlorinated cobalt dicarbollide (CCD) and polyethylene glycol (PEG) in a phenyltrifluoromethyl sulfone diluent (8). The CCD extractant molecule is shown in Figure 2. The CCD/PEG process is most efficient when the feed is < 1 M nitric acid; therefore, it can be used directly on the UREX process raffinate or on the codecontamination process raffinate, after an acid recovery process. Cesium and strontium, along with any barium or rubidium present, are extracted into the solvent. A 3 M nitric acid scrub is used to remove any trace actinides present in the solvent. Cesium and strontium are effectively stripped using a guanidine carbonate/ diethylenetriamine pentaacetic acid strip solution. Recent results indicate that a new, regenerable strip reagent, based on methylamine carbonate would significantly reduce the amount of organics in the cesium/strontium strip product and greatly simplify subsequent solidification operations (9). The cesium and strontium strip product may be solidified in a number of ways, namely sorption onto a zeolite-type matrix, mineralization by steam reforming, calcination, etc.

This process has been demonstrated in countercurrent flowsheet tests using both simulated and actual UREX and codecontamination flowsheet raffinates. Both tests demonstrated removal efficiencies for cesium and strontium of ~99% or greater, which is more than sufficient to eliminate cesium and strontium as main contributors to the short term heat load to the repository.

The second technology for the separation of cesium and strontium is based on a combined solvent containing two extractants (shown in Figure 3), 4′,4′,(5′)-Di-(t-butyldicyclo-hexano)-18-crown-6 (DtBu18C6) and Calix[4]arene-bis-(tert-octylbenzo-crown-6) (BOBCalixC6) combined with a phase modifier- 1-(2,2,3,3-tetrafluoropropoxy)-3-(4-*sec*-butylphenoxy)-2-propanol (Cs-7SB) in a branched aliphatic hydrocarbon diluent (Isopar® L). This solvent composition was based on the Strontium Extraction (SREX) process developed at Argonne National Laboratory and the Caustic Side Solvent Extraction (CSSX) process developed at Oak Ridge National Laboratory (for alkaline waste)(10,11). A simple combination of the two solvents produced unacceptable extraction results; however, it was found that the Cs-7SB modifier used in the CSSX process had a synergistic effect on the extraction of strontium. Therefore, the modifier used in the SREX process (TBP) was not needed in the new combined solvent. Preliminary batch contact testing of this Cs/Sr extraction process has been completed and results indicate that the process is effective at selectively extracting cesium and strontium from simulated UREX raffinates and that the cesium and strontium can be stripped from the solvent using dilute nitric acid (12).

The major differences between the two cesium and strontium separation processes are: 1) the CCD/PEG process is most effective if nitric acid

Downloaded by NORTH CAROLINA STATE UNIV on August 10, 2012 | http://pubs.acs.org
Publication Date: June 9, 2006 | doi: 10.1021/bk-2006-0933.ch003

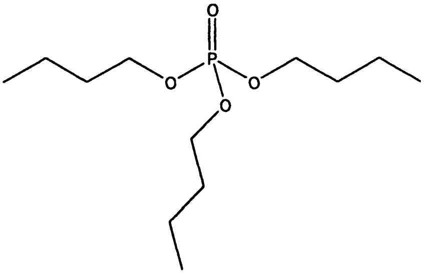

Figure 1. Tri-n-butyl phosphate

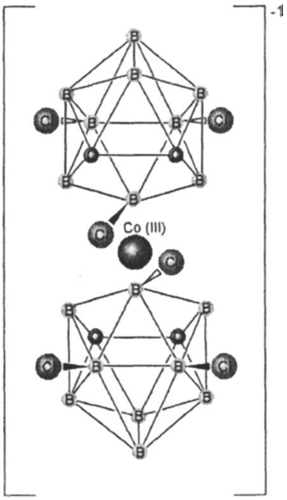

Figure 2. Hexachlorocobaltdicarbolide anion

Downloaded by NORTH CAROLINA STATE UNIV on August 10, 2012 | http://pubs.acs.org
Publication Date: June 9, 2006 | doi: 10.1021/bk-2006-0933.ch003

concentrations in the feed are less than 1 M, while the crown ether/calixarene solvent effectively extracts cesium and strontium at nitric acid concentrations between 1 and 2 M and 2) the stripping of cesium and strontium from the crown ether/calixarene solvent can be accomplished with dilute nitric acid rather than a concentrated carbonate/complexant solution, such as is required for the CCD/PEG extractant. It should be noted, however, that the development state of the CCD/PEG process is significantly more advanced than for the crown ether/calixarene solvent extraction process. No countercurrent flowsheet testing has been performed to date on the crown ether/calixarene solvent extraction process, while the CCD/PEG process has been successfully tested with UREX raffinates from simulated and actual spent nuclear fuel.

Downloaded by NORTH CAROLINA STATE UNIV on August 10, 2012 | http://pubs.acs.org
Publication Date: June 9, 2006 | doi: 10.1021/bk-2006-0933.ch003

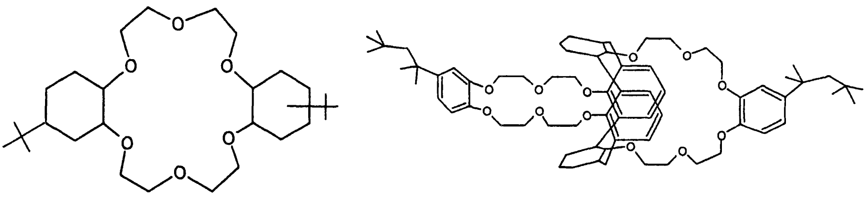

Figure 3. 4',4',(5')-Di-(t-butyldicyclo-hexano)-18-crown-6 (DtBu18C6) and Calix[4]arene-bis-(tert-octylbenzo-crown-6) (BOBCalixC6)

Group Transuranium Element Extraction

One of the goals of the AFCI program is to provide an enhanced proliferation resistant fuel cycle. In the initial phase of fuel processing, it is planned to keep the plutonium with the other TRU elements (neptunium, americium and curium) due to their self-protecting properties. Later phases of fuel processing could separate the desired TRU elements for preparation of fuel for either thermal or fast reactors. The key to realizing a benefit to the repository is to place the TRU's recovered during the initial spent fuel processing in a form that can be retrieved and processed, so that the actinides can be eventually transmuted, thereby keeping almost all of the TRU inventory out of the repository.

There are three possible approaches to the group management of the transuranics in the intial phase of fuel processing: 1) place all transuranium elements along with lanthanides and some other fission products (this is analogous to the cesium/strontium process raffinate) into a storage form for possible interim storage in the repository, 2) separate the transuranium actinides along with lanthanides from the remaining fission products for possible interim storage in the repository, 3) separate the transuranium actinides from the lanthanides and remaining fission products for possible interim storage in the repository.

The first approach is the simplest of the three options described above, and would require the least initial capital investment and technology development to implement. The raffinate from the cesium/strontium separation process would be solidified into a form that would provide adequate heat transfer properties. Ideally, this storage form would be readily dissolved in nitric acid, for future treatment to recover the TRU's for future transmutation in reactors. The separation of trivalent TRU's from lanthanides is a challenging technological problem that has been under intense study for the past several years. While much progress has been made in the development of extractants, there does not appear to be a technology currently ready for industrial-scale use. The approach of placing the TRU's and lanthanides together in interim storage would allow for a few additional decades of research and development of new separation technologies before such technology would need to be implemented.

The second approach would require an additional separation step following removal of the cesium and strontium. A process to separate transuranics and lanthanides from remaining fission products, activation products and other minor fuel components would be added. Two processes that have been extensively developed and tested are the Transuranium Extraction (TRUEX) process and the Diamide Extraction (DIAMEX) process (13,14). Both processes would produce a relatively pure TRU/lanthanide fraction and the raffinate would contain transition and noble metals. The primary difference between the processes is the composition of the extractants, with the diamide extractants following the C, H, O, N principle of containing only carbon, hydrogen, oxygen and nitrogen atoms to allow ease of incinerating spent solvent. Another extractant that exhibits high separation efficiencies for TRU's and lanthanides is N,N,N',N'-tetraoctyldiglycolamide or TODGA (15). The development of this extractant is new, but is under investigation by a number of research laboratories around the world. TODGA is soluble in n-dodecane, however had low loading capacities for Nd and had tendencies toward third phase formation. Addition of > 0.5 M N,N,-dihexyloctanamide (DHOA) to the solvent apparently resolves both issues.

The TRUEX process uses a solvent comprised of octyl (phenyl)-N,N-diisobutylcarbamoylmethylphosphine oxide (CMPO), shown in Figure 4, and tri-*n*-butyl phosphate in a paraffin hydrocarbon diluent. The TRUEX process is very effective at extracting 3, 4 and 6 valent metals from nitric acid solutions. Complexants, such as oxalic acid, can be added to reduce the extraction of transistion metals, such as zirconium and molybdenum. The TRUEX process has been successfully tested in centrifugal contactors with actual acidic radioactive waste streams at the INEEL (16).

The DIAMEX process originally utilized dimethyl-dibutyl-tetradecylmalonamide (DMDBTDMA) as the extractant in a hydrocarbon diluent. Recently, a new extractant, dimethyl-dioctyl-hexaethoxymalonamide

Downloaded by NORTH CAROLINA STATE UNIV on August 10, 2012 | http://pubs.acs.org
Publication Date: June 9, 2006 | doi: 10.1021/bk-2006-0933.ch003

(DMDOHEMA) has been developed that appears to have better extraction properties than DMDBTDMA.. Both extractant structures are shown in Figure 5. This new extractant has been tested in a countercurrent flowsheet test with actual concentrated high activity PUREX process raffinates (17). It should be noted that most development work with the DIAMEX and TRUEX processes has been performed with solutions containing little or no plutonium. It may be desirable to remove plutonium prior to the DIAMEX or TRUEX process if solvent loading becomes an issue.

Downloaded by NORTH CAROLINA STATE UNIV on August 10, 2012 | http://pubs.acs.org
Publication Date: June 9, 2006 | doi: 10.1021/bk-2006-0933.ch003

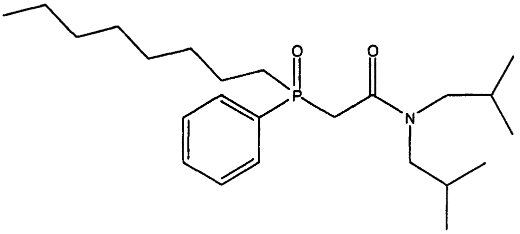

Figure 4. Octyl (phenyl)-N,N-diisobutylcarbamoylmethylphosphine oxide

The third approach would add an additional process after the TRUEX or DIAMEX process to separate trivalent actinides from lanthanides. The state of development of An/Ln partitioning technologies is less than for the other technologies described above. As stated above, most of the work done on An/Ln separation processes has focused on the separation of americium and curium from lanthanides, in the absence of plutonium. It would seem that the current state of development would necessitate the separation of plutonium, either by the codecontamination process or by another TBP-based neptunium-plutonium (NPEX) extraction process prior to the An/Ln separation process.

Trivalent actinide/lanthanide separation is difficult to accomplish due to the similarities in the chemical properties of the trivalent actinides and lanthanides. Various solvent extraction processes have been studied including: the extraction of the lanthanides from the trivalent actinides with the TALSPEAK process (18), the coextraction of the trivalent actinides and lanthanides, with selective stripping of the actinides from the lanthanides with the reverse TALSPEAK process (19), the di-isodecylphosphoric acid (DIDPA) process (20), the SETFICS process (21), the PALADIN process (22), selective actinide extraction (SANEX) processes using Cyanex 301 (23), the SANEX-III and SANEX-IV processes (24), as well as processes utilizing bis-triazinyl-1,2,4 pyridines (SANEX-BTP) (25).

Downloaded by NORTH CAROLINA STATE UNIV on August 10, 2012 | http://pubs.acs.org
Publication Date: June 9, 2006 | doi: 10.1021/bk-2006-0933.ch003

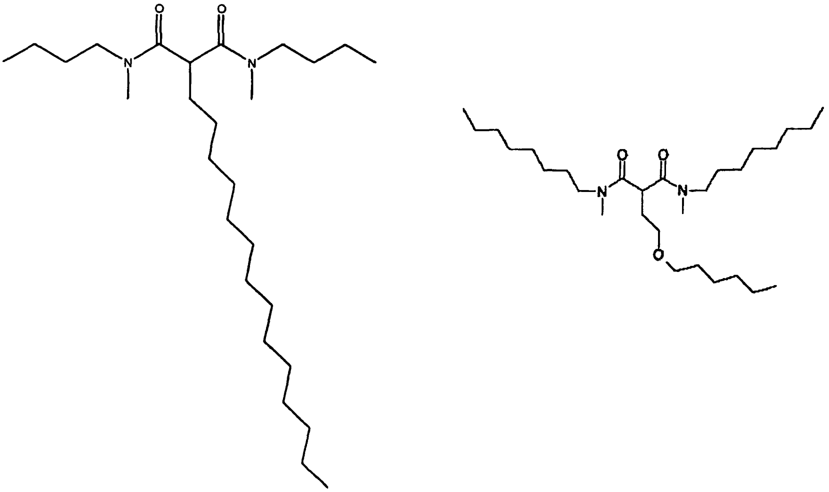

Figure 5. Dimethyl-dibutyl-tetradecylmalonamide (DMDBTDMA) and Dimethyl-dioctyl-hexaethoxymalonamide (DMDOHEMA)

Regardless of the approach, the final result would be to avoid permanent disposal of significant amounts of Pu, Np, Am and Cm in the repository, which could result in enhanced repository loading and performance.

Chemical Separations of Benefit to a Geologic Repository

In a previous study, the repository benefits of separating certain chemical elements from spent fuel and recycling them to alter the characteristics of the waste stream destined for a repository at Yucca Mountain were quantified (2). It was determined that the loading of such a repository is constrained by the decay heat generated in the emplaced materials, and that to improve the utilization of repository space, the decay heat characteristics must be modified by removing certain chemical elements from the waste. The recommended separations and the requirements are as follows:

The dominant contributors to the thermal load from the emplaced spent fuel or waste in a repository at Yucca Mountain that lead to reaching one or more of the temperature limits are plutonium and americium. Removal of these chemical elements, and recycling and transmuting them to reduce the inventory of these elements in the materials placed in the repository, is essential to increasing the repository drift loading. The measure of benefit is the amount of spent fuel (or waste therefrom) that can be placed per meter of repository drift. The benefit ranges from a factor of 5-6 in increasing the drift loading (or decreasing the repository size for a given capacity) as compared to the direct disposal of spent fuel, with waste placed in the repository at 25 years after reactor discharge. The required separation efficiency is estimated at 99 to 99.9%, with lower efficiencies reducing the benefit to repository loading, while higher efficiencies do not provide significant further increase unless many other materials are removed from the waste.

After the plutonium and americium have been removed, the next chemical elements that need to be considered are cesium and strontium, mainly for the heat produced by their short-lived decay products, barium and yttrium. Removing cesium and strontium, and sequestering them in a separate area of the repository or in another facility, would allow a substantial increase in the repository drift loading, up to a factor of 40-50 greater than the direct disposal case, for 99 to 99.9 % removal of plutonium, americium, cesium, and strontium, and when the waste is placed in the repository 25 years after reactor discharge. Further increases in separation efficiency do not result in further increases in repository loading unless other separations are performed.

The next most important chemical element is curium. In principle, with the subsequent separation of curium, loading increases of about a factor of 100 with respect to the direct disposal of spent fuel are possible. However, in considering a realistic recycling scenario for the plutonium and americium, assumed to be irradiation in a fast reactor, it was observed that the drift loading can be limited by the losses of these two elements from processing the spent fast reactor fuel. If a 1% loss is assumed in the processing of the fast reactor fuel, this reduced the potential increase in drift loading from a factor of 43 to 21, and dominated the decay heat generation. (Better separations appear to be needed for the fast reactor fuel due to the much higher actinide loading.) This emphasizes the need to reduce recycling losses of plutonium and americium below the 1% assumed in this study for the fast reactor before separation of curium will be effective.

The issue of peak dose rate can be addressed by removing and recycling the plutonium, americium, and neptunium, as these chemical elements are the dominant contributors to the peak dose rate. It should be noted that the estimated peak dose rate of 100 to 400 mrem/year is occurring at times well beyond the current 10,000 year regulatory period, about 250,000 years. Current estimates of repository performance indicate that the peak dose rate within the regulatory period is several orders of magnitude below the 15 mrem/year limit. Whether separations should be done to alter the estimated performance past the regulatory period appears to be an open question, although the potential for increased repository capacity would imply a need to evaluate the impact on the estimated peak dose rate to ensure that regulatory requirements are still satisfied.

It has been shown that removal of plutonium and americium has the potential for reducing the size of a repository at Yucca Mountain by a factor of

Downloaded by NORTH CAROLINA STATE UNIV on August 10, 2012 | http://pubs.acs.org
Publication Date: June 9, 2006 | doi: 10.1021/bk-2006-0933.ch003

5-6. Combining this with removal of cesium and strontium allows for much greater reductions in size, upwards of a factor of 40, although the use of realistic recycling options for the plutonium and americium emphasizes the need to effectively transmute these elements and to have very low losses for processing the recycled fuel, regardless of the manner in which the recycled material is treated (thermal reactor, fast reactor, etc.) To take advantage of such a potential increase in drift loading also requires the availability of waste forms that could be densely loaded with the remaining waste materials.

Examination of an alternative low temperature operating mode (LTOM) for a repository at Yucca Mountain shows that the same processing and recycling strategies would be effective for that case as well, yielding similar benefits. In summary, the study quantified benefits to a geologic repository that arise from certain spent fuel processing strategies, as would be examined as part of the AFCI program, with these benefits appearing to be relatively independent of the specific repository design decisions being considered for a repository at Yucca Mountain.

Downloaded by NORTH CAROLINA STATE UNIV on August 10, 2012 | http://pubs.acs.org
Publication Date: June 9, 2006 | doi: 10.1021/bk-2006-0933.ch003

Acknowledgements

This work was sponsored by the U.S. Department of Energy, Office of Nuclear Energy, Science and Technology under DOE Idaho Operations Office contract DE-AC07-99ID13727. The authors would like to acknowledge researchers at the INL (J. Law et al.); ANL (G. Vandegrift et al.); ORNL (E. Collins et al.); and SRNL (T. Rudisill et al.) who are actively developing many of the separation technologies described. The authors would also like to acknowledge support from Jim Laidler, AFCI National Technical Director for Separations.

References

1. Laidler, J. J.; Bresee, J. C., "The U.S. Advanced Fuel Cycle Initiative: Development of Separation Technologies," *proceedings of Advances for Nuclear Fuel Cycles (ATALANTE 2004)*, Nimes, France, June 2004.

2. Wigeland, R. A.; Bauer, T. H.; Fanning, T. H.; Morris, E. E.,"Spent Nuclear Fuels Separation and Transmutation Criteria for Benefit to a Geologic Repository," *proceedings of Waste Management '04,* Tucson, AZ, March 2004 (submitted to Nuclear Technology).

3. Swanson, J. L.; Pereira, C.; Vandegrift, G. F., "Preliminary Evaluation of Solvent Extraction and/or Ion Exchange Process for Meeting AAA Program

Multi-Tier Systems Recovery and Purification Goals," Argonne National Laboratory Report ANL-02/29, Argonne, IL, May 2002.

4. Thompson, M. C.; Norato, M. A.; Kessinger, G. F.; Pierce, R. A.; Rudisill, T. S.; Johnson, J. D., "Demonstration of the UREX Solvent Extraction Process with Dresden Reactor Fuel Solution," Westinghouse Savannah River Co. Report WSRC-TR-2002-00444, Aiken, SC, September 2002.

5. Vandegrift, G. F.; Regalbuto, M. C.; Aase, S. B.; Arafat, H. A.; Bakel, A. J.; Bowers, D. L.; Byrnes, J. P.; Clark, M. A.; Emery, J. W.; Falkenberg, J. R.; Gelis, A. V.; Hafenrichter, L. D.; Leonard, R. A.; Pereira, C.; Quigley, K. J.; Tsai, Y.; Vander Pol, M. H.; Laidler, J. J., "Lab-Scale Demonstration of the UREX+ Process," *proceedings of Waste Management '04*, Tucson, AZ, March 2004.

6. Collins, E. D.; Benker, D. E.; Spencer, B. B.; Baron, P.; Dinh, B.; Bond, W. D.; Campbell, D. O., "Development of the UREX+ Co-Decontamination Solvent Extraction Process," *proceedings of Global '2003*, New Orleans, LA, November 2003.

7. Vandegrift, G. F.; Regalbuto, M. C.; Pereira, C.; Bakel, A. J.; Aase, S. B.; Bowers, D. L.; Byrnes, J. P.; Clark, M. A.; Emery, J. W.; Falkenberg, J. R.; Hafenrichter, L. D.; Leonard, R. A.; Quigley, K. J.; Vander Pol, M. H.; Laidler, J. J., "Lab-Scale Demonstration of the UREX+2 Process using Spent Nuclear Fuel," *proceedings of Waste Management '05*, Tucson, AZ, March 2005.

8. Law, J. D.; Herbst; R. S.; Peterman, D. R.; Tillotson, R. D.; Todd, T. A. *Nuclear Technology*, **2004**, 147(2), 284-290.

9. Law, J. D.; Herbst, R. S.; Peterman, D. R.; Todd, T. A.; Romanovskiy, V. N.; Babain, V. A.; Smirnov, I. V. *Solvent Extraction and Ion Exchange*, **2005**, 23(1), 59-84.

10. Horwitz, E. P.; Dietz, M. L.; Fisher, D. E. *Solvent Extraction and Ion Exchange*, **1991**, 9(1), 1-25.

11. Bonnesen, P. V.; Delmau, L. H.; Moyer, B. A.; Leonard, R. A. *Solvent Extraction and Ion Exchange*, **2000**, 18 (6), 1079–1108.

12. Riddle, C. L.; Baker, J. D.; Law, J. D.; McGrath, C. A.; Meikrantz, D. H.; Mincher, B. J.; Peterman, D. R.; Todd, T. A. *Solvent Extraction and Ion Exchange*, **2005**, 23(3), 449-461.

Downloaded by NORTH CAROLINA STATE UNIV on August 10, 2012 | http://pubs.acs.org
Publication Date: June 9, 2006 | doi: 10.1021/bk-2006-0933.ch003

13. Horwitz, E. P.; Kalina, D. G.; Diamond, H.; Vandegrift, G. F.; Schulz, W. W. *Solvent Extraction and Ion Exchange*, **1985**, 3(1&2), 75.

14. Bisel, I.; Nicol, C.; Charbonnel, M. C.; Blanc, P.; Baron, P.; "Inactive DIAMEX Test with the Optimized Extraction Agent DMDOHEMA," *proceedings of Fifth Information Exchange Meeting on Actinide and Fission Product Partitioning and Transmutation*, Mol, Belgium, November 1998.

15. Tachimori, S.; Sasaki, Y.; and Suziki, S. *Solvent Extr. Ion Exch.*, **2002**, 20(6), 687-699.

16. Law, J. D.; Brewer, K. N.; Todd, T. A., in *Science and Technology for Disposal of Radioactive Tank Waste*, Schulz W. W.; Lombardo N. J.; Ed.; Plenum Publishing Co., NY, 1998, pp. 245-254.

17. Serrano-Purroy, D.; Baron, P.; Christiansen, B.; Madic, C.; Malmbeck, R.; Modolo, G.; Glatz, J. P.; "First Demonstration of MA Recovery from Genuine High Active Concentrate," *proceedings from the Sixth International Conference on Nuclear and Radiochemistry (NRC6),* Aachen, Germany, September 2004.

18. Weaver, B. and Kappelmann, F. A. "Talspeak: A New Method of Separating Americium and Curium from Lanthanides by Extraction from an Aqueous Solution of Aminopolyacetic Acid Complex with a Monoacidic Phosphate or Phosphonate," Oak Ridge National Laboratory Report ORNL-3559, Oak Ridge, TN, 1964.

19. Persson, G. E.; Svantesson, S.; Wingefors, S.; Liljenzin, J. O. *Solvent Extr. Ion Exch.*, **1986**, 2(89).

20. Kubota, M.; Yamaguchi, I.; Morita, Y.; Kondou, Y.; Shirahasi, K.; Yamagishi, I.; Fujiwara, T.; "Development of a Partitioning Process for the Management of High-Level Waste," *Proceedings of GLOBAL '93*, Seattle, WA, August 1993.

21. Funasaka, H.; Sano, Y.; Nomura, K.; Koma, Y.; Koyama, T. "Current Status of Research and Development on Partitioning of Long-Lived Radionuclides in JNC Japan Nuclear Cycle Development Institute," *Proceedings of ATALANTE 2000 Scientific Research on the Back-End of the Fuel Cycle for the 21st Century*, Avignon, France, October 2000.

Downloaded by NORTH CAROLINA STATE UNIV on August 10, 2012 | http://pubs.acs.org
Publication Date: June 9, 2006 | doi: 10.1021/bk-2006-0933.ch003

22. Heres, X.; Nicol, C.; Bisel, I.; Baron, P.; Ramain, L. "Paladin: A One Step Process for Actinides(III)/Fission Products Separation," *Proceedings of Global '99*, Jackson Hole, WY, August 1999.

23. Chen, J.; Zhu, Y. J.; and Jiao, R. Z. *Sep. Sci. Technol.* **1996**, 31(19), 2723.

24. Madic, C., Hudson, M. J., Liljezin, J. O., Glatz, J-P., Nannicini, R., Facchini, A., Kolarik, Z., and Odoj, R. *New Partitioning Techniques for Minor Actinides*, EUR 19149, European Commission, Luxembourg, ISBN 92-828-9696-X, 2000.

25. Madic, C., "Overview of the Hydrometallurgical and Pyro-Metallurgical Processes Studied Worldwide for the Partitioning of High Active Nuclear Wastes," *proceedings of the 6th International Exchange Meeting, "Actinides and Fission Product Partitioning and Transmutation*, Madrid, Spain, December 2000.

Downloaded by NORTH CAROLINA STATE UNIV on August 10, 2012 | http://pubs.acs.org
Publication Date: June 9, 2006 | doi: 10.1021/bk-2006-0933.ch003

Downloaded by UNIV MASSACHUSETTS AMHERST on August 9, 2012 | http://pubs.acs.org
Publication Date: June 9, 2006 | doi: 10.1021/bk-2006-0933.ch004

Chapter 4

Reprocessing Spent Nuclear Fuel with Supercritical Carbon Dioxide

Chien M. Wai

Department of Chemistry, University of Idaho, Moscow, ID 83844

Methods of dissolving uranium dioxide in supercritical fluid CO_2 are reviewed in this paper. Minimizing liquid waste generation, easy separation of solutes and tunable solvent strength are some of the advantages of the supercritical fluid extraction technology. Different approaches of utilizing this green technology for reprocessing spent nuclear fuels are summarized and an ideal dry process for the reprocessing is proposed. A current demonstration project using a CO_2-soluble tributylphosphate-nitric acid extractant for reprocessing spent nuclear fuels is described.

Introduction

Research in metal extraction utilizing supercritical fluid carbon dioxide (SF-CO_2) as a solvent started in the early 1990s (1-3). The reasons behind this technology development are mainly due to the changing environmental regulations and increasing costs for disposal of conventional liquid solvents. A difficulty encountered initially in this technology development is that metal ions are not soluble in SF-CO_2 because of the charge neutralization requirement and weak solute-solvent interactions. Carbon dioxide is a linear triatomic molecule. It has no dipole moment and is indeed a poor solvent for dissolving polar compounds and ionic species. However, when metal ions are bound to chelating agents, the resulting charge neutralized metal chelates may become soluble in SF-CO_2. Quantitative measurements of solubility of metal chelates in SF-CO_2

In Separations for the Nuclear Fuel Cycle in the 21st Century; Lumetta, G., et al.;
ACS Symposium Series; American Chemical Society: Washington, DC, 2006.

were first reported by Laintz et al. in 1991 (1). In this pioneering study, the authors showed that metal diethyldithiocarbamates exhibited limited solubilities in SF-CO_2 (~10^{-6} mol/L) under normal supercritical fluid extraction (SFE) conditions (1). An important observation noted in this report is that fluorine substitution in the chelating agent can significantly increase the solubility of the resulting metal chelates (1). For example, the solubilities of bis(trifluoroethyl)dithiocarbamate complexes with transition metals are typically two to three orders of magnitude higher than their non-fluorinated analogues. The idea of using fluorinated chelating agents for metal extraction in SF-CO_2 was inspired by the fact that perfluorinated compounds were used as blood substitutes because of their high solubilities for oxygen and carbon dioxide. The reverse is apparent true when CO_2 is used as a solvent and fluorinated compounds as solutes. Today, fluorinated compounds are considered "CO_2-philic" though the reasons are not well understood. Based on the initial solubility study, the same authors demonstrated in 1992 that Cu(II) ions spiked in liquid and solid samples could be effectively extraction into SF-CO_2 using bis(trifluoroethyl)dithiocarbamate as a chelating agent (2). Since then, a variety of chelating agents including β-diketones, organophosphorus reagents, and macrocyclic ligands have been tested for metal extraction in SF-CO_2 (3). The first of a series of U.S. patents related to the supercritical fluid-based metal extraction technology was awarded to Wai and Laintz in 1994 (4). Highly CO_2-soluble uranium complexes involving organophosphorus reagents were found later (5). Recently, direct dissolution of uranium oxides (UO_2, U_3O_8, and UO_3) and lanthanide oxides (Ln_2O_3) in supercritical CO_2 using a tri-n-butylphosphate-nitric acid complex as the extractant has been demonstrated (6-8). The *in situ* chelation-SFE technique for extracting metal ions appears attractive for nuclear waste management because it can greatly reduce the secondary waste generation compared with the conventional processes using organic solvents and aqueous solutions. Other advantages of using the SFE technology include fast extraction rate, capability of penetration into small pores of solid materials, and rapid separation of solutes by depressurization. The tunable solvation strength of SF-CO_2 also allows potential separation of metal complexes based on their difference in solubility and partition between the fluid phase and the matrix.

The nuclear industry became interested in this technology after several initial publications from the University of Idaho demonstrating effective extraction of urany and trivalent lanthanide ions using SF-CO_2 as a solvent (9-11). British Nuclear Fuels, plc. (BNFL) was the first company to explore potential uses of this technology for the nuclear industry by supporting research activities at the University of Idaho (USA), Leeds University (UK), and Khlopin Radium Institute (St. Petersburg, Russia) in 1994. The BNFL coordinator of this project, Neil Smart, spent two years at the University of Idaho conducting a series of experiments testing the possibility of using SF-CO_2 as a medium for

Downloaded by UNIV MASSACHUSETTS AMHERST on August 9, 2012 | http://pubs.acs.org
Publication Date: June 9, 2006 | doi: 10.1021/bk-2006-0933.ch004

extraction of uranium, thorium, and other metals relevant to reprocessing applications. In 1995, BNFL also signed a 2-year agreement with JAERI (Japan Atomic Energy Research Institute) with Chien Wai of University of Idaho and Tony Clifford of Leeds University as other participating members for exchange research information related to supercritical fluid technology for nuclear applications. JAERI started a SF-CO_2 extraction program around 1993 after Ken Laintz moved from Idaho to Japan for a post-doctoral appointment. The first publication from JAERI regarding SF-CO_2 extraction of lanthanides with TBP and β-diketone by Laintz and Tachikawa appeared in 1994 (12). Studies of uranyl and plutonium(IV) extraction from nitric acid solutions with TBP in SF-CO_2 were published later by Meguro, Yoshida, and others at JAERI (13,14). The possibility of using SF-CO_2 as a medium for reprocessing spent nuclear fuels was discussed by Smart et al. in 1998 (15). A demonstration of a SF-CO_2 technology for reprocessing spent nuclear fuel called Super-DIREX process was initiated in 2002 by a Japanese group involving Nagoya University, Mitsubishi Heavy Industries and Japan Nuclear Cycle Corp (16). In a period of about one decade, a simple laboratory study of SFE of metals from a scientific curiosity has led to an industrial demonstration of a supercritical fluid-based technology for reprocessing of spent nuclear fuels. The impact of this new green technology to the nuclear industry is still uncertain but the development of the technology is rapid. This article summarizes research activities in recent years regarding different approaches of using SF-CO_2 as a medium for reprocessing spent nuclear fuels.

Supercritical CO_2 Extraction of Uranium

Early reports in 1993-94 showed that lanthanide and actinide ions in solid and liquid materials can be extracted using a chelating agent such as a fluorinated β-diketone dissolved in SF-CO_2 (9-11). Among a number of commercially available fluorinated β-diketones, thenoyltrifluoroacetone (TTA) was often used because it is a solid at room temperature (m.p. 42 °C) and is easy to handle experimentally. A strong synergistic effect was observed for the extraction of uranyl and trivalent lanthanide ions when a mixture of tri-n-butylphosphate (TBP) and a fluorinated β-diketone was used as complexing agents in SF-CO_2 (10,11). TBP is highly soluble in supercritical CO_2 with solubility close to 10 % by mole under normal SFE conditions. Actually at a given temperature, TBP can be miscible with supercritical CO_2 above a certain pressure according to a recent phase diagram study of the TBP/CO_2 system (17). The synergistic extraction effect is probably due to an adduct formation with TBP replacing a coordinated water molecule in the complex leading to an enhanced solubility for the adduct complex in SF-CO_2. The solubility of uranyl-

Downloaded by UNIV MASSACHUSETTS AMHERST on August 9, 2012 | http://pubs.acs.org
Publication Date: June 9, 2006 | doi: 10.1021/bk-2006-0933.ch004

TTA-X adducts were measured later using a spectroscopic method where X included Lewis bases such as TBP, TEP (triethylphosphate), TBPO (tributylphosphine oxide), and TOPO (trioctylphosphine oxide). These organophosphorus reagents can all replace the coordinated H_2O through the electron donating P=O group forming adducts complexes with uranyl-TTA. The $UO_2(TTA)_2TBP$ was found to have the highest solubility in SF-CO_2 compared with the adducts formed by the other three organophosphorus reagents (5,18).

An important report in 1995 was the demonstration that in nitric acid solutions (1-6 M HNO_3), TBP and TBPO could extract uranyl (UO_2^{2+}) and thorium ions (Th^{4+}) effectively into SF-CO_2 (19). The extraction efficiencies for UO_2^{2+} and Th^{4+} using TBP saturated SF-CO_2 are comparable to those observed in solvent extraction with kerosene containing 19 % v/v TBP (19). The extraction of uranyl ions from a nitric acid solution with TBP in the SF-CO_2 system can be expressed by the following equation:

$$UO_2^{2+}{}_{(aq)} + 2\,NO_3^- + n\,TBP_{(sf)} \rightarrow [UO_2(NO_3)_2 \bullet nTBP]_{(sf)}$$

where the subscripts (aq) and (sf) denote the aqueous phase and the supercritical fluid phase, respectively. From a slope analysis of the distribution coefficient of uranium between the SF-CO_2 phase and the aqueous phase, the n value was estimated to be around 1.8 suggesting the extracted uranyl nitrate species was most likely of the form $UO_2(NO_3)_2 \bullet 2TBP$. This is similar to the stoichiometry of the complex observed in the conventional solvent extraction of uranyl from nitric acid solutions with TBP (20,21). It was also noted in this study that the nitric acid concentration in the aqueous phase was reduced after the SFE of uranium. Separate experiments with a nitric acid solution in contact with SF-CO_2 containing TBP revealed that HNO_3 could be extracted by the supercritical fluid phase (20,21). The changing in nitric acid concentration during the extraction probably caused deviation of the slope analysis. Nevertheless, the observation of nitric acid dissolution in SF-CO_2 in the presence of TBP is significant. It suggested that a CO_2 insoluble acid (e.g. nitric acid) could be carried into the SF-CO_2 phase by a CO_2-soluble Lewis base such as TBP for chemical reactions.

The solubilities of $(UO_2)(NO_3)_2 \cdot 2TBP$ in supercritical CO_2 in the temperature range 40 °C to 60 °C and pressure range 100 to 200 atm were measured using a spectroscopic method (5). The solubility of this important uranyl complex in SF-CO_2 reached 0.45 mol/L at 40 °C and 200 atm, a concentration comparable to that used in the conventional PUREX process. The solubility of $(UO_2)(NO_3)_2 \cdot 2TBP$ can be related to the density of the SF-CO_2 phase by the following equation:

$$\log S = k \log D + C$$

where S is the solubility in g/L, D is the density of the fluid phase (g/L), and k and C are constants (22). Figure 1 shows the linear relationship between S and D in logarithmic scale for $(UO_2)(NO_3)_2 \cdot 2TBP$. According to Figure 1, the

Downloaded by UNIV MASSACHUSETTS AMHERST on August 9, 2012 | http://pubs.acs.org
Publication Date: June 9, 2006 | doi: 10.1021/bk-2006-0933.ch004

solubility of $(UO_2)(NO_3)_2{\cdot}2TBP$ can be controlled by the density of the fluid phase. This relationship also works for the solubility of $UO_2(TTA)_2{\cdot}TBP$ in SF-CO_2. In comparison with $UO_2(NO_3)_2{\cdot}2TBP$, the solubility of $UO_2(TTA)_2{\cdot}TBP$ in supercritical CO_2 is about an order of magnitude lower (22). This information suggests that uranyl ions can be extracted by supercritical CO_2 with a mixture of TBP and a fluorinated β-diketone or with a mixture of TBP and nitric acid.

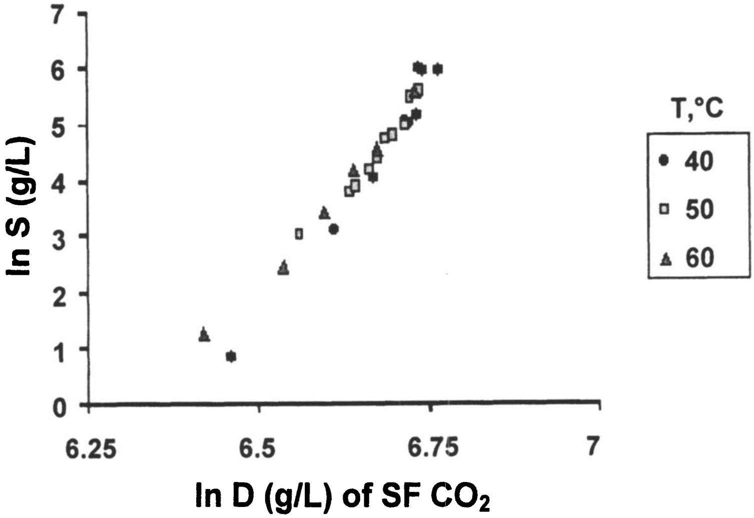

Figure 1. Plot of ln S (solubility) versus ln D (density) for $UO_2(NO_3)_2{\cdot}2TBP$ (Reproduced with permission from reference 5. Copyright 1998 Royal Society of Chemistry.)

Reprocessing Spent Nuclear Fuel in SF-CO_2

A discussion of potential applications of SF-CO_2 extraction technology for nuclear waste treatment and for reprocessing spent nuclear fuel was published in 1998 (15). Two methods were proposed in that report for reprocessing applications, a wet SF-PUREX process and a dry SF-CO_2 process for solubilizing uranium from its oxide. A possible scheme for the wet SF-PUREX process is illustrated in Figure 2. In this process, SF-CO_2 is utilized to replace the organic solvent conventionally used in the PUREX process. The advantages of the SF-PUREX process over the conventional PUREX process include high mass transport properties, faster extraction rate, and tunable distribution

Downloaded by UNIV MASSACHUSETTS AMHERST on August 9, 2012 | http://pubs.acs.org
Publication Date: June 9, 2006 | doi: 10.1021/bk-2006-0933.ch004

coefficient of SF-CO_2. Since nitric acid is required to dissolve the spent fuels, the wet SF-PUREX process would still produce acidic high level wastes like the PUREX process

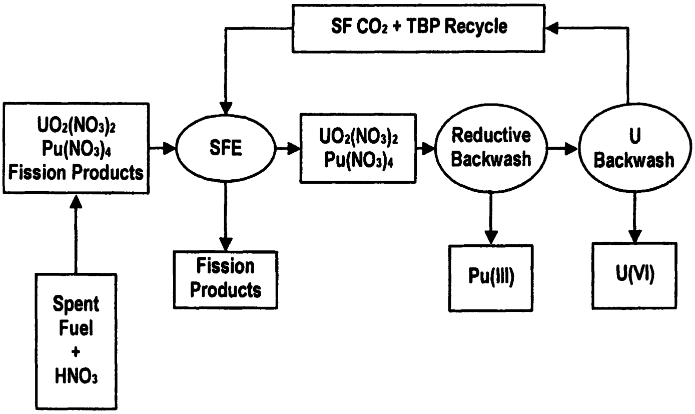

Figure 2. Schematic diagram of the wet SF-PUREX process (Reproduced with permission from reference 15. Copyright 1998 Royal Society of Chemistry.)

Downloaded by UNIV MASSACHUSETTS AMHERST on August 9, 2012 | http://pubs.acs.org
Publication Date: June 9, 2006 | doi: 10.1021/bk-2006-0933.ch004

The dry process was based on the observation that acidic ligands were able to react directly with and solubilize uranium from its oxide into an SF-CO_2 medium (23). Generation of liquid waste would be greatly reduced by a dry supercritical fluid process. In the conventional PUREX process approximately 30 liters of acidic raffainate are produced for the processing of 1 kg of uranium. Production of the acid waste in the dissolution step could be avoided in a dry supercritical dissolution process. The dissolution of UO_3 in SF-CO_2 can be expressed by the following equation:

$$UO_3\,(\text{solid}) + 2\ HL\ (\text{in SF}) + TBP\ (\text{in SF}) \rightarrow UO_2(L)_2TBP\ (\text{in SF}) + H_2O$$

The ligands mentioned in the report by Smart et al. include fluorinated β-diketones and TBP (15). Selective extraction of uranium from a range of other metal oxides likely to be present in spent nuclear fuel was also demonstrated in this report (15). For dissolution of solid UO_2, an oxidation step is necessary because uranium in the +4 oxidation state does not form stable complexes with commonly known ligands. An oxidizing agent such as H_2O_2 was found effective together with TBP and a fluorinated β-diketone for dissolution of UO_2 in SF-CO_2 (24).

Recent reports show that TBP forms a complex with nitric acid which is soluble in SF-CO_2 and is capable of dissolving uranium oxides directly (6,7). The complex can be easily prepared by mixing TBP with a concentrated nitric acid solution. Nitric acid dissolves in the TBP phase forming a Lewis acid-base complex of the general formula $TBP(HNO_3)_x(H_2O)_y$ which is separable from the remaining aqueous phase. The x and y values depend on the relative amount of TBP and nitric acid used in the preparation. The TBP-nitric acid complexes of different x and y values have been characterized by conventional titration methods as well as by proton nuclear magnetic resonance (NMR) spectroscopy (25). The NMR spectra indicate that the protons of HNO_3 and H_2O in the complex undergo rapid exchange and exhibited a single resonance peak that shifts upfield with increasing x/y ratio (25). The nature of the TBP-nitric acid complex is not well known. It probably resembles a solution of TBP-nitric acid with hydrogen bonding between the electron donating P=O group from TBP and the protons of HNO_3 and H_2O. When a TBP-nitric acid complex such as $TBP(HNO_3)_{0.7}(H_2O)_{0.7}$ is added to SF-CO_2, the fluid phase becomes cloudy suggesting formation of small acid droplets in the fluid phase. This can be attributed to an anti-solvent effect of SF-CO_2 which repels a fraction of the nitric acid in the TBP complex. Formation of small acid droplets was verified by NMR when the TBP-nitric acid complex was added to a solvent of low dielectric constant such as $CDCl_3$ (25). Dissolution of UO_2 by a TBP-nitric acid complex probably involves oxidation of the tetravalent uranium in UO_2 to the hexavalent uranyl by HNO_3 followed by formation of $UO_2(NO_3)_2{\bullet}2TBP$ which is known to have a high solubility in SF-CO_2. The dissolution reaction may be expressed by the following reaction:

$$3\ UO_2 + 8TBP{\bullet}HNO_3\ _{(sf)} \rightarrow$$
$$3\ UO_2(NO_3)_2{\bullet}2TBP\ _{(sf)} + 2\ TBP\ _{(sf)} + 2\ NO + 4\ H_2O\ _{(sf)}$$

Our experimental results also showed that after dissolution of UO_2 in a solid sample such as glass beads, sand or soil using $TBP(HNO_3)_{0.7}(H_2O)_{0.7}$, the solid matrix is dry. Small amount of water produced in the reaction shown above probably dissolves in CO_2 and is carried away by the fluid phase.

Dissolution of UO_2 by a TBP-nitric acid complex depends on the stoichiometry of the complex and the density of the supercritical fluid phase. Dissolution of UO_2 in SF-CO_2 using $TBP(HNO_3)_{1.8}(H_2O)_{0.6}$ is more rapid than $TBP(HNO_3)_{0.7}(H_2O)_{0.7}$ because of a higher nitric acid concentration provided by the former. The alkali metals, the alkaline earth metals, and a number of transition metals can not be extracted by the TBP-nitric acid complex in supercritical CO_2. Sonication can significantly enhance the dissolution rate of tightly packed UO_2 powders probably by increasing the transport of $UO_2(NO_3)_2(TBP)_2$ from the solid surface to the supercritical fluid phase (26).

In recent scientific meetings, this author has described an ideal dry process for reprocessing spent nuclear fuel using SF-CO_2 as a medium. A conceptual illustration of the dry SF-CO_2 reprocessing process is given in Figure 3. UO_2 and transuranic elements in spent fuel are dissolved in SF-CO_2 with a TBP-nitric acid complex leaving fission products including Cs and Sr behind. Stripping uranium from the supercritical fluid phase and regeneration of the ligand are important steps to make this process effective and environmentally sustainable.

Downloaded by UNIV MASSACHUSETTS AMHERST on August 9, 2012 | http://pubs.acs.org
Publication Date: June 9, 2006 | doi: 10.1021/bk-2006-0933.ch004

If the whole process shown in Figure 3 could be done in a pressurized CO_2 system, it would also be economically favorable.

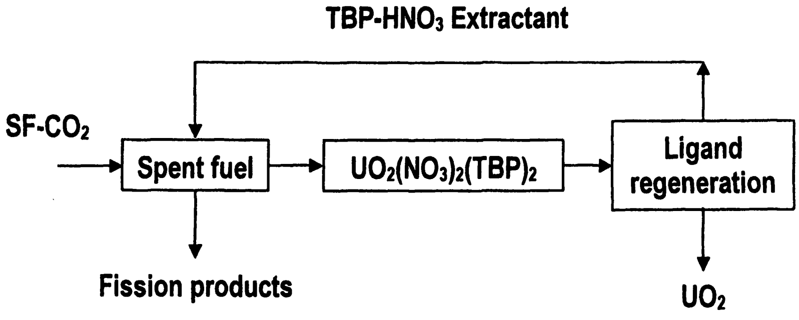

Figure 3. A conceptual illustration of a dry process for reprocessing spent nuclear fuel in SF-CO_2

Current Demonstration and Future Directions

A demonstration project testing dissolution of UO_2 directly from spent nuclear fuels for reprocessing in supercritical CO_2 called Super-DIREX process is currently being studied by a team in Japan. The Japanese demonstration project (2002-2005) involves Mitsubishi Heavy Industries, Japan Nuclear Cycle Corp., and Nagoya University with Professor Youichi Enokida of Nagoya University as the coordinator. The project is aimed at extracting uranium and plutonium from the mixed oxide fuel as well as the irradiated nuclear fuel using the $TBP(HNO_3)_{1.8}(H_2O)_{0.6}$ complex as an extractant in supercritical CO_2. A schematic diagram of the Super-DIREX process is shown in Figure 4. Fuel dissolution occurs via the formation of SF-CO_2 soluble uranyl nitrate and plutonium nitrate complexes with TBP as described in the previous section. TRU's are also expected to dissolve in the SF-CO_2 phase. Fission products remain as unreacted solids. Stripping of Uranium and plutonium from the supercritical fluid stream is accomplished by water following the conventional PUREX process. Stripping of uranium by water can be achieved at low nitrate concentration, e.g. 0.1 M nitric acid. Because the concentration of HNO_3 in the extractant $TBP(HNO_3)_{1.8}(H_2O)_{0.6}$ is very high, handling a large volume of aqueous stripping solution for uranium and plutonium recovery may still create an environmental problem for the Super-DIREX process. Nevertheless, this project should provide valuable information regarding dissolution of real nuclear

Downloaded by UNIV MASSACHUSETTS AMHERST on August 9, 2012 | http://pubs.acs.org
Publication Date: June 9, 2006 | doi: 10.1021/bk-2006-0933.ch004

fuels and safe handling of highly radioactive materials in a high-pressure supercritical fluid extraction system.

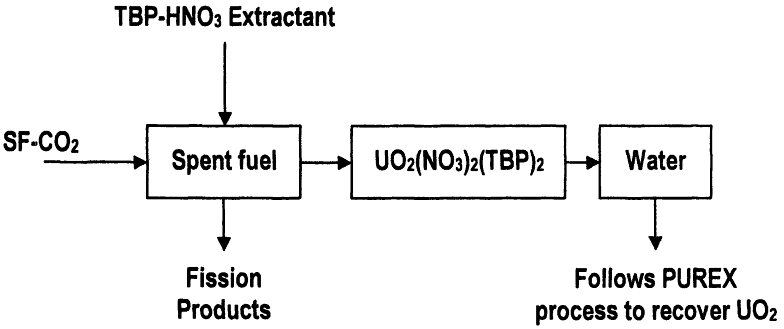

Figure 4. A conceptual illustration of the SUPER-DIREX process

New ideas are needed for recovery of uranium and for regeneration of TBP in SF-CO_2 solutions. Chemical reduction of transition metal β-diketonates to their metallic state in SF-CO_2 has been reported in recent years (27). For example, reduction of Cu-hexafluoroacetylacetone by hydrogen in SF-CO_2 can occur at low temperature using palladium as a catalyst (28). Converting uranyl salt to UO_2 with hydrogen is also possible at a relative high temperature using platinum as a catalyst. If $UO_2(NO_3)_2(TBP)_2$ could be converted to UO_2 in SF-CO_2 with regeneration of TBP, then the dry reprocessing process shown in Figure 3 would probably be economically more favorable and environmentally more acceptable. Research along this direction is currently in progress in our laboratory.

Acknowledgement

This work was partially supported by the DOE Office of Environmental Management, EMSP Program (grant number DE-FG07-98ER14913) and by a grant from Argonne National Lab (Argonne West). The author would like to thank Professor Youichi Enkoda of Nagoya University and Dr. Karen Howden and Mike Simpson of Argonne National Lab for valuable discussion.

Downloaded by UNIV MASSACHUSETTS AMHERST on August 9, 2012 | http://pubs.acs.org
Publication Date: June 9, 2006 | doi: 10.1021/bk-2006-0933.ch004

References

1. Laintz, K.E.; Wai, C.M.; Yonker, C.R.; Smith, R.D., *J. Supercrit. Fluids*, **1991**, 4, 194-198.
2 Laintz, K.E.; Wai, C.M.; Yonker, C.R.; Smith, R.D., *Anal. Chem.* **1992**, 64,2875-2878.
3. Wai, C.M.; Wang, S., *J. Chromatography A*, **1997**, 785, 369-383.
4. Wai, C.M.; Laintz, K.E., Supercritical Fluid Extraction, U.S. Patent No. 5,356,538, **1994**.
5. Carrott, M.J.; Waller, B.E.; Smart, N.G.; Wai, C.M. Chem. Commun. **1998**, 373-374.
6. Tomioka, O.; Meguro, Y.; Iso, S.; Youshida, Z.; Enokida, Y.; Yamamoto, I., *J. Nucl. Sci. Technol.* **2001**, 38, 1097.
7. Samsonov, M.D.; Wai, C.M.; Lee, S.C.; Kulyako, Y.; Smart, N.G., *Chem. Commun.* **2001**, 1868-1869.
8. Tomioka, O.; Enokida, Y.; Yamamoto, I. *J. Nucl. Sci. Technol.* **1998**, *35*, 513-514.
9. Lin, Y.; Brauer, R.D.; Lainta, K.E.; Wai, C.M., Anal. Chem. **1993**, *65*, 2549-2552.
10. Lin, Y.; Wai, C.M., *Anal. Chem.* **1994**, *66*, 1971-1975.
11. Lin, Y.; Wai, C.M.; Jean, F.M.; Brauer, R.D., *Environ. Sci. Technol.* **1994**, 28, 1190-1193.
12. Laintz, K.E.; Tichikawa, E., *Anal. Chem.* **1994**, *66*, 2190-2193.
13. Meguro, Y.; Iso, S.; Yoshida, Z., *Anal. Chem.* **1998**, *70*, 1262-1267.
14. Iso, S.; Uno, S.; Megur, Y.; Sasaki, T.; Yoshida, Z. *Progress in Nuclear Energy*, **2000**, *37*, 423-428.
15. Smart, N.G.; Wai, C.M.; Phelps, C., *Chem. Britain*, **1998**, 34, 34-36.
16. Enokida, Y.; Yamamoto, I.; Wai, C.M., **2003**, *in Supercritical Carbon Dioxide-Separations and Processes, ACS Symposium Series 860*, eds. Gopalan, A.S.; Wai, C.M.; Jacob, H.K., ACS, Washington D.C.,Chapter 2, p.10-22.
17. Joung, S.N.; Kim, S.J.; Yoo, K.P., *J. Chem. Eng. Data* **1999**, 44, 1034-1036.
18. Wai, C.M.; Waller, B., *Ind. Eng. Chem. Res.* **2000**, 39, 3837-3841.
19. Lin, Y.; Smart, N.G.; Wai, C.M., *Environ. Sci. Technol.* **1995**, 29, 2706-2708.
20. Lin, Y.; Supercritical Fluid Extraction and Chromatography of Metal Chelates and Organic Metallic Compounds, Ph.D. Dissertation, Department of Chemistry, University of Idaho, Moscow, Idaho, May 1997.
21. Wai, C.M.; Lin, Y.; Ji, M.; Toews, T.; Smart, N.G., **1999**, *in Metal Ion Separation and Preconcentration, ACS Symposium Series 716*, eds. Bond,

Downloaded by UNIV MASSACHUSETTS AMHERST on August 9, 2012 | http://pubs.acs.org
Publication Date: June 9, 2006 | doi: 10.1021/bk-2006-0933.ch004

A.H.; Dietz, M.L.; Roger, R.D., ACS, Washington, DC, Chapter 23, p. 390-400.

22. Wai, C.M., Supercritical Fluid Extraction Technology for Nuclear Waste Management, Chapter 5.1 in *Hazardous and Radioactive Waste Treatment Technologies Handbook*, Ed. C.H. Oh, CRC Press, Boca Raton, Florida, **2001**, p. 5.1.3-20.
23. Wai, C.M.; Smart, N.G.; Phelps, C., Extraction Meals Directly From Metal Oxides, U.S. Patent No. 5,606,724 , **1997**.
24. Trofimov, T.I.; Samsonov, M.D.; Lee, S.C.; Smart, N.G.; Wai, C.M., *J. Chem. Technol. Biotechnol.* **2001**, *76*, 1223-1226.
25. Enokida, Y.; Tomioka, O.; Lee, S.C.; Rustenholtz, A.; Wai, C.M., *Ind. Eng. Chem. Res.* **2003**, 42, 5037-5041.
26. Enokida, Y.; Sami, A.E., Wai, C.M., *Ind. Eng. Chem. Res.* **2002**, 41, 2282-2286.
27. Blackburn, J.M.; Long, D.P.; Cabanas, A.; Watkins, J.J. ***Science*** **2001**, *294*, 141-143.
28. Wai, C.M.; Ohde, H.; Kramer, S., U.S. Patent No. 6,653,236, **2003**.

Downloaded by UNIV MASSACHUSETTS AMHERST on August 9, 2012 | http://pubs.acs.org
Publication Date: June 9, 2006 | doi: 10.1021/bk-2006-0933.ch004

Downloaded by COLUMBIA UNIV on August 10, 2012 | http://pubs.acs.org
Publication Date: June 9, 2006 | doi: 10.1021/bk-2006-0933.ch005

Chapter 5

Dissolution of Irradiated Nuclear Fuel from the Big Rock Point Reactor

**Allen J. Bakel, Delbert L. Bowers, Kevin J. Quigley,
Monica C. Regalbuto, John A. Stillman, and George F. Vandegrift**

**Argonne National Laboratory, 9700 South Cass Avenue,
Argonne, IL 60439**

Summary

The Advanced Fuel Cycle Initiative (AFCI), funded by the Department of Energy, is developing proliferation-resistant technologies that allow safe and economical disposal of waste from reactors. A critical element is the separation of key radionuclides followed by either waste disposal, or conversion of long-lived isotopes to reactor fuel. A sample of Big Rock Point uranium oxide fuel was dissolved in nitric acid at elevated temperature to provide feedstock for the UREX+ demonstration. Elevated temperature led to the complete dissolution of noble metals at relatively low nitric acid concentrations. The conditions used in this study are not suitable for plant-scale application. Three products were obtained: (1) a dissolved fuel solution, (2) undissolved residue, and (3) leached cladding containing no observable undissolved fuel. Elemental analyses of the dissolved fuel, residue, and leached cladding are presented. The data show that 99% of the fuel, including the noble metals was dissolved. The small amount of residue contained primarily Zr, Mo, and Pu. While the total amount of residue is small, approximately 20% of the total Pu was found in the residue. Several proposals are made for the prevention of precipitation of the residue.

In Separations for the Nuclear Fuel Cycle in the 21st Century; Lumetta, G., et al.;
ACS Symposium Series; American Chemical Society: Washington, DC, 2006.

Downloaded by COLUMBIA UNIV on August 10, 2012 | http://pubs.acs.org
Publication Date: June 9, 2006 | doi: 10.1021/bk-2006-0933.ch005

Introduction

The Advanced Fuel Cycle Initiative (AFCI), funded by the Department of Energy's Office of Nuclear Energy, is developing advanced proliferation-resistant technologies that allow the safe and economical disposal of waste from nuclear reactors. A critical element of this initiative is the separation of key radionuclides followed by either superior waste disposal forms, or conversion of long-lived isotopes to reactor fuel. To that end, the AFCI is developing advanced fuel reprocessing systems that separate key radionuclides from spent fuel.

The UREX+ process is a series of five solvent-extraction process steps that separates irradiated nuclear fuel into seven product and waste streams: (1) U_3O_8 for recycle or disposal as LLW, (2) Np/Pu for mixed oxide fuel for thermal reactors, (3) Tc for disposal, (4) I for disposal, (5) Am/Cm for fast-reactor fuel, (6) Cs/Sr for decay storage, and (7) mixed short-lived fission products for repository disposal. The overall process was designed for $\geq$ 99% recovery of fission products and $\geq$ 99.99% of actinides. Decontamination factors are 10^3-10^8 as required by process goals. The complete UREX+ solvent extraction process was demonstrated in the Chemical Engineering Division (CMT) of Argonne National Laboratory (ANL) in FY 03.

The purpose of this work was to completely dissolve a pin of irradiated Big Rock Point uranium oxide fuel to provide high quality feedstock to the UREX+ demonstration done at ANL. In particular, we will monitor the dissolution of the noble metals, which are known to be problematic in fuel dissolution, and uranium, which makes up the bulk of the fuel. Any solids collected at the end of the dissolution will be characterized to determine their origin and effect on the dissolution product.

Experimental

Dissolver Equipment. Dissolution of irradiated fuel has previously been done in open vessels with HNO_3 and HF [1]. The presence of fluoride ion is undesirable for the proposed UREX+ process because Pu (IV) fluoride complexes are much stronger than other Pu (IV) complexes [2], and extract poorly with TBP [3]. Therefore, we dissolved irradiated nuclear fuel in pure nitric acid at an elevated temperature.

A stainless steel (304L) pressure vessel was designed and fabricated. The following criteria were to be met: 1) about 2.5 L in volume, 2) safe operation above 1000 psi, 3) resistance to nitric acid and 4) convenient operation inside a shielded cell facility. A photograph of the cylindrical vessel is shown in Figure 1. A mesh basket was used to hold the cladding/fuel pieces. The dissolver was equipped with a liquid inlet line, a gas vent valve, a pressure gauge, a pressure relief valve set at <1200 psi, and two thermocouples, one to be placed in the liquid phase and one in the vapor phase.

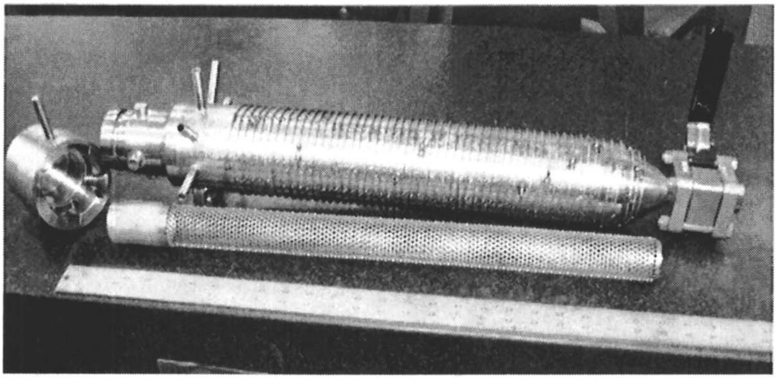

Figure 1. Photograph of the dissolver vessel before installation in the shielded cell.

Downloaded by COLUMBIA UNIV on August 10, 2012 | http://pubs.acs.org
Publication Date: June 9, 2006 | doi: 10.1021/bk-2006-0933.ch005

Process tests With Sintered UO_2. Previous work in our group [4] had shown that dissolution of UO_2 in HNO_3 in a closed dissolver proceeds by the following reaction:

$$UO_2 + 8/3HNO_3 \rightarrow UO_2(NO_3)_2 + 2/3NO + 4/3H_2O.$$

Scoping tests were done with pressed and sintered depleted UO_2 pellets to test the dissolver, to determine the dissolution behavior of the UO_2, and to measure the corrosion behavior of the vessel as a function of temperature. Because irradiated fuel has a different microstructure, different surface morphology and different composition than sintered UO_2, the results of these tests were not quantitatively applied to irradiated nuclear fuel. However, the observed temperature dependence of the dissolution and corrosion rate was used to determine the operational limits of the system.

A series of small scale dissolutions of depleted UO_2 pellets was carried out in 5.84 M HNO_3 at 125, 150, 175°C for 2 hours. Each solution was analyzed for U and H^+ concentrations, and the results are shown in Table 1. The U concentrations were measured by ICP/AES, and were all within 6% of the target. The H^+ concentrations were measured by titrations, and were all within 16% of the target. Data from the scoping tests (Table 1) confirmed that the observed residual pressure of generated gas is equal to or lower than predicted pressure calculated from the suggested chemical reaction and the ideal gas law. A portion of the generated gas might dissolve in the liquid at experimental temperature and pressure. These results suggest that the dissolution of UO_2 in nitric acid can be accurately represented by the reaction suggested [4].

Table 1. Results from dissolution tests

Test temperature (°C)	*U concentration (gU/L)*	*Total acidity (M)*	*Residual pressure observed, psi*	*Residual pressure expected, psi*
125	441	0.67	110	110
150	422	0.79	120	150
175	413	0.78	160	220

The extent of corrosion of the vessel during the dissolution tests was also investigated as a function of temperature. The corrosion of stainless steel is known to be temperature-dependant [5] therefore; the corrosion rate represented a limit on the operating temperature. Concentrations of Fe, Cr, and Ni were measured in the final solutions, and were used as qualitative measures of corrosion rates. The results in Table 2 show that the corrosion rate is significantly higher at 175°C, than at 150°C. Based on this data, the dissolutions were carried out at temperatures below 175°C.

Table 2. Metal concentrations measured in dissolver solutions from tests conducted at different temperatures

Temperature, °C	*Cr, μg/mL*	*Ni, g/mL*	*Fe, μg/mL*
125	13.4	10.0	182
150	22.5	12.1	126
175	104	59.0	446

Irradiated Fuel Dissolution. The first task in the dissolution was to choose the fuel/cladding sections to go into the first dissolution batch (Figure 2). Our initial examination of the sections suggested that about half of the sections were intact, i.e., no fuel had fallen out during the cutting, shipping and unpacking operations. A basket (Figure 1) was placed into the dissolver and 23 weighed fuel/cladding pieces were placed into the basket. The dissolver was sealed, the vent valve was closed, about 800 mL of the acid was pumped into the dissolver, and the heater was switched on.

After 8 hours at temperature, the dissolver was cooled overnight. The residual pressure, i.e., the pressure from generated gases, was 180 psi at room temperature. The brown residual gas was vented through a base scrubber. The dissolved fuel solution was then drained from the vessel and weighed. The vessel, basket and cladding pieces were rinsed three times with about 100 mL of dilute HNO_3. Solids were collected during the first two rinses; during the third rinse, no solid material was observed.

Downloaded by COLUMBIA UNIV on August 10, 2012 | http://pubs.acs.org
Publication Date: June 9, 2006 | doi: 10.1021/bk-2006-0933.ch005

Downloaded by COLUMBIA UNIV on August 10, 2012 | http://pubs.acs.org
Publication Date: June 9, 2006 | doi: 10.1021/bk-2006-0933.ch005

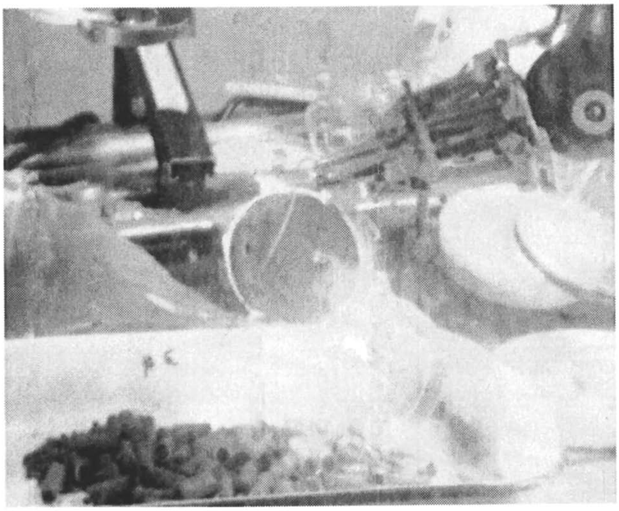

Figure 2. Photograph of fuel/cladding segments being poured from the shipping container into a pan for examination.

The leached cladding removed from the basket contained no visible undissolved fuel (Figure 3). The leached cladding hulls weighed 116.4 g, while the fuel/cladding sections added at the beginning of the first dissolution weighed 492.7 g. Therefore, 376.3 g of material, assumed to be fuel was dissolved. If we assume that 84% of the fuel is U, then 316.1 g of U were dissolved during the first batch dissolution. Two more batches were dissolved. The details of each batch and the calculated totals are shown in Table 3.

Table 3. Summary of masses of material dissolved and the products

	Dissolution 1	*Dissolution 2*	*Dissolution 3*	*Total*
Mass of Fuel/cladding (measured)	492.7 g	434.6 g	514.6 g	1442 g
Mass of Hulls (measured)	116.4 g	59.7 g	141.2 g	317.3 g
Mass of Fuel (by difference)	376.3 g	375.3 g	373.4 g	1125 g
*Mass of U (fuel *0.84)*	316.1 g	315.3 g	313.7 g	945.1 g
Mass of fuel solution (measured)	1279 g	1330 g	1229 g	3838 g
Volume of dissolved fuel solution	836 mL	869 mL	803 mL	2510 mL

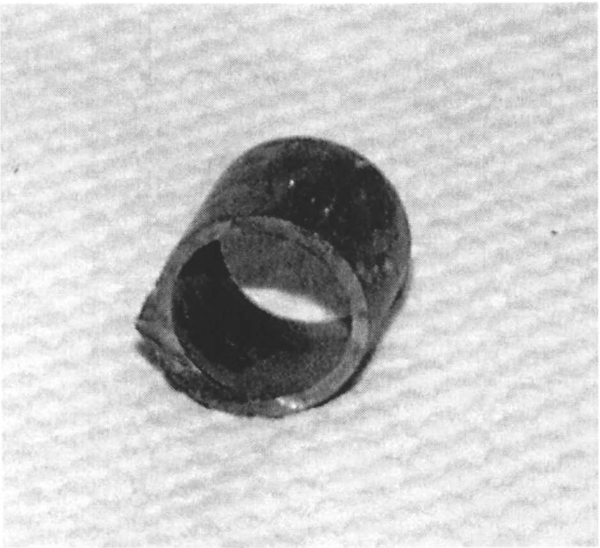

Figure 3. Photograph of a representative piece of cladding after fuel dissolution.

Downloaded by COLUMBIA UNIV on August 10, 2012 | http://pubs.acs.org
Publication Date: June 9, 2006 | doi: 10.1021/bk-2006-0933.ch005

Based on the data compiled in Table 3, we dissolved 1124.6 g of fuel (assuming that all of the mass lost during dissolution was fuel) and 945.1 g of U. The total mass of dissolved fuel solution was measured as 3838.3 g, and the density was determined to be 1.53 g/mL. This gives a total volume of 2.51 L of solution. This yields an estimated U concentration of about 377 g U/L.

The dissolved fuel was vacuum filtered using a Büchner funnel with a 90 mm Whatman 42 filter paper. A significant amount of solid material was removed from the solution during filtration. The filtered solution was used as the feedstock for the UREX+ demonstration. The solid removed was analyzed and results will be described later in this paper.

Results And Discussion

Estimation of fuel composition. As part of the UREX+ demonstration, process flowsheets were designed and modeled using the Argonne Model for Universal Solvent Extraction (AMUSE) code [6]. Accurate modeling results can be obtained only if the chemical composition of the feed, dissolved fuel in this case, is well known. The composition of the irradiated fuel from Big Rock Point reactor had not been determined analytically, so we estimated the dissolved fuel composition using the ORIGEN2 code. Input for the code includes burnup (30,100 MWd/MT), enrichment (4.6% ^{235}U), burnable poison content (1.2 %

Gd_2O_3), and cooling time (21 years) [7]. Additional input was derived from the known, or assumed operating parameters of the Big Rock Point boiling water reactor [8, 9].

The ORIGEN2 code [10] utilizes highly detailed nuclide depletion chains, tracking over 200 actinides and over 800 individual fission product isotopes. The code uses a point depletion model and pre-evaluated libraries of one-group neutron cross section data and decay parameters. Cross section libraries which have been evaluated for several reactor systems with their characteristic neutron spectra are available; specifically, a library for a UO_2-fueled BWR is available. Results generated by ORIGEN2 with these "generic" cross section libraries must be carefully considered. Recent comparisons of pressurized water reactor (PWR) spent fuel actinide concentrations generated by ORIGEN2 and the WIMS8 lattice code [11] exhibited differences of several percent for some of the higher mass actinides (isotopes of Pu, Am, and Cm). The higher mass actinides such as Pu-241, Am-241, and Cm-244 are important in spent fuel processing due to their contribution to decay heat and dose. WIMS8 utilizes a multi-group cross section library (172 groups) and two-dimensional spatial modeling to predict the nuclide reaction rates for the particular system under analysis. The code has built-in depletion chains that track the concentrations of 20 actinides, from U-233 to Cm-245. The code also tracks around 100 individual fission products that are important from a neutronics point of view. WIMS8 has been used extensively for PWR spent fuel characterization in the AFCI program. A WIMS8 model of a BWR fuel pin lattice was developed. The model was first benchmarked against spent fuel results reported by ORNL and other external references. The model was expanded to include heterogeneous fuel pin loadings, which are typical in BWR assemblies.

The elemental composition of the fuel was calculated using the procedure described above, and is shown in Table 4. The estimated composition was used to design a preliminary flowsheet for the UREX+ process for the demonstration.

Composition of the Dissolver Solution. Aliquots of the filtered dissolved fuel solution were analyzed using inductively-coupled plasma mass spectrometry (ICP-MS) and thermal ionization mass spectrometry (TIMS). The ICP-MS method separates complex mixtures of metal ion on the basis of their atomic mass. The TIMS method allows for the precise and accurate determination of isotope ratios and concentrations of U and Pu.

The concentration of metals measured by ICP-MS at any given atomic mass includes the concentrations of all of the isotopes of that mass. For example, the concentration of m/z = 241 (^{241}Pu + ^{241}Am) in the solution was measured as 0.336 parts per million (mg/L). Plutonium has several isotopes, including one with molecular weight of 240; no other isotope expected in the fuel occurs at this mass. Therefore, the m/z=240 data from ICP-MS represents only plutonium with no interference from other elements. The ratio of ^{240}Pu to ^{241}Pu was known from TIMS data. Therefore, the concentration of ^{241}Pu in the dissolved fuel can be

Downloaded by COLUMBIA UNIV on August 10, 2012 | http://pubs.acs.org
Publication Date: June 9, 2006 | doi: 10.1021/bk-2006-0933.ch005

Downloaded by COLUMBIA UNIV on August 10, 2012 | http://pubs.acs.org
Publication Date: June 9, 2006 | doi: 10.1021/bk-2006-0933.ch005

Table 4. Estimated elemental composition of an irradiated fuel rod from the Big Rock Point reactor calculated using the ORIGEN2 code.

Element	*g/MTHM in fuel*[1]	*g/906-g U*[2]	*g/L*[3]
Rb	3.45E+02	3.26E-01	1.30E-01
Sr	6.49E+02	6.12E-01	2.44E-01
Y	4.43E+02	4.17E-01	1.66E-01
Zr	3.49E+03	3.29E+00	1.31E+00
Mo	3.00E+03	2.83E+00	1.13E+00
Tc	6.97E+02	6.57E-01	2.62E-01
Ru	1.87E+03	1.76E+00	7.01E-01
Rh	3.85E+02	3.63E-01	1.45E-01
Pd	9.83E+02	9.27E-01	3.69E-01
Ag	5.50E+01	5.19E-02	2.07E-02
Cd	7.78E+01	7.34E-02	2.92E-02
Sn	7.90E+01	7.45E-02	2.97E-02
Sb	1.68E+01	1.58E-02	6.29E-03
Te	4.19E+02	3.95E-01	1.57E-01
Cs	1.99E+03	1.88E+00	7.49E-01
Ba	2.07E+03	1.95E+00	7.77E-01
La	1.10E+03	1.04E+00	4.14E-01
Ce	2.13E+03	2.01E+00	8.01E-01
Nd	3.67E+03	3.46E+00	1.38E+00
Sm	7.91E+02	7.46E-01	2.97E-01
Eu	9.81E+01	9.25E-02	3.69E-02
Gd	9.18E+03	8.65E+00	3.45E+00
U	9.60E+05	9.05E+02	3.61E+02
Np	3.65E+02	3.44E-01	1.37E-01
Pu	8.74E+03	8.24E+00	3.28E+00
Am	8.17E+02	7.70E-01	3.07E-01

[1] –grams of the indicated element per metric ton of fuel (on a heavy metal basis)

[2] –grams of the indicated element per the total amount of uranium dissolved (906 g).

[3] - These values are calculated assuming a final solution volume of 2.51 L

calculated using the total m/z=241 concentration from ICP-MS data and the ^{240}Pu to ^{241}Pu ratio from TIMS data. Such calculations were carried out at each m/z value. The total concentration of any element was calculated by the sum of the concentrations of all of its isotopes. For example, the total Pu concentration was calculated by summing the concentrations of ^{238}Pu, ^{239}Pu, ^{240}Pu, ^{241}Pu, and ^{242}Pu. The totals for the concentrations of each element present in the dissolved fuel are shown in Table 5.

Table 5. Elemental concentrations of dissolved fuel using ICP/MS and TIMS data, and the ORIGEN calculations.

Element	Measured concentrations, g/L	ORIGEN prediction, g/L
Rb	1.10E-01	1.30E-01
Sr	2.59E-01	2.44E-01
Y	1.47E-01	1.66E-01
Zr[2,3]	2.14E-01	1.31E+00
Mo[2]	1.63E-01	1.13E+00
Tc	2.55E-01	2.62E-01
Ru	7.75E-01	7.01E-01
Rh	1.70E-01	1.45E-01
Pd[2]	6.60E-02	3.69E-01
Ag[2]	7.11E-04	2.07E-02
Cd[3]	5.01E-02	2.92E-02
Sn[3]	6.19E-02	2.97E-02
Sb[3]	5.14E-01	6.29E-03
Te[2]	5.64E-02	1.57E-01
Cs	6.26E-01	7.49E-01
Ba[1]	1.36E+00	7.77E-01
La	3.88E-01	4.14E-01
Ce	6.70E-01	8.01E-01
Nd	1.39E+00	1.38E+00
Sm	2.69E-01	2.97E-01
Eu	3.59E-02	3.69E-02
Gd	2.64E+00	3.45E+00
U	3.61E+02	3.61E+02
Np	1.68E-01	1.37E-01
Pu[2]	2.68E+00	3.28E+00
Am	3.08E-01	3.07E-01

[1] - This value might include Xe that interferes at masses 134 and 135.

[2] – These elements are present in the residue.

[3] – These elements are present in the cladding

Downloaded by COLUMBIA UNIV on August 10, 2012 | http://pubs.acs.org
Publication Date: June 9, 2006 | doi: 10.1021/bk-2006-0933.ch005

In Separations for the Nuclear Fuel Cycle in the 21st Century; Lumetta, G., et al.;
ACS Symposium Series; American Chemical Society: Washington, DC, 2006.

Such calculations can only be made if accurate isotopic data are available. Results from TIMS analyses are ideal for this purpose. If the TIMS data were not available, the needed isotope ratios could be obtained from ORIGEN code results. Only U and Pu were analyzed by TIMS, isotope ratios for other elements were obtained from ORIGEN calculations. Table 5 compares the results of TIMS and the predictions from ORIGEN for individual isotopes of U and Pu. These results suggest that if TIMS data were not available, then ORIGEN results could also be used.

Data in Table 6 allows comparison of the measured elemental concentrations of the dissolved fuel and the concentrations predicted by the ORIGEN code calculations (Table 4). The agreement is good in most cases. This good agreement shows that the dissolution was successful. In particular, the results for the noble metals Ru and Rh show that the fuel dissolution was effective.

Downloaded by COLUMBIA UNIV on August 10, 2012 | http://pubs.acs.org
Publication Date: June 9, 2006 | doi: 10.1021/bk-2006-0933.ch005

Table 6. Concentrations of individual U and Pu isotopes from TIMS analyses and ORIGEN code predictions.

Isotope	*Results of TIMS analysis*	*Estimate from ORIGEN code*
^{233}U	<0.0005 % of total U	5.11E-07 % of total U
^{234}U	0.0295 ± 0.0005 % of total U	0.0278 % of total U
^{235}U	2.2347 ± 0.0005 % of total U	2.188 % of total U
^{236}U	0.5155 ± 0.0005 % of total U	0.4753 % of total U
^{238}U	97.2202 ± 0.0010 % of total U	97.31 % of total U
^{238}Pu	1.34 ± 0.01 % of total Pu	0.9397 % of total Pu
^{239}Pu	70.95 ± 0.22 % of total Pu	71.59 % of total Pu
^{240}Pu	21.84 ± 022 % of total Pu	20.00 % of total Pu
^{241}Pu	3.40 ± 0.03 % of total Pu	4.915 % of total Pu
^{242}Pu	2.47 ± 0.02 % of total Pu	2.560 % of total Pu
^{244}Pu	<0.02 % of total Pu	3.96E-07 % of total Pu

The measured concentrations of several elements do not agree with those predicted by ORIGEN code calculations (Table 5). These deviations can be explained by the formation of residue and the dissolution of a small amount of cladding. Zr, Mo, Te, and Pu are components of the undissolved residue to be described later. Pd and Ag are also minor components of the residue. These elements were removed from the dissolved fuel during formation of the residue, and are therefore found in the dissolved fuel in lower concentrations than predicted. Zr, Cd and Sn are components of the cladding, and might have leached from the cladding to the dissolved fuel. This would explain why they are found in the dissolved fuel in higher concentrations than expected. The relatively high concentration of Sb is difficult to explain, although it is a trace component of the cladding.

Based on the ICP-MS analysis of the dissolved fuel, a total of 906 g of U was dissolved. Based on bulk mass balance, a total of 945 g of U was removed from the cladding(Table 3). Therefore, about 39 g of U (corresponding to about 46 g of fuel, or about 4.1% of the total fuel mass) cannot be accounted for. The amount of fuel dissolved was estimated as the mass difference between the total charge (the cladding and the fuel) and the cladding remaining after the dissolution. We assumed that the change in mass was due entirely to the dissolution of fuel, and that all of the fuel dissolved. Accounting for the uncertainties in the measurements and in the assumptions made, the 4.1% of fuel is experimentally insignificant.

Downloaded by COLUMBIA UNIV on August 10, 2012 | http://pubs.acs.org
Publication Date: June 9, 2006 | doi: 10.1021/bk-2006-0933.ch005

Residue recovery and analysis. The dissolved fuel contained some undissolved material. The solutions were vacuum filtered through a Whatman 42 filter paper (90 mm) with a Büchner apparatus. The filter papers holding the solids were removed from the funnel and placed in a stainless steel tray to dry. A small amount of residue was also recovered by filtration of the rinse solutions described above. This small sample had been rinsed thoroughly during its collection, and was chosen for quantitative elemental analysis. A portion (87.5 mg) of the recovered residue was placed in a Teflon cup. Ten mL of a solution containing 94 vol % HNO_3, 5% HCl, and 1% HF was placed into the same Teflon cup and the cup was sealed as part of a Parr reaction vessel. The dissolution was carried out at 175°C for about 12 hours. The vessel was removed from the oven and cooled. The solution was removed and we observed that about 46 mg of residue had not dissolved. A second dissolution was carried out with the 46 mg of undissolved material in 10 mL of a solution containing 90 vol % HCl, and 10 vol % HNO_3, after which no residue could be seen in the Teflon cup. A composite of these two solutions was analyzed using ICP-MS. The composition is shown in elemental weight % in Table 7, and the total of all of the elements measured is only 51.24%. If the elements are present in the residue as their most stable oxides, then the total oxide weight % is about 70%. Additional analyses are underway to determine if other elements are present.

Zr, Mo, and Pu were the major constituents of the undissolved solids. The origin of the residue was not clear; it might have been undissolved material originally present in the irradiated fuel, or it might have been solids precipitated from the dissolved fuel solution. An understanding of the processes by which the residue was formed is important for efforts to prevent it.

Two solid phases have been previously reported in irradiated nuclear fuel residues, 1) a Zr-Mo-Pu oxide phase [12] and 2) a Mo-Tc-Ru-Rh-Pd alloy phase [13]. Zr, Mo and Pu are major components in the undissolved solids in this study, and Tc, Ru, Rh, and Pd are present in only small amounts (Table 7). We propose that the residue of our dissolution is composed primarily of the oxide phase, with only a small amount of the alloy. The Zr-Mo-Pu oxide phase has been suggested as a highly insoluble, Pu-bearing zirconium molybdate absent from the irradiated fuel, and is probably formed by precipitation [12].

Table 7. Composition of the residue from the spent fuel dissolution

element	*wt. %*[1]	*element*	*wt. %*[1]
Rb	0.0043	*Cs*	0.046
Sr	0.053	*Ba*[2]	0.44
Y	0.049	*La*	0.0021
Zr	12.84	*Ce*	0.0052
Mo	20.20	*Pr*	0.00089
Tc	0.16	*Nd*	0.0032
Ru	0.20	*Sm*	0.00021
Rh	0.019	*Eu*	.000072
Pd	0.036	*Gd*	0.0036
Ag	0.23	*U*	1.41
Cd	0.18	*Np*	0.0046
Sn	0.071	*Pu*	13.61
Sb	0.073	*Am*	0.00028
Te	1.29	*Total*	51.24

[1] based on metallic forms of elements

[2] This value might include Xe that interferes at masses 134 and 135

The origin of the residue is of interest. The zirconium in the residue could have come from two sources: (1) cutting debris from the zircalloy cladding and (2) fission product from the irradiated fuel. The zircalloy cladding would be expected to contain natural Zr, and would exhibit known natural isotopic ratios (Table 8). On the other hand, fission-product Zr would exhibit isotopic ratios similar to those calculated with the ORIGEN2 code (Table 8). The zirconium isotopic data strongly suggest that the Zr present in the residue comes primarily from fission products. Therefore, the major component of this material is clearly derived from the fuel, and is thought to be part of a compound not found in the irradiated fuel.

Cladding dissolution and analysis. Cladding pieces were collected after each of the three dissolution batches. For 906 g of U in the irradiated fuel, we collected 317 g of cladding hulls. One cladding piece was dissolved in two steps 1) with 6 M HF, and 2) in aqua regia, leaving no residue. This combined solution was analyzed using ICP-MS (Table 9). The Zr was the major component of the dissolved cladding. Sn, Pd, and Cd are known components of the Ziralloy-2. Small amounts of activation products (Sr, Y, Mo, Tc, Ru, Rh, Pd,

Downloaded by COLUMBIA UNIV on August 10, 2012 | http://pubs.acs.org
Publication Date: June 9, 2006 | doi: 10.1021/bk-2006-0933.ch005

Ag, Sb, Te, Cs and Ba) were also observed. More Mo than expected and a significant amount of Pu were detected in the dissolved cladding. These two components are probably from a small amount of residue stuck to the recovered cladding. The analysis of the cladding show that it contains very little undissolved fuel or residue.

Table 8. Isotopic distributions for Zr in samples of dissolved residue and cladding compared to distributions for natural Zr and fission-product Zr

m/z	*Residue-measured*	*Fission product-ORIGEN2 code*	*Natural abundance*
90	8.8%	7.9%	51.4%
91	19.8%	19.9%	11.2%
92	21.3%	21.5%	17.2%
94	24.8%	25.0%	17.4%
96	25.5%	25.8%	2.80%

Table 9. Composition of the dissolved cladding

Element	*wt %*	*Element*	*wt %*
Sr^3	1.37E-03	Ag^3	8.26E-03
Y^3	1.24E-03	Cd^2	2.07E-01
Zr^2	99.1	Sn^2	7.26E-01
Mo^3	1.67E-02	Sb^3	1.44E-04
Tc^3	5.29E-03	Te^3	4.59E-03
Ru^3	1.91E-03	Cs^3	1.02E-02
Rh^3	2.47E-04	$Ba^{1,3}$	5.27E-02
$Pd^{2,3}$	2.29E-01	*Pu*	1.50E-02

[1] - This value might include Xe that interferes at masses 134 and 135

[2] - These elements are known to be components of the Zircalloy-2 alloy

[3] – These elements are known to be activation products of the Zircaalloy-2 alloy.

Mass Balance Summary. Analyses of the dissolved fuel, the residue, and cladding were performed and related to the amount of each element expected based on the predicted composition of the irradiated nuclear fuel. The ORIGEN2 predictions were normalized to the amount of uranium measured in the dissolved fuel (906 g). Table 10 shows the amounts of each element expected and the amounts determined in the dissolved fuel, residue, and cladding as percentages of the expected element mass. The residue results are normalized to 12.7 g. The composition of the cladding is normalized to the total amount of cladding recovered (317.3 g). The percent recovery is the total of each element in the dissolved fuel, residue, and cladding, relative to the amount predicted.

Downloaded by COLUMBIA UNIV on August 10, 2012 | http://pubs.acs.org
Publication Date: June 9, 2006 | doi: 10.1021/bk-2006-0933.ch005

Table 10. Amounts of each element determined in 2.5 L of dissolved fuel, 12.7g of undissolved solids, and 317.3 g of cladding. These percentages were normalized to 100. The results of the ORIGEN2 calculation, normalized to 906 g of U are also shown.

Element	*Total mass expected, g*[1]	*Fraction of element mass in dissolver solution*	*Fraction of element mass in residue*[2]	*Fraction of element mass in cladding*[3]
Rb	3.26E-01	99.5 %	0.3 %	0.2 %
Sr	6.17E-01	98.4 %	0.9 %	0.7 %
Y	4.21E-01	97.4 %	1.6 %	1.00 %
Zr	3.16E+02	0.2 %	0.6 %	99.2 %
Mo	2.89E+00	13.2 %	84.9 %	1.9 %
Tc	6.74E-01	91.4 %	6.2 %	2.4 %
Ru	1.75E+00	98.5 %	1.2 %	0.3 %
Rh	3.64E-01	99.3 %	0.5 %	0.2 %
Pd	1.69E+00	36.3 %	0.6 %	63.1 %
Ag	7.56E-02	2.5 %	61.4 %	36.1 %
Cd	7.28E-01	15.7 %	2.8 %	81.5 %
Sn	2.37E+00	2.0 %	10.9 %	87.1 %
Te	4.10E-01	43.5 %	52.1 %	4.4 %
Cs	1.91E+00	97.5 %	0.5 %	2.0 %
Ba[4]	2.12E+00	93.7 %	1.7 %	4.6 %
La	1.06E+00	98.1 %	0.0 %	1.9 %
Ce	2.01E+00	99.9 %	0.0 %	0.1 %
Nd	3.47E+00	99.9 %	0.0 %	0.1 %
Eu	9.26E-02	99.9 %	0.0 %	0.1 %
Gd	8.67E+00	100.0 %	0.0 %	0.0 %
U	9.05E+02	100.0 %	0.0 %	0.0 %
Np	3.44E-01	99.8 %	0.2 %	0.0 %
Pu	8.24E+00	79.6 %	19.8 %	0.6 %
Am	7.70E-01	100.0 %	0.0 %	0.0 %

[1] – These values were calculated using ORIGEN, and normalized to 906 g of uranium

[2] – These values were calculated assuming a total of 12.7 g residue

[3] – These values were calculated assuming a total of 317.3 g cladding

[4] – This value might include Xe that interferes at masses 134 and 135

Downloaded by COLUMBIA UNIV on August 10, 2012 | http://pubs.acs.org
Publication Date: June 9, 2006 | doi: 10.1021/bk-2006-0933.ch005

Factors bearing on the formation of residue. Solid zirconium molybdate particles [$ZrMo_2O_7(OH)_2 \cdot 2H_2O$, references 14 and 15] have been reported in several studies of irradiated nuclear fuel dissolutions [12, 16]. The formation of zirconium molybdate precipitates from acidic solutions can be described using the equations given by Imumida and Kawamura [15]:

$$Mo^{+3} + 3H_2O \rightarrow MoO_3 + 6H^+ + 3e^-$$

$$MoO_3 + H_2O \rightarrow HMoO_4^- + H^+$$

$$Zr^{+4} + H_2O \rightarrow ZrO^{2+} + 2H^+$$

$$2HMoO_4^- + ZrO^{2+} + 2H_2O \rightarrow ZrMo_2O_7(OH)_2 \cdot 2H_2O.$$

Downloaded by COLUMBIA UNIV on August 10, 2012 | http://pubs.acs.org
Publication Date: June 9, 2006 | doi: 10.1021/bk-2006-0933.ch005

Several authors have suggested that a Pu-bearing zirconium molybdate phase is precipitated from nitric acid solutions of irradiated nuclear fuel and that its formation is relatively slow [15-19]. Therefore, we suggest that the formation of the Pu-bearing phase could be minimized by minimizing storage time. Three additional variables have been proposed as important for the formation of solids from dissolved fuel solutions [14, 19]: temperature, [H+] and [Mo] [Zr].

Several studies have shown that the zirconium molybdate phase is more soluble at low temperatures than at high temperatures. Specifically, higher temperatures favor the formation of the zirconium molybdate solids between 50 and 100°C [15, 18]. Therefore, dissolution and storage at relatively low temperatures would be expected to lower the risk of precipitation.

At the same time, the formation rate of a zirconium molybdate depends on the concentration of the dissolving acid solution [15, 18]. Izumida and Kawamura [15] showed that at room temperature, precipitate formed in HNO_3 solutions less than 1 M. Further, precipitate formed from 2 M HNO_3 at 50°C, but not at 30°C; while it precipitated from 6 M HNO_3 at 100°C, but not at 90°C [15]. Therefore, higher acid concentrations would be expected to lower the risk of precipitation.

Lowering the concentrations of Mo and Zr by diluting the solution prior to storage would be expected to inhibit the surface controlled initiation of precipitation [16]. However, the overall effect of diluting the solution is unknown. One consequence would be to increase the total volume of dissolved fuel to be fed into the process.

Ideally, to prevent the precipitation of the zirconium molybdate the dissolved fuel solution would be diluted with strong acid, and stored at low temperatures. On the other hand, if precipitation cannot be prevented, then the Pu in the residue might be recovered in a secondary treatment process. Dissolution of the residue in an acid solution containing HF would allow for recovery of the material.

Conclusions

Two conclusions can be drawn from this study, 1) the pin of fuel was effectively dissolved under the conditions used and 2) a small amount of residue rich in Zr, Mo, and Pu formed during or after dissolution.

Based on the elemental composition of the dissolved fuel, and comparison to the composition predicted, we successfully dissolved the irradiated nuclear fuel. The concentrations of noble metals (Ru, and Rh) showed that even these difficult elements were completely dissolved. Deviations of elemental concentrations in the fuel from expected concentrations can be explained by formation of a residue or the dissolution of a small amount of cladding.

Dissolution and analysis of the recovered residue showed that the major constituents were Zr, Mo, and Pu. This finding is consistent with previous studies that identified a Pu-bearing zirconium molybdate oxide phase. At the same time, the commonly-observed noble metal alloy was not observed. We propose that this oxide was precipitated from the dissolved fuel solution.

Downloaded by COLUMBIA UNIV on August 10, 2012 | http://pubs.acs.org
Publication Date: June 9, 2006 | doi: 10.1021/bk-2006-0933.ch005

References

1. C. M Slansky, "Preparation of Fuels for Processing," in: Chemical Processing of Reactor Fuels (ed. J. F. Flagg), Academic Press, New York, 1961.
2. E. A. Kyser, "Extraction of Plutonium into 30% Tributyl Phosphate from Nitric Acid Solutions Containing Fluoride, Aluminum, and Boron," *Sep. Sci. Tech.* **36**, 729-741 (2001).
3. R. L. Stevenson and P. E. Smith, "Aqueous Separation," in: Reactor Handbook, Volume II (eds S. M. Stoller, and R. B. Richards), Interscience Publishers, New York (1961).
4. B. Srinivasan, R. A. Leonard, S. B. Aase, G. F. Vandegrift, Moeridun, A. A. Rauf, H. Lubis, A. Hardi, S. Amini, and Y. Nampira, "Processing of LEU Targets for 99Mo Production—Dissolution of Metal Foils by Nitric Acid/Sulfuric Acid Mixtures," Proc. 1995 International Meeting on Reduced Enrichment for Research and Test Reactors (1995) Paper 3-2.
5. M. G. Fontana, and N. D. Greene, Corrosion Engineering, McGraw-Hill, New York, 1978

6. G. F. Vandegrift, M. C. Regalbuto, S. B. Aase, H. A. Arafat, A. J. Bakel, D. L. Bowers, J. P. Byrnes, M. A. Clark, J. E. Emery, J. R. Falkenberg, A. V. Gelis, L. D. Hafenrichter, R. A. Leonard, C. Pereira, K. J. Quigley, Y. Tsai, M. H. Vander Pol, and J. J. Laidler, "Lab-Scale Demonstration of the UREX+ Process," Proceedings of Waste Management 2004, International Symposium, Tucson, AZ, February 29-March 4, 2004.

7. K. N. Woods and L. F. Van Swam, *Extended Burnup Demonstration, Reactor Fuel Program, Semi-Annual Progress Report, January 1979 - September 1979*, Exxon Nuclear Company, XN-NF-80-25, December, 1980.

8. S. Glasstone and A. Sesonske, *Nuclear Reactor Engineering*, Van Nostrand Reinhold Company, pp. 748-754.

9. A. V. Nero, *A Guidebook to Nuclear Reactors*, University of California Press, pp. 94-108.

10. A. G. Croff, *ORIGEN2 – A Revised and Updated Version of the Oak Ridge Isotope Generation and Depletion Code*, Oak Ridge National Laboratory, ORNL-5621, July, 1980.

11. *WIMS: A Modular Scheme for Neutronics Calculations*, AEA Technology, 1999.

12. J. Lausch, R. Berg, L. Koch, M. Coquerelle, J. P. Glatz, C. T. Walker, and K. Mayer, "Dissolution Residues of Highly Burnt Nuclear Fuels," *J. Nucl. Mater.* **208,** 73-80 (1994).

13. H. Kleykamp, J. O. Paschoal, R. Pejsa, and F. Thommler, "Composition and Structure of Fission Product Precipitates in Irradiated Oxide Fuels: Correlation with Phase Studies in the Mo-Ru-Rh-Pd and BaO-UO_2-ZrO_2-MoO_2 Systems," *J. Nucl. Mater.* **130,** 426-433 (1985).

14. P. A. Anderson, "Laboratory Simulation of Hig-Level liquid Waste Evaporation and Storage," *Nucl. Tech.* **47**, 173-180 (1979).

15. T. Izumida, and F. Kawamura, "Precipitates Formation Behavior in Simulated High Level Liquid Waste of Fuel Reprocessing," *J. Nucl. Sci. Tech.* **27**, 267-274 (1990).

16. F. C. Doucet, D.T. Goddard, C. M. Taylor, I. S. Denniss, S. M. Hutchison, and N. D. Bryan, "The Formation of hydrated Zirconium Molybdate in Simulated Spent Nuclear Fuel Reprocessing Solutions," *Phys. Chem. Chem. Phys.,* **4**, 3491-3499 (2002).

Downloaded by COLUMBIA UNIV on August 10, 2012 | http://pubs.acs.org
Publication Date: June 9, 2006 | doi: 10.1021/bk-2006-0933.ch005

17. T. Adachi, M. Ohnuki, N.Yoshida, T. Sonobe, W. Kawamura, H. Takeishi, K. Gunju, T. Kimura, T. Suzuki, Y. Nakahara, T. Muromura, Y. Kobayashi, H. Okahita, and T. Yamamoto, "Dissolution Study of Spent PWR Fuel: Dissolution Behavior and Chemical Properties of Insoluble Residues," *J. Nucl. Mater.* **174,** 60-71 (1990).

18. M. H. Lloyd, "Instabilities and Solids Formation in LWR Reprocessing Solutions," *Trans. Amer. Nucl. Soc.* **24,** 233 (1979).

19. P. Baron, personal communication (2004).

Downloaded by COLUMBIA UNIV on August 10, 2012 | http://pubs.acs.org
Publication Date: June 9, 2006 | doi: 10.1021/bk-2006-0933.ch005

Downloaded by UNIV OF ARIZONA on August 9, 2012 | http://pubs.acs.org
Publication Date: June 9, 2006 | doi: 10.1021/bk-2006-0933.ch006

Chapter 6

Advanced PUREX Flowsheets for Future Np and Pu Fuel Cycle Demands

O. D. Fox, C. J. Jones, J. E. Birkett, M. J. Carrott, G. Crooks, C. J. Maher, C. V. Roube, and R. J. Taylor

Nuclear Sciences and Technology Services, B229 and BNFL Technology Centre, Sellafield CA20 1PG, United Kingdom

The reprocessing of nuclear fuel using PUREX-based solvent extraction has been undertaken in the UK on an industrial scale for over forty years. Current research includes the development of modified PUREX-style flowsheets for processing ever-increasing plutonium content fuels including MOX, fast reactor and even experimental and legacy fuels. Herein, results are presented on Np recovery in single cycle PUREX flowsheets using hydroxamic acids. Flowsheets have been demonstrated on a centrifugal contactor rig. Aspects of Np chemistry relevant to the use of hydroxamic acids in process flowsheets for U/Pu(&Np) separation are reported.

Introduction

The UK has undertaken Purex nuclear fuel reprocessing both in industrial deployment and research and development for over forty years.[1] Spent fuel from the UK's first generation of reactors, Magnox, are reprocessed at the Magnox reprocessing plant and those from the more modern oxide fuel reactors (e.g. AGRs, PWRs and BWRs) at the Thermal Oxide Reprocessing Plant (Thorp); both plants are located at the Sellafield site in Cumbria, UK.

In Separations for the Nuclear Fuel Cycle in the 21st Century; Lumetta, G., et al.;
ACS Symposium Series; American Chemical Society: Washington, DC, 2006.

Advances in Purex technology have reflected fuel cycle evolution: as evidenced through the development of flowsheets and equipment to reprocess both metal and oxide thermal reactor fuels. Research and development is continuing at BNFL in the area of aqueous (or solvent extraction) reprocessing to meet the anticipated future demands of the nuclear fuel cycle. This paper discusses how nuclear fuel cycles might develop in the future, how Purex technology may develop to respond to the challenges of advanced fuel cycle strategies and presents some current R&D work being undertaken within BNFL towards these ends.

Developments in Purex technology are subject to a number of drivers to which different countries may ascribe different priorities depending on their nuclear energy strategy.[1] At the more focussed level of developing future reprocessing plants three primary drivers of any development programme may be seen as:-

1. Reductions in reprocessing costs.
2. Reduction in effluent volumes.
3. Minimisation of waste production.

However, at a more strategic level other issues become important:-

- Reducing the radiotoxicity of high-level waste.
- Reducing or eliminating uncertainties about the long-term performance of waste repositories.
- Utilizing the energy potential in the fissionable isotopes present in spent fuel.
- Increasing the proliferation resistance of wastes and products.

Drivers 1 to 3 are not necessarily independent since reductions in effluent and waste production may, of themselves, reduce costs, but this may be at the expense of process changes in fuel preparation and solvent extraction which may increase costs elsewhere in the cycle.

A reduction in cost may be achievable by the use of intensified solvent extraction equipment. For example, there is current worldwide interest in the nuclear industry in the use of centrifugal contactors for liquid-liquid extraction in PUREX and waste partitioning processes. Besides BNFL, flowsheets utilizing centrifugal contactor equipment for solvent extraction are being developed by, amongst others, American,[2] European[3] and Japanese[4] groups. Centrifugal contactors offer a number of advantages over the pulsed-columns and mixer-settlers employed on current reprocessing plants. These include; reduced risk of criticality due to design geometry; variable flowrates allowing high through-put

Downloaded by UNIV OF ARIZONA on August 9, 2012 | http://pubs.acs.org
Publication Date: June 9, 2006 | doi: 10.1021/bk-2006-0933.ch006

of liquids and intensification of the process; compact equipment which markedly reduces capital costs; easy and rapid start-up and shut down procedures; short contact times with active feed reducing both radiolytic damage and hydrolysis of the TBP/hydrocarbon-diluent solvent.

Set against the process cost drivers, there may be strategic benefits from improved partitioning of actinides and Fission Products (FP) which may justify increases in reprocessing costs, if necessary. Elimination of 99.9% of the actinides can reduce the radiotoxicity of High Level Waste (HLW) from reprocessing by a factor of up to 100,000 compared to the direct disposal of spent fuel. Furthermore, the radiotoxicity of HLW is dominated by Fission Products (FP) for the first few hundred years but thereafter it is the presence of the TRans Uranium elements (TRU) which becomes the dominant contributor. Thus removing TRU from HLW can substantially reduce the time taken for it to decay to the radiotoxicity level of the natural uranium ore from which it originated. A target of less than 10^3 years, compared to *ca.* 10^6 years without TRU removal, seems possible and would simplify waste repository design. Retaining neptunium, americium and curium in recycled plutonium makes it substantially more radioactive and more proliferation resistant; but places much higher demands on reprocessing and fuel fabrication technology.

In order to derive significant benefits from segregating the TRU from HLW it is necessary to recycle and ultimately destroy the TRU in the nuclear fuel cycle through Partitioning and Transmutation (P&T). P&T offers the prospect of recovering energy from fissionable nuclides and consuming fissile material which might potentially be used in the production of fission weapons. P&T involves separating the FP from the actinides (Partition) so that the latter can be returned to a reactor for further irradiation (Transmutation). The recycled actinides may be removed by 'nuclear incineration' through fission or they may be converted to other fissile or short lived isotopes, these processes collectively being known as transmutation. The transmutation of actinides is more efficient if a fast neutron energy spectrum is used and so requires the use of Fast Reactors (FR) or Accelerator Driven Systems (ADS).

To fully close the fuel cycle with respect to TRU will require substantial investments in research and development to become viable. However, transmutation accompanied by multiple fuel recycle has the potential to reduce, by a factor exceeding 10^2, the time taken for the HLW to decay to the activity level of the natural uranium from which it originated.[2] Such a strategy helps to deal with objections about the long-term problem of nuclear wastes and about nuclear proliferation. If a transmutation strategy were adopted fuel reprocessing

Downloaded by UNIV OF ARIZONA on August 9, 2012 | http://pubs.acs.org
Publication Date: June 9, 2006 | doi: 10.1021/bk-2006-0933.ch006

would need to tolerate much higher radiation and heat outputs from spent fuel placing much greater demands on Purex technology and in the longterm requiring pyrochemical or other non-aqueous reprocessing techniques for multiply recycled fuel.[4] In the nearer term, work on aqueous reprocessing flowsheets needs to address the problem of the routing of transuranium elements in the Purex process, in particular removing them from the highly active waste.

Control of Np in Advanced Fuel Cycles

The first contactor in the PUREX process extracts and separates the U and Pu from the majority of highly active fission products and dissolved fuel cladding. In acidic solutions, Np exists largely as Np(IV), $[Np^{(V)}O_2]^+$ and $[Np^{(VI)}O_2]^{2+}$. Pentavalent Np is not significantly extracted into the TBP/alkane solvent; however, the tetra and hexa-valent Np ions are complexed by TBP and nitrate ions (see [1] and [2]) and extract into the U/Pu-loaded organic phase.

$$Np(IV) + 4NO_3^- + 2TBP \Leftrightarrow Np(NO_3)_4(TBP)_2 \qquad [\,1\,]$$
$$Np^{(VI)}O_2^{2+} + 2NO_3^- + 2TBP \Leftrightarrow Np^{(VI)}O_2(NO_3)_2(TBP)_2 \qquad [\,2\,]$$

In the next contactor the U/Pu split is achieved by introducing a solution of reducing agent, commonly U(IV), to convert the Pu present to inextractable Pu(III), which is then rejected to the aqueous phase. However, Np is reduced by U(IV) to Np(IV) and any Np in the solvent will, therefore, accompany the uranium stream. A consequence of this is the requirement to operate a Uranium Purification (UP) cycle to remove Np. Therefore if Np can be diverted from the U before the UP contactor – and sufficient DFs for Pu and other TRUs and FPs are obtained in prior contactors – then the UP cycle and all its plant footprint, operation, wastes and costs can be eliminated.

A number of options for Np routing have been considered, see Figure 1:

- Route Np with FPs and MAs in first extraction contactor; and thereby send Np with the HLW and eventual vitrification
- Remove Np immediately after U/Pu split contactor; that is, include a specific Np rejection contactor
- Remove Np in U/Pu split contactor i.e. co-recover Np/Pu; this removes the need for a separate Np rejection contactor.

For the first option Np would be directed with FPs and MAs and – depending on fuel cycle scenario – either be vitrified (most likely) or recovered with the MAs in a second Highly Active (HA) extraction cycle.

Downloaded by UNIV OF ARIZONA on August 9, 2012 | http://pubs.acs.org
Publication Date: June 9, 2006 | doi: 10.1021/bk-2006-0933.ch006

Downloaded by UNIV OF ARIZONA on August 9, 2012 | http://pubs.acs.org
Publication Date: June 9, 2006 | doi: 10.1021/bk-2006-0933.ch006

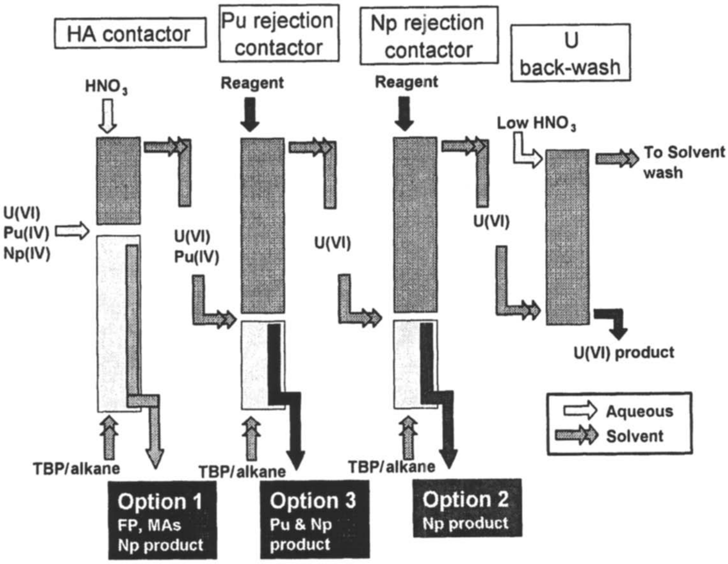
HA contactor
Pu rejection contactor
Np rejection contactor
U back-wash
HNO$_3$
Reagent
Reagent
Low HNO$_3$
To Solvent wash
U(VI)
Pu(IV)
Np(IV)
U(VI)
Pu(IV)
U(VI)
U(VI)
U(VI) product
Aqueous
Solvent
TBP/alkane
TBP/alkane
TBP/alkane
Option 1
FP, MAs
Np product
Option 3
Pu & Np
product
Option 2
Np product

Figure 1. Options for Np routing in a PUREX-style flowsheet including 1) directing with FPs and MAs in HA contactor, 2) production of a Np-only product by use of a specific Np rejection contactor and 3) co-recovery with Pu in the Pu rejection contactor

For the second option a specific Np rejection contactor is required, which is absent for options one and three. Separation of Np after the U/Pu split would keep the Pu product free of Np (which is a burnable neutron poison) and this would be the preferred option for Pu-only recycle fuel cycles. However, this generates a pure neptunium stream and there appears to be little current or anticipated demand for such a product.

The third option, which removes the need for a Np rejection contactor by producing a co-recovered Np/Pu product, is potentially the most convenient and justifiable option. Neptunium is a burnable poison (in thermal reactors) and could theoretically be included in a plutonium-based oxide fuel with adjustment to reactor operating conditions. In addition, recent concerns over nuclear weapons proliferation associated with the advancement of Pu-based fuels may be tempered by the manufacture of a Np-contaminated Pu product. Finally, Np is fissionable in fast reactors and therefore the fuel cycle can be closed with respect to Np in a P&T scenario. This Minor Actinide burning is also consistent with reducing the long-term radiotoxicity of the TRU elements in waste.

Use of Hydroxamic Acids in Advanced Fuel Cycles for Np and Pu control

Np rejection - routing option 2, a Np-only product

Routing option 2 requires a hydrophilic ligand that selectively complexes Np(IV) over U(VI) at very low pH values and is reasonably stable to both acid and radiolytic degradation for the time scale of the separation process.

Downloaded by UNIV OF ARIZONA on August 9, 2012 | http://pubs.acs.org
Publication Date: June 9, 2006 | doi: 10.1021/bk-2006-0933.ch006

BNFL identified hydroxamic acids (1) as suitable candidates for stripping tetravalent actinide cations into the aqueous phase while leaving hexavalent actinides in the TBP/OK phase.[5] Two hydrophilic hydroxamic acids, formo- and aceto-hydroxamic acid, (FHA & AHA) are considered suitable for this process as they form hydrophilic actinide complexes.

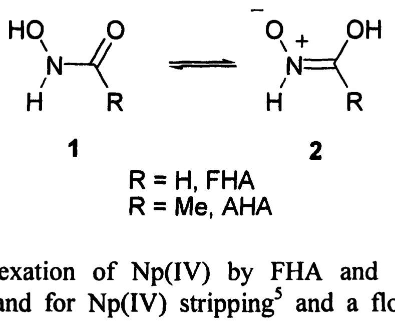

R = H, FHA
R = Me, AHA

Work on the complexation of Np(IV) by FHA and AHA confirmed the suitability of this ligand for Np(IV) stripping[5] and a flowsheet test of a Np rejection trial using AHA to selectively strip Np from a U-loaded solvent stream was undertaken at Sellafied. From the final Np concentrations in the exiting organic and aqueous solutions a decontamination factor (Np DF to uranium solvent product) of 270 was obtained.

Although successful, a number of problems were identified with the operation of the experimental rig and the analytical methods employed for data collection. The final value of the DF was limited either due to the analytical limit of neptunium detection and/or rig contamination. This problem arises from the difficulty of determining the concentration of low levels of Np in U-loaded solvent. In addition, early computational models over-predicted neptunium back-extraction due to over-optimistic predictions on the stage efficiencies for the 1-cm miniature annular centrifugal contactors employed.[6] A significant volume of work was undertaken to understand and address the rates of actinide mass transfer in miniature centrifugal contactors to improve process modelling of the experimental flowsheets.

Np Flowsheet Trial

A second Np rejection trial (Np02) was undertaken to optimise the flowsheet with respect to Np stripping and improve on analytical limits of detection, see Figure 2. Alterations were made to the flowsheet compared to the first Np rejection trial at Sellafield. Briefly, in order to improve the Np DF a decrease in the solvent:aqueous flowrate ratio in the Np stripping section was made, dropping from 6:1 in Np01 to 4.2:1 in Np02. Clearly, this would lead to higher U levels in the Np product, but there appears little justification for producing a Np product free of U if the Np is to be returned to fuel manufacture.

A glovebox-housed centrifugal contactor rig comprising three blocks of four-stage 1 cm centrifugal contactors was used to simulate the Np rejection contactor. The U- and Np-loaded solvent feed (SP1) entered at stage 17.

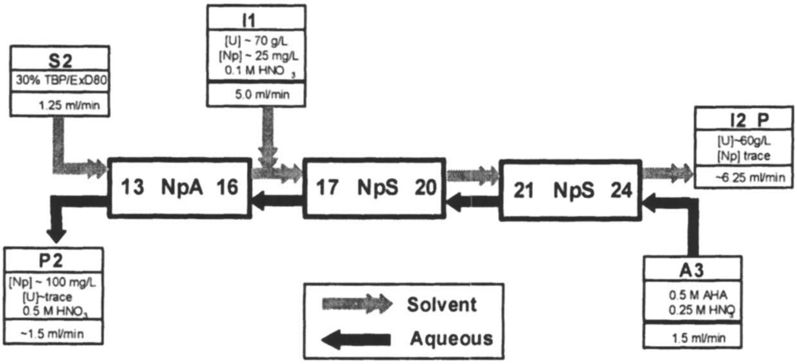

Figure 2. Flowsheet tested for Np rejection trial at Sellafield

Product streams and profile stage samples were analysed for metals (U, Np, Tc) and acidity. A range of methods were employed depending on the concentration of analyte, the concentrations of interfering species and the sample matrices present. The methods employed included: off-line spectrophotometry, titrations, inductively-coupled plasma mass spectrometry (ICP-MS), X-ray fluorescence (XRF), and both gamma and low energy photon spectroscopy (LEPS).

The concentration of Np in P2 aqueous product stream was monitored spectrophotometrically and showed that the Np concentration in the P2 aqueous product reached steady state after about 50 min. The absorption spectrum of the P2 product was characteristic of a Np(IV)AHA complex[8] (λ_{max} = 732 nm).

Downloaded by UNIV OF ARIZONA on August 9, 2012 | http://pubs.acs.org
Publication Date: June 9, 2006 | doi: 10.1021/bk-2006-0933.ch006

During the course of the trial four product samples were taken and analysed for U, Np and acidity. Mass balances for U, Np and acid were determined across the flowsheet, see Table I. Uranium mass balances were excellent, averaging 99% for all four product samples taken. Interestingly, although in-line spectrophotometry indicated that the Np in the aqueous product had reached steady state after less than an hour, the level of Np in the aqueous product measured by LEPS did not plateau until the final two product samples, after 2h 41 min and 3h 26 min. Similarly, good Np mass balances (96%) were not achieved until the final two samples; this is attributed to the gradual build-up of Np in the flowsheet during run up to steady state, a consequence of recycle in the U re-extraction cascade. Overall acid mass balances across the flowsheet were reasonably good.

Downloaded by UNIV OF ARIZONA on August 9, 2012 | http://pubs.acs.org
Publication Date: June 9, 2006 | doi: 10.1021/bk-2006-0933.ch006

Table I. Mass balances for Np rejection trial across four product samples

Time (Hr/mins)	*Uranium (%)*	*Neptunium (%)*	*Acidity (%)*
0.50	99	75	83
1.40	99	86	87
2.41	99	95	90
3.26	101	96	90

Aqueous and organic product streams for the Np rejection trial are given in Table II. From the four product samples taken during the course of the trial, decontamination factors (DFs) were calculated based on a feed (I1) of 31.4 mg/L Np, for the aqueous (P2) and analyses of the organic product (I2_P) streams (Table 3). These results showed that the Np was very effectively stripped from the U-loaded solvent. Long count times were employed to provide better confidence in the magnitude of the DFs obtained.

As mentioned previously, the mass balance for Np improves over the duration of the trial. In light of this, it is more reasonable to calculate the Np DF based on the final two product samples (at 2 h 40 mins and 3 h 30 mins) where the flowsheet is operating under steady-state conditions. *Based on this, an average DF of 2150 for Np decontamination of the U product was obtained.* In terms of Np recovery this corresponds to approximately 99.95%. This exceeds the proposed requirement for 99.9% MA recovery in Advanced Fuel Cycles in order to minimise losses of long-lived TRUs. The aqueous flowrate was increased in this trial in order to maximise Np DFs and ensure the backwash of a modest mass of uranium. The levels of U (<0.5 g/L) in the Np product are regarded as acceptable considering the final projected usage of such a Np product.

Table II. Aqueous (P2) and Organic (I2_P) product streams for Np rejection trial

I2_P Organic	*Time (hrs/mins)*	*[U] g/L*	*[Np] mg/L*	*Np DF to U product*	*Acidity (M)*
1	0.50	60	0.007	3589	0.04
2	1.40	60	0.005	5024	0.04
3	2.41	60	0.014	1794	0.04
4	3.26	61	0.010	2512	0.04

P2 Aqueous	*Time (hrs/mins)*	*[U] g/L*	*[Np] mg/L*	*Acidity (M)*
1	0.50	0.43	78.8	0.49
2	1.40	0.44	90.2	0.52
3	2.41	0.42	99.1	0.54
4	3.26	0.52	101.0	0.54

After the final product sample was taken, profile samples taken across the 12–stages. The Np solvent and aqueous profile samples are shown in Figure 3. In the solvent profile a small amount of Np recycle is observed between stages 13 – 17 due to the introduction of fresh solvent at stage 13. A modest rise in Np solvent concentration at the feed plate (stage 17) is observed. From hereon, with increasing stage number, the concentration of Np in the solvent falls steadily until the Np Limit of Detection (LOD) is reached (~ 0.5 mg/L Np). The LOD differs from the product samples because both the volume of sample and the count times for profile samples are reduced.

In the aqueous profile the concentration of Np across stages 13 – 15 is approximately 90 mg/L, as expected. A modest increase in Np aqueous concentration is seen at stage 16, which suggests a small amount of Np is being recycled between stages 16 and 17. Across stages 17 – 24 the aqueous concentration of Np falls steadily and consistently as the Np is effectively scrubbed from the uranium-loaded stream.

The U- solvent and aqueous profiles are shown in Figure 4. A steady drop in both aqueous and solvent U concentration across the U re-extract cascade, stages 13 – 17, is evident. The aqueous U concentration at stage 13 of 0.4 g/L is consistent with the four product samples taken during the trial. Above the feed plate the U solvent concentration reaches a maximum at approximately 80 g/L

Downloaded by UNIV OF ARIZONA on August 9, 2012 | http://pubs.acs.org
Publication Date: June 9, 2006 | doi: 10.1021/bk-2006-0933.ch006

(stages 17 – 20); from hereon the concentration falls steadily to 60 g/L at stage 24. The U aqueous concentration profile shows a smooth and steady increase to ~40 g/L at stages 19 and 20 and a gradual drop to ~27 g/L over stages 21 to 24. This hump in U concentration across the Np stripping contactors is expected due to the lower acidity of the AHA stripping feed.

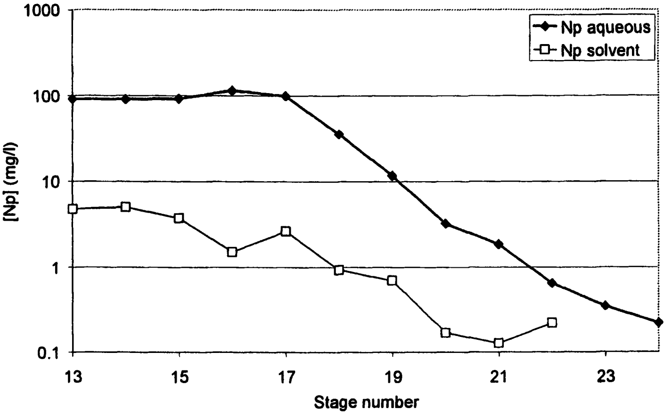

Figure 3. Np profiles for second for Np rejection trial at Sellafield

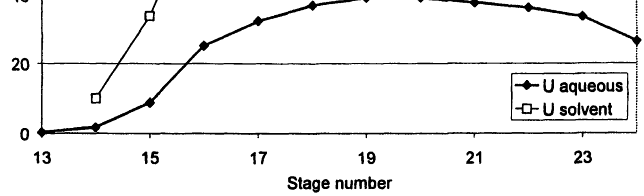

Figure 4. U profiles for second for Np rejection trial at Sellafield

Downloaded by UNIV OF ARIZONA on August 9, 2012 | http://pubs.acs.org
Publication Date: June 9, 2006 | doi: 10.1021/bk-2006-0933.ch006

Summary

A Np rejection trial was undertaken to demonstrate the selective stripping of Np(IV) from a U/Np-loaded solvent using a hydrophilic complexant, AHA. Excellent mass balances for Np and U were observed and a reasonably good mass balance for acidity was achieved. Based on product streams for the flowsheet at steady state, a Np DF of 2150 was achieved, which corresponds to approximately 99.95% Np recovery.

From trials run at Sellafield, it appears relatively simple to tune a Np(IV) rejection flowsheet to achieve the required Np DF in the U solvent product and to maintain an acceptable loss of U to the Np product stream. Indeed, the efficiency of the hydroxamic acid backwash suggests that a number of parameters (*e.g.* aqueous flowrate, number of contactor stages) could be relaxed to further optimise the flowsheet, depending on either the demands of the fuel cycle or engineering.

Downloaded by UNIV OF ARIZONA on August 9, 2012 | http://pubs.acs.org
Publication Date: June 9, 2006 | doi: 10.1021/bk-2006-0933.ch006

Np/Pu co-recovery - routing option 3, a Np/Pu product

The hexavalent, NpO_2^{2+}, is in equilibrium with the pentavalent form and, in nitric acid solutions, the fate of the equilibrium is controlled by the concentration of nitrous acid. Notably, the pentavalent form of Np is essentially inextractable and the hexavalent form highly extractable in to TBP-alkane mixtures.

$$2NpO_2^+ + NO_3^- + 3H^+ \Leftrightarrow 2NpO_2^{2+} + HNO_2 + H_2O$$

$$K = \frac{[Np(VI)][HNO_2]^{1/2}}{[Np(V)][NO_3^-]^{1/2}[H^+]^{3/2}}$$

The equilibrium constant for this reaction was determined by Sidall and Dukes, and at 25 °C is 4.00 E-4.[9] Due to the high extractability of nitrous acid into TBP/diluent mixtures this equilibrium is shifted towards Np(VI) and for this reason in the PUREX process Np is extracted – in the hexavalent form - to a somewhat varying degree depending on the process conditions (e.g. residence time and acidity). A significant mass of Np therefore accompanies the U and Pu into the split contactor.

Plutonium will readily exist in the tetravalent state under PUREX conditions and it is in this, its most extractable, oxidation state that extraction occurs in all primary extraction cycles. Due to its high charge, stability constants for complexation with simple ligands are invariably higher than those with U(VI) and this phenomenon is exploited in the complexant stripping of Pu from organic

U-loaded streams.[10] The most studied ligand for complexant stripping of Pu is the sulphate anion. Indeed, a flowsheet based on sulphate stripping was designed and operated at Dounreay (UK) for the reprocessing of fast reactor fuel. However, this method suffers from the salt-loading of the waste streams and the corrosive nature of the sulphate anion.

Alternatives based on organic anions derived from common weak acids have been proposed; most notably, formate, acetate and lactate.[10] Studies on the use of complexant stripping led to the proposition of the use of hydroxamic acids. Interest in the use of hydroxamic acids arose because of the noted differences in the stability constants of Pu(IV) and U(VI) for a series of organic soluble hydroxamates. Subsequently, the use of formohydroxamic acid as a stripping agent for Pu(IV) was investigated in the early 1990s through a collaboration of BNFL with AEA-T; much of this early work has now been reviewed.[11]

Downloaded by UNIV OF ARIZONA on August 9, 2012 | http://pubs.acs.org
Publication Date: June 9, 2006 | doi: 10.1021/bk-2006-0933.ch006

Recent work at BNFL has focused on the use of hydroxamic acids for Pu(IV) at high Pu loadings; that is, concentrations of Pu that may arise from the reprocessing of MOX and fast reactor fuels.[12] A programme of research is underway focused on flowsheet testing and chemical and engineering studies to support operation and further understanding of such flowsheets. However, the focus of this paper is on the Np routing under such circumstances.

In addition to complexation, hydroxamic acids are reducing agents. The reduction of Np(VI) to Np(V) by FHA is rapid (99% reduction after 0.045 s) and has been investigated in some detail using stopped-flow near-infrared spectrophotometry.[13] In 2M HNO_3 at 22 °C the reduction was described by the following second order rate equation:

$$-\frac{d[NpO_2^{2+}]}{dt} = k[NpO_2^{2+}][FHA] \text{ where } k = 1.17\text{E}3 \text{ M}^{-1} \text{ s}^{-1}$$

Therefore hydroxamic acids can be used to reduce extractable Np(VI) to inextractable Np(V) and to strip Pu(IV). Clearly, FHA is unusually effective at reducing Np(VI), being significantly more rapid than both U(IV) and hydroxylamine.[14]

Previous work had shown that the stripping of Np(IV) by hydroxamic acids in 1-cm centrifugal contactors was relatively slow compared to that of U(VI) extraction or back-wash.[7] Although the rate of reduction of Np(VI) by FHA is fast it was considered that it could limit the efficiency of Np(VI) stripping from U-loaded solvent. Therefore experiments were performed to determine whether in a single stage centrifugal contactor the efficiency of Np(VI) stripping is rapid enough. The extent of Np(VI) reduction being dependent upon the residence time of the emulsion in the contactor which is in turn dependent on the flowrate of liquids through it.

Experiments were performed using a single stage 1-cm centrifugal contactor to investigate Np(VI) rejection by AHA in the presence and absence of U. From the results on mass transfer (E) obtained (Figure 5) it can be seen that Np(VI) [as Np(V)] will be effectively back-washed from a U-loaded stream by AHA, and that the stage efficiencies for this backwash (under the conditions of the experiment) are comparable to those for the backwashing of Np(IV) with AHA. Therefore, Np(VI) is expected to be effectively backwashed along with Pu in a U/Pu split contactor.

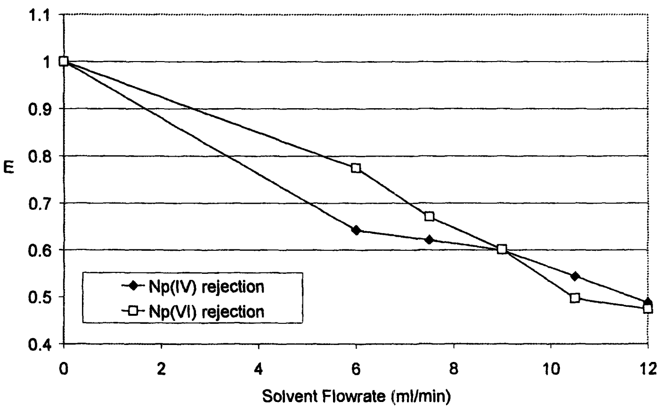

Figure 5. Comparison of Np(IV) and Np(VI) rejection rates in a single stage centrifugal contactor

Conclusions

Reducing the time taken for highly active waste from spent nuclear fuel reprocessing to decay to the radiotoxicity level of the uranium ore from which it was extracted is an important goal. In order to reduce this decay time by a factor of at least 100 it will be necessary to implement a P&T fuel cycle with very efficient (99.9%+) TRU recoveries. In order to direct Np away from the HAR in an aqueous Purex process it is necessary to extract the Np along with the U and Pu in the first solvent extraction cycle. Experimental work on neptunium recovery from uranium loaded solvent using complexant stripping of Np(IV) with AHA has shown that better than 99.9% Np recovery is possible by this means. Furthermore, Np(VI) reduction by AHA is not a limiting factor in the recovery of neptunium from the solvent, so that AHA might be used in an

Downloaded by UNIV OF ARIZONA on August 9, 2012 | http://pubs.acs.org
Publication Date: June 9, 2006 | doi: 10.1021/bk-2006-0933.ch006

advanced Purex process to produce either a pure Np product stream or a mixed Pu/Np product stream as required.

References

1. Denniss, I. S. and Jeapes, A. P., *Reprocessing irradiated fuel, The Nuclear Fuel Cycle: From Ore to Waste*, Ed. Wilson, P. D., OUP, UK, 1996.
2. Laidler, J. J.; Burris, L.; Collins, E. D.; Duguid, J.; Henry, R. N.; Hill, J.; Karell, E. J.; McDeavitt, S. M; Thompson, M.; Williamson, M. A.; Willit, J. L.; *Prog. Nuclear Energy*, **2001**, *38*, 65.
3. Madic, C.; Hudson, M. J.; Liljenzin, J. O.; Glatz, J. P.; Nannicini, R.; Facchini, A.; Kolarik, Z.; Odoj, R.; *EURATOM EU Report EU19149 EN*, **2000**.
4. Nomura, S.; Aoshima, A.; Koyama, T.; Myochin, M.; Global **2001**, Paris.
5. Taylor, R. J.; May, I.; Wallwork, A. L.; Denniss, I. S.; Hill, N. J.; Galkin, B. Ya.; Zilberman, B. Ya; Federov, Yu. S; *J. Alloys Comp.*, **1998**, *271-273*, 535.
6. Denniss, I. S.; Birkett, J. E.; May, I.; Gaubert, E.; Jobson, M.; Taylor, R. .J; Contribution P2-18, Atlante **2000**.
7. May, I.; Birkett, E.J; Denniss, I.S.; Gaubert, E. T.; Jobson, M.; Contribution 01-05, Atalante **2000**.
8. May, I; Taylor, R. J. and Brown, G.; *J. Alloys Comp.*, 1998, 271-273, 650.
9. Sidall, T. H. and Dukes, E. K., *J. Am. Chem. Soc.*, **1959**, *81*, 790.
10. Miles, J. H.; *Separation of Pu and U, Science and technology of TBP (Vol. III) Applications of TBP in nuclear fuel reprocessing, (Ed., W. W. Schulz, L. L. Burger, J. D. Navratil, K. P. Bender,* CRC Press Inc., Florida, 1990
11. Fox, O. D. and Taylor, R. J.; paper in preparation for submission to Solvent Extraction and Ion Exchange.
12. Fox, O. D. and Taylor, R. J.; *AIP Conf. Proc. Plutonium Futures*, **2003**, *673(1)*, 282.
13. Colston, B. J.; Choppin, G. R. and Taylor, R. J.; *Radiochim. Acta*, **2000**, *88*, 329.
14. Koltunov, V. S. and Tikhonov, M. F.; *Radiokhimiya*, **1977**, *19*, 611.

Downloaded by UNIV OF ARIZONA on August 9, 2012 | http://pubs.acs.org
Publication Date: June 9, 2006 | doi: 10.1021/bk-2006-0933.ch006

Downloaded by CORNELL UNIV on August 10, 2012 | http://pubs.acs.org
Publication Date: June 9, 2006 | doi: 10.1021/bk-2006-0933.ch007

Chapter 7

Haze Formation and Behavior in Liquid–Liquid Extraction Processes

Stuart T. Arm[1] and Jon A. Jenkins[2]

[1]**Pacific Northwest National Laboratory, 902 Battelle Boulevard, P.O. Box 999, Richland, WA 99352**
[2]**AEA Technology plc, 329 Harwell, Didcot, Oxfordshire OX11 0QJ, United Kingdom**

Aqueous haze formation and behavior was studied in the liquid-liquid system tri-n-butyl phosphate in odorless kerosene and 3M nitric acid with uranyl nitrate and cesium nitrate representing the major solute and an impurity, respectively. A pulsed column, mixer-settler and centrifugal contactor were chosen to investigate the effect of different turbulence characteristics on the manifestation of haze since these contactors exhibit distinct mixing phenomena. The dispersive processes of drop coalescence and breakage, and water precipitation in the organic phase were observed to lead to the formation of haze drops of ~1 μm in diameter. The interaction between the haze and primary drops of the dispersion was critical to the separation efficiency of the liquid-liquid extraction equipment. Conditions of high power input and spatially homogeneous mixing enabled the haze drops to become rapidly assimilated within the dispersion to maximize the scrub performance and separation efficiency of the equipment.

Introduction

This chapter describes the manifestation and significance of aqueous phase entrainment in the continuous organic phase of a liquid – liquid extraction process employed to separate uranium and plutonium from irradiated nuclear fuel. The most widely used liquid – liquid extraction process employs an extractant, tri-n-butyl phosphate (TBP) dissolved in an organic diluent to selectively extract uranium and plutonium from impurities dissolved in a nitric acid solution. Examples of diluent include dodecane, used in the USA and odorless kerosene (OK) used in the United Kingdom. An organic phase consisting of 20 volume percent TBP in OK (20% TBP/OK) contacted with 3M nitric acid was used throughout this work.

Downloaded by CORNELL UNIV on August 10, 2012 | http://pubs.acs.org
Publication Date: June 9, 2006 | doi: 10.1021/bk-2006-0933.ch007

Process Equipment for Liquid – Liquid Extraction

The entrainment characteristics of dispersed aqueous phase drops into the continuous organic phase product was expected to be affected by the turbulence structure within the dispersion. In turn, the turbulence structure is dependent upon the geometric and dynamic characteristics of the process equipment. Therefore, three types of liquid – liquid contactor commonly employed for irradiated fuel processing were studied and are described below.

The Gravity Mixer-Settler

The gravity mixer-settler is a discrete contactor that has been employed extensively from the earliest processing facilities. As illustrated in figure 1, it consists of a mixing chamber into which the aqueous and organic phases are fed. A dispersion of aqueous drops is formed by the action of an impeller. The dispersion flows over a weir and into the settling section where drops coalesce and settle by gravity. The length of the settler should be sufficient for drops to have settled out of the continuous phase.

The Centrifugal Contactor

Another discrete contactor is the centrifugal contactor, which is considered the base-line technology for future fuel processing facilities and is schematically illustrated in figure 2. The two liquid phases enter into an annulus bounded by the fixed contactor housing and an internal rotor that spins at several thousand revolutions per minute. The shear forces generated by the spinning rotor and the stationary vanes at the base produces the dispersion. It is in the annulus that the principal mass transfer takes place. The dispersion is then pumped up inside the rotor where the centrifugal forces facilitates separation of the dispersion into aqueous and organic phases. The separated phases pass over weirs, into their respective collector rings and thereby exit the contactor.

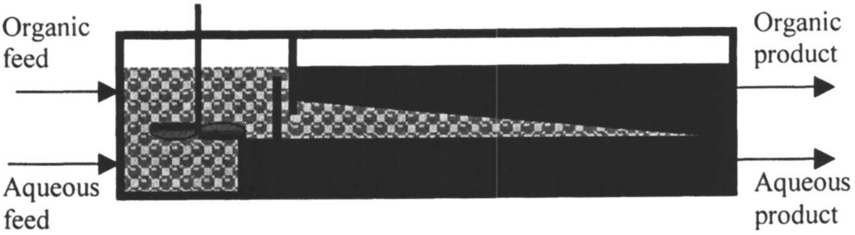
Organic feed
Aqueous feed
Organic product
Aqueous product

Figure 1. Schematic of the Gravity Mixer-Settler

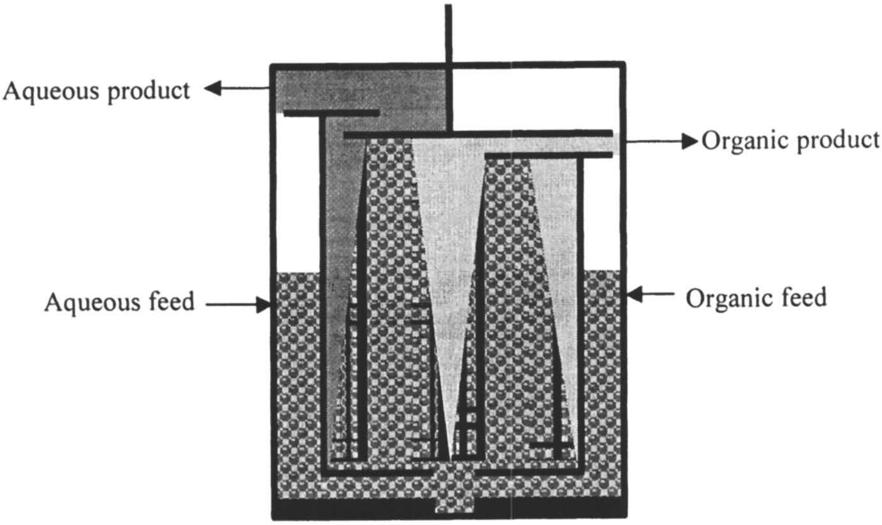
Aqueous product
Organic product
Aqueous feed
Organic feed

Figure 2. Schematic of the Centrifugal Contactor

Connection of Discrete Contactors

Discrete contactors are typically connected to provide countercurrent contact of the organic and aqueous phases. Haze formation and behavior was

Downloaded by CORNELL UNIV on August 10, 2012 | http://pubs.acs.org
Publication Date: June 9, 2006 | doi: 10.1021/bk-2006-0933.ch007

studied in a bank of centrifugal contactors consisting of both extraction and scrub sections. Figure 3 illustrates the process. In the extraction section of four contactors, aqueous feed is countercurrently contacted with the organic phase. For the PUREX process, uranium, plutonium and small quantities of fission products are extracted into the organic phase in the extraction section. The organic phase exits the extraction section and feeds the scrub section where it is countercurrently contacted with dilute (~0.1M) nitric acid to strip extracted fission products. The scrub section consists of eight contactors.

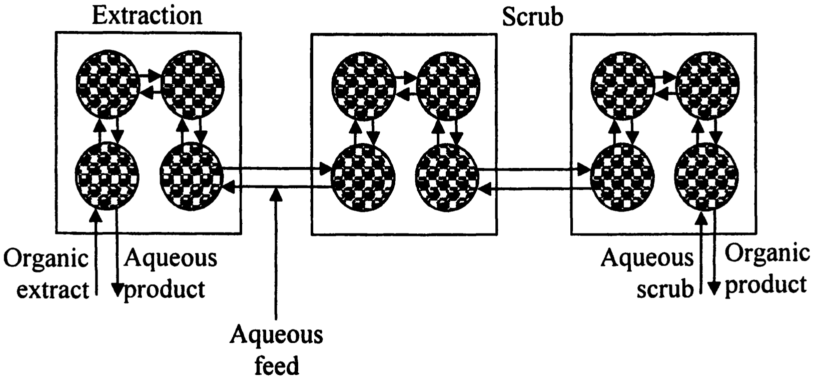

Figure 3. Countercurrent connection of discrete contactors

Downloaded by CORNELL UNIV on August 10, 2012 | http://pubs.acs.org
Publication Date: June 9, 2006 | doi: 10.1021/bk-2006-0933.ch007

The Pulsed Column

The pulsed column is a differential type of contactor employed in the most modern commercial irradiated fuel processing facilities (e.g. the Thermal Oxide Reprocessing Plant, operated by British Nuclear Fuels, plc.). The pulsed column, illustrated in figure 4, consists of a column containing an axial arrangement of perforated plates, top and bottom settlers and a pulse limb. The light, organic phase is fed just above the bottom settler and forms the continuous phase. The heavy aqueous phase enters below the top settler and forms the dispersed phase as it passes through the nozzles of the perforated plates. The pulse, applied to the continuous phase, provides the dynamic force for the dispersed phase to overcome the surface tension forces that would otherwise retain the heavy phase on the plates. Drops of the dispersed phase coalesce in the bottom settler before the heavy phase passes from the column. The height of the top settler should be sufficient for drops to settle from the continuous phase before it also passes from the column.

Extraction and scrub sections may be incorporated into a single pulsed column, as illustrated in figure 4. In this case, the organic feed enters the bottom of the column, the aqueous feed part way up and then the scrub feed enters at the top. Aqueous and organic products exit the column at the column's bottom and top, respectively.

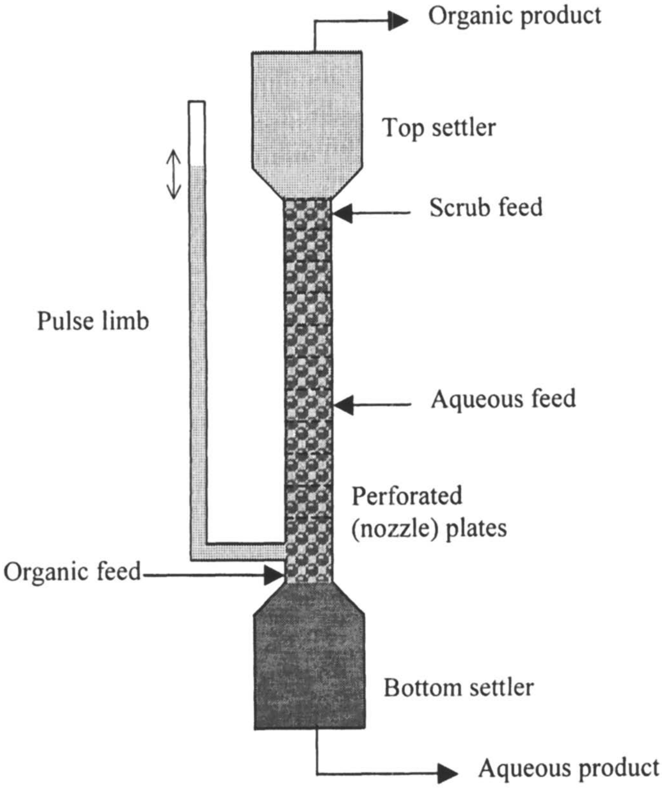
Organic product
Top settler
Scrub feed
Pulse limb
Aqueous feed
Perforated (nozzle) plates
Organic feed
Bottom settler
Aqueous product

Figure 4. Schematic of a pulsed column

Downloaded by CORNELL UNIV on August 10, 2012 | http://pubs.acs.org
Publication Date: June 9, 2006 | doi: 10.1021/bk-2006-0933.ch007

Hypotheses for Haze Formation and Behavior

This section defines haze and discusses hypotheses for its formation and behavior that can be compared to the phenomena experienced in actual process equipment.

Haze Formation

Haze Definition

For the purposes of this study, haze drops are defined as the secondary drops of a dispersion with diameters of approximately 1 μm since they will be most easily entrained into the continuous phase product. Primary drop breakage and water precipitation are the primary means of haze formation in the 20% TBP/OK – 3M nitric acid system.

Haze Formation by Primary Drop Breakage

Secondary or haze drops will be formed as the fluid inertial, or turbulent, forces overcome the surface tension forces constraining the primary drops such that they break apart. Turbulence consists of the apparently random motion of fluid eddies that act to generate shear forces across drops. As illustrated in figure 5, the eddy causes the drop to deform, generating a neck that breaks at a critical eddy size, as a result of Rayleigh instabilities, to produce primary and secondary drops.

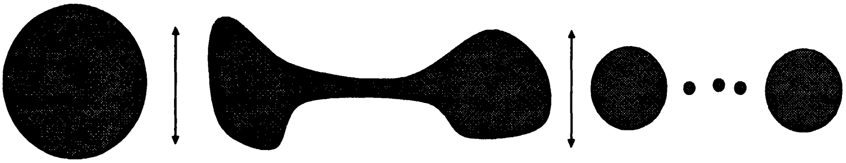

Figure 5. Illustrative Mechansim of Drop Deformation and Breakage

The size of the secondary drops can be approximately predicted by considering equations for thin film rupture and jet break-up. Ruckenstein and Jain (1) considered the Navier Stokes equations and intermolecular forces to derive the critical wavelength of perturbations that would rupture a free thin film,

$$\lambda_{crit} = h_d^2 \sqrt{\left(\frac{4\pi^3\gamma}{A_H}\right)} \qquad (1)$$

In equation 1, A_H is the Hamaker Constant (~10^{-20}J), h_d is the average film thickness (m) and γ is the interfacial tension (Nm^{-1}). In addition, Coyle et al. (2) derived the volume of a drop formed from a jet breaking as a result of Rayleigh

Downloaded by CORNELL UNIV on August 10, 2012 | http://pubs.acs.org
Publication Date: June 9, 2006 | doi: 10.1021/bk-2006-0933.ch007

instabilities, $v_d = \pi\lambda h_j^2$, where h_j is the jet radius (m) and λ is the wavelength of the disturbance. A wavelength, or eddy size, of size 45 μm is therefore calculated to create secondary drops of 1 μm diameter by putting $h_j = h_d$.

In the spectrum of eddy sizes, the smallest eddies have a size such that their Reynolds number is unity. On this basis, Kolmogoroff defined the length of the smallest eddy size, l_k, as

$$l_k = \left(\frac{\mu_c^3}{\rho_c^2 P_v} \right)^{1/4} \tag{2}$$

In equation 2, μ_c is the continuous phase viscosity (Nsm^{-2}), ρ_c is the continuous phase density (kgm^{-3}) and P_v is the power input per unit volume (Wm^{-3}), which is a characteristic operating parameter of the process mixing equipment. Therefore, the secondary drop size can be predicted from the operating characteristics of the process equipment. The value of P_v for a l_k of 45 μm is 2400 Wm^{-3} for the system 20% TBP/OK – 3M nitric acid.

Haze Formation by Precipitation

Haze drops are also formed in the organic phase by water precipitation as a result of metal extraction. The solubility of water in 20% TBP/OK decreases as the concentrations of extracted metals, particularly uranium, increases. Therefore, the organic phase becomes increasingly super-saturated in water as uranium extraction proceeds and this is relieved by precipitation of the excess water. In a combined extraction – scrub counter-current process, most haze drops will be precipitated close to the aqueous phase feed point.

Haze Behavior

Haze drops are important in considering the performance of liquid – liquid extraction processes because they act as 'sinks' for relatively inextractable metals and may become easily entrained into the organic phase product due to their small size. Entrainment into the organic phase becomes increasingly probable the larger the smallest turbulent eddies compared to the haze drops because the haze drops will exist in a viscous fluid regime. In a viscous fluid regime, the haze drops are more likely to follow the fluid streamlines around the primary drops than to collide and coalesce. An important concept in considering the contactor performance is to recognize that precipitated haze represents a

Downloaded by CORNELL UNIV on August 10, 2012 | http://pubs.acs.org
Publication Date: June 9, 2006 | doi: 10.1021/bk-2006-0933.ch007

deviation from the equilibrium drop dispersion generated from the drop breakage and coalescence processes. The rate at which the equilibrium dispersion is re-established after haze precipitation will depend upon the turbulence characteristics of the equipment.

Overview of Experimental Methods

Gravity Mixer-Settler Experiments

Gravity mixer-settler experiments were performed batch-wise in a baffled 200 mL capacity beaker. A Rushton type impeller provided fluid agitation with its speed measured by an optical tachometer. Experiments were performed by first adding the organic phase and then the aqueous phase beneath the organic phase by pipette. Agitation was initiated and continued for the desired time. The phases were allowed to separate for the desired time once agitation was terminated.

Downloaded by CORNELL UNIV on August 10, 2012 | http://pubs.acs.org
Publication Date: June 9, 2006 | doi: 10.1021/bk-2006-0933.ch007

Pulsed Column Experiments

Pulsed column experiments were performed in a pilot plant consisting of a glass column 11 m tall and 10 cm diameter packed with nozzle plates spaced 5 cm apart. The aqueous feed was introduced to the column 3 m below the scrub feed. Organic phase samples were extracted from the column using a sampler constructed from PTFE.

Centrifugal Contactor Experiments

Centrifugal contactor experiments were performed using a single contactor with a rotor 5.5 cm diameter and 12 cm tall providing a a mixing annulus 6.4 mm wide. Experiments were also performed in a pilot plant consisting of four extraction and eight scrub contactors. Sampling of the organic phase exiting each contactor was performed from a drain valve.

Analytical Techniques

Samples of the organic phase were analyzed by Karl Fischer titration for their dissolved and total (i.e. dissolved and entrained) water content. The dissolved water concentration was determined on a sub-sample from near the surface of the sample, after allowing entrained water to settle. The total water concentration was then determined by performing the titration on the entire sample.

The size distribution of drops entrained in the organic phase were analyzed using a Malvern Mastersizer laser spectrometer. Samples were analyzed for drop size distribution within a few minutes of them being taken.

Results from Gravity Mixer-Settler

Haze formation by drop breakage were expected from the gravity mixer-settler since the predicted power input was typically 1200 Wm^{-3} providing smallest eddies of size 50 μm. Some persistence of precipitated haze was expected since the turbulence energy is distributed in a spatially inhomogeneous manner. Figure 6 confirms these expectations. A first set of experiments were performed with organic and aqueous phases pre-equilibrated with uranium to investigate the formation of haze drops from drop breakage. Concentrations of entrained haze were approximately 0.04 volume% for mixing times up to 120 seconds. A further set of mass transfer experiments were performed to investigate haze precipitation. Figure 6 shows the concentration of entrained precipitated haze (the difference between the profiles) decreased from 0.08 volume% to 0.03 volume% for mixing times of 23 seconds to 120 seconds. The precipitated haze represents a deviation from the equilibrium drop dispersion and the latter becomes re-established as mixing progresses.

Figures 7 and 8 illustrate the results from the laser spectrometer for the mixing times of 23 and 120 seconds. Drops of diameter greater than approximately 8 μm are primary drops and will not be discussed further. The figures show a difference in the proportion of entrained haze drops, typically 1 μm diameter, generated in the presence and absence of mass transfer that diminishes as mixing progresses. The results from the laser spectrometer again illustrate the equilibrium drop dispersion becoming re-established as mixing progresses.

Results from the Pulsed Column

Precipitated haze was expected to persist through the scrub section of the column. The smallest eddy size of 150 μm generated from a power input of approximately 100 Wm^{-3} would not have generated haze drops by drop breakage. In addition, the precipitated haze drops exist in a viscous fluid regime and follow the fluid streamlines around the primary drops rather than undergoing coalescence.

Downloaded by CORNELL UNIV on August 10, 2012 | http://pubs.acs.org
Publication Date: June 9, 2006 | doi: 10.1021/bk-2006-0933.ch007

Downloaded by CORNELL UNIV on August 10, 2012 | http://pubs.acs.org
Publication Date: June 9, 2006 | doi: 10.1021/bk-2006-0933.ch007

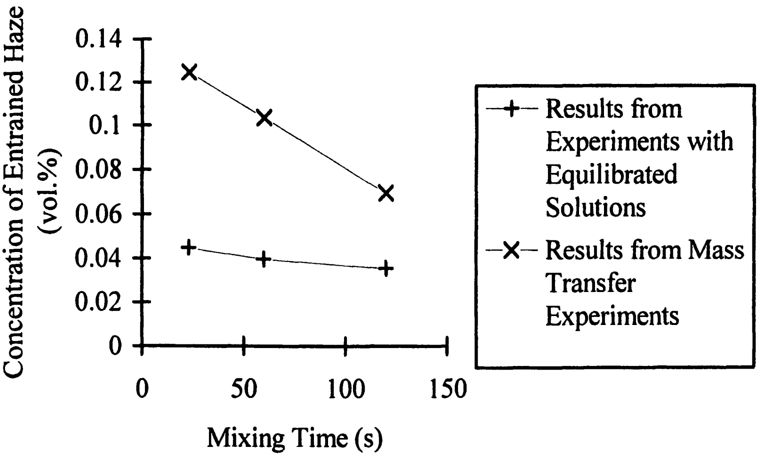

Figure 6. Concentration of Entrained Haze as a Function of Mixing Time

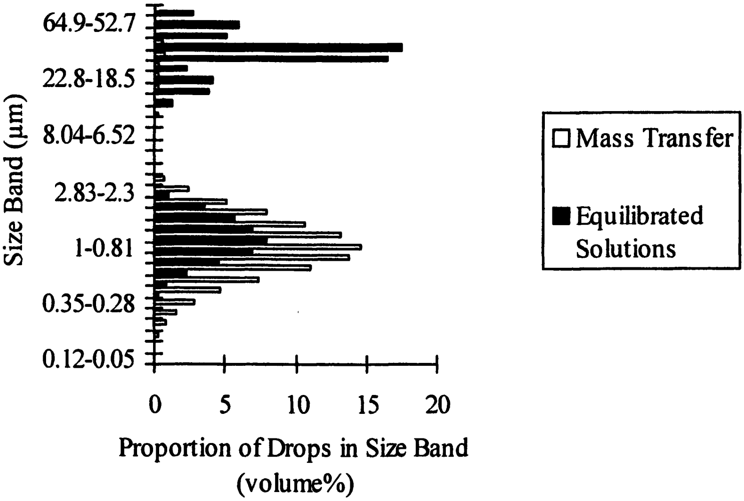

Figure 7. Entrained Drop Size Distribution in the Presence and Absence of Mass Transfer for a Mixing Time of 23 seconds

Figure 9 presents the dissolved and entrained water concentration profiles from the pulsed column pilot plant. The uranium bearing aqueous feed is introduced approximately 3 m below the scrub feed. The dissolved water concentration decreases through the extraction section as uranium is extracted into the organic phase. The dissolved water concentration remains constant through the scrub section since there is no uranium extraction into the organic phase. The concentration of entrained aqueous phase is negligible through the extraction section 5 m below the scrub feed. However, the concentration of entrained aqueous phase increases to approximately 0.1 volume% closer to the aqueous feed point, where most of the uranium mass transfer occurs, as haze is precipitated and entrained. There is a spike in the entrained aqueous phase concentration at the aqueous feed point but this is considered mainly constituted of bulk aqueous phase entrained directly into the sample from the aqueous feed distributor. In the scrub section, the concentration of entrained aqueous phase remains constant at approximately 0.1 volume% indicating the persistence of haze precipitated close to the aqueous feed point.

Downloaded by CORNELL UNIV on August 10, 2012 | http://pubs.acs.org
Publication Date: June 9, 2006 | doi: 10.1021/bk-2006-0933.ch007

Results from the Centrifugal Contactor

Haze formation from drop breakage was expected to be significant in the centrifugal contactor since the smallest eddies generated from a power input of 40,000 Wm^{-3} were predicted to be approximately 20 μm diameter. The precipitated haze was expected to become rapidly assimilated with the haze drops formed by drop breakage since the mixing energy is concentrated into a small volume.

Figure 10 illustrates the size distribution of drops entrained from the centrifugal contactor in the absence of mass transfer. Drops of size greater than approximately 8 μm again represent the primary drops and are not discussed further. The figure clearly shows the generation and entrainment of haze from drop breakage. The haze drops become smaller with increasing rotor speed and, therefore, decreasing eddy size.

Haze entrainment is further illustrated in figure 11 as a function of rotor speed. At low rotor speeds, haze entrainment slightly decreases as the rotor speed is increased, which can be attributed to improved phase separation due to increased centrifugal forces inside the rotor. However, improving phase separation at higher rotor speeds is less significant than the increasing mixing intensity in generating smaller drops that are harder to separate. Therefore, the entrained haze concentration increases with increasing rotor speed at higher speeds.

Downloaded by CORNELL UNIV on August 10, 2012 | http://pubs.acs.org
Publication Date: June 9, 2006 | doi: 10.1021/bk-2006-0933.ch007

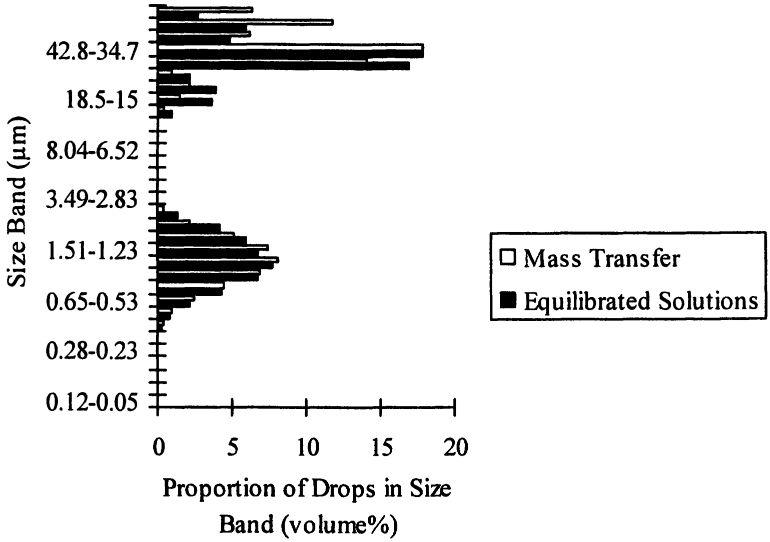

Figure 8. Entrained Drop Size Distribution in the Presence and Absence of Mass Transfer for a Mixing Time of 120 seconds

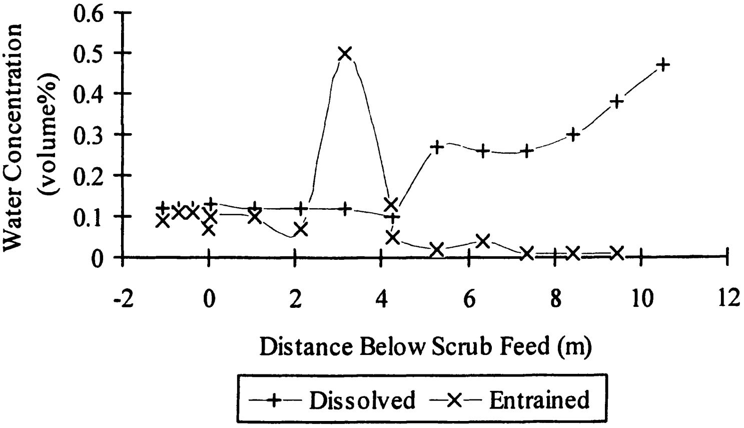

Figure 9. Water Concentration Profiles from the Pulsed Column Pilot Plant

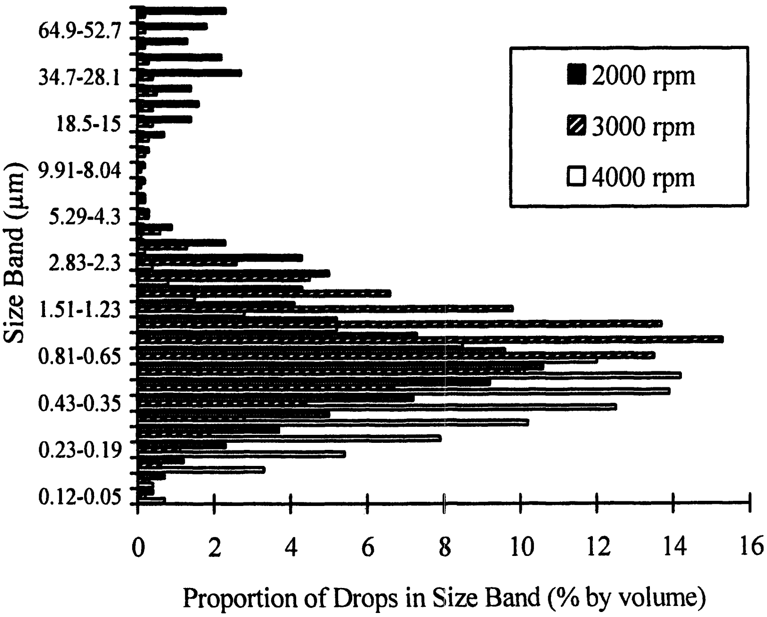

Figure 10. Size Distribution of Entrained Aqueous Drops in the Centrifugal Contactor (no mass transfer)

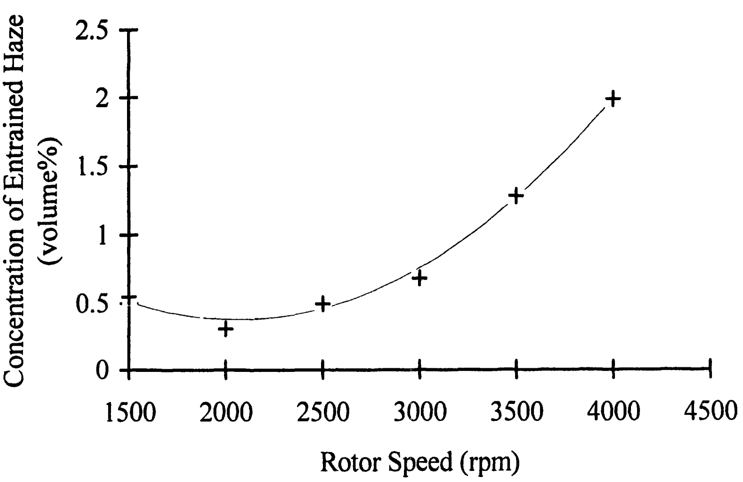

Figure 11. Entrained Haze in the Centrifugal Contactor as a Function of Rotor Speed

Downloaded by CORNELL UNIV on August 10, 2012 | http://pubs.acs.org
Publication Date: June 9, 2006 | doi: 10.1021/bk-2006-0933.ch007

Figure 12 illustrates the profiles of dissolved and entrained water in the centrifugal contactor pilot plant. As in the pulsed column, the concentration of dissolved water decreased in the extraction section as uranium was extracted into the organic phase. As expected, there was no evidence of precipitated haze entrained into the organic phase product from the fourth stage where most of the uranium mass transfer occurred. The concentration of entrained haze increased in each of the scrub stages presumably due to contactor hydrodynamics since no significant mass transfer occurs throughout this section. However, the reason for this phenomenon is not readily explained. These results demonstrate the importance of haze generated from drop breakage for centrifugal contactors and that precipitated haze is an insignificant contributor to entrainment.

Downloaded by CORNELL UNIV on August 10, 2012 | http://pubs.acs.org
Publication Date: June 9, 2006 | doi: 10.1021/bk-2006-0933.ch007

Implications of Haze Entrainment for Organic Phase Product Purity

The major source of impurities in the organic phase product are in the entrained haze drops because they act as 'aqueous sinks' in which the impurities are dissolved. The mechanism by which these impurities are scrubbed from the organic phase depends upon the haze behavior and, therefore, the mixing intensity in the contactor.

Haze drops fully participate in the drop dispersal and coalescence processes in contactors for which the power input is greater than approximately 1000 Wm^{-3} (i.e. centrifugal contactors and gravity mixer-settlers). Impurities dissolved in the entrained drops are successively mixed with the bulk aqueous phase in each stage. Therefore, the concentration of impurities in the organic phase is successively reduced by dilution.

For pulsed columns and other contactors with power inputs less than approximately 1000 Wm^{-3}, haze drops are only formed by precipitation and they do not participate in the drop dispersal and coalescence processes. The concentration of impurities in the haze drops can only be reduced by mass transfer through the organic phase and into the scrub aqueous phase. However, such mass transfer is insignificant due to the low extractability of impurities into the organic phase and the low bulk interfacial area of scrub drops. Therefore, haze drops and their impurity content persist through the scrub section into the organic phase product.

Conclusions

The formation and behavior of aqueous hazes is determined by the mixing characteristics of the contactor type.

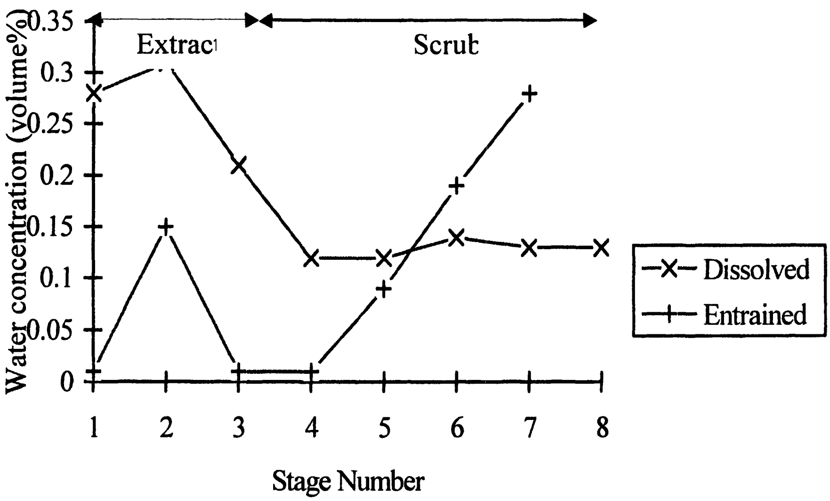

Figure 12. Entrained and dissolved water concentration profiles from the centrifugal contactor pilot plant

- Haze drops are generated from primary drop breakage in contactors of high mixing intensity, such as centrifugal contactors and gravity mixer-settlers. In addition, haze is precipitated in all equipment when water supersaturation in the organic phase is relieved during uranium extraction.
- Precipitated haze drops persist in a laminar flow environment in contactors of low mixing intensity, such as pulsed columns. In contactors of high mixing intensity, the haze drops fully participate in the drop dispersal and coalescence processes.

Other aspects of this work has focused on the impact of haze entrainment on product purity by measuring the concentrations of impurities (e.g. cesium) in haze drops and the organic phase. These results show the purity of the organic phase product is largely determined by the presence of entrained aqueous hazes because they act as 'sinks' for impurities of low extractability.

- The impurity content of haze drops is reduced by dilution with the bulk aqueous phase in contactors of high mixing intensity.
- In contactors of low mixing intensity, there is no significant reduction in the impurity concentration.

Downloaded by CORNELL UNIV on August 10, 2012 | http://pubs.acs.org
Publication Date: June 9, 2006 | doi: 10.1021/bk-2006-0933.ch007

References

1. Ruckenstein, E.; Jain, R. K. Spontaneous Rupture of Thin Liquid Films. J. Chem. Soc., Faraday Trans. II **1974**, *70*.
2. Coyle, R.W.; Berg, J.C.; Niwa, J.C. Liquid-liquid Jet Break-up Under Conditions of Relative Motion, Mass Transfer and Solute Adsorption. Chem. Eng. Sci. **1981**, *36*.

Downloaded by CORNELL UNIV on August 10, 2012 | http://pubs.acs.org
Publication Date: June 9, 2006 | doi: 10.1021/bk-2006-0933.ch007

Downloaded by STANFORD UNIV GREEN LIBR on August 9, 2012 | http://pubs.acs.org
Publication Date: June 9, 2006 | doi: 10.1021/bk-2006-0933.ch008

Chapter 8

Comparison of Uranyl Third-Phase Formation in 30% TBP–Nitric Acid in Dodecane and HPT Using UV-Visible Spectroscopy

J. Plaue[1], S. Goeury[2], J. Petchsaiprasert[2], M. Draye[3], J. Foos[3], and K. Czerwinski[2,3]

[1]Defense Nuclear Facilities Safety Board, 625 Indiana Avenue, NW, Suite 700, Washington, DC 20004
[2]Department of Chemistry, University of Nevada at Las Vegas, 4505 Maryland Parkway, Las Vegas, NV 89154–4003
[3]Conservatoire National des Arts et Métiers, 11 Rue Pierre et Marie Curie, 75005 Paris, France

Third phase formation behavior was studied in the uranyl / 30% tri-*n*-butyl phosphate/high molar nitric acid system. Using metal ion titration coupled with UV-visible spectroscopy, a comparison was made between the diluents dodecane and hydrogenated polypropylene tetramer (HPT). This work presents the first quantitative comparison of dodecane with HPT, which is commonly used in the French reprocessing program. As anticipated, higher metal loading prior to third phase formation was observed in the HPT system due to the branched configuration of the diluent. Spectral evidence of differences in speciation between each phase, as well as a change in the single organic phase speciation prior to phase splitting is presented.

In Separations for the Nuclear Fuel Cycle in the 21st Century; Lumetta, G., et al.;
ACS Symposium Series; American Chemical Society: Washington, DC, 2006.

Introduction

There exists a lack of quantitative information regarding third phase formation in solvent extraction systems. Historically, the primary methods relied upon determination of the phase split boundary though visual identification. This process has been shown to be error prone and has resulted in inconsistencies across the literature (*1*). This chapter attempts to quantitatively dissect third phase formation using ultraviolet-visible spectroscopy. While general spectroscopic studies of the third phase have been performed previously, this work utilized multiple spectroscopic titrations to elucidate changes in the speciation of uranium as the third phase is formed. In addition, a comparison is made between the diluents *n*-dodecane and hydrogenated polypropylene tetramer (HPT). Branched hydrocarbons, such as HPT, have been reported to have higher resistance to third phase formation, and are commonly used in the French reprocessing industry. Little published data is available on the behavior or composition of HPT, however it is commonly assumed to be a branched dodecane. While the range of acid conditions studied is limited and under non-typical conditions, they are important to understanding the system chemistry and can be applied to off-normal plant scenarios.

Downloaded by STANFORD UNIV GREEN LIBR on August 9, 2012 | http://pubs.acs.org
Publication Date: June 9, 2006 | doi: 10.1021/bk-2006-0933.ch008

Third phase formation is the phenomenon in which the organic phase of a normal two-phase solvent extraction systems splits into heavy and light phases, thereby creating a three-phase system. Historically, the study of third phase formation in solvent extraction systems has exclusively focused on defining the boundaries where it may occur. Typically, results are reported as limiting organic concentrations (LOC), which is the maximum concentration of metal found in the organic phase prior to a visual observation of phase splitting. Although the effects of several variables (nitric acid and extractant concentrations, temperature, diluent and, extractant types, and ionic strength) have been studied on the formation boundaries (*2-5*), very little progress has been made on the formation mechanism or characterization of third phase species. A complete understanding of the third phase phenomenon is important from a process safety perspective. Serious upsets, such as criticality or runaway reactions, can result from third phase formation.

Uranyl third phase formation has been the focus of renewed studies (*6-7*). Unique spectra were identified for the third phase, while the normal organic phase spectra closely resembled that of the light organic phase. These results suggested an abrupt change in the uranyl speciation rather than the progressive buildup of insoluble organic complexes. However, these UV-Visible spectroscopy results contradicted several other reports tending to show third phase formation as the result from an aggregation-type process (*8-9*). The primary evidence for this conclusion is based upon small angle neutron scattering measurements indicating the presence of reverse micelle which interact more strongly with increasing organic metal concentration. These techniques were initially developed for other systems involving other extractants (*10-11*), but the results in the TBP systems have lead to various models for prediction of third phase formation (*12-13*). This chapter does not attempt to propose a unique model, but rather add to the small body of work on this topic, especially with respect to the diluent HPT.

Downloaded by STANFORD UNIV GREEN LIBR on August 9, 2012 | http://pubs.acs.org
Publication Date: June 9, 2006 | doi: 10.1021/bk-2006-0933.ch008

Methods

Stock solutions of uranyl nitrate were prepared at constant nitric acid concentration by dissolution of known quantities of $UO_2(NO_3)_2 \cdot 6H_2O$ (Merck) in nitric acid solutions. Organic extraction phases were prepared using 30 vol. % tri-*n*-butyl phosphate (Aldrich 97 %) with respective diluents; *n*-dodecane (Prolabo) and hydrogenated polypropylene tetramer (Novasep SAS, France). The conditions examined are given in Table 1. All work was performed at room temperature of approximately 22 °C. Equal volumes (4 – 7 mL) of organic and aqueous phases were contacted and vigorously mixed for a period of 10 minutes using a wrist action shaker. After centrifuging, samples of each phase were drawn off and

Downloaded by STANFORD UNIV GREEN LIBR on August 9, 2012 | http://pubs.acs.org
Publication Date: June 9, 2006 | doi: 10.1021/bk-2006-0933.ch008

spectra taken using a Cary 5E UV-visible spectrometer with precision quartz cuvettes (1 cm path length) measured against a deionized water reference cell. Four sets of spectra were collected for each sample and the average used in analysis performed with Microsoft Excel™ software. Samples were returned, and a small volume of aqueous uranyl ion was titrated into the system at constant acid molarity. Phase volumes were determined by mass using density measurements. Using this methodology, spectral evidence of third phase behavior was collected before and after phase separation was observed. Extinction coefficients for aqueous phase uranyl nitrate were determined using laboratory prepared samples. Acid concentration in each phase was determined by titration with a Metrohm titration apparatus. The organic phase was washed twice with water to remove the acid, and oxalate was added to the aqueous phase to bind the uranium and prevent complexation with hydroxide during the titration. Material balance calculations enabled determination of total organic phase metal content, from which extinction coefficients for the light and heavy organic phases were determined.

Table 1. Experimental conditions

Diluent	*$[HNO_3]$ M*	*$[UO_2^{2+}]_{aq}$ M*
Dodecane	11, 11.5, 12, 13, 14, 14.2	0-0.65
HPT	12, 13, 14	0.1-0.75

Results and discussion

Organic acid phase concentration

The titration data showed a distinct change in organic phase acid concentration upon third phase formation. In the presence of a single organic phase, the acid concentration in the organic phase tends to increase with increasing aqueous acid concentration in the absence of uranium (Table 2). For comparison purposes, the experimental distribution values are compared to model predictions using the Argonne Model for Universal Extraction (AMUSE) (14). When uranium is present in the system, a decrease in the single phase organic acid concentration with increasing uranium organic phase concentration is observed (Table 3).

The data presented in Table 3 provide averages of the measured nitric acid concentration under set phase conditions. Additional measurements taken as the system was loaded with uranium indicate trends. In the single organic phase, the organic nitric acid concentration is observed to decrease on approach of the phase split. Upon phase splitting, there is a pronounced decrease in organic nitric acid concentration in the light phase. Further measurements taken as uranium is added to the system show a decrease in the light organic phase acid concentration. However, the heavy organic phase experiences a dramatic increase in nitric acid concentration. The total acid concentration in the heavy phase is generally higher than any other organic phase conditions, particularly at higher total acid concentrations. This behavior indicates a minimum nitric acid concentration is required for the formation of the heavy organic phase under a set of given initial conditions. These observations are seen for both the dodecane and HPT systems studied.

For both the dodecane and HPT organic phases, the nitric acid distribution increases with increasing total nitric acid concentration. This trend differs with the nitric acid distribution in the absence of uranium (Table 2), where the distribution decreases and reaches a minimum with increasing total nitric acid concentration. For the single and light phase there is a similar decrease in acid distribution with increasing uranium concentration at a given initial nitric acid concentration. However, as shown in Figure 1, differences between the nitric acid distributions for the organic diluents are evident. For the dodecane, the heavy organic phase has a higher nitric acid distribution compared to the HPT systems, indicating a lower acid concentration in the HPT

Downloaded by STANFORD UNIV GREEN LIBR on August 9, 2012 | http://pubs.acs.org
Publication Date: June 9, 2006 | doi: 10.1021/bk-2006-0933.ch008

Table 2. Nitric acid concentrations in mol/L for single organic phase in dodecane with no uranium

$[HNO_3]_{aq\ int}$	*$[HNO_3]_{org}$*	*$[HNO_3]_{org}/[HNO_3]_{aq}$*	*AMUSE*
8	1.09±0.08	0.157	0.170
9	1.12±0.07	0.142	0.163
10	1.20±0.02	0.136	0.157
11	1.20±0.01	0.122	0.155
12	1.30±0.01	0.121	0.153
13	1.39±0.01	0.120	0.150
14	1.51±0.03	0.121	0.146
14.2	1.55±0.03	0.120	0.145

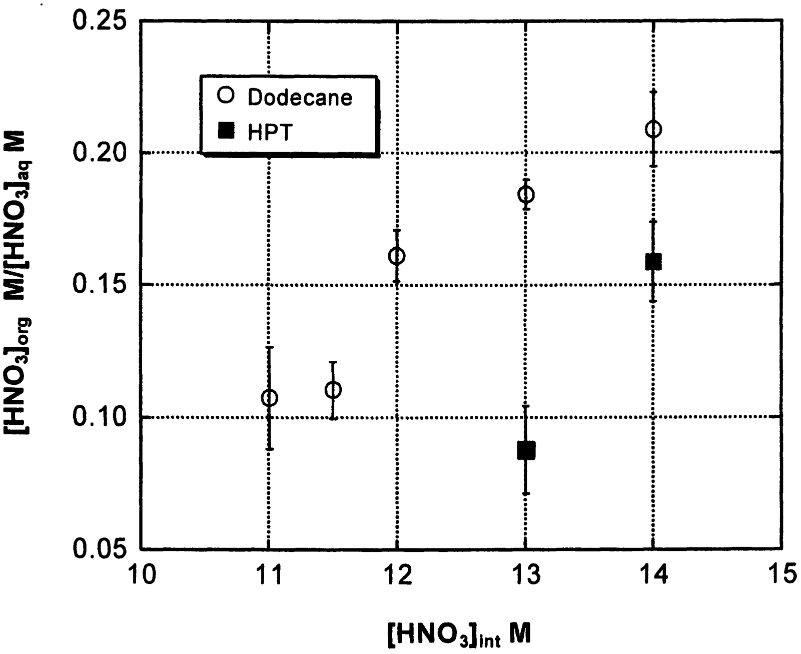

Figure 1. Nitric acid distribution between the heavy organic phase and aqueous phase for dodecane and HPT diluents as a function of total nitric acid concentration.

Downloaded by STANFORD UNIV GREEN LIBR on August 9, 2012 | http://pubs.acs.org
Publication Date: June 9, 2006 | doi: 10.1021/bk-2006-0933.ch008

Downloaded by STANFORD UNIV GREEN LIBR on August 9, 2012 | http://pubs.acs.org
Publication Date: June 9, 2006 | doi: 10.1021/bk-2006-0933.ch008

Table 3. Average organic phase nitric acid concentration in mol/L for dodecane diluent in the presence of uranium. The uranium concentration is 110% of the LOC for the nitric acid concentration

Aqueous	*Single phase*	*Heavy phase*		*Light phase*	
$[HNO_3]$	$[HNO_3]$	$[HNO_3]$	$[UO_2^{2+}]$	$[HNO_3]$	$[UO_2^{2+}]$
11	0.65±0.17	1.07±0.15	0.381±0.021	0.384±0.048	0.0968±0.009
11.5	0.84±0.08	1.23±0.11	0.343±0.018	0.474±0.211	0.0502±0.0048
12	1.14±0.04	1.93±0.10	0.193±0.008	0.797±0.157	0.0177±0.0016
13	1.44±0.11	2.42±0.14	0.0791±0.0068	0.762±0.167	5.06±0.81E-3
14	1.31±0.15	2.93±0.18	0.0200±0.0017	0.026±0.024	1.88±0.21E-3

third phase. As apparent in the comparison of the uranium concentration described below, the acid behavior is opposite of the uranium behavior, where the formation of the HPT third phase requires a higher uranium concentration.

Organic uranium phase concentration

The uranium concentration in the organic phase was observed to increase with increasing total uranium concentration, regardless if the organic is composed of a single phase or two phases. For the two phase organic condition, there is a noticeable difference in the uranium concentration and increase due to total uranium present (Figure 2). For the single phase system, the expected increase in organic uranium concentration is consistent with the expected distribution behavior. This trend is continued with the heavy organic phase upon formation of the second phase. The light phase exhibits only the slightest organic uranium concentration increase. These observations are consistent with all the conditions examined, including both HPT and dodecane diluents.

As previously stated, the organic uranium behavior differs from the observed nitric acid organic phase behavior for the heavy and light organic phases. This appears to indicate a radical difference in the extracted uranium species in the heavy and light phase. However, if the ratio of organic acid to uranium is evaluated, similarities between the light and heavy organic phase are recognizable (Figure 3). The ratio decreases with increasing total uranium for both the light and heavy organic phases. Furthermore, the ratio values are similar with the largest differences at outset of the phase splitting. For all systems examined, the acid to uranium ratio of the two organic phases converge under the highest total uranium initial concentrations. This indicates there are similarities between the extracted organic uranium species in each phase. At the initial onset of third phase it appears the heavy phase has a relatively larger acid concentration. This can be attributed to the extraction of nitric acid by either uncomplexed TBP or

Downloaded by STANFORD UNIV GREEN LIBR on August 9, 2012 | http://pubs.acs.org
Publication Date: June 9, 2006 | doi: 10.1021/bk-2006-0933.ch008

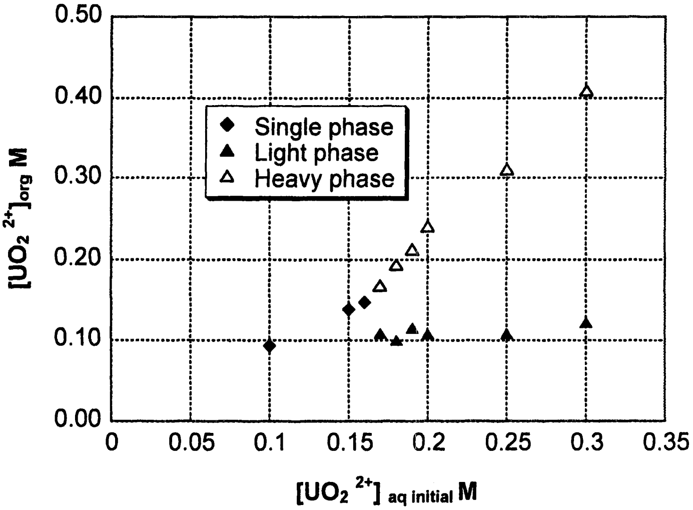

Figure 2. Organic uranium concentration for the 12 M HNO_3/30 % TBP in dodecane system

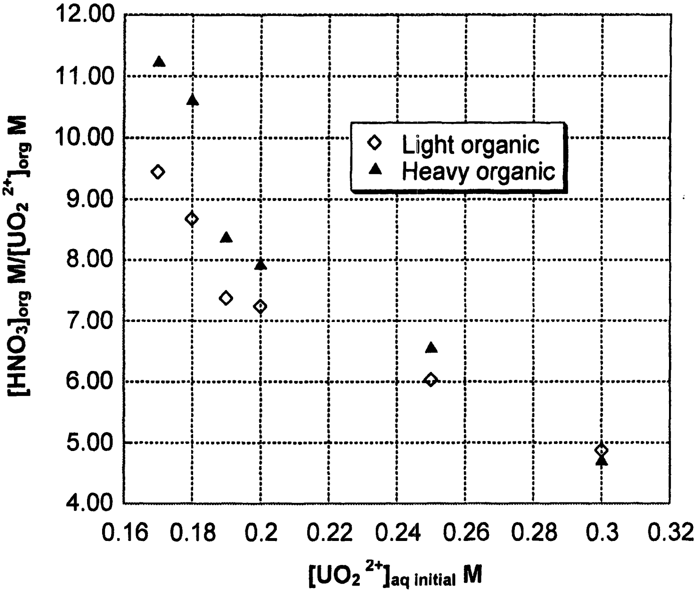

Figure 3. Organic acid to uranium concentration ratio for the light and heavy organic phase in the 12 M HNO_3/30 % TBP in dodecane system

Downloaded by STANFORD UNIV GREEN LIBR on August 9, 2012 | http://pubs.acs.org
Publication Date: June 9, 2006 | doi: 10.1021/bk-2006-0933.ch008

through the extracted uranium organic moiety. As the overall uranium concentration is increased, both phases exhibit a similar response in the acid to uranium ratio. As the organic phases begin to become saturated with uranium, the relative difference between the phases is minimized; indicating phase separations are driven by intramolecular characteristics.

Spectral Features and Trends

Overall, the spectra collected here closely resemble the literature for uranyl nitrate in tributyl phosphate systems (*15*). Significant maxima were observed at 403, 414, 425, 437 and 452 nm. The spectra in HPT appear to have more pronounced peaks, especially for wavelengths greater than 415 nm. The prominent difference between the diluents is a deepening of the minima at 420 and maxima at 425 nm as compared to the peak absorbance at 415 nm. The maximum at 485 nm is also more visible in the HPT system. An interesting spectroscopic feature is observed at 492 nm (Figure 4). A peak is present for the single and heavy organic phase, but is nearly absent for the light organic phase. This indicates a pre-existing species is in the single phase that dominates the heavy phase when it is formed. This observation can support the formation of micelles leading to the development of the organic phase split. The molar absorptivities for the different phases are determined from the spectroscopic data (Table 4). There is very little difference between the different diluents. However, a larger molar absorptivity is observed in the heavy phase with each diluent.

Further evidence of spectral change, particularly between 420 nm and 480 nm, as a function of metal loading is provided in

Downloaded by STANFORD UNIV GREEN LIBR on August 9, 2012 | http://pubs.acs.org
Publication Date: June 9, 2006 | doi: 10.1021/bk-2006-0933.ch008

Downloaded by STANFORD UNIV GREEN LIBR on August 9, 2012 | http://pubs.acs.org
Publication Date: June 9, 2006 | doi: 10.1021/bk-2006-0933.ch008

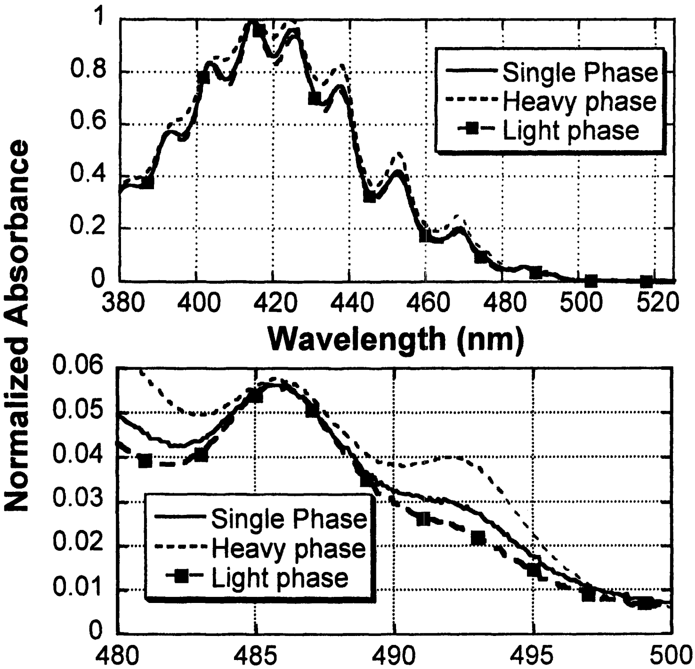

Figure 4. Absorbance spectra for the 14 M HNO_3/30% TBP in HPT system

Table 4. Molar Absorptivities (L $mol^{-1}cm^{-1}$) for the organic phases with uranium

Diluent	*Phase*	*414 nm*	*425 nm*	*437 nm*	*452 nm*
Dodecane	Light	10.9±1.0	10.1±0.8	7.65±0.56	3.92±0.31
Dodecane	Heavy	11.3±1.0	11.3±0.9	9.14±0.80	4.84±0.48
HPT	Light	10.7±0.8	9.87±0.71	7.51±0.37	3.91±0.29
HPT	Heavy	12.0±1.0	12.0±1.0	9.72±0.82	5.51±0.45

Figure 5. When evaluating the spectroscopic minimum at 420 nm, a subtle but progressive decrease in absorbance is observed as the system approaches the phase split point, followed by a continued decrease in light phase absorbance. At approximately 30 % above and below the visual split point, the behavior becomes stable. It is clear that within this region, the extinction coefficients are deviating from the single phase for the resulting heavy and light organic phases and subsequently provide evidence of progressive changes in the uranyl chemical environment upon third phase formation. Furthermore, the extracted uranium species, either through the addition of nitric acid or intramolecular interaction, are different, not only between the heavy and light phases, but also between the normal and light phases. Previous investigations have disagreed on the speciation of uranyl in the heavy phase. Boukis and Solovkin (*5,16*) both suggest spectral evidence of the uranyl trinitrato species, $H[UO_2(NO_3)_3] \cdot 2TBP$, in the third phase. However, others (*8*) have dismissed this evidence as inconclusive and instead suggest an average composition with consistent stoichiometry, but different coordination denoted as the extended disolvate; $UO_2(NO_3)_2 \cdot 2TBP \cdot HNO_3$.

Third phase susceptibility is graphically compared for the two diluents studied in Figure 6. Both diluents follow the same general trend of decreasing loading with increasing acid concentration. Overall, the results indicate substantially better performance for the branched HPT ranging from approximately two to six times higher loading for the acid concentrations studied.

Conclusions

Differences in the chemical composition of the resulting organic phases due to phase splitting were observed for 30% TBP with dodecane and HPT as diluents. A strong variation in the acid concentration between the single organic phase, light organic phase, and heavy organic phase was observed. The acid

Downloaded by STANFORD UNIV GREEN LIBR on August 9, 2012 | http://pubs.acs.org
Publication Date: June 9, 2006 | doi: 10.1021/bk-2006-0933.ch008

Downloaded by STANFORD UNIV GREEN LIBR on August 9, 2012 | http://pubs.acs.org
Publication Date: June 9, 2006 | doi: 10.1021/bk-2006-0933.ch008

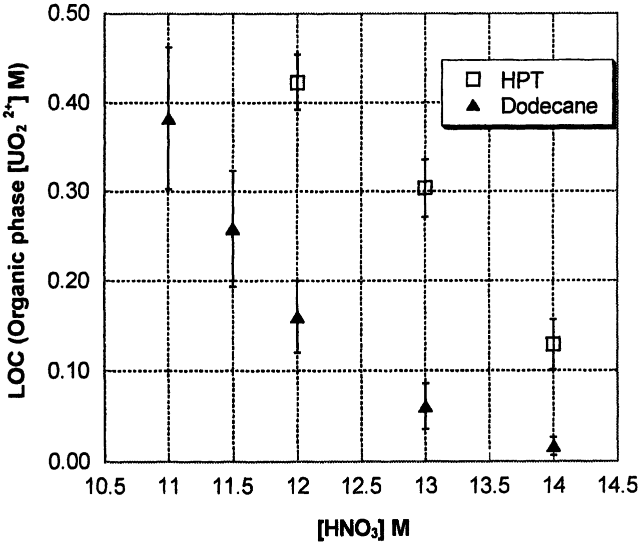

Figure 5. Trends observed at the 420 nm minima in 13 M HNO_3 systems

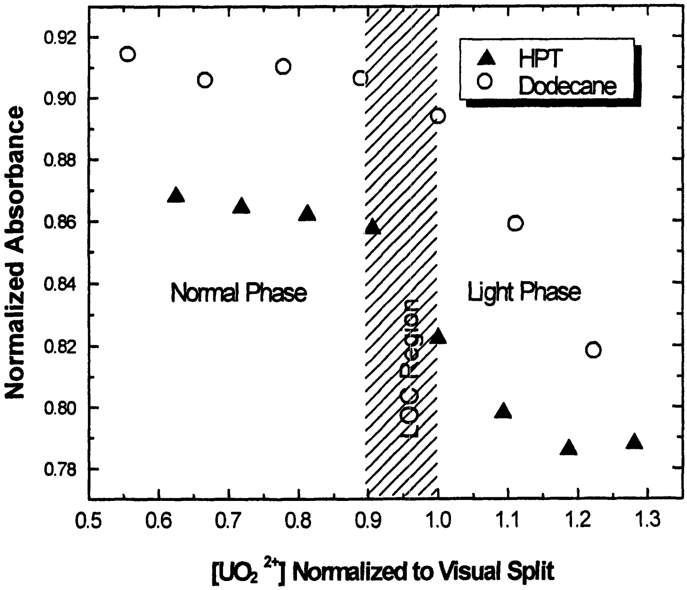

Figure 6. Comparison of LOC in dodecane and HPT

concentration of the heavy organic phase was consistently found to be greater than the light phase or the single phase in the presence of uranium at a constant total acid concentration and offers a method for the determination of third phase formation. This trend was also observed with the organic uranium concentration. Similarities were observed with the ratio of nitric acid to uranium for the light and heavy phases. The main difference was observed in conditions immediately after third phase formation, where the acid ratio for the heavy phase was higher, supporting an acidic extracted uranium complex as the third phase species. However, upon high uranium loading, the ratio differences between the phases disappeared. Variations in the UV-visible absorbance between the phases was noted and demonstrated as a method for identification of third phase formation. The spectroscopic data provided molar absorptivities for uranyl in the light and heavy phase. The LOC results show that HPT requires a higher uranyl concentration to form the third phase than dodecane. However, this initial result with uranium must be examined in the plutonium system for an evaluation of benefits of HPT in an extraction process.

Downloaded by STANFORD UNIV GREEN LIBR on August 9, 2012 | http://pubs.acs.org
Publication Date: June 9, 2006 | doi: 10.1021/bk-2006-0933.ch008

**Disclaimer

The views expressed are solely those of the author and no official support or endorsement of this article by the Defense Nuclear Facilities Safety Board or the federal government is intended or should be inferred.

Acknowledgements

The authors wish to acknowledge the useful discussions and donation of diluent by Dr. Christophe Moulin. Additionally, the authors thank Dr. Candido Pereira and Dr. Artem Gelis for their assistance with the AMUSE predictions. Partial financial support

for this work is from Conservatoire National des Arts et Métiers, Paris, France.

References

1. Rao, P.R.; Kolarik, Z. *Solvent Extr. Ion Exch.*, **1996**, 14(6), 955-993.
2. Mills, A.L. *Solvent Ext. Chem.*, **1967**, 322-326.
3. Mason, C.; Thompson, R.; Tolchard, A.C. *I. Chem. E. Symposium Series,* **1987**,103, 75-85.
4. Horner, D.E. ORNL-4724, Oak Ridge National Laboratory, Oak Ridge, TN, 1971.
5. Boukis, N.; Kanellakopulos, B. Kernforschungszentrum Karlsruhe, Germany, June 1983.
6. Jensen, M. P.; Chiarizia, R.; Ferraro, J. R.; Borkowski, M.; Nash, K. L.; Thiyagarajan, P; Littrell, K. C. In *Proc. Internat. Solv. Extr. Conf. ISEC 2002,* Sole K. C., Cole P. M., Preston J. S., Robinson D. J., Eds.; S. African Inst. Mining and Metallurgy, **2002**, 1137-1142.
7. Borkowski, M.; Ferraro, J. R.; Chiarizia, R.; McAllister, D. R. *Solvent Extr. Ion Exch.*, **2002**, 20(3), 313-330.
8. Chiarizia, R.; Jensen, M. P.; Borkowski, M.; Ferraro, J. R.; Thiyagarajan, P; Littrell, K. C. *Solvent Extr. Ion Exch.*, **2003**, 21(3), 423-433.
9. Chiarizia, R.; Jensen, M. P.; Borkowski, M.; Ferraro, J. R.; Thiyagarajan, P; Littrell, K. C. *Sep. Sci. Technol.*, **2003**, 38, 3313-3331.
10. Erlinger, C.; Belloni, L.; Zemb, Th.; Madic, C. *Langmuir*, **1999**, 15, 2290-2300.
11. Erlinger, C.; Gazeau, D.; Zemb, T.; Madic, C.; Lefrançois, L.; Hebrant, M.; Tondre, C. *Solvent Extr. Ion Exch.,* **1998**, 16, 707-738.

Downloaded by STANFORD UNIV GREEN LIBR on August 9, 2012 | http://pubs.acs.org
Publication Date: June 9, 2006 | doi: 10.1021/bk-2006-0933.ch008

Downloaded by STANFORD UNIV GREEN LIBR on August 9, 2012 | http://pubs.acs.org
Publication Date: June 9, 2006 | doi: 10.1021/bk-2006-0933.ch008

12. Lefrancois, L.; Belnet, F.; Noel, D.; Tondre, C. *Sep. Sci. Technol.*, **1999**, 34(5), 755-770.
13. Chiarizia, R.; Jensen, M. P.; Borkowski, M.; Thiyagarajan, P; Littrell, K. C. *Solvent Extr. Ion Exch.* **2004**, 6, 799-808.
14. Vandegrift, G.F.; Regalbuto, M.C. *Proceedings of the Fifth International Conference on Radioactive Waste Management and Environmental Remediation*, Vol. 1, Cross-cutting Issues and Management of High Level Waste and Spent Fuel, Berlin, Germany, September 3-7, **1995**, 457.
15. Federov, Y.S.; Zilverman, B.Y. *Radiochemistry*, **2000**, 42(3), 242-246.
16. Solovkin, A. S.; Povitskii, N. S.; Lunichkina, K. P. *Russian J. Inorg. Chem.* **1960**, 5, 1026-1028.

Downloaded by UNIV MASSACHUSETTS AMHERST on August 10, 2012 | http://pubs.acs.org
Publication Date: June 9, 2006 | doi: 10.1021/bk-2006-0933.ch009

Chapter 9

A New Interpretation of Third-Phase Formation in the Solvent Extraction of Actinides by TBP

R. Chiarizia[1], M. P. Jensen[1], M. Borkowski[1,2], and K. L. Nash[1,3]

[1]**Chemistry Department, Argonne National Laboratory, 9700 South Cass Avenue, Argonne, IL 60439**
[2]**On leave from INCT, 03–195 Warsaw, Poland. Current address: Los Alamos National Laboratory, Carlsbad Operations, Carlsbad, NM 88200**
[3]**Current address: Chemistry Department, Washington State University, P.O. Box 644630, Pullman, WA 99164**

Third phase formation, i.e., the separation of a second heavy organic phase, is a largely unexplained phenomenon which is observed in solvent extraction of metal species (for example, in the extraction of actinides by tri-*n*-butyl phosphate, TBP, in aliphatic diluents). Structural approaches for explaining organic phase splitting, based on concepts borrowed from the field of colloid chemistry, have recently appeared in the literature. In this chapter, we summarize the results of our recent small-angle neutron scattering (SANS) investigation of third phase formation in the extraction of uranyl and thorium nitrates by TBP in *n*-alkanes. An interpretation of the mechanism of third phase formation, founded on the application of Baxter's "sticky spheres" model, is presented.

In Separations for the Nuclear Fuel Cycle in the 21st Century; Lumetta, G., et al.;
ACS Symposium Series; American Chemical Society: Washington, DC, 2006.

Introduction

Studies of solvent extraction of metal species are generally performed at low concentrations of cations and extractant. Under these conditions, it is usually straightforward to determine the stoichiometry of the metal-extractant complexes formed in the organic phase. The complexes identified in this way, however, exist only under conditions of high dilution, where ideal behavior of the solute species can be assumed. It is generally impossible to extrapolate the results obtained at very low metal and extractant concentrations to the conditions usually met in practical applications of solvent extraction, where the extractant concentration is generally high and the organic phase often approaches the saturation limit with respect to the extracted species.

Under these more realistic conditions, the discrete metal-extractant entities familiar to coordination chemists can undergo polymerization or association phenomena leading to the formation of much larger species whose behavior can be quite different from that of the complexes found in dilute solutions. Examples of this type of behavior have been reported earlier (*1-5*). The authors of these studies observed the formation of very large cylindrical aggregates upon loading the organic phase with progressively higher concentrations of certain metal ions. The extractants used in these works, octyl(phenyl)-N,N-diisobutylcarbamoylmethylphosphine oxide (CMPO) (*1,2*), and dialkyl esters of diphosphonic acids (*3-5*), were bifunctional molecules, containing one P=O and one C=O, or two P=O donor groups, respectively. In these systems, polymeric species in the presence of high metal concentrations are not surprising, as metal ions can promote polymerization by bridging functional groups of different extractant molecules.

Association phenomena in the organic phase, however, are also expected to take place at high concentrations of the metal-extractant complexes when the extractant is a monofunctional compound, such as, for example, tri-*n*-butyl phosphate (TBP). In nonpolar diluents, polar species are subjected to attractive van der Waals interactions which can lead to self-assembly of solutes into much larger species.

Another phenomenon typically observed in solvent extraction systems involving nonpolar diluents at high loading of the organic phase is that of third phase formation, i.e., the splitting of the organic phase into two layers. The light layer contains most of the diluent and low concentrations of extractant and solutes, while the heavy or "third" phase is a highly concentrated solution of extractant and solutes. In spite of the abundant literature on the subject discussed in a recent review paper (*6*), a comprehensive description of the energetic and structural aspects of third phase formation is still lacking. Most of the attention in previous works, in fact, has focused on the conditions under which third phase formation is observed or avoided. Preventing third phase formation is of

Downloaded by UNIV MASSACHUSETTS AMHERST on August 10, 2012 | http://pubs.acs.org
Publication Date: June 9, 2006 | doi: 10.1021/bk-2006-0933.ch009

paramount importance in solvent extraction systems of nuclear interest (e.g., TBP–*n*-alkane systems) to avoid accidentally assembling a critical mass of fissionable materials in third phases.

The physico-chemical origin of the phenomenon of third phase formation is still matter of debate. The traditional explanation is based on simple solubility concepts (*7*), i.e., to insufficient solubility of the polar metal-ligand complexes in the nonpolar organic phase diluents. More recently, other attempts to interpret third phase formation have been reported. According to Osseo-Asare and his microemulsion model (*8*), the third phase observed when alkane solutions of TBP are used to extract mineral acids and metal salts from highly acidic aqueous solutions corresponds to the middle phase of a Winsor III system, in which the microemulsion (middle phase) is in equilibrium with both the aqueous and the oil phase. Other authors have semi-quantitatively predicted third phase formation in the extraction of nitric acid by alkyl-substituted malonamides in *n*-dodecane by using the Flory-Huggins theory of polymer solutions and the theory of regular solutions (*9*).

Third phase formation can also be considered as the final step of an aggregation process involving the organic phase species. Thiyagarajan *et al.* were the first to hypothesize that the self-association of the metal-extractant complexes may represent an intermediate stage between a homogeneous solution of monomers or very small particles, and the separation of a second organic phase (*1,2*). Following this hypothesis, and profiting from our own experience on similar systems (*3-5*), we decided to revisit from an aggregation standpoint third phase formation in the extraction of actinides by TBP in *n*-alkanes.

Our initial objective was to relate third phase formation in TBP solvent extraction systems with the formation of large self-assembled species in the organic phase (*10-12*). In the course of our investigations, however, we realized that a more realistic interpretation of third phase formation could be achieved by using a model in which the major emphasis was placed not on particle growth but, rather, on particle interactions (*13-15*). Similar conclusions have been independently arrived at by other investigators (*16,17*).

In this chapter we review our most important results obtained in the extraction of actinide nitrates by TBP in *n*-alkanes and summarize our conclusions on the mechanism and energetics of third phase formation.

Downloaded by UNIV MASSACHUSETTS AMHERST on August 10, 2012 | http://pubs.acs.org
Publication Date: June 9, 2006 | doi: 10.1021/bk-2006-0933.ch009

Measurements and Calculations

Small-angle neutron scattering (SANS) measurements are particularly suitable for the determination of the morphology (shape and size) of the aggregates formed in the organic phase by the extractants used in solvent extraction systems. The SANS technique is based on the different ability of the hydrogen and deuterium atoms to scatter neutrons. If the extractant is dissolved in a deuterated diluent, the scattered neutrons will highlight those volumes of the solution that are occupied by the extractant molecules and their aggregates, thus allowing measurement of their morphology.

Measurements

In our investigations, we used deuterated diluents (*n*-dodecane or *n*-octane) for TBP (20% v/v or 0.73 M). Aliquots of the TBP solutions were loaded by extracting progressively increasing amounts of $UO_2(NO_3)_2$ or $Th(NO_3)_4$ up to the LOC (limiting organic concentration) condition and beyond. The LOC condition represents the critical metal concentration in the organic phase, i.e., the highest concentration achievable under the specific conditions of the experiment without organic phase splitting. The details of solution preparation and characterization can be found in the original publications (*10-15*).

The SANS measurements were performed at the time-of-flight small-angle neutron diffractometer (SAND) at the Intense Pulsed Neutron Source (IPNS) of Argonne National Laboratory. For each sample the data were collected as scattered intensity, I(Q) (cm^{-1}) vs momentum transfer, $Q = (4\pi/\lambda)\sin(\theta)$ ($Å^{-1}$), where θ is half the scattering angle and λ is the wavelength of the probing neutrons.

Calculations

The intensity of the scattered neutrons can be exprressed as (*18*):

$$I(Q) = N_p V_p^2 (\Delta\rho)^2 P(Q) S(Q) + I_{inc} \tag{1}$$

where N_p is the number of scattering particles per unit volume, V_p is the particle volume, $(\Delta\rho)^2$ is the contrast factor determined from the scattering length densities of extractant and solvent, P(Q) is the single particle form factor, which describes the angular scattering distribution as a function of particle size and shape, S(Q) is the structure factor which contains information on the interaction between particles, and I_{inc} is the incoherent scattering background.

Our SANS measurements revealed a sharp increase in the scattering intensity at low Q values for solutions containing progressively higher concentrations of extracted metal species. For the interpretation of our SANS measurements we used two different models: 1) the "particle growth model", in which increased scattering intensity was attributed solely to an increase in the

Downloaded by UNIV MASSACHUSETTS AMHERST on August 10, 2012 | http://pubs.acs.org
Publication Date: June 9, 2006 | doi: 10.1021/bk-2006-0933.ch009

size of the scattering entities; 2) the "particle interaction model", in which the scattering intensity increased as a consequence of increasingly strong interactions between small particles.

Particle Growth Model

This model implies that interactions between particles are absent or negligible. By setting S(Q) = 1, eq 1 reduces to:

$$I(Q) = N_p\, V_p^2\, (\Delta\rho)^2\, P(Q) + I_{inc} \qquad (2)$$

Our SANS data were fitted by using eq 2 and the form factor for an ellipsoid of rotation (*11-13*). Since at Q=0, P(Q) = 1, after subtraction of the incoherent scattering background from the intensity values, eq 2 becomes:

$$I(0) = N_p\, V_p^2\, (\Delta\rho)^2 \qquad (3)$$

The I(0) values from the ellipsoid of rotation fit were used in eq 3 to calculate the molecular weight of the extractant aggregates, and hence n, the average aggregation number of TBP in the aggregates.

Particle Interaction Model

This model implies the ability to mathematically express the structure factor, S(Q) to account for interactions between particles in solution. This can be done by using Baxter's model for hard-spheres with surface adhesion (a.k.a. the "sticky spheres" model) (*19*). This model allows the calculation of the energy of interaction between small particles assumed as incompressible spheres and provides analytical expressions for the structure factor, S(Q).

According to Baxter's model, an approximate value of the potential energy of attraction (which is negative) between two hard spheres, U(r), expressed in k_BT units (where k_B = Boltzmann constant), is given by the following equation:

$$U(r) = \lim_{\delta \to d_{hs}} \ln\left[12\tau\left(\frac{\delta - d_{hs}}{d_{hs}}\right)\right] \qquad (4)$$

where d_{hs} is the diameter of the incompressible (hard) spheres and (δ-d_{hs}) represents the width of a narrow square attractive well. When the distance between the left edges of two particles is larger than d_{hs} but smaller than δ (i.e.,

Downloaded by UNIV MASSACHUSETTS AMHERST on August 10, 2012 | http://pubs.acs.org
Publication Date: June 9, 2006 | doi: 10.1021/bk-2006-0933.ch009

for $d_{hs} < r < \delta$), the particles experience attraction. Use of eq 4 requires knowledge of the parameter τ. The reciprocal of τ, τ^{-1}, is the "stickiness parameter" and its value is higher when the adhesion between particles is stronger. The limit in eq 4 implies that the calculation of the interparticle attraction potential energy is valid only when the attractive well is extremely narrow, i.e., when its width is within 10% of the particle diameter ($(\delta - d_{hs}) / d_{hs} \leq 0.1$).

The following analytical expressions for the structure factor S(Q) in terms of the parameter τ were used in our calculations (with $x = Qd_{hs}$ and η = particle volume fraction) (*13-16,20*):

$$S(Q) = [1-C(Q)]^{-1} \tag{5}$$

$$\begin{aligned} C(Q) = -24\eta x^{-6}\{\alpha x^3(\sin x - x\cos x) + \beta x^2[2x\sin x - (x^2-2)\cos x - 2] + \\ 0.5\eta\alpha[(4x^3-24x)\sin x - (x^4-12x^2+24)\cos x + 24]\} + \\ -2\eta^2\lambda^2(1-\cos x)x^{-2} + 2\eta\lambda x^{-1}\sin x \end{aligned} \tag{6}$$

$$\alpha = (1 + 2\eta - \mu)^2 / (1-\eta)^4 \tag{7}$$

$$\beta = -[3\eta(2+\eta)^2 - 2\mu(1+7\eta+\eta^2) + \mu^2(2+\eta)] / [2(1-\eta)^4] \tag{8}$$

$$\mu = \eta\lambda(1-\eta) \tag{9}$$

$$\gamma = \eta(1+0.5\eta) / [3(1-\eta)^2] \tag{10}$$

$$\varepsilon = \tau + [\eta / (1-\eta)] \tag{11}$$

$$\lambda = (6/\eta)[\varepsilon - (\varepsilon^2 - \gamma)^{0.5}] \tag{12}$$

By introducing in eq 1 the relations:

$$N_p = N_{TBP} / n \tag{13}$$

$$V_p = n\, V_{TBP} \tag{14}$$

where N_{TBP} and V_{TBP} are the number of TBP molecules per unit volume and the TBP molecular volume, respectively, one obtains:

$$I(Q) = (\Delta\rho)^2 N_{TBP} V_{TBP} V_p P(Q) S(Q) + I_{inc} \tag{15}$$

Downloaded by UNIV MASSACHUSETTS AMHERST on August 10, 2012 | http://pubs.acs.org
Publication Date: June 9, 2006 | doi: 10.1021/bk-2006-0933.ch009

Downloaded by UNIV MASSACHUSETTS AMHERST on August 10, 2012 | http://pubs.acs.org
Publication Date: June 9, 2006 | doi: 10.1021/bk-2006-0933.ch009

Eq 15 was used for the Baxter model calculations by obtaining S(Q) from eqs 5 – 12 and expressing P(Q) as the form factor of a sphere (*18*) with a radius $R = d_{hs}/2$:

$$P(Q) = \{\frac{3[\sin(QR) - QR\cos(QR)]}{(QR)^3}\}^2 \tag{16}$$

The three parameters I_{inc}, d_{hs} and τ were used as independent fit parameters and were optimized using the nonlinear curve fitting features of the Origin™ program (Microcal™ Software, Inc.).

Results and Discussion

Composition of the organic phases

Under the experimental conditions of this work, HNO_3 exists in the organic phase predominantly as a 1:1 complex with TBP (*10-12*). $UO_2(NO_3)_2$ is extracted by TBP in the form of the disolvate $UO_2(NO_3)_2 \cdot 2TBP$ (*21*). $Th(NO_3)_4$ exists in TBP solutions as disolvate and trisolvate species (*6*). When extracted by TBP containing high concentrations of HNO_3, the metal nitrates displace some of the acid from the organic phase as a result of the competition between metal nitrates and HNO_3 for the P=O groups of the extractant.

Table I reports the composition of the LOC organic phases obtained in the extraction of $UO_2(NO_3)_2$ from 10 M aqueous HNO_3, and of $Th(NO_3)_4$ under a variety of aqueous phase conditions.

Table I. Composition of the LOC Samples

Metal Ion	*$[HNO_3]_{aq,init}$ M*	*$[Metal]_{org}$ M*	*$[HNO_3]_{org}$ M*
UO_2^{2+}	10.0	0.23	0.27
Th^{4+}	1.0	0.18	0.079
Th^{4+}	2.5	0.20	0.20
Th^{4+}	5.0	0.16	0.33
Th^{4+}	7.5	0.13	0.48

Note: 0.73 M TBP in *n*-dodecane for UO_2^{2+} and *n*-octane for Th^{4+} (*13-15*).

The data in Table I for the Th^{4+} case indicate that the LOC condition always corresponds to a total nitrate concentration in the organic phase of about 1 M, independent of the initial aqueous acidity. The existence of this critical concentration alone, however, does not provide information on the mechanism and energetics of phase splitting.

Particle Growth Model

Figure 1 shows, as an example, the SANS data and the ellipsoid of rotation fit for a series of 0.73 M TBP solutions in *n*-octane containing progressively higher concentration of $Th(NO_3)_4$ extracted from 2.5 M HNO_3. The figure clearly shows the very pronounced increase in scattering at low Q values observed when increasing amounts of $Th(NO_3)_4$ are transferred into the organic phase displacing some of the nitric acid. The good fit in Figure 1 indicates that the scattering increase can be well modeled by assuming that upon extraction of more $Th(NO_3)_4$ the ellipsoidal particles in solution grow in size. The minor and major axes of the ellipsoid of rotation corresponding to the LOC condition in Figure 1 are 24 and 216 Å long, respectively (*15*).

The average TBP aggregation number, n, was calculated for all the investigated samples by using eq 3. Although the highest n values calculated for the extraction of $UO_2(NO_3)_2$ were close to 6 (*10,11*), in the case of $Th(NO_3)_4$ a very steep increase in the n values was observed when the LOC condition was approached (*12,14,15*). Figure 2 shows how n increases with the progressive extraction of $Th(NO_3)_4$, reaching values as high as ~40 for the LOC solutions. Since there is no literature precedent for such large aggregates of TBP-metal salts in organic solutions, the suspicion arose that these results were due to the oversimplification of assuming ideal behavior of solutes, thus neglecting solute-solute interactions. Interparticle interactions, in fact, are likely to take place in solutions containing high concentrations of TBP.

Particle Interaction Model

The possibility of using a particle interaction model to interpret our SANS data was suggested by the similarities existing between third phase formation in solvent extraction and cloud-point phase separation, a reversible critical phenomenon usually observed for aqueous solutions of nonionic surfactants (*22*). It has been reported that in these systems, phase separation is not preceded by aggregate size growth but, rather, by increasingly long-ranged spatial

Downloaded by UNIV MASSACHUSETTS AMHERST on August 10, 2012 | http://pubs.acs.org
Publication Date: June 9, 2006 | doi: 10.1021/bk-2006-0933.ch009

Downloaded by UNIV MASSACHUSETTS AMHERST on August 10, 2012 | http://pubs.acs.org
Publication Date: June 9, 2006 | doi: 10.1021/bk-2006-0933.ch009

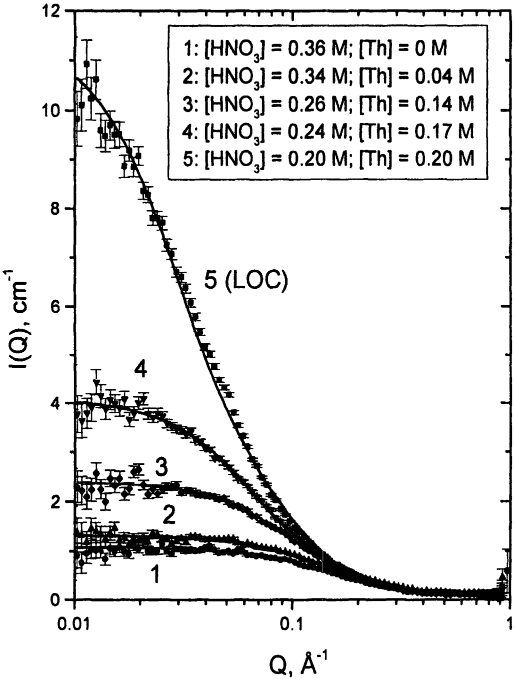

Figure 1. SANS data and ellipsoid of rotation fit (particle growth model) for 0.73 M TBP in perdeutero-n-octane containing increasing concentrations of $Th(NO_3)_4$ extracted from 2.5 M HNO_3. Concentrations are those actually present in the organic phase samples.

Downloaded by UNIV MASSACHUSETTS AMHERST on August 10, 2012 | http://pubs.acs.org
Publication Date: June 9, 2006 | doi: 10.1021/bk-2006-0933.ch009

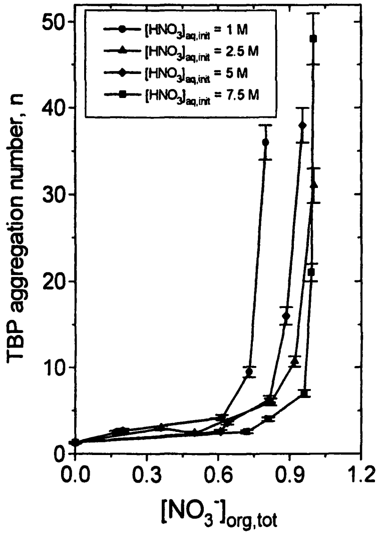

Figure 2. Apparent TBP aggregation number, n, as a function of total nitrate concentration in the organic phase upon extraction of $Th(NO_3)_4$ *by 0.73 M TBP in perdeutero-n-octane from 1, 2.5, 5 and 7.5 M* HNO_3*, respectively, as calculated using the particle growth model (data from Reference 15).*

correlations between small micelles, characterized by critical concentration fluctuations due to attractive intermicellar interactions (*23*).

The extension of concepts developed for aqueous surfactants to TBP phase behavior is justified by the fact that practically all metal extractants, including TBP, can be considered as amphiphiles, since their molecules possess polar groups capable of reacting with metal species and organophilic chains that make them soluble in organic diluents. The links of TBP phase behavior in solvent extraction to colloid chemistry are reinforced by Osseo-Asare's pioneering work on TBP micellization, which showed that TBP does form small reverse micelles in nonpolar organic diluents (*24*). We were further encouraged in attempting a particle interaction approach to our TBP systems by similar studies on the phase behavior properties of other extractants, such as alkylsubstituted malonamides (*16,25*).

Our SANS data were interpreted by using the Baxter model and eqs 5-16. Figure 3 shows, as an example, the very good fit obtained for the same samples as in Figure 1. The n, d_{hs} and τ^{-1} values obtained for the LOC samples from the Baxter model fit are reported in Table II together with the U(r) values calculated by using eq 4 with $(\delta - d_{hs})/d_{hs} = 0.1$.

Table II. Baxter Model Results for the LOC Samples

Metal Ion	$[HNO_3]_{aq,init}$ *M*	*n*	d_{hs} *Å*	τ^{-1} k_BT	*U(r)* k_BT
UO_2^{2+}	10.0	3.7±0.4	14.7±0.6	7.1±0.1	-1.78±0.01
Th^{4+}	1.0	4.1±0.4	15.3±0.5	9.6±0.6	-2.08±0.01
Th^{4+}	2.5	3.6±0.4	14.7±0.5	9.7±0.4	-2.09±0.01
Th^{4+}	5.0	3.4±0.4	14.4±0.5	9.9 ±0.4	-2.11±0.01
Th^{4+}	7.5	3.4±0.4	14.4±0.6	10.2±0.4	-2.14±0.01

Note: 0.73 M TBP in *n*-dodecane for UO_2^{2+} and *n*-octane for Th^{4+} (*13-15*).

The results in Table II indicate that according to the particle interaction model, the TBP aggregation number remains small, in the 3 to 4 range, even for the LOC samples, in agreement with previous observations (*24*). The d_{hs} values in Table II agree with molecular modelling calculations showing that a reverse micelle containing three TBP molecules has a diameter ≥14.2 Å (*13*). The interacting micelles, however, interpenetrate to some extent, since the interparticle correlation distance is always about 2 Å smaller than the corresponding d_{hs} value (*13-15*).

The critical value of the stickiness parameter, τ^{-1}, is ~7 for the diluent *n*-dodecane (in which phase splitting is achieved more readily) and ~10 for for *n*-

Downloaded by UNIV MASSACHUSETTS AMHERST on August 10, 2012 | http://pubs.acs.org
Publication Date: June 9, 2006 | doi: 10.1021/bk-2006-0933.ch009

Downloaded by UNIV MASSACHUSETTS AMHERST on August 10, 2012 | http://pubs.acs.org
Publication Date: June 9, 2006 | doi: 10.1021/bk-2006-0933.ch009

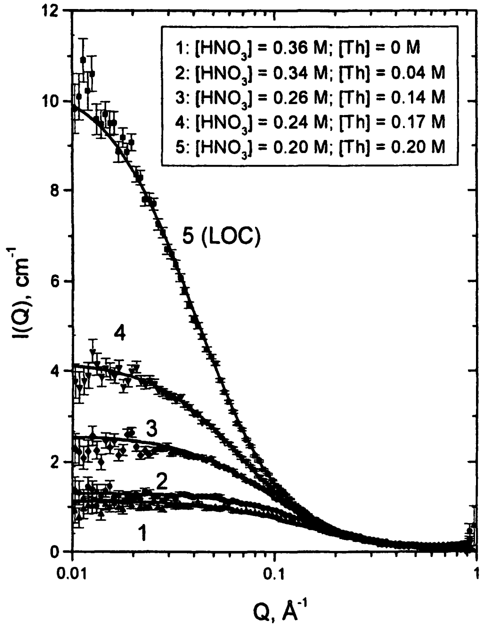

Figure 3. SANS data and Baxter model fit for 0.73 M TBP in perdeutero-n-octane containing increasing concentrations of $Th(NO_3)_4$ *extracted from 2.5 M* HNO_3*. Concentrations are those actually present in the organic phase samples.*

octane. It is indicative that the same critical value of τ^{-1} is obtained for all Th^{4+} LOC samples. The critrical τ^{-1} value, therefore, is a constant characteristic of each solvent extraction system, independent of the chemical conditions under which metal extraction took place.

Figure 4 shows how U(r) evolves as a function of the total nitrate concentration in the organic phase for the extractioin of $Th(NO_3)_4$ from aqueous phases having different HNO_3 concentrations. The results for all four series of measurements exhibit a steep increase in attractive potential energy (more negative U(r) values), as the LOC condition is approached, leading to third phase formation. The separation of most of the solute particles in a third phase takes place when the energy of attraction between the particles in solution becomes larger than about twice the average thermal energy k_BT.

Conclusions

SANS data for the extraction of $UO_2(NO_3)_2$ and $Th(NO_3)_4$ by *n*-alkane solutions of TBP were interpreted according to two different models. According to the particle growth model, the increase in scattering intensity in the low Q range, observed when increasing amounts of metal nitrates are transferred into the organic phase, arises from the formation of very large ellipsoidal "super-aggregates" containing up to ~40 TBP monomers. However, the existence in solution of these aggregates is unlikely.

An alternative model, the Baxter model for hard-spheres with surface adhesion, interpreted our SANS data as arising from interactions between small reverse micelles containing 3 to 4 TBP molecules. The interaction between the micelles was quantified through the potential energy of attraction, U(r), which increased sharply when third phase formation was approached, reaching a critical value of ~2 k_BT at the point of phase splitting.

The application of the Baxter model to our SANS data provides a plausible explanation for third phase formation in the TBP-actinide-*n*-alkane systems. The small reverse micelles formed by TBP in the organic phase are subjected to two contrasting physical forces. Thermal energy, k_BT, tends to keep the micelles dispersed in the solvent, while intermicellar attraction causes micellar adhesion. The latter factor becomes stronger as increasing amounts of polar solutes are transferred into the organic phase. As long as these two energies are comparable, the organic phase remains stable. The separation of most of the solute particles in a third phase takes place when the energy of attraction between the particles in solution becomes about twice the average thermal energy.

Although our investigations have been so far limited to TBP, our results (*13-15*), together with those obtained by other investigators for TBP and for other extractants (*16,17,25*) indicate that the Baxter model provides an

Downloaded by UNIV MASSACHUSETTS AMHERST on August 10, 2012 | http://pubs.acs.org
Publication Date: June 9, 2006 | doi: 10.1021/bk-2006-0933.ch009

Downloaded by UNIV MASSACHUSETTS AMHERST on August 10, 2012 | http://pubs.acs.org
Publication Date: June 9, 2006 | doi: 10.1021/bk-2006-0933.ch009

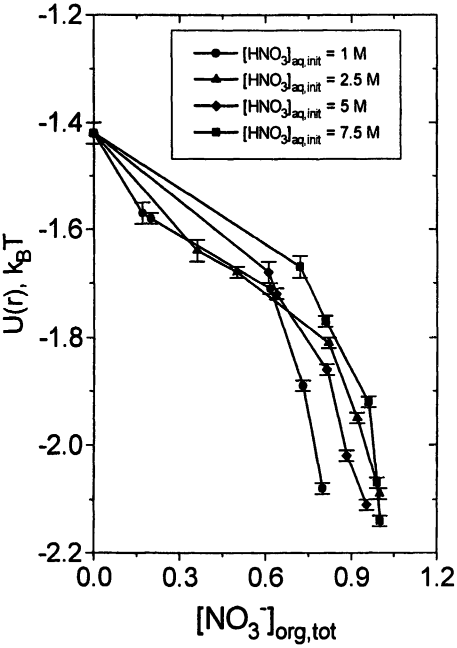

Figure 4. Intermicellar energy of attraction, U(r) (in k_BT units) as a function of total nitrate concentration in the organic phase upon extraction of $Th(NO_3)_4$ by 0.73 M TBP in perdeutero-n-octane from 1, 2.5, 5 and 7.5 M HNO_3, respectively (data from Reference 15).

interpretation of the mechanism and energetics of third phase formation in solvent extraction which is very likely of general validity.

Acknowledgments

We thank P. Thyagarajan, K. C. Littrell and D. G. Wozniak (IPNS) for help provided during the SANS measurements and data interpretation.

This work was funded by the U. S. Department of Energy, Office of Basic Energy Science, Division of Chemical Science. The submitted manuscript has been created by the University of Chicago as Operator of Argonne National Laboratory ("Argonne") under Contract No. W-31-109-ENG-38 with the U.S. Department of Energy. The U.S. Government retains for itself, and others acting on its behalf, a paid-up, nonexclusive, irrevocable worldwide license in said article to reproduce, prepare derivative works, distribute copies to the public, and perform publicly and display publicly, by or on behalf of the Government.

Downloaded by UNIV MASSACHUSETTS AMHERST on August 10, 2012 | http://pubs.acs.org
Publication Date: June 9, 2006 | doi: 10.1021/bk-2006-0933.ch009

References

1. P. Thiyagarajan, H. Diamond and E. P. Horwitz, *J. Appl. Cryst.* **1988**, *21*, 848-852.
2. H. Diamond, P. Thiyagarajan and E. P. Horwitz, *Solvent Extr. Ion Exch.* **1990**, *8*, 503-513.
3. R. Chiarizia, V. Urban, P. Thiyagarajan and A. W. Herlinger, *Solvent Extr. Ion Exch.* **1998**, *16*, 1257-1278.
4. R. Chiarizia, V. Urban, P. Thiyagarajan and A. W. Herlinger, *Solvent Extr. Ion Exch.* **1999**, *17*, 113-132.
5. R. Chiarizia, V. Urban, P. Thiyagarajan and A. W. Herlinger, *Solvent Extr. Ion Exch.* **1999**, *17*, 1171-1194.
6. Vasudeva Rao, P. R.; Kolarik Z. *Solvent Extr. Ion Exch.* **1996**, *14*, 955-993.
7. Marcus Y.; Kertes, A. S. Ion Exchange and Solvent Extraction of Metal Complexes; Wiley Interscience: New York, NY, 1969, p 715.
8. Osseo-Asare, K. In *Metal Separation Technologies Beyond 2000: Integrating Novel Chemistry with Processing*; Liddel, K. C., Chaiko, D. J., Eds.; The Minerals, Metals & Materials Society: Warrendale, PA, 1999, pp 339-346.
9. Lefrançois, L.; Belnet, F.; Noel, D.; Tondre, C. *Sep. Sci. Technol.* **1999**, *34*, 755-770.
10. Chiarizia, R.; Jensen, M. P.; Borkowski, M.; Ferraro, J. R.; Thiyagarajan, P; Littrell, K. C. *Solvent Extr. Ion Exch.* **2003**, *21*, 1-27.

11. Chiarizia, R.; Jensen, M. P.; Borkowski, M.; Ferraro, J. R.; Thiyagarajan, P; Littrell, K. C. *Sep. Sci. Technol.* **2003,** *38,* 3313-3331.
12. Borkowski, M.; Chiarizia, R.; Jensen, M. P.; Ferraro, J. R.; Thiyagarajan, P; Littrell, K. C. *Sep. Sci. Technol.* **2003,** *38,* 3333-3351.
13. Chiarizia, R.; Nash, K. L.; Jensen, M. P.; Thiyagarajan, P; Littrell, K. C. *Langmuir*, **2003,***19*, 9592-9599.
14. Chiarizia, R.; Thiyagarajan, P.; Jensen, M. P.; Borkowski, M.; Littrell, K. C. In *Proceedings of Hydrometallurgy 2003,* Young, C. A., Alfantazi, A. M., Anderson, C. G., Dreisinger, D. B., Harris, B., James, A., Eds.; The Minerals, Metals & Materials Society: Warrendale, PA, 2003, Vol. 1, pp 917-928.
15. Chiarizia, R.; Jensen, M. P.; Borkowski, M.; Thiyagarajan, P.; Littrell, K. C. *Solvent Extr. Ion Exch.* **2004,** *22*, 1-27.
16. Erlinger, C.; Belloni, L.; Zemb, Th.; Madic, C. *Langmuir* **1999**, *15*, 2290-2300.
17. Nave, A.; Mandin, C.; Martinet, L.; Berthon, L.; Testard, F.; Madic, C.; Zemb, Th. *Phys. Chem. Chem. Phys.* **2004**, *6*, 799-808.
18. Pedersen, J. S. *Adv. Colloid Interface Sci.* **1997**, *70*, 171-210.
19. Baxter, R. J. *J. Chem. Phys.* **1968**, *49*, 2770-2774.
20. Menon, S. V. G.; Kelkar, V. K.; Manohar, C. *Phys. Rev. A*, **1991**, *43*, 1130-1133.
21. McKay, H.A.C. In *Proceedings International Conference on Peaceful Uses of Atomic Energy*, Geneva, Aug. 8-20, 1955, United Nations: New York, NY, 1956, Vol. 7, pp 314-317.
22. Rosen, M.J. *Surfactants and Interfacial Phenomena*, Second Edition; Wiley: New York, 1989, pp 171-206.
23. Hayter, J. B. In *Physics of Amphiphiles: Micelles, Vesicles and Microemulsions*; Degiorgio, V., Corti M., Eds.; Elsevier: Amsterdam, 1985; pp 59-93.
24. Osseo-Asare, K. *Adv. Colloid Interface Sci.* **1991**, *37*, 123-173.
25. Erlinger, C.; Gazeau, D.; Zemb, T.; Madic, C.; Lefrançois, L.; Hebrant, M.; Tondre, C. *Solvent Extr. Ion Exch.* **1998**, *16*, 707-738.

Downloaded by UNIV MASSACHUSETTS AMHERST on August 10, 2012 | http://pubs.acs.org
Publication Date: June 9, 2006 | doi: 10.1021/bk-2006-0933.ch009

Downloaded by UNIV OF GUELPH LIBRARY on August 9, 2012 | http://pubs.acs.org
Publication Date: June 9, 2006 | doi: 10.1021/bk-2006-0933.ch010

Chapter 10

The Interaction of Ammonium Carbamate with Uranyl and Molybdenum Containing Species Derived from PUREX Processing

Mark D. Ogden[1,3], Jun Jiang[1], Iain May[1], Mark J. Sarsfield[1], and Phil Mayhew[2]

[1]Centre for Radiochemistry Research, Department of Chemistry, The University of Manchester, Manchester M13 9PL, United Kingdom
[2]NSTS, B170, BNFL, Sellafield, Cumbria CA20 1PG, United Kingdom
[3]Current address: Department of Chemistry, Washington State University, P.O. Box 644630, Pullman, WA 99164–4630

Multiple spectroscopic techniques have been utilized to investigate the complex equilibria governing the chemistry of ammonium carbamate in aqueous solution, in the absence and in the presence of uranyl (UO_2^{2+}) and phosphomolybdate $[PMo_{12}O_{40}]^{3-}$. Ammonium carbamate does not interact directly with these species but rather decomposes to produce carbonate ions in a particularly reactive form. The dissolution of $[UO_2(DBP)_2]$ (DBP = dibutylphosphate) by high concentrations of ammonium carbamate is shown to occur *via* ligand substitution of DBP by CO_3^{2-}. Dissolution of $Cs_3[PMo_{12}O_{40}]$ by ammonium carbamate occurs *via* initial formation of $[P_2Mo_5O_{23}]^{6-}$ and, ultimately, production of PO_4^{3-} and MoO_4^{2-}.

In Separations for the Nuclear Fuel Cycle in the 21st Century; Lumetta, G., et al.;
ACS Symposium Series; American Chemical Society: Washington, DC, 2006.

Introduction

Irradiated nuclear fuel is a very complex mixture containing about 1/3 of the periodic table. When spent nuclear fuel is dissolved in nitric acid and contacted with tributyl phosphate (TBP) during fuel reprocessing, many reactions may occur. There is potential to form a range of insoluble species, particularly when solutions are concentrated by evaporation, as occurs prior to high activity liquor storage or vitrification. Phases of particular interest are hydrous zirconium molybdate $ZrMo_2O_7(OH)_2(H_2O)_2$ (ZM), cesium phosphomolybdate $Cs_3PMo_{12}O_{40}$ (CPM), zirconium dibutylphosphate $Zr(DBP)_2(NO_3)_2$ (ZrDBP) and uranyl dibutylphosphate $UO_2(DBP)_2$ (UDBP). DBP is a degradation product of TBP and is formed as a result of hydrolysis and radiolysis. It is, therefore, useful to identify a complexant or solvent which both could be used to remove such precipitates and is compatible with nuclear fuel reprocessing plant operation. It has been found that an aqueous solution of ammonium carbamate (ACm) ($NH_4O_2CNH_2$) is an effective reagent for the redissolution of these solids, although the mechanism of redissolution is unclear (*1*).

Dissociation of ACm into water does not yield a solution of NH_4^+ and $H_2NCO_2^-$. Instead it forms an equilibrium mixture with HCO_3^-, CO_3^{2-}, and NH_3 (*2-4*). This equilibrium has been studied in some detail by Wen and Brooker using Raman and ^{13}C NMR spectroscopies (*5*). Ammonium bicarbonate, ammonium carbonate, and sodium carbonate mixed with ammonium chloride interact via the same equilibria as ammonium carbamate when dissolved in water. Several possible equilibria govern a complex interchange between carbonate, bicarbonate, carbamate, ammonium, and free ammonia, as follows:

$$H_2NCOO^-_{(aq)} + OH^-_{(aq)} \leftrightarrows CO_3^{2-}{}_{(aq)} + NH_{3\,(aq)}$$

$$H_2NCOO^-_{(aq)} + H_3O^+_{(aq)} \leftrightarrows NH_{3\,(aq)} + CO_{2\,(aq)} + H_2O_{(l)}$$

$$NH_{3\,(aq)} + H_2O_{(l)} \leftrightarrows NH_4^+{}_{(aq)} + OH^-_{(aq)}$$

$$NH_4^+{}_{(aq)} + H_2O_{(l)} \leftrightarrows NH_{3\,(aq)} + H_3O^+_{(aq)}$$

$$CO_3^{2-}{}_{(aq)} + H_2O_{(l)} \leftrightarrows HCO_3^-{}_{(aq)} + OH^-_{(aq)}$$

$$CO_3^{2-}{}_{(aq)} + NH_4^+{}_{(aq)} \leftrightarrows HCO_3^-{}_{(aq)} + NH_{3\,(aq)}$$

It has been reported in the literature that the carbamate anion can behave either as a bidentate or monodentate ligand (*6-7*), and that the carbamate ligand is always coordinated through the oxygen donor atoms. Bidentate coordination of carbamate through the two O-donor would have the same bonding mode as the carbonate anion.

Downloaded by UNIV OF GUELPH LIBRARY on August 9, 2012 | http://pubs.acs.org
Publication Date: June 9, 2006 | doi: 10.1021/bk-2006-0933.ch010

In this paper, we report results of investigations into the possible mechanism by which ACm dissolves the various PUREX solid phases listed above while identifying the complexes present in the resulting solution. Only high stoichiometric ratios (above 1:3 metal to ligand) will be considered in this paper as these conditions are similar to dissolution conditions that could be used in a plant. Characterisation of the solids and solutions produced at low stoichiometric ratios (below and including 1:3 ratios) have been described elsewhere (*1*).

Experimental

General

All chemicals were reagent grade, purchased from Aldrich or BDH and used without purification. Distilled deionised water was used throughout all experiments. Solution UV/Vis spectroscopic data were collected in a 1 mL quartz cell, referenced against water. These experiments were performed primarily using a Perkin Elmer Lambda 5 and an Uvikon 941 plus UV/Vis spectrometer. Solid state infrared (IR) data were collected on a Bruker Equinox 55 spectrometer using a "Golden gate" Attenuated Total Reflectance (ATR) attachment, with a resolution of 4 cm^{-1}. Data were typically collected for 32 scans in the mid-IR region (4000-400 cm^{-1}) using a 2-3 mg sample of material. A Bruker FRA 106/S Raman instrument, with a coherent laser (1064 nm, 400 mW), was used to collect the Raman scattering from solid samples (10-20 mg) held in the laser beam path, solution samples (1.5 cm^3) were measured using a mirrored cuvette. Solid samples were run for 100 scans whereas solution samples were collected overnight to provide better signal to noise ratios. ^{13}C and ^{31}P solution NMR were recorded on a Bruker Avance Ultrashield^{TM} 400 MHz spectrometer, in 5 mm diameter NMR tubes, using a D_2O lock. ^{31}P NMR chemical shifts were referenced against 85% H_3PO_4. For ^{13}C NMR the chemical shifts were referenced to an internal 2% d_4-methanol spike. Elemental analysis for U and Mo were carried out using a Fisons Horizon Elemental Analysis ICP-OES at the Microanalysis Lab in the Chemistry Department of the University of Manchester. Thermogravimetric analysis (TGA) curves were recorded on a Mettler Toledo TGA/SDTA 851^e analyser. Samples were heated in crucibles between 25 and 1000 °C at a heating rate of 5 °C per minute, under a continuous stream of nitrogen. Single crystal X-ray diffraction data was collected at ambient temperature on a Rigaku RAXIS diffractometer in the Crystallography Department at the University of Manchester.

Downloaded by UNIV OF GUELPH LIBRARY on August 9, 2012 | http://pubs.acs.org
Publication Date: June 9, 2006 | doi: 10.1021/bk-2006-0933.ch010

Stoichiometric reactions of the uranyl ion and ACm

In initial trial studies, aliquots of 0.02 M uranyl nitrate solution were reacted with varying concentrations (0.02-0.4 M) of ACm and the formation of any precipitates was monitored visually. Spectroscopic investigation of both the solid and solution phases was carried out. Solution and solid phases above metal to ligand ratios of 1:3 were repeated with ^{15}N labeled ACm, which had been previously prepared as described elsewhere (*8*), with the addition of an argon blanket. All the solutions and products formed were analyzed spectroscopically and compared directly with complexes from non-labeled ACm.

The interaction between ACm and UDBP

UDBP was prepared by reacting aqueous uranyl nitrate (0.1 M) with dibutylphosphoric acid (HDBP) in a molar ratio of 1:3. The solid formed was analysed using elemental analysis, Raman, IR, and TGA. TGA was consistent with decomposition of the ligand to gaseous products with the formation of uranium trioxide (UO_3). Loss of 40.2% of the starting mass can be attributed to removal of 2 DBP molecules, each minus a single oxygen from the uranium center. The IR spectrum was compared with that in the literature (*9*) and was found to match directly, supporting the suggestion that the product is a polymeric $UO_2(DBP)_2$ previously reported (*10*). The Raman peaks at 1124 and 1447 cm^{-1} are assigned to symmetric and antisymmetric stretches of a bridging phosphate (*10*) that would be found in a polymeric species.

The solid UDBP (0.21 mM) was contacted with solution of ACm (0.42 M) until complete dissolution took place and the resulting solution was investigated using UV/Vis, ^{13}C NMR, and ^{31}P NMR spectroscopies, the pH was initially between 6.5 and 7.0 and increased to 9.44 after dissolution.

The interaction between ACm and CPM

$H_3PMo_{12}O_{40}$ and $CsNO_3$ solutions were mixed together with stirring in a 1:3 molar ratio. An immediate yellow precipitate, $Cs_3PMo_{12}O_{40}.xH_2O$ (CPM), was formed and was air dried after separation by centrifugation. TGA, solid Raman, and IR were obtained. From the TGA results, the number of waters in the formula was calculated from the weight loss below 200 °C, corresponding to the evaporation of water. The water content varies from 9-14 per equivalent of phosphomolybdate depending on the drying method and time ($Cs_3PMo_{12}O_{40}.9H_2O$- $Cs_3PMo_{12}O_{40}.14H_2O$). In the solid Raman spectra, the band observed at 997 cm^{-1} is the characteristic symmetric Mo-O stretch in

Downloaded by UNIV OF GUELPH LIBRARY on August 9, 2012 | http://pubs.acs.org
Publication Date: June 9, 2006 | doi: 10.1021/bk-2006-0933.ch010

$[PMo_{12}O_{40}]^{3-}$, comparable to that observed for $H_3PMo_{12}O_{40}$ (*1*). In the solid IR, the band at 1060 cm^{-1} is assigned to the P-O stretch and the band at 950 cm^{-1} assigned to the terminal Mo-O stretch of an α Keggin structure $[PMo_{12}O_{40}]^{3-}$ (*12, 13*). A mass equivalent of 1 mol/L of solid CPM in 1 mL D_2O was reacted directly with increasing molar ratios of ammonium carbamate. The resulting solutions were analysed using solution Raman and ^{31}P NMR spectroscopies.

Results and Discussion

The interaction of ACm with the uranyl ion at high stoichiometric ratios

The UV/Vis spectrum of the uranyl ion in solutions containing high concentrations of ACm displays a single band around 440 nm, split by vibronic coupling (Figure 1). The pattern of the vibronic coupling gives and indication of the effect of bonding in the equatorial plane around the uranyl (UO_2^{2+}) center (*14*).

The vibronic coupling of the uranyl species in ACm is similar to that of the carbonate species (*14*). This implies that either the carbamate anion is bonding to the UO_2^{2+} center in a manner similar to that of carbonate (CO_3^{2-}), or that carbamate readily decomposes to carbonate which forms the known $UO_2(CO_3)_3^{4-}$ complex with UO_2^{2+}.

In the ^{13}C NMR spectrum of the uranyl ion in excess ^{15}N labeled ACm solution (Figure 2) three peaks can be seen at 168.9 ppm, 166.9 ppm, and 162.9 ppm. The peak at 166.9 ppm is a doublet that is a assigned to free carbamate in solution (*5*) with a coupling constant (J value) of 4 Hz, which is a typical J value for carbamate species (*15, 16*). The splitting arises from the coupling of the ½ spins of ^{13}C and ^{15}N. There is no shift or broadening of the ^{13}C carbamate peak, or change in the J value, in comparison with the initial ammonium carbamate solution, as would be expected if the carbamate were bound to the uranyl. The peak at 162.9 ppm is a broad singlet that is assigned to free carbonate and bicarbonate undergoing proton transfer. The peak at 168.9 ppm is uncoupled and can unambiguously be assigned to carbonate bound to uranyl.

In the ^{15}N NMR of labeled ACm solution there are two resonances at 75 ppm and 15 ppm. The peak at 15 ppm is assigned to the ammonium ion undergoing proton exchange with ammonia in solution. The peak at 75 ppm has been assigned to the free carbamate anion in solution. There is no change in the carbamate peak in the presence of the uranyl ion indicating that there is no interaction between the uranyl center and carbamate. Collectively, these

Downloaded by UNIV OF GUELPH LIBRARY on August 9, 2012 | http://pubs.acs.org
Publication Date: June 9, 2006 | doi: 10.1021/bk-2006-0933.ch010

Downloaded by UNIV OF GUELPH LIBRARY on August 9, 2012 | http://pubs.acs.org
Publication Date: June 9, 2006 | doi: 10.1021/bk-2006-0933.ch010

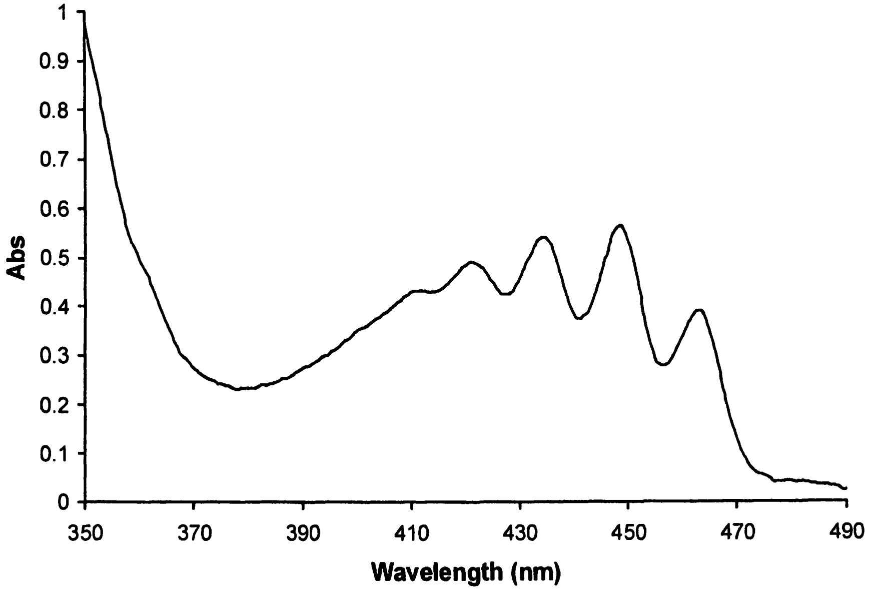

Figure 1. UV/Vis absorption spectra of the uranyl ion in high concentration ammonium carbamate solution.

Downloaded by UNIV OF GUELPH LIBRARY on August 9, 2012 | http://pubs.acs.org
Publication Date: June 9, 2006 | doi: 10.1021/bk-2006-0933.ch010

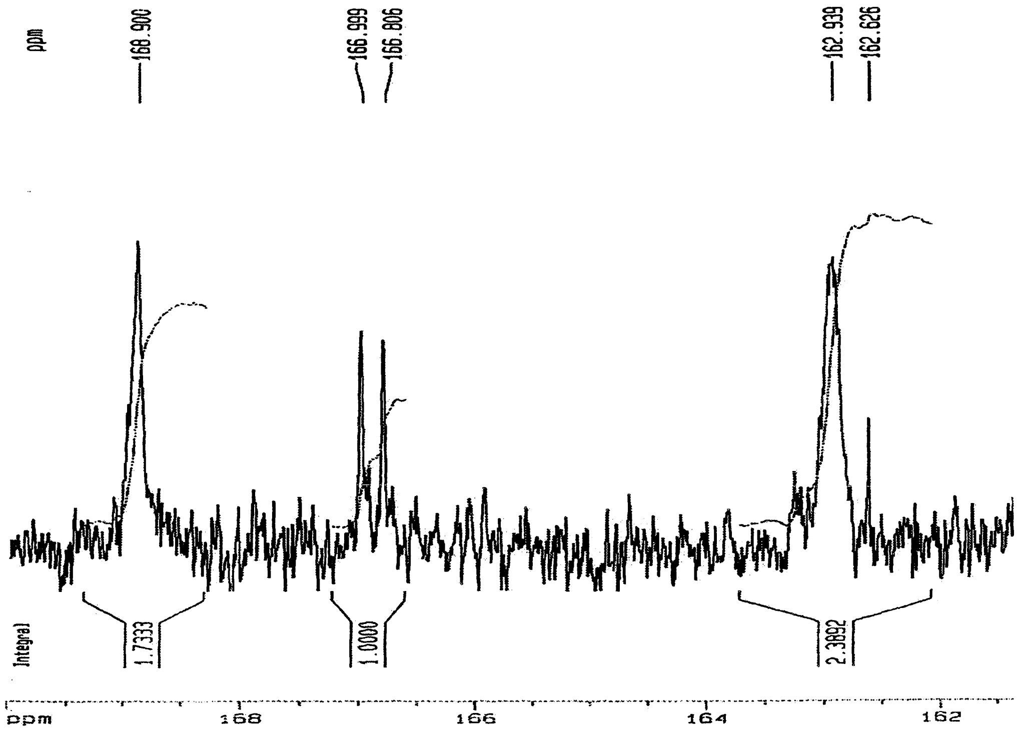

Figure 2. ^{13}*C NMR spectrum of* UO_2^{2+} *in high concentration* ^{15}*N labeled ammonium carbamate solution.*

In Separations for the Nuclear Fuel Cycle in the 21st Century; Lumetta, G., et al.;
ACS Symposium Series; American Chemical Society: Washington, DC, 2006.

observations indicate that the most likely species of uranyl present in solutions of high concentration ACm is $UO_2(CO_3)_3^{4-}$.

Uranyl nitrate (0.1 M), when mixed with a concentrated solution of carbamate (2.0 M) and allowed to stand for several days, produced a lemon yellow crystalline precipitate (product **1**). The same lemon yellow crystals were produced by uranyl nitrate in ^{15}N enriched ACm solution (product **2**).

Key stretches in the solid state IR spectra of **1** and **2** and their assignments are given in Table I. If carbonate is bound to the uranyl, a group of characteristic vibrational frequencies (ν_1, ν_2, ν_3, ν_4) for the carbonate ligand (*17*) would be expected. The ν_3 carbonate vibration will be split by 160-190 cm^{-1} (*18*) on coordination to uranyl and hence maybe diagnostic of the coordination mode of the carbonate. For carbamate, 12 stretches in the IR are anticipated. The key areas that are not overlapped by the ammonium cation and the uranyl stretches are the ν_9 antisymmetric CO_2^- stretch at around 1520-1525 cm^{-1}. The C-N stretch would appear between 1404 and 1455 cm^{-1} (*19*). Symmetric stretches ν_4 and ν_6 would appear around 1115 cm^{-1} and 840-825 cm^{-1}. The antisymmetric CO_2^- stretch would appear around 690-720 cm^{-1}. Around 660 cm^{-1} ν_7 CO_2^- bends would be expected. NH_2 stretches for the $^-O_2CNH_2$ ligand would appear around 3440 (ν_8), 3295 (ν_1), 1620 (ν_2), 1261 (ν_{10}), 1040 (ν_5) (*20*). These NH_2 stretches can shift in position depending on the degree of hydrogen bonding in the crystal.

Table I. IR assignments for 1 and 2

Product 1	*Product 2*	*Assignment*
Peak Wavenumbers (cm^{-1})	*Peak Wavenumbers (cm^{-1})*	
1521	1524	v_4 CO_3^{2-}
1444		v_4 NH_4^+
	1364	v_1 CO_3^{2-} antisymmetric
1347		v_1 CO_3^{2-} antisymmetric
	1181	$^{15}NH_4^+$ stretch
	1083	$^{15}NH_4^+$ stretch
1053	1053	v_2 CO_3^{2-} stretch
891	889	UO_2^{2+} antisymmetric stretch
844	844	v_3 CO_3^{2-} deformation
720	719	v_5 CO_3^{2-} deformation
691	691	v_3 CO_3^{2-} deformation

Downloaded by UNIV OF GUELPH LIBRARY on August 9, 2012 | http://pubs.acs.org
Publication Date: June 9, 2006 | doi: 10.1021/bk-2006-0933.ch010

Downloaded by UNIV OF GUELPH LIBRARY on August 9, 2012 | http://pubs.acs.org
Publication Date: June 9, 2006 | doi: 10.1021/bk-2006-0933.ch010

Both spectra have a matching peak at around 720 cm^{-1} that is a characteristic out of plane deformation of a carbonate ligand (*14, 21, 22*). If carbamate was bound to the uranyl metal center, a significant shift to lower wavenumbers in all of the C-O stretches would be expected in the IR of **2**. There are no significant changes in the C-O stretches when comparing the products **1** and **2**. There is also no visible C-N stretch, or NH_2 ν_2 and ν_{10} in both spectra. The slight shift in C-O stretches between **1** and **2** is due to the change in hydrogen bonding associated with the presence of a ^{15}N ammonium counter cation. The peaks at 1181 cm^{-1} and 1083 cm^{-1} in the IR of **2** have been assigned using $^{15}NH_4Cl$ (although there is a slight increase of the wavenumber values in **2** due to hydrogen bonding).There is little or no change in the Raman spectra of **1** and **2**. There is no shift in the C-O deformations as would be expected if the carbon were bound to a heavier nitrogen atom. The shift of 1 cm^{-1} in the symmetric CO_2^- stretch of **2** is due to the change in hydrogen bonding. The crystals of **1** are monoclinic, a = 10.68, b = 9.38, c = 12.85, β = 96°27', Z = 4. The space group is C2/c. The linear uranyl group is perpendicular to the equatorial plane in which three bidentate ligands are chelated. This structure is identical to one reported previously (*23*) for $(NH_4)_4[UO_2(CO_3)_3]$. Isotopic labelling has made it possible to identify the solid species without ambiguity suggesting that the species crystallizing at high concentrations of ACm is $(NH_4)_4[UO_2(CO_3)_3]$.

The interaction of ACm with UDBP

The solution UV/Vis spectrum from the dissolution of UDBP by ACm produces a pattern of peaks identical to that of UO_2^{2+} in ACm as shown in Figure 1. This suggests that one of the species formed in solution after the breakdown of UDBP by ACm is $UO_2(CO_3)_3^{4-}$.

In the ^{13}C NMR spectrum of UDBP dissolved in ACm solution seven peaks can be seen. The assignments, J values, and chemical shift are given in Table II. The peak at 163 ppm is assigned to free carbonate/bicarbonate in equilibrium; the peak at 166 ppm is assigned to free carbamate (*5*). The peaks below 70 ppm are assigned to the DBP unit. This region of the spectrum is similar to that observed for HDBP in ammonium hydroxide with little or no change in the J values for the carbon to phosphorus coupling, showing that the alkyl chains are unaffected by pH.

The ^{31}P NMR spectra of HDBP and its deprotonated species in ammonium hydroxide are significantly different. The peak at 0.7 ppm is assigned to the

Table II. ^{13}C NMR peak assignment for the dissolution of UDBP by ammonium carbamate solution

Peak (ppm)	*J value (Hz)*	*Assignment*
168	-	$UO_2(\underline{C}O_3)_3^{4-}$
166	-	$H_2N\underline{C}O_2^-$
163	-	$H\underline{C}O_3^-/\underline{C}O_3^{2-}$
67	23.82	$(CH_3CH_2CH_2\underline{C}H_2)_2\text{-O-}PO_2^-$
33	28.17	$(CH_3CH_2\underline{C}H_2CH_2)_2\text{-O-}PO_2^-$
19	-	$(CH_3\underline{C}H_2CH_2CH_2)_2\text{-O-}PO_2^-$
14	-	$(\underline{C}H_3CH_2CH_2CH_2)_2\text{-O-}PO_2^-$

deprotonated species in ammonium hydroxide, a shift of 2.4 ppm from the −1.7 ppm found for HDBP. In the ^{31}P NMR spectrum of UDBP dissolved in ACm there is a single phosphorus peak at 1.00 ppm. This indicates that the DBP is deprotonated and shows that further decomposition of the DBP has not occurred (*24*). From the multiple spectra collected the species found in solution are DBP^-, HCO_3^-, CO_3^{2-}, $H_2NCO_2^-$, and $UO_2(CO_3)_3^{4-}$.

Therefore, in the dissolution of UDBP by high concentrations of ACm, carbonate complexation seems to be the mechanism by which dissolution occurs. The complex equlibria that exists in solution producing HCO_3^-, CO_3^{2-}, and $H_2NCO_2^-$ act as a buffer which can prevent the hydrolysis of the uranyl carbonate species. A possible equation for the dissolution of UDBP by ACm could be:

$$UO_2(DBP)_{2\,(s)} + 3NH_4O_2CNH_{2\,(aq)} + 3H_2O_{(l)} \leftrightarrows UO_2(CO_3)_3^{4-}{}_{(aq)} + 6\,NH_4^+{}_{(aq)} + 2DBP^-{}_{(aq)}$$

The interaction between ammonium carbamate and CPM

Upon addition of ACm solution to solid CPM, in all cases gas evolution was observed. The Raman spectra of the CPM dissolution show no activity until after the addition of more than 2 molar equivalents of ammonium carbamate. Subsequent additions of ammonium carbamate produce species active in two regions in the solution Raman. One at 895-900 cm^{-1} and the other at 930-940 cm^{-1} (pH 6.2-9.2). In all the Raman spectra obtained during the dissolution experiments, including pH ≥ 6.4, there is a peak at 896 cm^{-1}, characteristic of the monomeric molybdate unit, MoO_4^{2-} (*12, 25, 26*). As the pH increases this peak increases in size. Formation of this product is indicative of an acid:base reaction between $PMo_{12}O_{40}^{3-}$ and $H_2NCO_2^-/HCO_3^-/CO_3^{2-}$ resulting in the break up of the

Downloaded by UNIV OF GUELPH LIBRARY on August 9, 2012 | http://pubs.acs.org
Publication Date: June 9, 2006 | doi: 10.1021/bk-2006-0933.ch010

heteropolymolybdate cluster. The second region is a complex envelope of peaks occurring between 940 cm^{-1} and 930 cm^{-1}. The peak at 940 cm^{-1} is assigned to the spectrum of $Mo_7O_{24}^{6-}$. The band at 930 cm^{-1} shifts as the pH changes. This feature has previously been assigned to the protonation/deprotonation equilibria associated with the $P_2Mo_5O_{23}^{6-}$ species (*27, 28*) *e.g.*

$$P_2Mo_5O_{23}^{6-}{}_{(aq)} + 2H^+{}_{(aq)} \leftrightarrows HP_2Mo_5O_{23}^{5-}{}_{(aq)} + H^+{}_{(aq)} \leftrightarrows H_2P_2Mo_5O_{23}^{4-}{}_{(aq)}$$

Raman measurements indicate that at these low ammonium carbamate concentrations, there is only sufficient base for partial breakdown of the $PMo_{12}O_{40}^{3-}$ to smaller isomolybdate and phosphomolybdate species (Figure 3). At the higher pH values of 7.26-9.23 molybdenum is present predominantly as the MoO_4^{2-} unit. A full summary of the peaks present and pH's is given in Table III.

Table III. Raman assignment for the dissolution of CPM by ammonium carbamate

Band position (cm^{-1})	*Assignment*	*pH range when visible*
896	MoO_4^{2-}	6.44-9.23
927-923	$P_2Mo_5O_{23}^{6-}$	6.70-7.26
941-939	$Mo_7O_{24}^{6-}$	6.70-7.08

^{31}P NMR spectra show one clear peak in the range of 2.6 ppm – 3.0 ppm attributed to PO_4^{3-} (*15*). The changes in chemical shift and broadness of the signal are related to the extent of its protonation. This is in accord with the Raman results, showing that $PMo_{12}O_{40}^{3-}$ is broken down to simpler anions by the action of the basic ammonium carbamate solution, liberating free phosphate. Below an initial ammonium carbamate concentration of 1.5 M, a second signal is observed between 2.0 and 2.2 ppm, attributed to $P_2Mo_5O_{23}^{6-}$, again in accord with the Raman results (*29*).

Literature reports (*12, 30*) indicate that in an equilibria system of H^+-MoO_4^{2-}-HPO_4^{2-} a pentamolybdodiphosphate ($P_2Mo_5O_{23}^{6-}$) is readily formed at low pH values. Even at low concentration of P and Mo, all the Mo will be bound in a $P_2Mo_5O_{23}^{6-}$ species. It is also found that regardless of concentration of Mo or P at pH values above 6.0 all phosphorus is bound as $P_2Mo_5O_{23}^{6-}$ and little or no additional complexes are formed. Therefore the $P_2Mo_5O_{23}^{6-}$ fragment is formed by a recombination of PO_4^{3-} and MoO_4^{2-} in aqueous solution. A general equation for the dissolution of CPM by ammonium carbamate could be written:

Downloaded by UNIV OF GUELPH LIBRARY on August 9, 2012 | http://pubs.acs.org
Publication Date: June 9, 2006 | doi: 10.1021/bk-2006-0933.ch010

Downloaded by UNIV OF GUELPH LIBRARY on August 9, 2012 | http://pubs.acs.org
Publication Date: June 9, 2006 | doi: 10.1021/bk-2006-0933.ch010

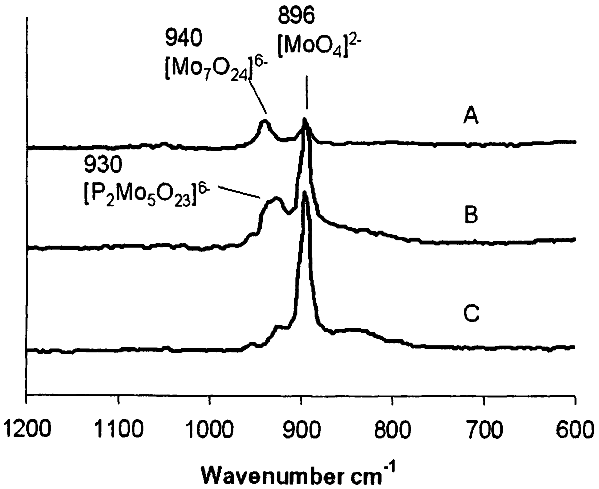

Figure 3. Raman Spectra of the final solutions after the dissolution of cesium phosphomolybdate in various concentrations of ammonium carbamate solutions (A=0.2, B=0.6, C=1.0 $mol{\cdot}L^{-1}$ $NH_4O_2CNH_2$)

$$Cs_3PMo_{12}O_{40\,(s)} + 12NH_4O_2CNH_{2\,(aq)} + 12H_2O_{\,(l)} \rightarrow 3Cs^+_{\,(aq)} + HPO_4^{2-}{}_{(aq)} + 12MoO_4^{2-}{}_{(aq)} + 23NH_4^+{}_{(aq)} + 12CO_{2\,(g)} + NH_{3\,(aq)}$$

Removal of gaseous CO_2 from the aqueous system appears to drive this reaction to the right. At low carbamate/carbonate:CPM ratios (*ca.*<20:1), there is incomplete reaction, with only partially hydrolysed molybdate $Mo_7O_{24}^{6-}$ and phosphomolybdate $P_2Mo_5O_{23}^{6-}$ species present in solution and some undissolved solids remaining.

Downloaded by UNIV OF GUELPH LIBRARY on August 9, 2012 | http://pubs.acs.org
Publication Date: June 9, 2006 | doi: 10.1021/bk-2006-0933.ch010

Conclusions

Carbamates in Future Nuclear Fuel Cycles

ACm is a particularly effective reagent for dealing with a number of PUREX derived solids because it combines a multitude of unique features, including;

1. Complexation (as carbonate ion).
2. Highly reactive carbamic acid intermediate.
3. Buffering
4. Production of a variety of gaseous by products.
5. No production of by product solid waste.

Throughout this research the authors have found no evidence for the carbamate anion coordinating to a metal centre like CO_3^{2-} and many of the mechanistic details of why ACm is an effective dissolution agent still remain a mystery. From the interaction of ammonium carbamate with the uranyl ion and the UDBP dissolution studies, it is clear that ammonium carbamate dissolves the solid yielding a U(VI) carbonate complex. Quantitatively the rate of dissolution is slower than the CPM dissolution. While ACm dissolves CPM faster than Na_2CO_3, in this case Na_2CO_3 should dissolve UDBP faster than ACm. This is due to the dissolution process being driven by coordination of carbonate. There is clearly more $[CO_3]^{2-}$ available for coordination to the metal in Na_2CO_3 solution than in $NH_4O_2CNH_2$. The nature of the species produced in solution is highly dependant on the proportion of $[HCO_3]^-$ present in solution (*31*). The presence of bicarbonate in solution as a source of protons prevents the hydrolysis and condensation of the carbonate species (*31*) and maintains the monomeric carbonate complex $[M(CO_3)_x^{y-2x}]$ in solution *e.g.*

$$M^{y+}_{(aq)} + xCO_3^{2-}{}_{(aq)} \rightarrow [M(CO_3)_x]^{y-2x}{}_{(aq)}$$

Dissolution of UDBP depends on the formation of U(VI) carbonate complexes, and thus a reagent yielding more carbonate in solution would be a more effective agent. Although a metal carbonate would provide more complexation per molar equivalent it would produce a greater amount of waste needing disposal.

It is clear that ACm can dissolve CPM by base hydrolysis of the Keggin phosphomolybdate anion to give MoO_4^{2-} and release PO_4^{3-}. This is the reverse process of how the Keggin structure is formed in the first place:

$$HPO_4^{2-}{}_{(aq)} + 12MoO_4^{2-}{}_{(aq)} + 24H^+{}_{(aq)} \rightarrow PMo_{12}O_{40}^{3-}{}_{(aq)} + 12H_2O_{(l)}$$

A qualitative investigation of the dissolution rate indicated clearly that CPM dissolution by carbamate is faster than CPM dissolution by sodium carbonate. The key to the different rates is the fact that carbamate will protonate to form unstable carbamic acid (*5*), which will immediately decompose to yield NH_3 and CO_2, with the majority of the CO_2 gas being liberated before any further reaction with water to yield bicarbonate. It is this liberation of CO_2 that drives the reaction forward and increases the rate of CPM dissolution. Conversely carbonate is protonated only to bicarbonate, remaining in solution and equilibrium with the remaining carbonate. This ability to release CO_2 is down to both the instability of the carbamic acid intermediate and the control of pH in an appropriate range to facilitate greater venting of CO_2 to the atmosphere. Dissolution rates for CPM and ZM by ACm along with a further quanitative investigation of the dissolution mechanisms are discussed more fully elsewhere in the literature (*32*)

ACm is a simple ligand containing only C, H, N, and O, the species that it produces in solution from the dissolution of PUREX derived solids can be broken down by back washing with acid and by changing the pH of the system a variety of gaseous products can be removed from solution reducing the amount of waste needing to be treated. ACm can also be inexpensively made from CO_2 and NH_3.

We have shown in this paper two examples of how ammonium carbamate can play an important role in waste minimization for the development of advanced reprocessing schemes.

Acknowledgements

The authors would like to acknowledge the assistance of Dr Madeline Helliwell at the University of Manchester in obtaining the X-ray crystallography

Downloaded by UNIV OF GUELPH LIBRARY on August 9, 2012 | http://pubs.acs.org
Publication Date: June 9, 2006 | doi: 10.1021/bk-2006-0933.ch010

data. We would also like to thank Prof. Francis Livens and Prof. Richard Winpenny for their help and guidance. For the constructive criticism of this paper the authors would like to thank the Ken Nash, Sue Clark, and Paul Benny groups at Washington State University. Funding for this project was provided by British Nuclear Fuels Ltd.

References

1. Ogden, M. D. MPhil thesis, The University of Manchester, Manchester, UK, 2004.
2. Burrows, G. G.; Lewis. G. N. *J. Am. Chem. Soc.* **1912,** *34,* 993-995.
3. Briggs, T. R.; Migrdichian, V. J. *Phys. Chem.* **1924,** *28,* 1121-1135.
4. Christensson, F.; Koefoed, H. C. S.; Petersen, A. C.; Rasmussen, K. *Acta Chem. Scand. A* **1978,** *32,* 15-17.
5. Wen, N.; Brooker, M. H. *J. Phys. Chem.* **1995,** *99,* 359-368.
6. Meyer, F.; Pritzkow, H. *Chem. Commun.* **1998,** 1555-1556.
7. Bang, E.; Monsted, O. *Acta Chem. Scand. A.* **1982,** *36,* 353-359.
8. Brooks, L. A.; Audrieth, L. F. *Inorg. Synth.* **1946,** *2,* 85-87.
9. Sokhina, L. P.; Bogdanov, F. A.; Solovkin, A. S.; Teterin, E. G.; Shesterikov, N. N. *Zh. Neorg. Khim.* **1976,** *21,* 2471-2478.
10. Burns, J. H. *Inorg. Chem.* **1983,** *22,* 1174-1178.
11. Edwards, H. G. M.; Hughes, M. A.; Smith, D. N.; Courtney, B. *J. Mol. Struct.* **1995,** *351,* 65-76.
12. Rocchiccioli-Deltcheff, C.; Fournier, M.; Franck, R.; Thouvenot, R. *Inorg. Chem.* **1983,** *22,* 207-216.
13. Thouvenot, R.; Fournier, M.; Franck, R.; Rocchiccioli-Deltcheff, C. *Inorg. Chem.* **1984,** *23,* 598-605.
14. Clark, D. L.; Hobart, D. E.; Neu, M. P. *Chem. Rev.* **1995,** *95,* 25-48.
15. Berger, S. *Tetrahedron* **1978,** *34,* 3133-3136.
16. Berger, S.; Roberts, J. D. *J. Am. Chem. Soc.* **1974,** *96,* 6757-6759.
17. Allen, P. G.; Bucher, J. J.; Clark, D. L.; Edelstein, N. M.; Ekberg, S. A.; Gohdes, J. W.; Hudson, E. A.; Kaltsoyannis, N.; Lukens, W. W. *Inorg. Chem.* **1995,** *34,* 4797-4807.
18. Jolivet, J. P.; Taravel, T. B.; Lorenzelli, V. J. *J. Mol. Struct.* **1980,** *60,* 93-98.
19. Galperin, V. A.; Finkelshtein, A. I. *Zh. Prikl. Spektr.* **1972,** *17,* 468-471.
20. Frasco, D. L. *J. Chem. Phys.* **1964,** *41,* 2134-2140.
21. Anderson, A.; Chieh, C.; Irish, D. E.; Tong, J. P. K. *Can. J. Chem.* **1980,** *58,* 1651-1658.
22. Rofail, N. H. *Mater. Chem. Phys.* **1994,** *36,* 241-245.

Downloaded by UNIV OF GUELPH LIBRARY on August 9, 2012 | http://pubs.acs.org
Publication Date: June 9, 2006 | doi: 10.1021/bk-2006-0933.ch010

23. Graziani, R.; Bombieri, G.; Forsellini, E. J. C. S. *J. Chem. Soc., Dalton Trans.* **1972,** *19,* 2059-2061.
24. Maya, L.; Begun, G. M. *J. Inorg. Nucl. Chem.* **1981,** *43,* 2827-2832.
25. Griffith, W. P.; Lesniak, P. J. B. *J. Chem. Soc. A* **1969,** *7,* 1066-1071.
26. Himeno, S.; Niiya, H.; Ueda, T *Bull. Chem. Soc. Jpn.* **1997,** *70,* 631-637.
27. Rob van Veen, J. A.; Sudmeijer, O.; Emeis, C. A.; de Wit, H. J. *J. Chem. Soc., Dalton Trans.* **1986,** *9,* 1825-1831.
28. Briand, L. E.; Valle, G. M.; Thomas, H. J. *J. Mater. Chem.* **2002,** *12,* 299-304.
29. Teterin, E. G.; Shesterikov, N. N.; Krutikov, P. G.; Solovkin, A. S. *Zh. Neorg. Khim.* **1971,** *16,* 780-784.
30. Pettersson, L.; Andersson, I.; Ohman, L. O. *Inorg. Chem.* **1986,** *25,* 4726-4733.
31. Veyland, A.; Dupont, L.; Rimbault, J.; Pierrard, J. C.; Aplincourt, M.; Bourg, S.; Nuzillard, J. M.; Angiboust, J. F. *Helv. Chim. Acta* **1999,** *82,* 2003-2014.
32. Jiang, J.; May, I.; Sarsfield, M. J.; Ogden, M.; Fox, D. O.; Jones, C. J.; Mayhew, P. *J. Solution Chem.* in press.

Downloaded by UNIV OF GUELPH LIBRARY on August 9, 2012 | http://pubs.acs.org
Publication Date: June 9, 2006 | doi: 10.1021/bk-2006-0933.ch010

Chapter 11

Plutonium Peroxide in Process Chemistry: Oxidation State, Coordination Chemistry, and Solubility

Glenn A. Fugate and James D. Navratil

Department of Environmental Engineering and Science,
Clemson University, Clemson, SC 29634

Downloaded by UNIV OF GUELPH LIBRARY on August 10, 2012 | http://pubs.acs.org
Publication Date: June 9, 2006 | doi: 10.1021/bk-2006-0933.ch011

Summary

Successful development of advanced processing of nuclear fuels to recycle plutonium and uranium, or to partition and transmute less useful species, will rely substantially on reagents and materials that contribute minimally to the creation of solid wastes. In this context, hydrogen peroxide can be a practical reagent in future process design, particularly for aqueous processing of high purity plutonium. H_2O_2 can be used to adjust the oxidation state, to purify or to separate plutonium in the laboratory or in industrial processes. Plutonium forms two soluble complexes with peroxide and a precipitate that can include a variety of anions. The precipitate forms in two different crystalline phases with the hexagonal phase having more advantageous properties for precipitation processes. Formation of the precipitate during oxidation adjustment steps must be monitored to avoid criticality concerns during large-scale processing operations. The Savannah River Site and other facilities have used the formation of a peroxide solid to purify the material during the production of plutonium metal. In this chapter, we describe the features of plutonium interactions with H_2O_2.

Introduction

Hydrogen peroxide has been an important reagent in the historical development of actinide chemistry and remains useful in the current laboratory and process chemistry of plutonium. This compound is a convenient reagent for the adjustment of the oxidation state of dissolved plutonium and has been employed as a precipitant in the purification of plutonium from impurities for weapons applications. As a product of the radiolysis, H_2O_2 can appear in solution as a degradation product of water, hence its chemistry in contact with actinides and fission products is a matter of clear relevance to all nuclear fuels processing.

As a possible reagent for use in future nuclear fuel cycles, it is noteworthy that the byproducts of H_2O_2, oxygen, protons and water, do not contribute to the volume of generated wastes. Furthermore, precipitation of plutonium peroxides can also be an important criticality concern for any large-scale process where Pu-H_2O_2 solids can potentially occur. It is clearly important that the chemistry of actinide interactions with H_2O_2 be well understood under most conditions. Fortunately, a considerable amount of information is already available on this chemistry, as will be described below.

Downloaded by UNIV OF GUELPH LIBRARY on August 10, 2012 | http://pubs.acs.org
Publication Date: June 9, 2006 | doi: 10.1021/bk-2006-0933.ch011

Oxidation State Chemistry

The standard potentials of hydrogen peroxide, shown in equations 1, 2 and 3, indicate that this reagent can be a strong oxidizing agent (equations 1 and 2) or a weak reducing agent (equation 3), depending upon solution conditions. Hydrogen peroxide is thermodynamically unstable and so is subject to disproportionation as shown by combining equations 1 and 3. The different electrochemical properties of this molecule allow the simultaneous oxidation and reduction of plutonium species (*1*).

$$H_2O_2 + 2\,H^+ + 2\,e^- = 2\,H_2O \qquad E^0 = 1.77\ V \qquad (1)$$

$$HO_2^- + H_2O + 2\,e^- = 3\,OH^- \qquad E^0 = 0.87\ V \qquad (2)$$

$$O_2 + 2\,H^+ + 2\,e^- = H_2O_2 \qquad E^0 = 0.68\ V \qquad (3)$$

Plutonium (VI) ions are rapidly reduced to the pentavalent oxidation state upon the addition of excess hydrogen peroxide in acidic solutions. The reaction typically occurs within minutes and has been characterized by the rate law:

$$\frac{-d[\mathrm{Pu\ (VI)}]}{dt} = k\,[\mathrm{Pu\ (VI)}]\,[H_2O_2]\,[H^+]^{-1} \qquad (4)$$

where k = 0.38 ± 0.1, 0.75 ± 0.1 and 0.37 ± 0.1 minute^{-1} for perchlorate, nitrate and sulfate media, respectively, in media of 1 M ionic strength at 22°C *(1)*. The reduction of the pentavalent oxidation state by hydrogen peroxide occurs very slowly, typically taking hours. Formation of the IV oxidation state occurs as a result of disproportionation of plutonium (V) when the concentration of that species is sufficiently high.

Hydrogen peroxide can simultaneously oxidize plutonium from III to IV and reduce plutonium from IV to III in the same solution. The half life of each reaction is mreasured in minutes. The equilibrium generally favors the trivalent oxidation state in dilute hydrochloric, nitric or perchloric acid systems while the equilibrium shifts to the tetravalent oxidation state in strongly complexing media such as sulfuric acid *(2)*. The formation of plutonium (IV) peroxide complexes can further shift the equilibrium to favor the tetravalent oxidation state. A net effect of this equilibrium is the catalytic destruction of hydrogen peroxide *(3)*.

Downloaded by UNIV OF GUELPH LIBRARY on August 10, 2012 | http://pubs.acs.org
Publication Date: June 9, 2006 | doi: 10.1021/bk-2006-0933.ch011

Coordination Complexes

The discovery of the coordination complex formed between plutonium and hydrogen peroxide was first noted by Cunningham and Werner during the initial isolation of plutonium *(4)*. The precipitate has been shown to form by the stepwise addition of peroxide to a dinuclear plutonium (IV) species, forming brown and red aqueous complexes and a green precipitate.

Brown Plutonium (IV) Peroxide Complex

Connick and McVey studied the formation of peroxide complexes in acidic systems containing plutonium in different oxidation states *(2)*. No evidence of complex formation was observed for the V and VI plutonium oxidation states, although the generation of oxygen and the appearance of Pu(III) and Pu(IV) indicated that the hydrogen peroxide was behaving as a reducing agent. The addition of hydrogen peroxide to a solution of plutonium (IV) produced an immediate change of color in the solution from brown to a deep brown. Further addition of hydrogen peroxide caused the solution to change rapidly to red before a green precipitate appears. No oxygen generation was observed during this process, indicating that the species are soluble complexes with plutonium (IV). These results are consistent with other work that examined the UV-visible-NIR spectrum of plutonium, noting that the characteristic bands of the tetravalent oxidation state were observed when a sample of plutonium peroxide precipitate was dissolved in 10 N hydrochloric acid *(5)*.

The visible spectra of plutonium (IV) and the brown and red peroxide complexes are shown in Figure 1 with the peaks summarized in Table I. The reported molar extinction coefficients are based upon the initial plutonium concentration. The brown complex was noted to form upon the addition of up to one half equivalent of hydrogen peroxide. The spectra were fit using several different models that included plutonium (III), plutonium (IV), the brown complex and the red complex. The only consistent fit was produced by assuming that two plutonium (IV) atoms were complexed by one peroxide molecule. The fit produced an equilibrium constant of 7.0×10^7 for the equation K_1 = [brown complex] / $[Pu^{4+}]^2$ $[H_2O_2]$ in 0.5 M hydrochloric acid *(2)*. The stability of the brown complex was monitored as the acidity was varied between 0.2 and 1 M hydrochloric acid. The increase of the concentration of plutonium (IV) with increasing acidity indicated that the complex also contained one hydroxide group. The structure of the complex, shown in Figure 2, most likely includes a peroxy bridge between the plutonium atoms. The hydroxide group may also bridge the plutonium atoms or may be localized around a single atom. The complex formation is given by the reaction:

$$2\,Pu^{4+} + H_2O_2 + H_2O = [Pu(OO)(OH)Pu]^{5+} + 3\,H^+ \qquad (5)$$

where OO is the peroxide molecule. The equilibrium quotient for this reaction is:

$$K_{brown} = \frac{[Pu(OO)(OH)Pu^{5+}][H^+]^3}{[Pu^{4+}]^2[H_2O_2]} \qquad (6)$$

where the value of K_{brown} has been reported as 8.8×10^6 *(2)*.

Red Plutonium (IV) Peroxide Complex

A red plutonium peroxide complex is instantly generated upon the addition of up to one half an equivalent of hydrogen peroxide to a solution of the brown complex. Addition of more than one total equivalence of hydrogen peroxide results in the formation of green plutonium peroxide precipitate. An equilibrium quotient of 145 was determined for the equation K_2 = [red complex] / [brown complex] $[H_2O_2]$ in 0.5 M hydrochloric acid by a fit of the spectroscopic data that included plutonium (III) and (IV), the brown complex and the red complex

Downloaded by UNIV OF GUELPH LIBRARY on August 10, 2012 | http://pubs.acs.org
Publication Date: June 9, 2006 | doi: 10.1021/bk-2006-0933.ch011

Downloaded by UNIV OF GUELPH LIBRARY on August 10, 2012 | http://pubs.acs.org
Publication Date: June 9, 2006 | doi: 10.1021/bk-2006-0933.ch011

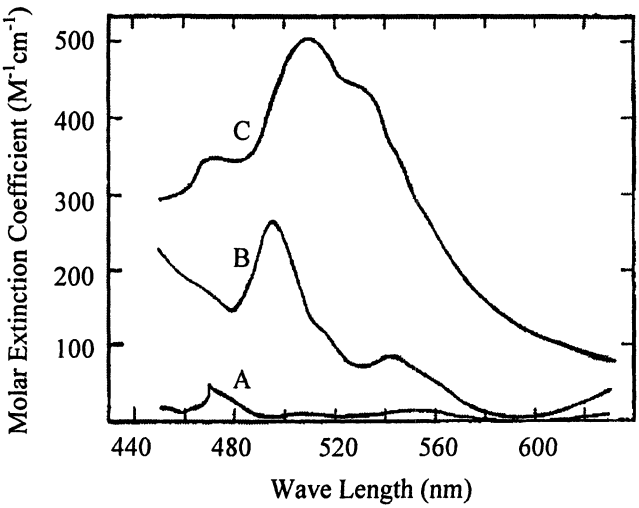

Figure 1. Spectra of (A) plutonium (IV), (B) brown plutonium hydrogen peroxide complex and (C) red plutonium hydrogen peroxide complex in 0.5 M HCl at 25°C (Reproduced with permission from reference 2. Copyright 1949 ACS.).

Table I. Summary of the Peaks from Plutonium Peroxide Species *(2).*

Species	*Peak (nm)*	*Molar Extinction Coefficient (M^{-1} cm^{-1})*
Plutonium (IV)	470.0	56
Brown Complex	495.5	266
Red Complex	510.0 530.0	441

(2). Experiments at 0.2 and 0.5 M hydrochloric acid indicated an inverse relationship between increasing acidity and the stability of the red complex, suggesting that the complex contains a hydroxide group or that one of the peroxy atoms is protonated. The structure of the complex most likely consists of either one bridging peroxide molecule with a hydroxide group and a protonated peroxide group associated with one of the plutonium atoms or as two bridging peroxide molecules as shown in Figure 3. The formation of this complex can be expressed by the reaction:

$$2\,Pu^{4+} + 2\,H_2O_2 = [Pu(OO)_2Pu]^{4+} + 4\,H^+ \qquad (7)$$

where OO represents the peroxy molecule. The corresponding equilibrium quotient can be expressed by the equation:

$$K_{red} = \frac{[Pu(OO)_2Pu^{4+}][H^+]^4}{[Pu^{4+}]^2[H_2O_2]^2} \qquad (8)$$

where K_{red} has been reported as 6.3 x 10^8 *(2)*.

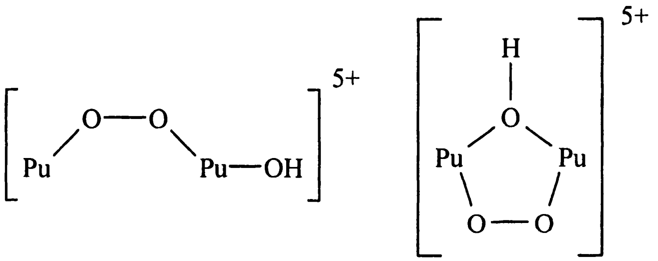

Figure 2. Potential structures of the brown complex of plutonium (IV) with hydrogen peroxide.

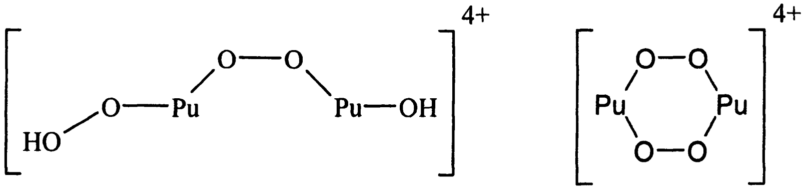

Figure 3. Potential structures of the red complex of plutonium (IV) hydrogen peroxide.

Downloaded by UNIV OF GUELPH LIBRARY on August 10, 2012 | http://pubs.acs.org
Publication Date: June 9, 2006 | doi: 10.1021/bk-2006-0933.ch011

Other Plutonium Peroxide Complexes

Nash *et al.* reported a transient reddish brown complex formed between plutonium (VI) and hydrogen peroxide in solutions containing high concentrations of bicarbonate *(6)*. This observation has been confirmed by Runde *et al (7)*. The plutonium (VI) complex was examined by stopped-flow spectrophotophotometric techniques with the spectrum reported for the species shown in Figure 4. The complex is short lived and is proposed to be an intermediate in the reaction pathway of the reduction of plutonium (VI) to (V). Comparison to peroxide complexes for uranium (VI) and neptunium (VI) in carbonate media lead the authors to suggest that the interaction between the actinide (VI) interaction and hydrogen peroxide occurs through the "yl" oxygen instead of the equatorial plane of the dioxocation *(6)*. More recent work suggests that peroxide can form a coordination directly with plutonium (VI), effectively competing with and displacing a carbonate from the inner sphere of the ion *(7,8)*.

Musikas noted the formation of a red complex in 1 M sodium hydroxide solutions at 0°C that were attributed to plutonium (V) peroxide *(9)*. The spectrum reported for the red complex is nearly the same as the summation of the spectra reported for the plutonium (VI) complexes with carbonate and peroxide in Nash *et al. (6)*. A plutonium (V) complex should be stable at higher temperatures because of the slow kinetics of the reduction of the pentavalent oxidation state by hydrogen peroxide. The unusual oxidation state analysis performed by Musikas may also suggest that the reported complex could be the transient plutonium (VI) peroxide species *(9)*.

Downloaded by UNIV OF GUELPH LIBRARY on August 10, 2012 | http://pubs.acs.org
Publication Date: June 9, 2006 | doi: 10.1021/bk-2006-0933.ch011

Plutonium Peroxide Precipitate

The precipitation of plutonium using hydrogen peroxide was originally noted during the development of the first plutonium purification procedure *(4)*. The precipitate was noted to be dark green and have an approximate solubility of 23 g plutonium per liter in a solution of 1 molar nitric acid and 6 molar hydrogen peroxide *(4)*.

Studies have examined the effects of media, temperature and impurities on the formation of the plutonium peroxide precipitate. Koshland *et al.* demonstrated that the plutonium ion was in the tetravalent oxidation state by titrations of precipitate slurries with permanganate, iodide or stannous ion *(10)*. The number of peroxide oxygen atoms per plutonium was determined to be approximately 3. This stoichiometry was reproducible under a variety of temperature and media conditions. Prolonged drying was noted to reduce the ratio of peroxy atoms to plutonium from 3 to 2. The change in the material during drying suggests that different plutonium peroxide environments may exist within the precipitate and that one of the peroxide molecules may be less strongly bound to the metal ion.

Downloaded by UNIV OF GUELPH LIBRARY on August 10, 2012 | http://pubs.acs.org
Publication Date: June 9, 2006 | doi: 10.1021/bk-2006-0933.ch011

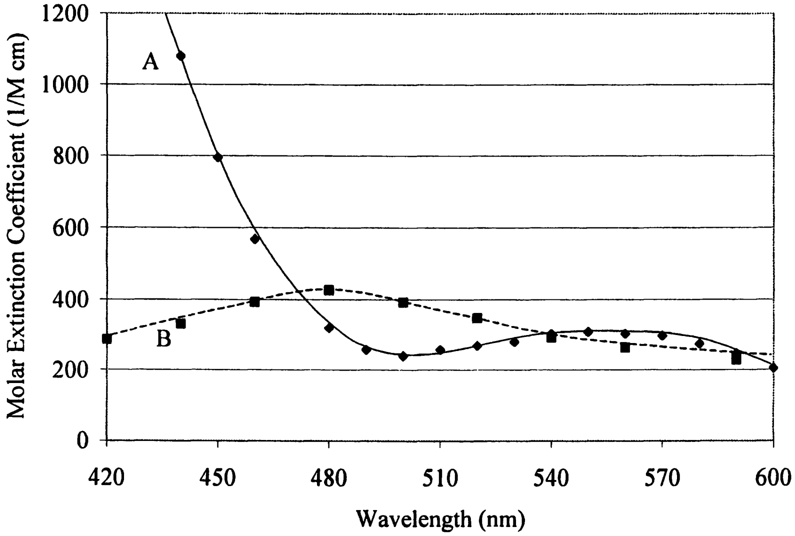

Figure 4. Spectra of (A) plutonium (VI) carbonate complex and (B) plutonium (VI) hydrogen peroxide complex in 0.05 M $NaHCO_3$ at 25°C (Reproduced with permission from reference 6. Copyright 1980 Elsevier.).

Downloaded by UNIV OF GUELPH LIBRARY on August 10, 2012 | http://pubs.acs.org
Publication Date: June 9, 2006 | doi: 10.1021/bk-2006-0933.ch011

Hopkins determined that plutonium formed a mixed peroxide precipitate with the general formula of $Pu^{4+}(R^{-})_{4-x}(O^{-})_x$ where R is an anion, x is the number of peroxide atoms and 4-x is the number of anion equivalents per plutonium *(5)*. A formula of $PuR_{0.85}O_{3.15}$ was determined for a material precipitated from 1.0 M nitric acid. Hamaker and Koch noted that the plutonium peroxide precipitate typically has 3 charge equivalents of peroxide per plutonium with the additional equivalence being another anion such as sulfate, nitrate, chloride or hydroxide *(11)*. Sulfate-containing precipitates appear to have increased stability, as this ion was found as the dominant non-peroxide anion component of the materials formed from all but the mostly highly purified nitric acid and hydrochloric acid solutions. Pure precipitates consisting of a single anion were difficult to obtain and typical materials contained sulfate and one or more of the anions: hydroxide, nitrate and chloride. The solubility of the precipitates can be categorized by the main anion present in the material and ranged from: 3.3 to 10.7 mg per liter for sulfate, 15 to 62 mg per liter for nitrate and 153 to 245 mg per liter for chloride *(11)*. Leary et al. later showed that purer materials are composed of plutonium (IV) and have an average peroxide atom to plutonium ratio of 3.03 ± 0.04 *(12)*. The composition is consistent with a study using thermogravimetric analysis coupled with X-ray and gas sampling which produced a thermogram for the peroxide precipitate. The thermogram has three regions that can be characterized as: loss of water below 90°C, decomposition of peroxide between 140 and 170°C and decomposition of nitrate and hydroxide between 210 and 290°C *(13)*.

Two different crystal phases have been observed for plutonium peroxide precipitates using X-ray powder diffractometry *(10, 11, 14)*. The first structure was characterized as a cubic face-centered with lattice constant a = 16.5 ± 0.1 Å *(14)*. The second structure is two-dimensional hexagonal with lattice constant a_1 = 4.00 ± 0.02 Å *(14)*. Both crystalline forms can be prepared with a variety of non-peroxide anion compositions *(10)*. The two-dimensional hexagonal structure is similar to the precipitate of thorium peroxide that has been suggested to be composed of hexagonal structures of thorium and peroxide linked together by anions and water *(11)*. A similar lattice structure was proposed for the hexagonal plutonium peroxide. Hexagonal crystal structures were obtained for materials containing sulfate and nitrate. This can only occur if these anions are interstitially located, most likely connecting the hexagonal plutonium peroxide units. Structures formed predominantly with chloride and containing minimal amounts of sulfate tend to preferentially form the cubic face-centered structure *(11)*.

Leary *et al.* have shown that the crystal structure also is dependent upon acidity with lower acidities favoring the formation of cubic face-centered structure *(12)*. The concentrations of hydrogen peroxide and sulfate have little effect upon the crystal structure. Additionally, crystal structures of plutonium peroxide and perchlorate could not be obtained, as the resulting material is colloidal.

Other actinides also form mixed precipitates with hydrogen peroxide. Thorium peroxide solids reported by Hamaker and Koch have the empirical formula $Th(R)_x(O^-)_y$. In the species where R is nitrate, x is typically 0.5 and y ranges between 2.91 and 3.22 (in acidic nitrate media) whereas when R is sulfate, x is 0.94 and y is 1.94 to 2.00 in sulfate media *(12, 15)*. Koshland *et al.* found two peroxy atoms per thorium for precipitates in 0.067 N sulfuric acid *(10)*. The acid concentration influenced the precipitate crystal phases. An orthorhombic phase with lattice constants a_1 = 16.4 ± 0.1 Å, a_2 = 10.3 ± 0.1 Å and a_3 = 4.23 ± 0.05 Å was formed in 0.33 M sulfuric acid. This crystal structure has four molecules per unit cell *(10)*. In 0.033 M sulfuric acid, a two-dimensional hexagonal phase forms with a lattice constant a_1 = 4.15 ± 0.02 Å that is isomorphous with the hexagonal crystalline form of plutonium peroxide *(10)*. Evidence for the existence of peroxide complexes of Np(IV) *(16, 17)*, Np(VI) *(18)* and U(VI) *(19-24)* have been shown, but these species appear to have very complex solution chemistry and tend to be more soluble than the Pu(IV) peroxide complex.

Downloaded by UNIV OF GUELPH LIBRARY on August 10, 2012 | http://pubs.acs.org
Publication Date: June 9, 2006 | doi: 10.1021/bk-2006-0933.ch011

Plutonium Processing - Precipitation

The formation of plutonium peroxide is an excellent concentration and purification procedure for the processing of plutonium and has been commonly used in the preparation of plutonium metal *(12, 25, 26)*. Leary *et al.* have listed initial masses of impurities introduced into the feed solution and the final mass of the impurity from the plutonium peroxide precipitate. Of the 26 elements analyzed in the study only thorium and uranium were coprecipitated by peroxide. Iron and other impurity ions capable of forming reduction-oxidation cycles with plutonium or hydrogen peroxide are significantly more important, as they can both consume hydrogen peroxide and affect the process chemistry by altering the plutonium oxidation state *(12, 26-28)*.

The crystal structure is highly dependent upon the acidity of the precipitation solution with the hexagonal structure forming preferentially as the acidity increases *(12)*. The hexagonal crystal structure is more desirable for processing conditions as it has better settling properties. Mainland *et al.* described the process used at the Savannah River Site to produce the high purity hexagonal plutonium peroxide nitrate solid that is used in the production of plutonium metal, shown in Figure 5 *(25)*. It was possible to remove the sulfate addition step (that had been used to improve the precipitate properties) by careful control of the conditions of the system. This adjustment provided a significant benefit in time, productivity and batch size for the next step in the plutonium metal production process, fluorination, as it was possible to eliminate

Downloaded by UNIV OF GUELPH LIBRARY on August 10, 2012 | http://pubs.acs.org
Publication Date: June 9, 2006 | doi: 10.1021/bk-2006-0933.ch011

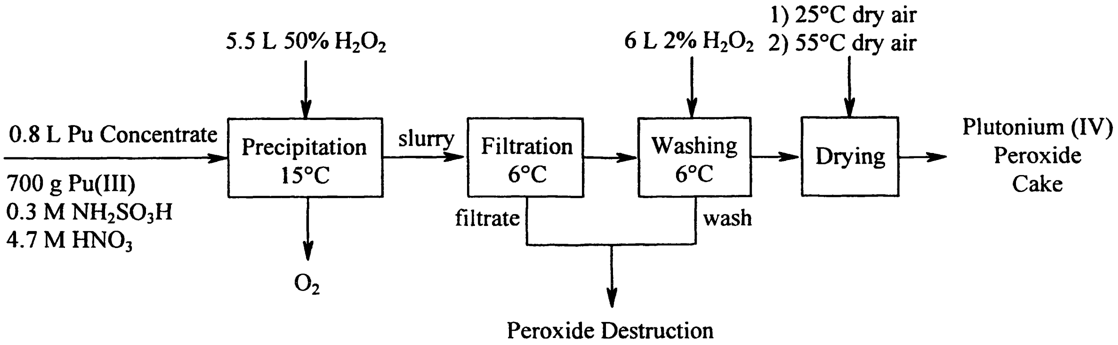
5.5 L 50% H_2O_2
6 L 2% H_2O_2
1) 25°C dry air
2) 55°C dry air
0.8 L Pu Concentrate
700 g Pu(III)
0.3 M NH_2SO_3H
4.7 M HNO_3
Precipitation
15°C
slurry
Filtration
6°C
Washing
6°C
Drying
Plutonium (IV)
Peroxide
Cake
O_2
filtrate
wash
Peroxide Destruction

Figure 5. The SRS plutonium peroxide precipitation process (Adapted with permission from reference 25. Copyright 1961 ACS.).

additional processing to remove sulfate *(25)*. The plutonium peroxide precipitation process has been further refined by studies of factors that influenced the rate of filtration including nitric acid concentration, hydrogen peroxide concentration and addition rate, effect of impurities, digestion time and temperature upon the filtration time of plutonium peroxide *(29)*.

Plutonium Processing – Oxidation State Adjustment

Hydrogen peroxide also can be a convenient reagent to adjust the oxidation state of plutonium during processing *(30)*. The reagent is available in high purity and high concentration, is easily diluted and has reaction byproducts that are readily removed from the system. On the other hand, the possible formation of undesirable plutonium solids can lead to criticality concerns in large-scale operations. Maillard and Adnet studied the conditions and kinetics of Pu(IV) peroxide precipitate from a Pu(VI) solution at 35°C in nitric acid media *(31)*. The conditions of precipitation depended upon the acidity, the plutonium concentration and the concentration ratio of hydrogen peroxide to plutonium (VI) as shown in Figure 6. Increasing acidity, decreasing Pu(VI) concentration and decreasing hydrogen peroxide to plutonium concentration ratio all decreased precipitation. The reduction of plutonium (VI) occurred within minutes in a 1 M plutonium, 2 M nitric acid system with $[H_2O_2]/[Pu\ (VI)]$ of 1.45 at 35°C. The mixture of III and IV oxidation states present initially was converted entirely to plutonium (IV) after 10 minutes. The presence of silver, a catalyst often used in the dissolution of plutonium dioxide, had no effect upon the rate of plutonium reduction, while the rate was significantly altered by changes in the concentration of plutonium and temperature.

Summary

Under suitable conditions, hydrogen peroxide can be a convienent reagent in both laboratory and industrial scale plutonium chemistry. The formation of a precipitate can be used to concentrate plutonium as a plutonium peroxide solid and to purify plutonium from many common impurity ions. The presence and crystalline form of the plutonium precipitate can be controlled by factors such as acidity, plutonium concentration, addition rate of hydrogen peroxide and the concentration of hydrogen peroxide. The oxidation state of plutonium can be adjusted using hydrogen peroxide without the introduction of counter ions that may affect later processes or purity of the material. Hydrogen peroxide is readily available in high purity, can be easily destroyed and its degradation products, oxygen, protons and water, do not add significant volume or toxicity to

Downloaded by UNIV OF GUELPH LIBRARY on August 10, 2012 | http://pubs.acs.org
Publication Date: June 9, 2006 | doi: 10.1021/bk-2006-0933.ch011

Downloaded by UNIV OF GUELPH LIBRARY on August 10, 2012 | http://pubs.acs.org
Publication Date: June 9, 2006 | doi: 10.1021/bk-2006-0933.ch011

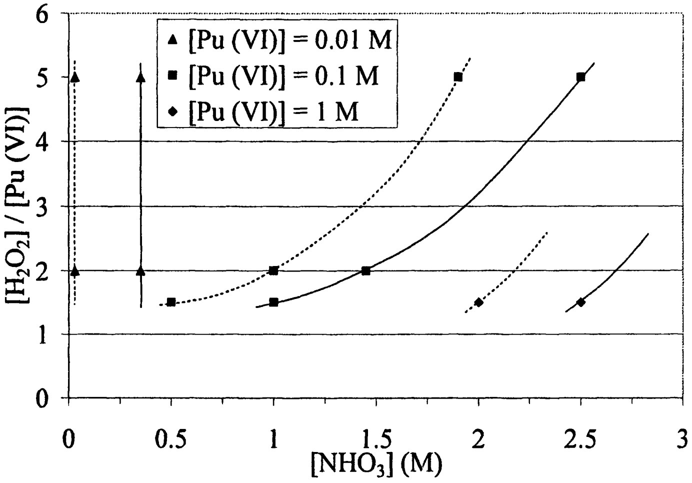

Figure 6. Domains of plutonium (IV) peroxide precipitation based upon initial concentrations of plutonium (VI), nitric acid and hydrogen peroxide to plutonium (VI) concentration ratio at 35°C Dashed lines indicate the maximum acidity where precipitates were stable and solids lines indicate minimum acidity where no precipitates were observed. (Reproduced with permission from reference 31. Copyright 2001 Oldenbourg).

generated wastes. Because hydrogen peroxide is a common product of the radiolysis of water, its chemistry with plutonium and other actinide elements must be considered in the design of any large scale process due to criticality and safety concerns.

References

1. Lesigne, B. "Kinetic Study of Hexavalent Plutonium Reduction by Hydrogen Peroxide in Acid Solutions" Commissariat a l'Energie Atomique Report 3168, 1967.
2. Connick, R.E.; McVey, W.H. *J. Am. Chem. Soc.* **1949**, 71, 1534.
3. Elson, R.E. "The Homogeneous Decomposition of Hydrogen Peroxide by Plutonium (IV)" Lawrence Radiation Laboratory report UCRL-6536, 1961.
4. Cunningham, B.B.; Werner, L.B. *J. Am. Chem. Soc.* **1949**, 71, 1521.
5. Hopinks, H.H., Jr. *Transuranium Elements*; Seaborg, G.T.; Katz, J.J.; Manning, W.M., Eds.; McGraw Hill: New York, 1949; pp 635-636.
6. Nash, K.L.; Noon, M.E.; Fried, S.; Sullivan, J.C. *Inorg. Nucl. Chem. Lett.* **1980**, 16, 33.
7. Runde, W.; Peper, S.M.; Scott, B.L.; Jarvinen, G. "Structure and Stability of Peroxo Complexes of Uranium and Plutonium in Carbonate Solutions" Actinides 2005, Abstract Paper 2C01.
8. Peper, S.M.; Brodnax, L.F.; Field, S.E.; Zehnder, R.A.; Valdez, S.N.; Runde, W.H. *Ind. Eng. Chem. Res.* **2004**, 43, 8188-8193.
9. Musikas, C. *Radiochem. Radioa. Let.* **1971**, 7, 375.
10. Koshland, D.E., Jr.; Kroner, J.C.; Spector, L. *Transuranium Elements*; Seaborg, G.T.; Katz, J.J.; Manning, W.M., Eds.; McGraw Hill: New York, 1949; Vol. 1, pp 731-739.
11. Hamaker, J.W.; Koch, C.W. *Transuranium Elements*; Seaborg, G.T.; Katz, J.J.; Manning, W.M., Eds.; McGraw Hill: New York, 1949; Vol. 1, pp 666-681.
12. Leary, J.A.; Morgan, A.N.; Maraman, W.J. *Ind. Eng. Chem.* **1959**, 51, 27.
13. Moseley, J.D.; Robinson, H.N. *T. Am. Nucl. Soc.* **1966**, 9, 20
14. Mooney, R.C.L.; Zachariasen, W.H. *Transuranium Elements*; Seaborg, G.T.; Katz, J.J.; Manning, W.M., Eds.; McGraw Hill: New York, 1949; Vol. 2, pp 1442-1447.
15. Hamaker, J.W.; Koch, C.W. "A Study of the Peroxides of Thorium" US Atomic Energy Commission Report TID-5223, 1957, pp 318-338.
16. Moskvin, A.I. *Radiochemistry* **1968**, 10, 13.
17. Burgener, C.S.; Sullivan, J.K. *Inorg. Chem.* **1970**, 9, 2604.

Downloaded by UNIV OF GUELPH LIBRARY on August 10, 2012 | http://pubs.acs.org
Publication Date: June 9, 2006 | doi: 10.1021/bk-2006-0933.ch011

18. Musikas, C. *J. Chim. Phys.* **1974**, 71, 197.
19. Gayer, K.H.; Thompson, L.C. *Canad. J. Chem.* **1958**, 36, 1649.
20. Gilpatrick, L.O.; Jolley, M.J.; Kelley, M.J., Silverman, M.D.; Watson, G.M. "The Concentration of Peroxide in Uranyl Sulfate Solutions at Incipient Precipitation", Oak Ridge National Laboratory Report CF-59-10-121, 1959.
21. Kamarov, E.V. *Rus. J. Inorg. Chem.* **1959**, 4, 591.
22. Moskvin, A.I. *Sov. Radiochem.* **1968**, 10, 10.
23. Dojic, R.; Branica, M. *Electroanal.* **1992**, 4, 151.
24. Dojic, R.; Raspor, B.; Branica, M. *Croat. Chem. Acta* **1993**, 66, 262.
25. Mainland, E.W.; Orth, D.A.; Field, E.L.; Radke, J.H. *Ind. Eng. Chem.* **1961**, 53, 685.
26. Marsh, S.F.; Matinez, E.A.; Day, R.S.; Nixon, A.E. "Reduction of Pu(VI) with Hydrogen Peroxide: Effects of Plutonium, Peroxide, and Iron Concentrations and of Reaction Time" Los Alamos National Laboratory Report LA-12554, 1993.
27. Sill, C.W.; Percival, D.R.; Williams, R.L. *Anal. Chem.* **1970**, 42, 1273.
28. Miner, F.J.; Hagan, P.G. *Ind. Eng. Chem. Process Des. Develop.* **1972**, 11, 547.
29. Hagan, P.G.; Miner, F.J. *ACS Symposium Series 117: Actinide Separations*; Navratil, J.D.; Schulz, W.W., Eds. American Chemical Society: Washington, DC, 1980.
30. Marsh, S.F.; Gallegos, T.D. "Chemical Treatment of Plutonium with Hydrogen Peroxide before Nitrate Anion Exchange Processing" Los Alamos National Laboratory Report LA-10907, 1987.
31. Maillard, C.; Adnet, J.-M. *Radiochem. Acta* **2001**, 89, 485.

Downloaded by UNIV OF GUELPH LIBRARY on August 10, 2012 | http://pubs.acs.org
Publication Date: June 9, 2006 | doi: 10.1021/bk-2006-0933.ch011

Chapter 12

Crystallization of Uranium Complexes for Partitioning of Spent Nuclear Fuel

Don Mullins[1], Gordon Jarvinen[1], Michael Mayne[1], Doris Ford[1], Kristy Long[1], Heidi Reichert[1], Phillip Palmer[2], C. Drew Tait[2], D. Webster Keogh[1], and Pamela Gordon[2]

[1]Nuclear Materials and Technology Division and [2]Chemistry Division, Los Alamos National Laboratory, Los Alamos, NM 87545

Downloaded by CORNELL UNIV on August 9, 2012 | http://pubs.acs.org
Publication Date: June 9, 2006 | doi: 10.1021/bk-2006-0933.ch012

Previous work in Germany and Japan has indicated that crystallization of uranyl nitrate at low temperatures from nitric acid solution could be a useful process for removing most of the uranium from spent light water reactor (LWR) fuel following the dissolution of the fuel in nitric acid. The crystallization process could potentially reduce the cost of LWR fuel partitioning because it selectively removes most of the uranium which is about 96% of the LWR spent fuel mass (metal basis). Subsequent separation processes would only need to handle the smaller volume of remaining actinides and the fission products. We are evaluating an approach to separating uranyl nitrate from spent fuel dissolver solutions by water and nitric acid distillation, a continuous adiabatic reduced-pressure crystallizer Initial work to define the process flowsheet and obtain data on optimum crystallization conditions and the purity of the uranium product are described.

In Separations for the Nuclear Fuel Cycle in the 21st Century; Lumetta, G., et al.;
ACS Symposium Series; American Chemical Society: Washington, DC, 2006.

Introduction

The mission of the Advanced Fuel Cycle Initiative (AFCI) of the Office of Nuclear Energy Science and Technology of the U.S. DOE is to develop and demonstrate technologies that will enable the transition to a long-term and economically and politically viable advanced nuclear energy cycle. Development of separations technologies under the AFCI has multiple goals: reducing the cost of geological disposal of high-level nuclear waste and indefinitely delaying the need for a second repository, diminishing inventories of plutonium, and recovering the energy value in spent nuclear fuel. The industrial spent fuel inventory in the U.S. will reach the Yucca Mountain statutory capacity of 70,000 tonnes within a decade. If we only retain the current level of nuclear generating capacity and spent fuel generation rate of 2,000 t/year, an equivalent amount of spent fuel will accumulate by about 2040. An increased role for nuclear power will generate even more spent fuel. The AFCI can ameliorate the spent fuel disposal requirements by extending the time at which a second repository is needed and enable this growth in nuclear generating capacity. This capability can be secured by developing treatment technologies that are economically attractive, environmentally sound, and responsive to concerns with diversion of nuclear materials and the proliferation of nuclear weapons worldwide.

Prior reports from Germany and Japan have indicated that crystallization of uranyl nitrate complexes at low temperatures from nitric acid solution could be a useful process for removing most of the uranium from nitric acid dissolver solutions of spent light-water reactor (LWR) fuel (*1-2,5-6*). The uranyl nitrate crystallization process was considered as an alternative to using the typical PUREX solvent extraction system for recovering the uranium. The process potentially could reduce the cost of LWR fuel partitioning because it provides a selective and compact process for removing most of the uranium which is about 96% of the LWR spent fuel mass. Subsequent separation processes (e.g., PUREX-type liquid-liquid extractions) would only need to handle the smaller volume of other actinides and fission products. In addition, bench scale work has shown it is possible to remove substantial amounts of plutonium (and likely neptunium as well) in the crystallization process by oxidizing these metal ions to the hexavalent state, and by co-crystallizing the Pu(VI) and Np(VI) with the U(VI) nitrates.(*1,2*) The work reported here was begun to evaluate the capability of crystallization processes to remove uranium and other actinides selectively from nitric acid solutions and the potential to reduce the cost of LWR spent fuel processing relative to the baseline PUREX process.

Downloaded by CORNELL UNIV on August 9, 2012 | http://pubs.acs.org
Publication Date: June 9, 2006 | doi: 10.1021/bk-2006-0933.ch012

Downloaded by CORNELL UNIV on August 9, 2012 | http://pubs.acs.org
Publication Date: June 9, 2006 | doi: 10.1021/bk-2006-0933.ch012

A variety of approaches have been evaluated to recover uranyl nitrate from spent light water reactor fuel dissolved in nitric acid, including low-temperature crystallization methods studied in Germany and Japan. The previous crystallization methods have been batch bench-scale tested in aqueous nitric acid solutions and produced modest yet encouraging decontamination factors (DFs). Bench-scale work on uranyl nitrate crystallization in Germany showed hexavalent actinides can be selectively crystallized (95% yield) from cold nitric acid solutions (-20 to -40°C) and result in tri- or hexahydrate forms depending on conditions. DFs of 100-1000, with the elements; Rb, Sr, Y, Zr, Mo, Ru, Rb, Pd, Cd, Te, Cs, Ba, La, were achieved after two successive batch crystallizations (*2*). An example from the ongoing Japanese work proposed a process that would cool the 40° C nitric acid dissolver solution to 10°C and recover approximately 60% of the uranium as nitrate crystals. Bench-scale test solutions included thirteen fission products. The process produced DFs of 2 to 9 from these fission products with no crystal washings and 10 to 100 after three washes (*2*). This result indicates that there is limited occlusion within the crystals with a significant hold-up of unwanted fission products on the crystal surface.

Continuous processing has the potential to vastly improve decontamination performance; comparison of batch and continuous processing in distillation, for example, demonstrates that significant advantages reside within continuous processing. Thus, a novel process using a continuous adiabatic reduced-pressure crystallizer has been developed at Los Alamos National Laboratory and is the first process of its kind to be tested. The crystallizer vessel chosen is a vertical circulating loop where the solution will be cooled and concentrated by the evaporation of a portion of the nitric acid and water at reduced pressure; uranyl nitrate hexahydrate crystallizes from this supersaturated solution. The distilled acid will be recycled for use in the fuel dissolver, for crystal washing or for dissolving washed crystals. Operation of this unit, which has been improved after physical (slurry) tests, is expected to produce a uranium oxide product that can be recycled, or disposed of as low-level nuclear waste.

Organization of Development

Three parallel tasks must be undertaken to successfully run the actinide crystallization process: an understanding of the physical chemistry of uranyl nitrate crystallization, the development of a physical crystallizer unit operation, and the ability to operate and optimize the continuous crystallization process.

Physical Chemistry of Crystallization

The pertinent physical chemistry includes phase equilibria, the physical characteristics of the crystals, co-crystallization with other salts, the effect of temperature and nitric acid strength on solubility, and the effect of precipitation rates on crystal quality. For example, Np(VI) and Pu(VI) will co-crystallize with U(VI) under oxidizing conditions (*1*).

It is important to understand the kinetics of crystallizing uranyl nitrate so that correct residence times can be achieved in the continuously operating loop crystallizer. The residence time has a strong effect on production of crystals that are easy to wash and purify, with the objective being to produce a small size distribution of properly sized crystals. Carefully designed tests were planned in a series of small bench scale crystallizers having a volume of 100-500 mls. The first bench crystallizer assembled includes heating, cooling and vacuum systems. as shown in Figure 1.

Tests to obtain kinetic data on crystal growth began using calcium nitrate tetrahydrate and were designed to provide input on the rate of crystallization and size and morphology of crystals formed under conditions relevant to the loop crystallizer. Calcium nitrate tetrahydrate was used, as it is readily available commercially and is a well characterized starting material which can be recrystallized from nitric acid solutions at conditions similar to the process to be used for uranyl nitrate. The bench-top batch crystallizer unit was run several times with reproducible results. Starting concentrations of solutions with ~4 molar $Ca(NO_3)_2$ and 1.3 to 1.6 molar HNO_3 at a total volume of 120 to 150ml were used. The crystallizer was operated about 50 minutes under vacuum with a liquid removal rate of about 0.5 ml/min before fine crystals were visible in the solution. After running for another 10 minutes crystals had grown large enough to fall out of solution (~1mm diameter rods 1.5 to 4mm in length). After 21 minutes ~a 1 cm deep layer of crystals had accumulated on the bottom of the crystallizer. Based on the data from these runs it was estimated that the residence time in the loop crystallizer would be approximately 30 minutes (time from the formation of fines till the crystals have grown to an acceptable size for removal).

The first experiments using uranium solutions to test uranyl nitrate crystallization in the bench-scale crystallizer contained no surrogate fission products. These tests evaluated parameters such as time, temperature, and molarity of the U and nitric acid solution.

Uranyl nitrate can crystallize from nitric acid with various amounts of water of hydration. Literature methods were used to prepare the initial hexa- and dihydrates of uranyl nitrate and the waters of hydration were measured using thermal gravimetric analysis (TGA). The TGA data were in good agreement with the published literature on the hydrates. (*3*) Several uranyl nitrate crystallization runs have been made using the bench-scale unit at between 29-31°C with initial acid concentrations of 2M, 6M, and 10M. Nitric acid and water are distilled away at reduced pressure until shortly after crystallization begins. The pressure

Downloaded by CORNELL UNIV on August 9, 2012 | http://pubs.acs.org
Publication Date: June 9, 2006 | doi: 10.1021/bk-2006-0933.ch012

Downloaded by CORNELL UNIV on August 9, 2012 | http://pubs.acs.org
Publication Date: June 9, 2006 | doi: 10.1021/bk-2006-0933.ch012

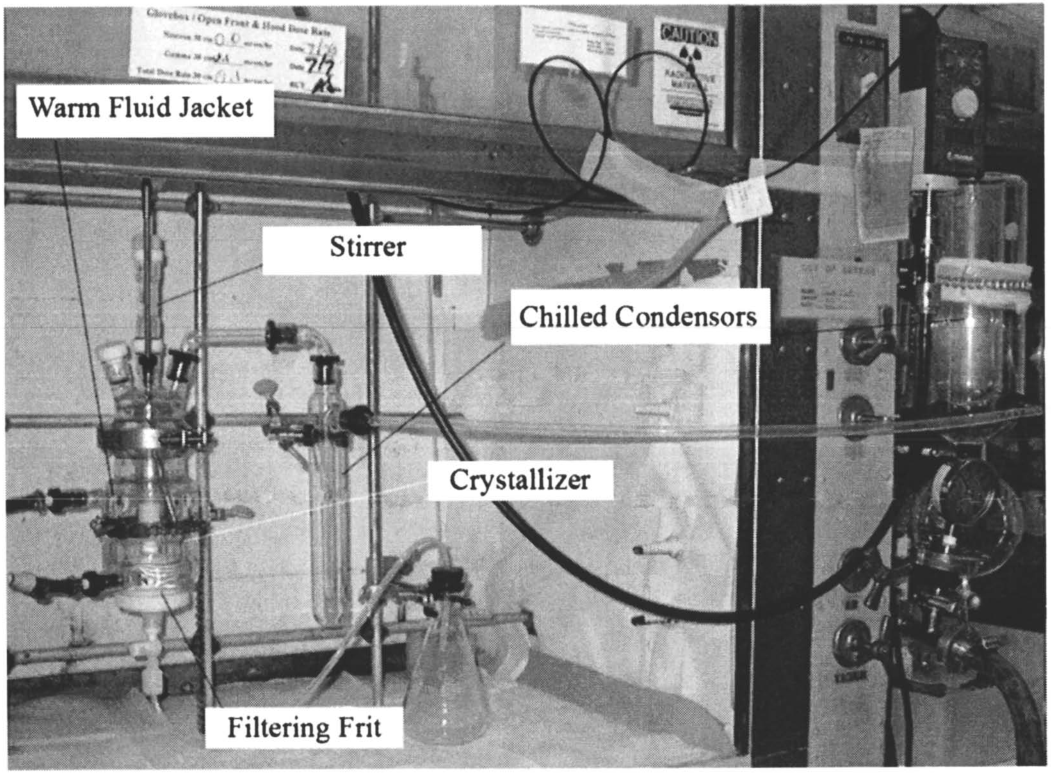
Warm Fluid Jacket
Stirrer
Chilled Condensors
Crystallizer
Filtering Frit
CAUTION

Figure 1. Bench-scale batch crystallizer for initial uranyl nitrate crystallization runs at 30℃.

In Separations for the Nuclear Fuel Cycle in the 21st Century; Lumetta, G., et al.;
ACS Symposium Series; American Chemical Society: Washington, DC, 2006.

applied differed depending upon the acid concentration, but we tried to keep it in the range of 20-10 mmHg. Very small crystals formed initially during each run and proceeded to grow in size and settled on the bottom of the (stirred) glass vessel. Once the crystals formed and settled to the bottom the run was stopped The crystals were collected by filtration and examined under a microscope. Densities of the solutions are measured before and after the runs. The nitric acid and uranium concentrations are also measured in the filtrate solution. The crystals grown from the 2M runs are multi-faceted rods 0.1 to 0.2 mm in diameter and 0.1 to 0.5 mm in length. The crystals from the 6 M runs are blocks or plates 0.1 to 0.5 mm thick and 0.5 mm square. The crystals grown in the 10 M runs are smaller blocks about 0.1 to 0.2mm on a side. Thermogravimetric analysis of the crystals indicates that all are primarily the hexahydrate although the crystals from higher acid crystals do appear to have somewhat less than six waters of hydration. There is no direct indication of two crystal types in the microscopy. These runs have provided useful density and concentration data for improving the mass balances and better defining the operating conditions for the loop system. The size distribution of the crystals appears narrower in the bench-scale equipment runs compared with the crystals grown in the previous vial tests based on the initial microscopic examination. A narrower size distribution is expected to result in better washing characteristics. The solution density, nitric acid concentration, and uranium concentration data from the series of uranyl nitrate crystallization runs correlate well with model results interpolated from literature values. This validates the modeling work and the planned operating parameters for the crystallization test runs.

Downloaded by CORNELL UNIV on August 9, 2012 | http://pubs.acs.org
Publication Date: June 9, 2006 | doi: 10.1021/bk-2006-0933.ch012

Crystallizer Unit Operation

The physical hardware, the crystallizer and its associated equipment, have undergone rigorous cold physical tests that include vapor handling and control as well as separation of solid phases from the (slurry). The initial test crystallizer (Figure 2) ran in a non-radiological laboratory using air, water, steam, and glass beads to confirm operability of various systems without the presence of uranyl nitrate or nitric acid.

The resulting physical properties of phases were comparable to process phases expected in the crystallizer, as the density difference between water and glass beads is similar to anticipated liquid and crystal density difference in actual unit operation.

Glass beads in sizes similar to the expected crystal size distribution were obtained and a further refining of the tests was concluded. The circulation of the crystallizer was tested by introducing a Gaussian size distribution of glass beads with water; the proper performance of the slurry lines and pumps as well as an appropriate no-clog valve design was established. The accurate operation of the control system was verified, and the combination densitometer/flowmeter was successfully tested. The circulation slurry velocity in the crystallizer was indirectly measured using a variable frequency ultraviolet strobe light combined with digital photography. This is used to compare the slurry velocity in the crystallizer to the settling velocities of various sizes of particles. Careful observation of flow patterns in the initial loop crystallizer revealed different flow velocity needs in various zones of the loop. The measured velocities obtained with the strobe were correlated with the observed slurry suspension characteristics. The study of this initial crystallizer design led to an improved version, which has been fabricated to include two or three different diameters in the sections of the loop. Another issue involved gas/liquid phase separation at the crystallizer vapor exit, which required a de-entrainment section that was designed and connected to the crystallizer.

Downloaded by CORNELL UNIV on August 9, 2012 | http://pubs.acs.org
Publication Date: June 9, 2006 | doi: 10.1021/bk-2006-0933.ch012

Optimization of Continuous Crystallization

Certainly the third task, of actually learning how to operate and optimize the continuous crystallizer, must wait for the concurrent maturing of the chemistry and process engineering. The preparation, equipment, and control system are in the final stages of development, while the maintenance of steady-state operation and consistent uniform crystal production with minimal occlusions and physical damage are to be mastered. The authorization documentation to operate the improved version of the loop crystallizer with uranium and nitric acid has been approved.

Actinide Crystallization Process Description

The Actinide Crystallization Process (ACP) currently under development uses an adiabatic flash crystallizer to crystallize uranyl nitrate hydrates from spent fuel dissolved in nitric acid. The crystallizer vessel is a vertical circulating loop. This configuration has been in industrial use for decades (*4*). The circulating solution is cooled and concentrated by evaporation of some of the nitric acid and water at reduced pressure. Uranyl nitrate hydrates crystallize from the supersaturated solution. The distilled acid and water will be recycled for further use in the plant. Unlike the PUREX Process there are no additional solutions used such as extraction solvents.

The current process modeling indicates that two stages of crystallization will be needed to obtain uranium recoveries in the 95-99% range. Figure 3 describes the process flows for the two-stage crystallizer.

Downloaded by CORNELL UNIV on August 9, 2012 | http://pubs.acs.org
Publication Date: June 9, 2006 | doi: 10.1021/bk-2006-0933.ch012

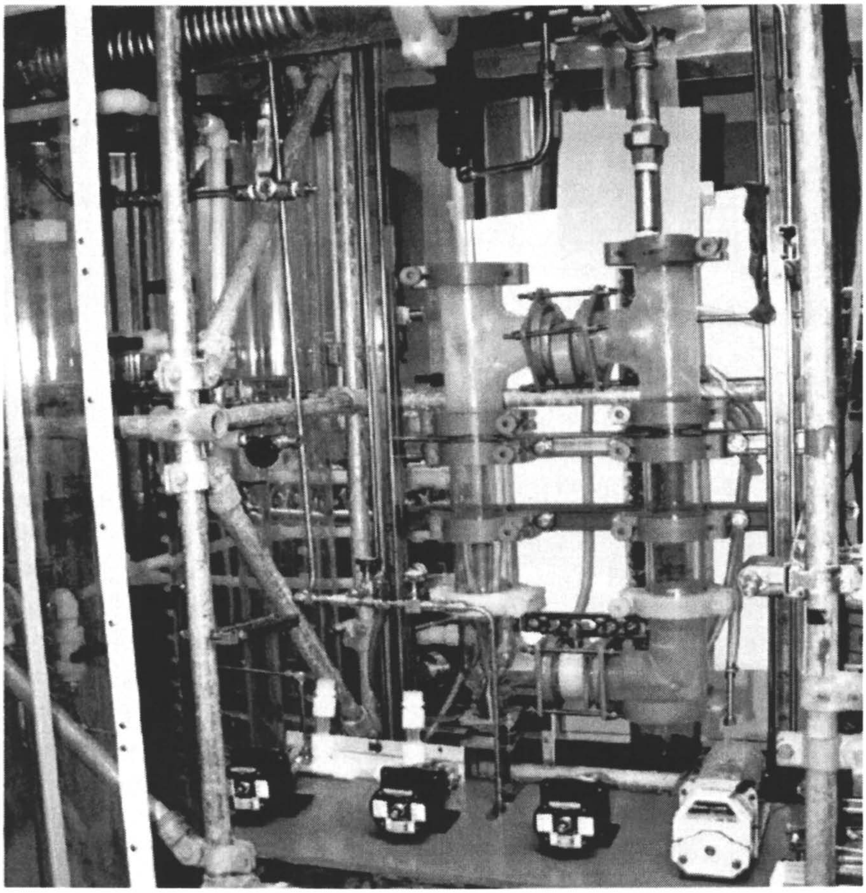

Figure 2. Initial design of ACP crystallizer

The primary crystallizer will operate near ambient temperature at about 15 torr of pressure. The crystallizer feed containing the spent fuel dissolved in nitric acid will be preheated. The feed enters and flashes at the bottom of one leg of the crystallizer. The flashed vapor lifts the liquid and circulates the crystallizer slurry. This avoids the need for a pumping propeller and the associated maintenance cost. The evaporation rate is controlled to maintain a uranium concentration in the solution for optimal crystal growth. The growth of the crystals is also controlled by a system to remove a slipstream of very small crystals or "fines," dissolve the fines by heating the solution, and return this solution to the feed stream. A portion of the circulating slurry is sent to a metal filter where the crystals are collected and washed. Slurry flow switches from one filter to another when the filter is full. Crystals in the first bed are purified and then dissolved. Purification is accomplished with two counter current rinses, followed by introduction of a nitric acid stream that partially dissolves the crystals and produces the fresh rinse solution. The remaining net UNH crystals are then dissolved and sent to rotary calcination or on to another crystallization step for more purification. Figure 4 depicts the test loop for a single-stage crystallizer with fines removal.

The filtrate solution from the first crystallizer is partly re-circulated as feed to the first crystallizer to maintain the liquid volume needed to suspend the crystals. The remaining filtrate is fed to the secondary lower-pressure crystallizer. The present model of the second unit indicates an operating temperature near -18°C and pressure at about 1 torr. The concentration and cooling of the solution again induces crystallization of uranyl nitrate hydrates. The reduced uranyl nitrate solubility at lower temperature results in a fission-product-containing effluent with the desired low uranium concentration.. A 95-99% recovery of uranium appears quite achievable at this stage of the flowsheet development. The crystals filtered from the second crystallizer will be dissolved in nitric acid and returned as feed to the first crystallizer. The filtrate or effluent from the second crystallizer will contain the fission products and transuranic elements and residual uranium in nitric acid solution. This effluent solution will be sent to other separation units in the plant to recover transuranic elements and selected fission products. Solubility data indicates that technetium will not be removed at room temperature, so an additional process would be needed for its recovery.

Extensive data on uranyl nitrate solubility as a function of nitric acid concentration and temperature exist. (*5*). There are very comprehensive vapor-liquid equilibrium databases for the aqueous nitric acid system. These data were used in developing the preliminary mass and energy balances. Key parts of the solubility data have been verified by experiments in the bench-scale crystallizer.

Downloaded by CORNELL UNIV on August 9, 2012 | http://pubs.acs.org
Publication Date: June 9, 2006 | doi: 10.1021/bk-2006-0933.ch012

Downloaded by CORNELL UNIV on August 9, 2012 | http://pubs.acs.org
Publication Date: June 9, 2006 | doi: 10.1021/bk-2006-0933.ch012

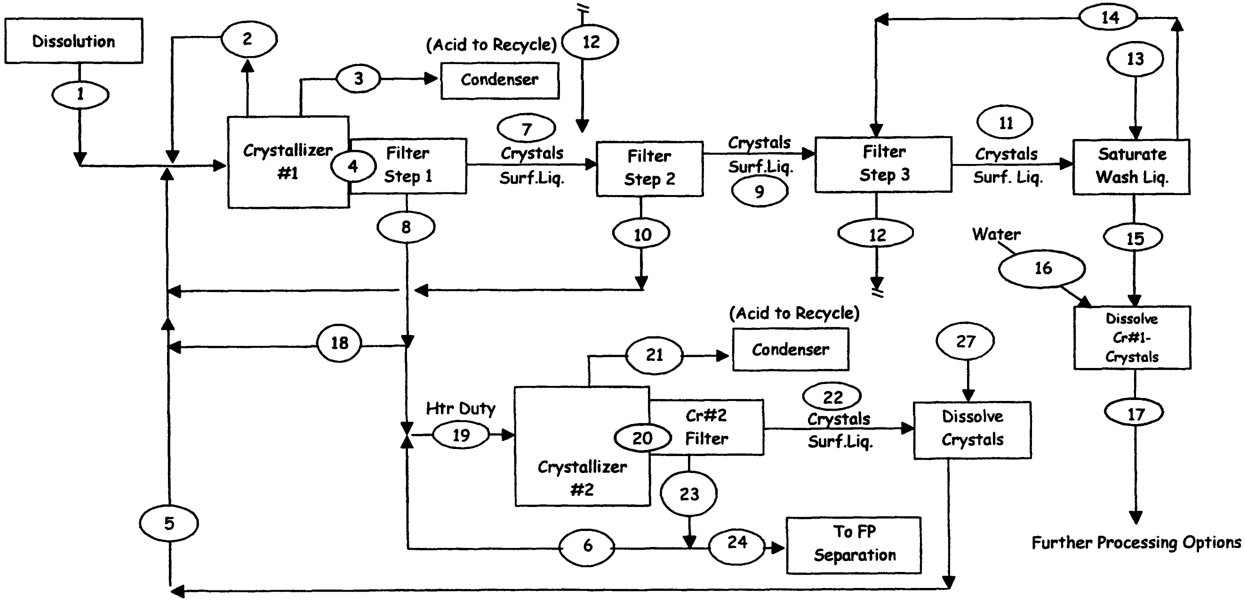
Dissolution
1
2
3
Condenser
(Acid to Recycle)
12
Crystallizer #1
4
Filter Step 1
7
Crystals Surf.Liq.
Filter Step 2
Crystals Surf.Liq.
9
Filter Step 3
11
Crystals Surf. Liq.
Saturate Wash Liq.
14
13
8
10
12
15
Water
16
Dissolve Cr#1-Crystals
17
Further Processing Options
18
(Acid to Recycle)
21
Condenser
27
Htr Duty
19
20
Cr#2 Filter
22
Crystals Surf.Liq.
Dissolve Crystals
Crystallizer #2
23
5
6
24
To FP Separation

Downloaded by CORNELL UNIV on August 9, 2012 | http://pubs.acs.org
Publication Date: June 9, 2006 | doi: 10.1021/bk-2006-0933.ch012

Figure 3. Process flow diagram mass balance of uranyl nitrate crystallization. Stream Names for crystallizer (xtyler) process

1. *Feed from dissolution*
2. *Fines removal/recycle*
3. *Evaporated nitric acid/H_2O*
4. *Slurry removal to filter*
5. *Recycle dissolved sec-xtyls*
6. *Recycled sec-xtyler filtrate.*
7. *Unrinsed UNH xtyls in filter*
8. *Mother liquor from slurry filtn*
9. *UNH xtyls after sec rinse*
10. *Xtyl rinse liquor recycle*
11. *UNH xtyls after primary rinse*
12. *Sec (c'rcurrent) xtyl rinse*
13. *Acid/H_2O for (satd) xtyl rinse*
14. *Primary xtyl rinse solution*
15. *Purified UNH xtyls*
16. *H_2O- dissolve purified UNH xtyls*
17. *Uranyl nitrate soln product*
18. *Filtrate recycle to xtyler*
19. *Secondary xtyler total feed*
20. *Slurry from sec xtyler to filter*
21. *Vaporized acid/H_2O from sec-xtyler*
22. *Slurry removal from sec-xtyler to filter*
23. *Secondary xtyler filtrate*
24. *Product stream to FP/Ac sepn*

Downloaded by CORNELL UNIV on August 9, 2012 | http://pubs.acs.org
Publication Date: June 9, 2006 | doi: 10.1021/bk-2006-0933.ch012

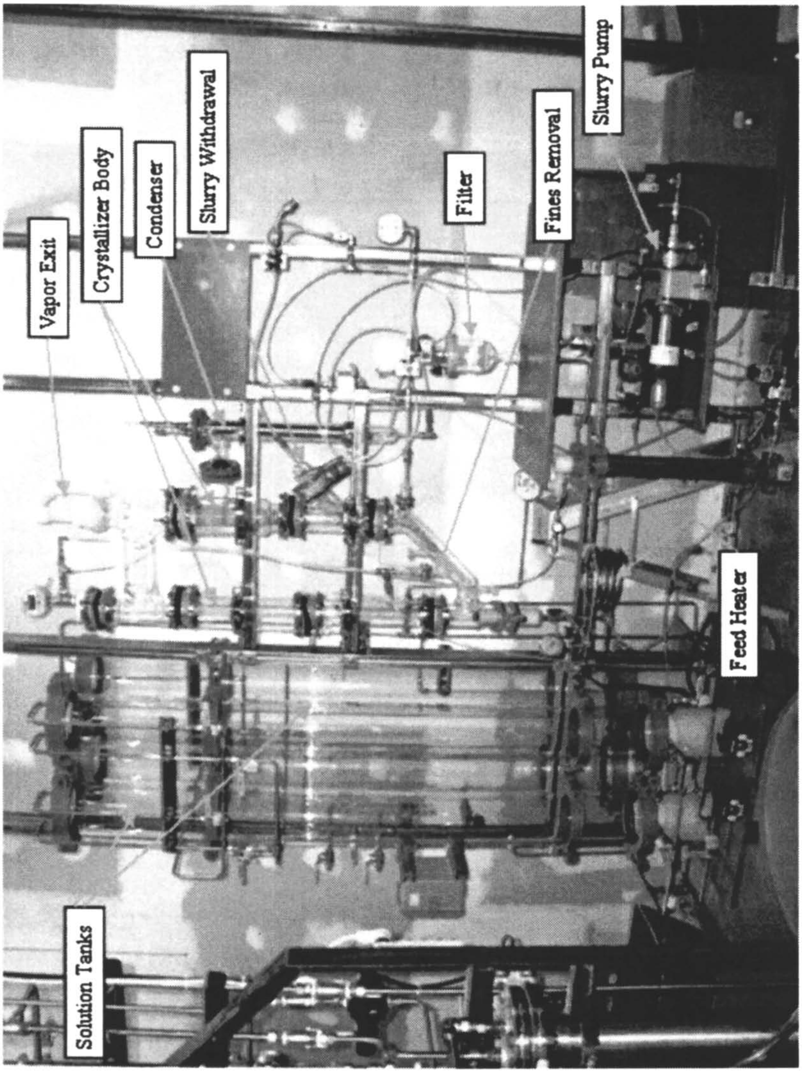
Vapor Exit
Crystallizer Body
Condenser
Slurry Withdrawal
Filter
Fines Removal
Slurry Pump
Feed Heater
Solution Tanks

Figure 4. Final design of ACP unit crystallizer and equipment.

Mathematical Process Models

Mathematical modeling of the process is essential. The interaction of acid-water vapor-liquid equilibria and uranyl nitrate solubility demand that difficult calculations be solved. There are at least five recycle streams whose material balances must be converged.

A model is used to estimate decontamination. The basis for this model is that the filtered crystals have a portion of the filtrate remaining upon their surface. It is assumed that if these crystals are mixed with a portion of rinsing solution, all of the liquid will become the same composition, and the liquid will end up in equilibrium (saturated) with the uranyl nitrate crystals, and that the same amount of liquid (as there was initially) will remain on the crystals. Decontamination is then achieved by diluting the filtrate that is present on the crystal surface. It is worthy of note that when uranyl nitrate changes between solid and solution phases, the waters of hydration are also changing phase.

Downloaded by CORNELL UNIV on August 9, 2012 | http://pubs.acs.org
Publication Date: June 9, 2006 | doi: 10.1021/bk-2006-0933.ch012

Mathematical Model Verification

Data obtained thus far on the bench-scale batch crystallizer have been incorporated into the crystallizer model property database. For the ternary system of water, acid, and uranyl nitrate, both measured solubility and measured liquid specific gravities have been incorporated. The solubilities have matched well with published data. In earlier studies it has been shown that density increases linearly with increasing concentration of uranyl nitrate or HNO_3 and decreases with rising temperature. (6) The measured data obtained has been correlated to estimate the specific gravities using the composition of uranyl nitrate, water, and acid.

Verification of the crystal washing model first requires an understanding of the things that could be different from our assumptions:

- There are occlusions, or holes, within the crystals in which filtrate could reside and not be exposed to the rinse liquid.
- There could be co-crystallization of another metal salt that is a part of the crystal structure.
- Different salts could crystallize separately from the uranyl nitrate hydrate salts.

Tests are underway in the bench-scale crystallizer with surrogate fission products added in concentrations representing spent LWR fuel composition. Results from these tests will be used to test the assumptions listed above.

Conclusion

The general crystallization approach and equipment discussed above are well established in industrial practice. Highly radioactive solutions have been processed at Hanford using evaporators for many years. (10) Although the task at Hanford has been to reduce waste volumes, the equipment is similar and some of the challenges are similar such as handling the slurry produced by the evaporators. Crystallization of strontium, americium, and curium have been accomplished in the past using batch crystallization operations.

The proposed ACP appears capable of meeting the recovery and uranium purity requirements of the AFCI. Decontamination factors for uranyl nitrate crystals from fission products in tests using simulant solutions in the literature (*1-2, 7-9*) and in our own tests give average values around 100. These DFs suggest that several successive crystallizations might be needed for the uranium to meet the required specifications. The mass balance uses a model for washing the crystals based on retention of a certain volume percent of mother liquor by the crystals and dilution of the retained liquid by the wash. The model predicts that very high DF are attainable. We certainly feel the DFs will improve substantially with well-controlled crystal growth and efficient washing methods. Work scheduled for the AFCI program will refine the DF, but tests of the loop crystallizer in continuous operation will provide the best data (short of hot cell testing with spent fuel). The nitric acid stream containing the purified uranyl nitrate could feed to a direct denitration process to yield UO_3 or U_3O_8 for storage or disposal.

The literature data and our own experiments on crystallization of uranyl nitrate from simulant solutions have not indicated that there are any fission products that appear to crystallize under the conditions tested. We have not run many tests in the higher concentration and lower temperatures of the secondary crystallizer. The presence of a variety of fission product elements does not appear to have any effect on the size or shape of the uranyl nitrate hydrate crystals compared to crystals obtained from pure uranyl nitrate solutions.

Reduced storage tankage required for the ACP will lower capital and operating costs compared to the PUREX system. The process also produces a more concentrated effluent stream for fission product and transuranic separations. This could reduce tank volumes for interim storage tanks. Acid removed from the adiabatic reduced-pressure crystallizer by evaporation can be recycled to other plant operations.

References

1. Henrich, E.; Bauder, U.; Marquardt R.; Druckenbrodt W.G.; Wittmann K.A., A concept for product refining in the PUREX process, Atomkernenrgie Kerntechnik, 1986, 48 (4), 241- 245.

Downloaded by CORNELL UNIV on August 9, 2012 | http://pubs.acs.org
Publication Date: June 9, 2006 | doi: 10.1021/bk-2006-0933.ch012

2. Takata, T.;Koma, Y.; Sato, K.; Kamiya, M.; Shibata, A.; Nomura, K.; Ogino, H.; Koyama, T.; Aose, S. Conceptual Design Study on Advanced Aqueous Reprocessing System for Fast Reactor Fuel Cycle Journal of Nuclear Science and Technology, Vol. 41, No.3. 307-314 2004
3. Dash, S.; Kamruddin, M.; Bera, S.;, Ajikumar, P. K.; Tyagi, A. K.; Narasimhan, S. V.; Raj, B. Temperature Programmed Decomposition of Uranyl Nitrate Hexahydrate Journal of Nuclear Materials 264 (1999) 271-282
4. *Encyclopedia of Separation Science*; Cooke, M. and Poole, C. F., Eds.: Academic Press: San Francisco, CA 2000; Vol 1, 78-80.
5. Gaunt J.; Bastien I.J. and Adelman M. Phase Equilibrium for the Ternary System Uranyl Nitrate - Nitric Acid – Water, Canadian J. Chem., 1963, 527-530 and references therein.
6. Slipyan,T.A.; Karpacheva, S.M. Physicochemical Properties of Nitric acid Solutions of Uranyl Nitrate and Determination of their Composition by Density, Electric Conductivity and Index of Reflection Radiokhimiya, Vol II, No 3, 1960, 369-376.
7. Nomura K.; Shibata A., Aoshima A. Study on Uranium Crystallization for Advanced Reprocessing, Japanese Atomic Energy Research Institute Conference, 2002, 004, 213-216.
8. Kikuchi T.; Koyama T.; Homma S. Development of Reprocessing Process by Plutonium Cocrystallization, Plutonium Futures – The Science 2003 Conference Transactions, G.D. Jarvinen, Ed., pp. 42-44, American Institute of Physics, 2003.
9. Mullins D., Jarvinen G., Mayne M., Ford D., Long K., Reichert H., Palmer P., Evaluation of Uranyl Nitrate Crystallization for Spent Nuclear Fuel Separations ATALANTE 2004
10. HNF-14755 Campbell, T. A.; Documented Safety Analysis for the 242-A Evaporator; Richland, WA 99352 2003 457pp,

Downloaded by CORNELL UNIV on August 9, 2012 | http://pubs.acs.org
Publication Date: June 9, 2006 | doi: 10.1021/bk-2006-0933.ch012

Downloaded by STANFORD UNIV GREEN LIBR on August 10, 2012 | http://pubs.acs.org
Publication Date: June 9, 2006 | doi: 10.1021/bk-2006-0933.ch013

Chapter 13

Potential Application of Kläui Ligands in Actinide Separations

Gregg J. Lumetta[1], Bruce K. McNamara[1], Timothy L. Hubler[1], Dennis W. Wester[1], Jun Li[1], and Stan L. Latesky[2]

[1]Pacific Northwest National Laboratory, P.O. Box 999,
Richland, WA 99352
[2]Science and Math Division, The University of the Virgin Islands,
John Brewer Bay Road, St. Thomas, Virgin Islands 00802

We have undertaken a systematic experimental and computational study of the complexation of $Cp^*Co[P(O)(OR)_2]_3^-$ (Cp^* = pentamethylcyclopentadienyl) ligands with f-block metal ions (i.e., lanthanides and actinides). As part of this work, the complexation of La^{3+} ion with $Cp^*Co[P(O)(OR)_2]_3^-$ ligands has been studied as the alkyl group was systematically varied from methyl to n-propyl (R = $-CH_3$, $-CH_2CH_3$, and $-CH_2CH_2CH_3$). For ligands in which R = $-CH_3$ or $-CH_2CH_3$, complexes with ligand-to-La stoichiometries of 1:1 and 2:1 were formed. In contrast, only the 1:1 complex was isolated when R = $-CH_2CH_2CH_3$. Computational modeling indicates that the coordination number for La in the 1:1 and 2:1 complexes is 8 and 9, respectively. A prototypical extraction chromatography resin containing $Cp^*Co[P(O)(OEt)_2]_3^-$ (**1b**) has been prepared. The resin consists of 0.75 wt% **1b** on Amberlite® XAD-7. This resin strongly sorbs Am^{3+} and Pu^{4+}. The sorption of these ions decreases with increasing nitric acid concentration, but this effect is more pronounced for Am^{3+}. This allows for convenient separation of Am^{3+} from Pu^{4+} by simple adjustments in the HNO_3 concentration. The tripodal geometry of **1b** disfavors the complexation of UO_2^{2+}, so sorption of U(VI) by the **1b**-containing resin is weak.

In Separations for the Nuclear Fuel Cycle in the 21st Century; Lumetta, G., et al.;
ACS Symposium Series; American Chemical Society: Washington, DC, 2006.

Introduction

Lanthanide and actinide ions tend to form stable complexes with chelating ligands containing hard donor atoms such as the oxygens of carboxylate and phosphonate. Among some of the most interesting ligands of this type are the anionic half-sandwich chelates $CpCo[P(O)(OR)_2]_3^-$ (Cp = cyclopentadienyl, R = CH_3, C_2H_5, etc.), which were first discovered by Harder, Dubler and Werner (1) and then studied in detail by Kläui and coworkers (2-6). This class of ligands is commonly referred to as "Kläui ligands." These ligands typically form coordination complexes as tripodal chelates involving the three terminal oxygens of the phosphonates.

Our attention was drawn to reports of complexes of lanthanides (and yttrium) (7-15) and actinides (16-17) with $CpCo[P(O)(OR)_2]_3^-$ ligands because of the extensive use of related organophosphorus compounds—tri-butylphosphate, carbamoylmethylenephosphine oxides, and diphosphonates—in the processing of materials containing lanthanides and actinides (18). The Kläui ligands have two features that distinguish them from the typically used organophosphorus extractants. First, they are negatively charged whereas the other organophosphorus extractants are neutral. This feature would reduce the energy penalty associated with co-extraction of hydrophilic anions (e.g., nitrate) during the transfer of f-block ions into an organic phase. Second, the tendency of the Kläui ligands to bind in a tripodal fashion would presumably disfavor binding of these ligands to the linear actinyl ions (e.g., UO_2^{2+}) that typically only accept donor ligands at the equatorial plane. Hence, it was hypothesized that Kläui ligands might display unique selectivity that could be exploited in actinide separations. Initial work in our laboratory has supported this supposition.

In this chapter, we provide a brief overview of studies conducted to probe the coordination chemistry of Kläui ligands with f-block ions. Included are discussions of the spectroscopic characterization of the complexes formed in solution, computational modeling of the geometries and electronic properties of the complexes, and the results of initial experiments with a prototypical extraction chromatography resins containing Kläui ligands.

Experimental

Preparation of the ligands. The Kläui ligands investigated in this work were anionic ligands of the type (η^5-pentamethylcyclopentadienyl)tris-(dialkylphosphito-P)cobalt(III), $Cp^*Co[P(O)(OR)_2]_3^-$ [R = CH_3 (**1a**), CH_2CH_3 (**1b**) or $CH_2CH_2CH_3$ (**1c**); Figure 1]. The ligands were prepared according to a published method [19]. To summarize the synthesis, $Co(acac)_3$ was reacted with

Downloaded by STANFORD UNIV GREEN LIBR on August 10, 2012 | http://pubs.acs.org
Publication Date: June 9, 2006 | doi: 10.1021/bk-2006-0933.ch013

Downloaded by STANFORD UNIV GREEN LIBR on August 10, 2012 | http://pubs.acs.org
Publication Date: June 9, 2006 | doi: 10.1021/bk-2006-0933.ch013

LiCp* in THF. Upon filtration and removal of THF *in vacuo*, the contents were then refluxed in neat $HOP(OR)_2$ to give $[Cp^*Co\{P(O)(OR)_2\}_3]_2Co$ in high yield. Reaction of the latter compound with NaCN in the presence of oxygen produced the sodium salt of the ligand $[Cp^*Co\{P(O)(OR)_2\}_3]Na$. The dimethylphosphonate derivative was crystallized from acetone and water in 25% yield, and the diethylphosphonate and di-n-propylphosphonate derivatives were crystallized by cooling warm cyclohexane solutions in 80% and 70% yield, respectively. The complexes were characterized by FTIR (4) and $^{13}C\{^1H\}$ and $^{31}P\{^1H\}$ NMR spectroscopies. *FTIR:* **1a**—δ(P=O), 601(s); ν(P=O), 1142(vs); **1b**—δ(P=O), 601(s); ν(P=O), 1143(vs); **1c**—δ(P=O), 596(s); ν(P=O), 1141(vs). *^{13}C NMR (25% CD_3CN, 75% CCl_4):* **1a**—$C_5(CH_3)_5$, 99.9; $C_5(CH_3)_5$, 10.6; PO-**C**-, 51.3; **1b**—$C_5(CH_3)_5$, 99.2; $C_5(CH_3)_5$, 10.8; PO-**C**-, 59.2; PO-C-**C**-, 17.1; **1c**—$C_5(CH_3)_5$, 99.2; $C_5(CH_3)_5$, 10.8; PO-**C**-, 65.3; PO-C-**C**-, 24.5; PO-C-C-**C**, 11.2. *^{31}P NMR (25% CD_3CN, 75% CCl_4):* **1a**—112.5; **1b**—111.0; **1c**—109.6.

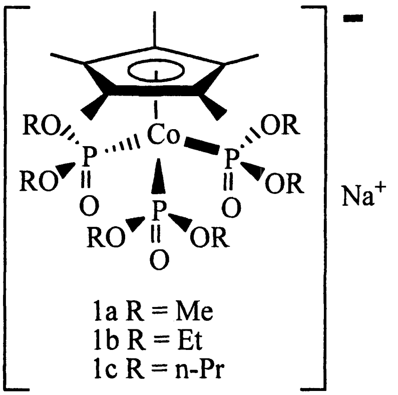

Figure 1. General structure of the Kläui ligands

Preparation of $[La(NO_3)_{3-x}1_x]$ (x = 1, 2) complexes. $La(NO_3)_3{\bullet}6H_2O$ was obtained from Alfa Chemicals and used without further purification. The isolation of 1:1 and 2:1 complexes (i.e., x = 1 and x = 2) of **1a** and **1b** with La^{3+} was accomplished by adding a CH_3CN solution (0.5 mL) containing a slight stoichiometric excess of $La(NO_3)_3{\bullet}6H_2O$ (0.0169 mmol La) to a solution of the Kläui ligand in 0.5 mL of CCl_4. The reaction quickly produced a white precipitate ($NaNO_3$) that was removed by passing through a 0.45-μm filter. The solvents were removed by gently heating to dryness in air. The residue was taken up in CCl_4, and the excess insoluble La nitrate was filtered from the solution. The solvent was allowed to evaporate slowly overnight to yield crystals of the desired complexes. The same process was followed to prepare the 1:1 **1c**/La complex, but attempts to prepare the 2:1 **1c**/La complex failed.

Preparation of the 1b/XAD-7 resin. The **1b**/XAD-7 resin was prepared by adapting the method described by Horwitz et al. (20) in which **1b** is physically sorbed onto a macroreticular resin. The Amberlite® XAD-7HP (16-50 mesh; Supelco Separation Technologies, Bellefonte, Pennsylvania; ~60 g) was washed with ~200 mL of deionized water and the wash water was removed by vacuum filtration. The water-washing process was repeated twice more. The XAD-7 was then washed in a similar manner with methanol (3 times), toluene (3 times), and CH_2Cl_2 (2 times), successively. Residual solvents were removed under vacuum at 100 °C using a rotary evaporator. To load the Kläui ligand onto the washed XAD-7 resin, a solution consisting of 0.3209 g of **1b** dissolved in 45 mL of CH_2Cl_2 was added to the flask containing the washed resin. The solvent was removed using a rotary evaporator yielding approximately 41 g of **1b**-loaded resin. To remove residual solvents, the resin was placed in a vacuum (550 mm Hg) oven at 60 °C for longer than one week. The resin was analyzed for Co by Desert Analytics (Tucson, Arizona), which indicated that the **1b**/XAD-7 resin contained 0.75 wt% **1b**.

Resin batch contacts. The resin batch contacts were performed by gently mixing 5 mL of the appropriately spiked nitric acid solution with nominally 50 mg of the **1b**/XAD-7 resins for at least 24 hours. Each isotope was measured independently. Americium-241 was procured from Isotope Products Laboratories (Valencia, California). Plutonium-239 and ^{233}U were obtained from existing Pacific Northwest National Laboratory stocks. The stock Pu solution (in 1 M HNO_3) was adjusted to Pu(IV) by treatment with sodium nitrite; spectrophotometric examination of the resulting solution indicated only the presence of Pu(IV). The solutions were agitated with a J-KEM BTS 3000 oscillating mixer (St. Louis, Missouri) equipped with a thermostated aluminum block. The aluminum block was drilled with holes suitable for holding the 20-mL high-density polyethylene vials used in the experiments, and it was controlled to 25 ± 1°C. Selected kinetic experiments confirmed that 24 hours was sufficient time to attain equilibrium under these conditions.

Aliquots (0.1-mL) of each solution were taken before and after equilibration with the resin for liquid scintillation counting. In the case of the equilibrated solution, the solution was passed through a 0.45-μm polysulfone filter membrane before sampling. Each aliquot was dissolved in 5 mL of Ultima Gold XR liquid scintillation cocktail (Packard BioScience, Meriden, Connecticut). The relative alpha activity of the samples was determined by liquid scintillation counting using a Packard Tri-Carb® 2260XL. The batch-sorption coefficients (K_d) were calculated according to the following equation:

$$K_d = \frac{A_i - A_f}{A_f} \times \frac{V}{m}$$

Downloaded by STANFORD UNIV GREEN LIBR on August 10, 2012 | http://pubs.acs.org
Publication Date: June 9, 2006 | doi: 10.1021/bk-2006-0933.ch013

where V is the volume of solution (5 mL), m is the mass of resin used, A_i and A_f are the initial and final activity of the radionuclide in the solution, respectively. Selected points were performed in duplicate and the results of these duplicates are shown on the plots discussed below. The relative percent difference between the mean and the standard deviation ranged from 2 to 38%.

Column experiments. For column chromatography experiments, a weighed amount of resin was slurried in deionized water and loaded into a small plastic column (inner diameter ~7 mm). Feed solutions spiked with ^{239}Pu were loaded onto the column, and the column was eluted in varying ways as described in the Results and Discussion section. All flow through the columns was driven by gravity with no active control over the flow rate. The flow rate was estimated to be 4.7 mL/min by measuring the flow of water through a column set up similar to that used in the Pu experiments. Samples were taken and analyzed by liquid scintillation counting (LSC) as described above. The feed solutions consisted of simply nitric acid, or a test solution consisting of HNO_3 (0.1 M = Test Solution #1 or 1.0 M = Test Solution #5), 0.0712 M Al, 0.0018 M Ca, 0.0163 M Fe, 0.007 M Na, and 0.93 M Li—all metal cations added as the nitrate salts. The latter solutions were designed to mimic the solutions that would be generated by dissolving Rocky Flats Soil Number 1 (National Institute of Standards and Technology Standard Reference Material 4353) using a lithium perborate fusion followed by nitric acid digestion. This standard material is often used to test protocols for analyzing radiologically contaminated soils.

Spectroscopic Characterization of Lanthanum(III) Kläui Complexes

Complexes of the type $[La(NO_3)_{3-x}\mathbf{1}_x]$ can be prepared by adding a stoichiometric amount of the Kläui ligand **1** to lanthanum nitrate. The stepwise complexation of La^{3+} is represented by Equations 1 and 2. Table I presents key

$$La(NO_3)_3 + Na\mathbf{1} \longrightarrow [La(NO_3)_2\mathbf{1}] + NaNO_3 \qquad (1)$$

$$[La(NO_3)_2\mathbf{1}] + Na\mathbf{1} \longrightarrow [La(NO_3)\mathbf{1}_2] + NaNO_3 \qquad (2)$$

spectral data for the sodium salts of the Kläui ligands, the 1:1 and 2:1 La^{3+} complexes. The assignment of these La:ligand ratios is assumed based on stoichometric ratio of La:ligand used and on the electrostatic consideration. Figure 2 presents example FTIR spectra for **1b** and its La^{3+} complexes. The complexes $[La(NO_3)_2\mathbf{1a}]$ and $[La(NO_3)_2\mathbf{1b}]$ display broad υ(P=O) bands, shifted to lower energy compared to the sodium salt of the ligand. The magnitude of this shift is similar for the **1a** and **1b** complexes (35 to 38 cm^{-1}). The υ(P=O) band for **1c** also shifts to lower energy upon complexation to La^{3+}, but the magnitude

Downloaded by STANFORD UNIV GREEN LIBR on August 10, 2012 | http://pubs.acs.org
Publication Date: June 9, 2006 | doi: 10.1021/bk-2006-0933.ch013

of the shift is somewhat less, perhaps indicating weaker binding of this ligand to the metal center. The correlation of the P=O vibrational frequencies and the Kläui-La binding strengths are consistent with computational modeling on the Kläui -La complexes (see below). The $^{31}P\{^1H\}$ NMR spectra of the $[La(NO_3)_2\mathbf{1}]$ complexes display single peaks shifted downfield by ~6 ppm from that of the sodium salt ligand.

The complexes $[La(NO_3)(\mathbf{1a})_2]$ and $[La(NO_3)(\mathbf{1b})_2]$ are also characterized by shifting of the υ(P=O) band to lower energy. In this case, identical shifts of -24 cm^{-1} are observed indicating similar binding of the ligands to La^{3+} in these complexes. Likewise, similar shifts in the ^{31}P resonances relative to the sodium salt of the ligands are observed in the **1a** and **1b** complexes. The $^{31}P\{^1H\}$ NMR spectra of the $[La(NO_3)(\mathbf{1a})_2]$ and $[La(NO_3)(\mathbf{1b})_2]$ complexes also display single peaks shifted downfield from that of the sodium salt of the ligand. In this case, the shift is ~4.5 ppm.

The complex $[La(NO_3)(\mathbf{1c})_2]$ could not be isolated in pure form, thus no spectral data for this complex is presented in Table I. We have observed some evidence for the formation of this complex (^{31}P resonance at 113.9 ppm in the NMR spectrum) when excess **1c** is added to a La^{3+} solution, but it is always present as a mixture with $[La(NO_3)_2\mathbf{1c}]$. This observation also indicates that **1c** binds La^{3+} less strongly than **1a** and **1b**.

Density Functional Theory Calculations of Lanthanum(III) Kläui Complexes

To gain further insight into the structural features and electronic properties of the La(III)/Kläui ligand complexes, density functional theory (DFT) calculations were performed on complexes with ligand:La stoichiometries of 1:1 and 2:1. To simplify the calculations the Kläui ligand used for these calculations was $(\eta^5\text{-}C_5H_5)Co[P(O)(OMe)_2]_3^-$ (referred to here as L_{OMe}); that is, ligand **1a** with the methyl groups on the pentamethylcyclopentadiene ring replaced by hydrogen atoms. Relativistic DFT calculations were performed using the *Amsterdam Density Functional* (ADF 2004) code (21-23). The local density approach with the exchange-correlation functional of Vosko-Wilk-Nusair (VWN-5) (24) was used for geometry optimization and the single-point energy calculations were performed at the optimized geometries using generalized gradient approach of Perdew and Wang (PW91) (25-26). The mass-velocity and Darwin relativistic effects were treated within the zero-order-regular-approach (ZORA) (27). The $[1s^2]$ cores for C, N, and O, $[1s^2\text{-}2p^6]$ cores for P and Co, and the $[1s^2\text{-}4d^{10}]$ core for La were frozen via the frozen core approximation. Slater-type-orbital (STO) basis sets of double-zeta with one polarization function were

Downloaded by STANFORD UNIV GREEN LIBR on August 10, 2012 | http://pubs.acs.org
Publication Date: June 9, 2006 | doi: 10.1021/bk-2006-0933.ch013

Table I. Selected Spectral Data for the Kläui Ligands and Their La(III) Complexes

Compound	*FTIR (KBr Pellet), cm^{-1}* ν(P=O)	Δν(P=O)	*$^{31}P\{^1H\}$ NMR, ppm*[(a)] δ	Δδ
NaIa	1142	N/A [(b)]	112.5	N/A
NaIb	1143	N/A	111.0	N/A
NaIc	1141	N/A	109.6	N/A
[La(NO$_3$)$_2$(**1a**)]	1104	-38	118.6	6.1
[La(NO$_3$)(**1a**)$_2$]	1118	-24	117.2	4.7
[La(NO$_3$)$_2$(**1b**)]	1108	-35	116.8	5.8
[La(NO$_3$)(**1b**)$_2$]	1119	-24	115.4	4.4
[La(NO$_3$)$_2$(**1c**)]	1113	-28	115.9	6.3

(a) The solvent for the NMR measurements consisted of 0.25 mL CD_3CN plus 0.75 mL CCl_4. Phosphorus-31 chemical shifts are relative to an internal standard of 85% H_3PO_4 in D_2O.

(b) N/A = not applicable

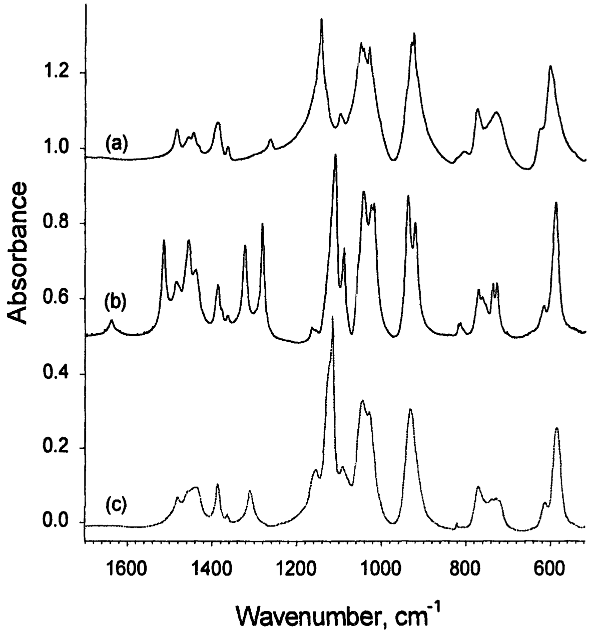

Figure 2. FTIR spectra of the sodium salt of ligand 1b (a), the 1:1complex (b), and 2:1complex (c) of this ligand with La^{3+}

Downloaded by STANFORD UNIV GREEN LIBR on August 10, 2012 | http://pubs.acs.org
Publication Date: June 9, 2006 | doi: 10.1021/bk-2006-0933.ch013

used for the valence orbitals of C, N, O, H, P and basis set of triple-zeta with one polarization function was used for the La (28). The structures of the calculated species were fully optimized with energy gradient converging to 10^{-3} Hartree/angstrom. Numerical integration accuracy of INTEGRATION=6.0 was used throughout.

For the La-Kläui complexes in solution, the number of coordinated water molecules is unknown experimentally. It is thus interesting to determine the coordination polyhedron around the La atom through computational modeling. The La atom has large ionic radius relative to the other lanthanide atoms, allowing coordination number (CN) as high as eight or even nine (e.g., in $La(H_2O)_9^{3+}$). Our initial trial geometries of the 1:1 and 2:1 La complexes were chosen in which two water ligands were directly coordinated to the La center. However, after a long time optimal geometry search, the DFT calculation suggested one water molecule is pushed out of the primary coordination shell, indicating that it becomes too crowded for La to have two water molecules as ligands in the coordination polyhedra of the 1:1 and 2:1 La complexes.

Figure 3 shows the optimized structure for the 1:1 complex and Figure 4 shows the optimized structure for the 2:1 complex. The coordination number for the 1:1 complex is eight, with the primary La coordination shell being occupied by the tridentate Kläui ligand, two bidentate nitrate ligands, and one coordinated water molecule. One the other hand, the coordination number for the 2:1 complex is nine, with the primary La coordination shell being occupied by two tridentate Kläui ligands, one bidentate nitrate ligand, and one coordinated water molecule. Interestingly for both complexes, the calculations suggest the presence of a second water molecule in the second coordination sphere which is hydrogen-bonded to oxygen atoms in the primary coordination sphere.

In general, La can adopt structures with coordination numbers of either eight or nine, depending upon the size and binding strengths of the ligands. For example, the La atom is considered to have coordination number nine in $LaVO_4$, but eight of the La-O distances are averaged to 2.56 Å whereas the ninth La-O is much longer (~2.89 Å) (29). To further corroborate the coordination numbers, we also performed geometry optimizations on the nine-coordinate 1:1 and eight-coordinate 2:1 Kläui-La complexes. It turns out that these species have higher energies (~8-9 kcal/mol) than the corresponding eight-coordinate 1:1 and nine-coordinate 2:1 complexes, respectively. The optimized bonding energies and their differences for the 1:1 and 2:1 Kläui-La complexes are listed in Table II. While a definite conclusion about the coordination numbers in these La complexes must still be verified experimentally, similar calculations performed on $[La(L_{OMe})_2(H_2O)_2]Cl$ provided reasonable agreement with the experimentally reported crystal structure (9).

Downloaded by STANFORD UNIV GREEN LIBR on August 10, 2012 | http://pubs.acs.org
Publication Date: June 9, 2006 | doi: 10.1021/bk-2006-0933.ch013

Downloaded by STANFORD UNIV GREEN LIBR on August 10, 2012 | http://pubs.acs.org
Publication Date: June 9, 2006 | doi: 10.1021/bk-2006-0933.ch013

Table II. Total bonding energy and energy difference of eight- and nine-coordinate Kläui-La complexes with stoichiometry 1:1 and 2:1

	CN=8	CN=9	ΔE (eV)	ΔE (kcal/mol)
1:1	-391.4036	-391.0657	+0.3379	7.8
2:1	-655.9702	-656.3482	-0.3780	8.7

* The total bonding energies are in eV.

It is interesting to compare the calculated bonding strengths of the P=O bonds with the experimentally observed vibrational frequencies of the P=O stretching modes. In the Kläui ligands, the oxygen lone-pairs of the three P=O units serve as electron donors to the binding metal ions. One can expect that the stronger the binding ability of the Kläui ligand to the metal ions, the weaker the P=O bonds. Our calculations show that the Mulliken overlap populations, a rough measure of the bonding strengths, of the P=O bonds decrease from 0.86 for free Kläui ligand, to 0.68 for the 2:1 complex and to 0.65 for the 1:1 complex. These results indicate that the Kläui -La binding is stronger in the 1:1 complex than in the 2:1 complex, consistent with the increase of the P=O stretching frequency from the 1:1 to 2:1 complex, as shown in Table I. Indeed the calculated Mulliken overlap populations of La-O(L_{OMe}) in the 1:1 and 2:1 complexes are 0.21 and 0.17, respectively.

Actinide Separations Using Kläui-Ligand Resin

Batch Equilibrium Measurements

Figure 3 presents the Am(III), Pu(IV), and U(VI) K_d as a function of nitric acid concentration for sorption onto the **1b**/XAD-7 resin. Blank experiments performed under identical conditions but using XAD-7 resin (without **1b**) indicated little adsorption of the actinide ions on the resin, so the adsorption indicated in Figure 3 is due to the ligand on the resin. Americium(III) and Pu(IV) are adsorbed strongly to the **1b**/XAD-7 resin at the lower acid concentrations. The sorption of Am(III) drops off rapidly with increasing HNO_3 concentration whereas the sorption of Pu(IV) decreases more gradually with increasing HNO_3. Indeed Pu(IV) is strongly retained on the resin even at 7 M HNO_3. This result suggests a generally higher affinity of **1b** for Pu(IV) compared to Am(III) since the protons from HNO_3 appear to more readily displace the Kläui ligand from Am(III) than from Pu(IV). This may simply be a reflection of the higher charge-to-ionic radius for Pu(IV).

The **1b**/XAD-7 resin showed little affinity for U(VI). The low sorption of U(VI) is assumed to be due to the geometrical mismatch of the tripodal ligand

Downloaded by STANFORD UNIV GREEN LIBR on August 10, 2012 | http://pubs.acs.org
Publication Date: June 9, 2006 | doi: 10.1021/bk-2006-0933.ch013

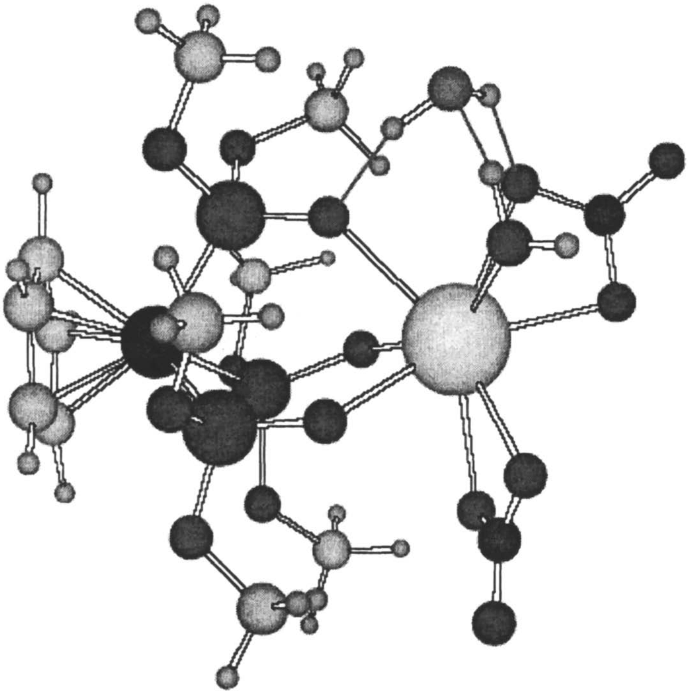

Optimized bond lengths of $(L_{OMe})La(H_2O)(NO_3)_2.(H_2O)$

Bond	*Average*	*Details*
La-O (NO_3)	2.518	2.483, 2.495, 2.537, 2.557
La-O (L_{OMe})	2.420	2.368, 2.286, 2.505
La-O (H_2O)	2.492	2.492
P=O (L_{OMe})	1.528	1.518, 1.530, 1.536
Co-P (L_{OMe})	2.122	2.109, 2.127, 2.131

Figure 3. The optimized structure of $(L_{OMe})La(H_2O)(NO_3)_2.(H_2O)$

Downloaded by STANFORD UNIV GREEN LIBR on August 10, 2012 | http://pubs.acs.org
Publication Date: June 9, 2006 | doi: 10.1021/bk-2006-0933.ch013

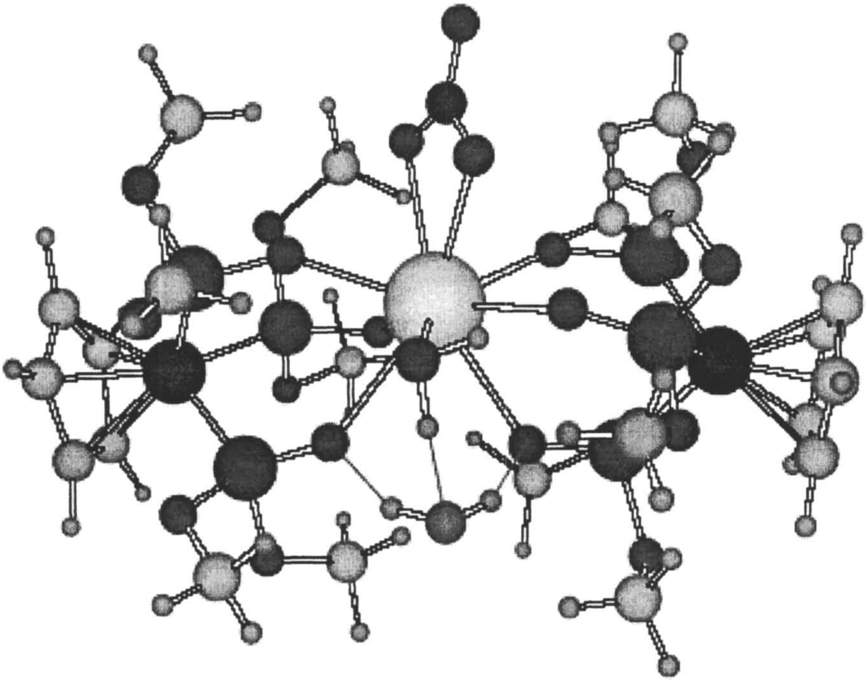

Optimized bond lengths of $(L_{OMe})_2La(H_2O)(NO_3)_2.(H_2O)$

Bond	*Average*	*Details*
La-O (NO_3)	2.559	2.529, 2.588
La-O (L_{OMe})	2.486	2.383, 2.415, 2.433, 2.520, 2.568, 2.594
La-O (H_2O)	2.611	2.611
P=O (L_{OMe})	1.521	1.518, 1.514, 1.531, 1.513, 1.522, 1.525
Co-P (L_{OMe})	2.121	2.114, 2.128, 2.124, 2.131, 2.114, 2.114

Figure 4. The optimized structure of $(L_{OMe})_2La(H_2O)(NO_3).(H_2O)$

Downloaded by STANFORD UNIV GREEN LIBR on August 10, 2012 | http://pubs.acs.org
Publication Date: June 9, 2006 | doi: 10.1021/bk-2006-0933.ch013

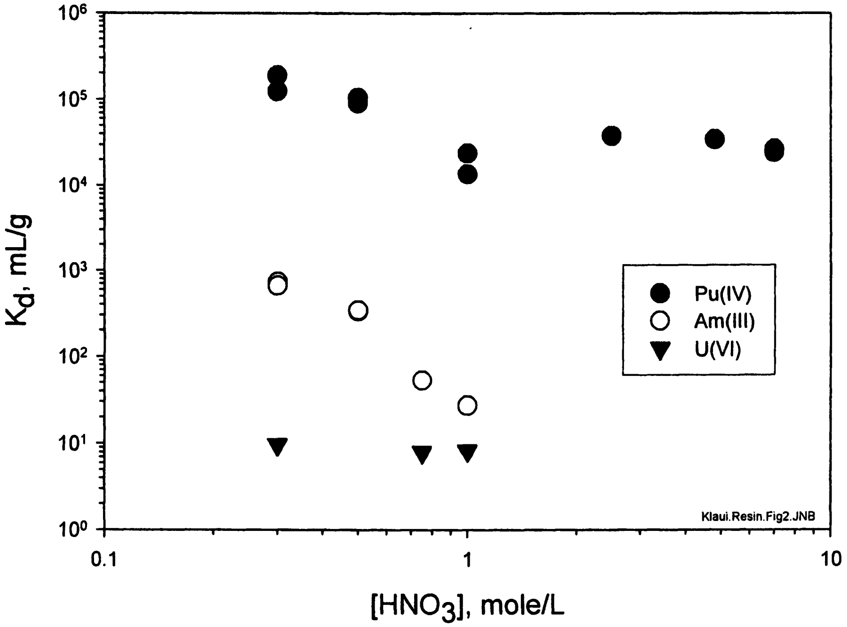

Figure 5. Batch distribution data for sorption of Am(III), Pu(IV), and U(VI) on the 1Et/XAD-7 resin (adapted from ref. 30, copyright 2004, Taylor & Francis)

Downloaded by STANFORD UNIV GREEN LIBR on August 10, 2012 | http://pubs.acs.org
Publication Date: June 9, 2006 | doi: 10.1021/bk-2006-0933.ch013

1b and the pentagonal or hexagonal planar coordination environment preferred by the linear trans-dioxo UO_2^{2+} ion (31). Indeed, preliminary results of computational modeling on $UO_2(L_{OMe})_2$ indicate that the Kläui ligand is forced to become bidentate.

To determine the influence of competing ions on the ability of the **1b**/XAD-7 resin to sorb Pu(IV), the batch K_d for Pu(IV) was determined in 1 M HNO_3 in the presence of varying concentrations of Fe(III), Al(III), and Ca(III). Figure 4 presents the results. Aluminum(III) and Ca(II) have little effect upon the sorption of Pu(IV) even at 0.1 M. In contrast, the presence of Fe(III) dramatically reduces the ability of the **1Et**/XAD-7 resin to sorb Pu(IV) under these conditions, with a three order-of-magnitude decrease observed at 0.1 M Fe(III). Nevertheless, in dynamic column experiments, the resin strongly retained Pu(IV); this is discussed in more detail below.

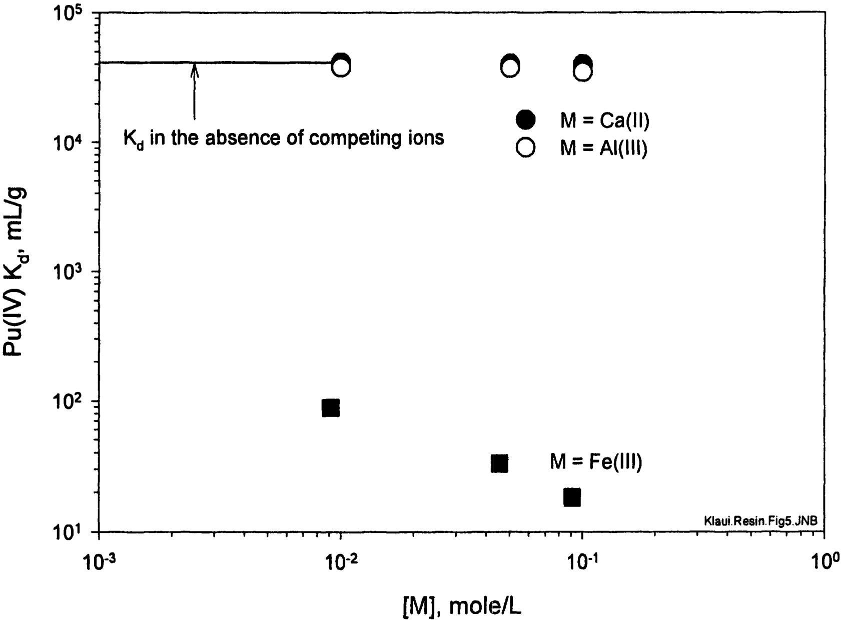

Figure 6. Effect of Al(III), Ca(II), and Fe(III) on the sorption of Pu(IV) on the 1Et/XAD-7 resin from 1 M HNO_3. (adapted from ref. 30, copyright 2004, Taylor & Francis)

Column Experiments

To determine the sorption behavior of Pu(IV) on the **1Et**/XAD-7 resin under dynamic column conditions, 0.9 mL of ^{239}Pu-spiked ~0.04 M HNO_3 was loaded onto a column containing 0.256 g of the **1Et/XAD-7** resin. The column was eluted with 0.1 M HNO_3, collecting the eluate in two 5-mL fractions. The column was then eluted with 1 M HNO_3 (two 5-mL fractions collected), and finally 7 M HNO_3 (seven 5-mL fractions and one 4-mL fraction collected). Table III summarizes the behavior of Pu in this column experiment. The results indicate very strong retention of Pu on the column. Ninety-nine percent of the alpha activity remained on the column during the course of the experiment. Approximately 1% of the Pu eluted in the first few fractions, which might be due to the presence of a small amount of Pu(III) and Pu(VI) in the Pu tracer solution, which could not be detected spectrophotometrically. However, this experiment clearly showed the strong affinity of the **1Et/XAD-7** resin for Pu(IV).

Table II. Result of First Pu(IV) Column Experiment: No Competing Ions

Description	*Vol., mL*	*Alpha cpm/mL*	*Pu cpm*	*%Pu*	*Cumulative %Pu*
Starting Solution	0.9	3.02E+06	2.72E+06	100%	N/A
Loaded solution +					
0.1 M HNO_3	5	1.87E+03	9.34E+03	0.34%	0.34%
0.1 M HNO_3	5	2.80E+01	1.40E+02	0.01%	0.35%
1 M HNO_3	5	8.84E+02	4.42E+03	0.16%	0.51%
1 M HNO_3	5	5.98E+02	2.99E+03	0.11%	0.62%
7 M HNO_3	5	1.25E+03	6.25E+03	0.23%	0.85%
7 M HNO_3	5	7.50E+01	3.75E+02	0.01%	0.86%
7 M HNO_3	5	3.60E+01	1.80E+02	0.01%	0.87%
7 M HNO_3	5	2.80E+01	1.40E+02	0.01%	0.88%
7 M HNO_3	5	3.00E+01	1.50E+02	0.01%	0.88%
7 M HNO_3	5	4.30E+01	2.15E+02	0.01%	0.89%
7 M HNO_3	5	2.70E+01	1.35E+02	0.00%	0.89%
7 M HNO_3	5	5.60E+01	2.80E+02	0.01%	0.90%

To determine the retention of Pu(IV) on the **1Et/XAD-7** resin in the presence of competing ions, a second column experiment was performed using Test Solution #1 spiked with ^{239}Pu(IV). In this second test, 0.3 g of resin was wet-packed into a small disposable plastic column. The column was first pretreated with 3 mL of 0.1 M HNO_3, and then a 1-mL aliquot of Pu-spiked Test Solution 1 was loaded onto the column. The column was eluted with 1) 5 mL of

Downloaded by STANFORD UNIV GREEN LIBR on August 10, 2012 | http://pubs.acs.org
Publication Date: June 9, 2006 | doi: 10.1021/bk-2006-0933.ch013

0.1 M HNO_3, 2) 5 mL of 1.0 M HNO_3, and 3) three 5-mL portions of 9 M HCl. Finally, the column was washed with 10 mL of deionized water. Table III summarizes the results. The results indicate that 98% of the Pu was retained on the column through this process, indicating strong retention of Pu(IV) even in the presence of high concentrations of competing ions. Note that the Fe(III) concentration in the feed solution was 0.0163 M, which, according to Figure 4, should result in a significant reduction in the Pu(IV) K_d.

Table III. Results of Second Column Test: Competing Ions Present

Description	*Vol., mL*	*Alpha cpm/mL*	*Pu cpm*	*%Pu*	*Cumulative %Pu*
Starting Solution	1	3.79×10^6	3.79×10^6	100%	N/A
0.1 M HNO_3[(a)]	8	9.80×10^2	7.84×10^3	0.2%	0.2%
1.0 M HNO_3	5	1.37×10^3	6.85×10^3	0.2%	0.4%
First 5 mL 9 M HCl	5	2.32×10^3	1.16×10^4	0.3%	0.7%
Second 5 mL 9 M HCl	5	4.18×10^3	2.09×10^4	0.6%	1.2%
Third 5 mL 9 M HCl	5	5.36×10^3	2.68×10^4	0.7%	2.0%
Column Wash	10	1.12×10^3	1.12×10^4	0.3%	2.2%

(a) Includes the initial column pretreatment with 0.1 M HNO_3, the loaded sample solution, and the 0.1 M column eluate.

The results of the column experiments described above present a quandary. Namely, the resin binds Pu(IV) so strongly that it is difficult to elute the Pu from the column for further processing or analysis. We are currently exploring a number of options for eluting the loaded Pu including reduction to Pu(III) and removing the Pu/**1b** complex by washing the column with an organic solvent such as methanol.

Conclusion

We have demonstrated the complexation of La^{3+} ion with Kläui ligands **1a**, **1b**, and **1c**. Based on the stoichiometric mixtures examined, it appears that ligands **1a** and **1b** form both 1:1 and 2:1 complexes with La^{3+}, whereas only the 1:1 La^{3+} complex could be isolated with ligand **1c**. The experimentally observed

Downloaded by STANFORD UNIV GREEN LIBR on August 10, 2012 | http://pubs.acs.org
Publication Date: June 9, 2006 | doi: 10.1021/bk-2006-0933.ch013

P=O stretching vibrational frequencies indicate that the binding ability of the Kläui ligands to the La^{3+} ion decrease as **1a** > **1b** > **1c** and the Kläui ligand is bound stronger in the 1:1 complex than in the 2:1 complex, as predicted by the computational modeling. Theoretical geometry optimizations predict coordination number of 8 and 9 for the 1:1 and 2:1 Kläui-La complexes. The affinity of **1b** for Am^{3+} and Pu^{4+} ions has been demonstrated using a resin consisting of the ligand loaded onto a macroreticular support. On the other hand, the **1b**-containing resin had little affinity for UO_2^{2+}, which is presumably due to unfavorable coordination of the normally tripodal Kläui ligand in the equatorial plane of the uranyl ion. The extraction data suggest that efficient separation of these ions can be achieved by simple changes in the acid concentration. Americium(III) and Pu(IV) can be coextracted at low acid concentration, cleanly separating them from U(VI). The Am(III) can be separated from the Pu(IV) simply by increasing the acid concentration. Although Fe(III) severely suppresses Pu(IV) sorption under equilibrium conditions, the ability of the resins to separate Pu(IV) under dynamic column conditions is maintained, even in the presence of relatively high concentrations of Fe(III).

Downloaded by STANFORD UNIV GREEN LIBR on August 10, 2012 | http://pubs.acs.org
Publication Date: June 9, 2006 | doi: 10.1021/bk-2006-0933.ch013

Acknowledgements

This research was supported by the U.S. Department of Energy through the Laboratory Directed Research and Development Program at the Pacific Northwest National Laboratory, which is operated for DOE by Battelle under Contract DE-AC06-76RL01830. This research was performed in part using the MSCF in EMSL, a national scientific user facility sponsored by the U.S. DOE, OBER and located at PNNL. The authors thank B. M. Rapko for reviewing the manuscript.

References

1. Harder, V.; Dubler, E.; Werner, H. *J. Organomet. Chem.* **1974**, *71*, 427-433.
2. Kläui, W.; Werner, H. *Angew. Chem. Int. Ed. Engl.* **1976**, *15*, 172-173.
3. Kläui, W.; Neukomm, H.; Werner, H. *Chem. Ber.* **1977**, *110*, 2283-2289.
4. Kläui, W.; Dehnicke, K. *Chem. Ber.* **1978**, *111*, 451-468.

5. Kläui, W. *Z. Naturforsch. B: Anorg. Chem. Org. Chem.* **1979**, *34*, 1403-1407.

6. Kläui, W. *Angew. Chem. Int. Ed. Engl.* **1990**, *29*, 627-637.

7. Kläui, W. *Helv. Chim. Acta* **1977**, *60*, 1296-1303.

8. Liang, L.; Stevens, E. D.; Nolan, S. P. *Organometallics* **1992**, *11*, 3459-3462.

9. Cho, I. Y.; Yeo, H. J.; Jeong, J. H. *Acta Crystallogr. Sect. C: Cryst. Struct. Commun.* **1995**, *51*, 2035-2037.

10. Kim, N. H.; Yeo, H. J.; Jeong, J. H. *Bull. Korean Chem. Soc.* **1996**, *17*, 483-485.

11. Kim, K.-C.; Park, Y.-C.; Jeong, J. H. *Bull. Korean Chem. Soc.* **1997**, *18*, 670-672.

12. Englert, U.; Ganter, B.; Wagner, T.; Kläui, W. *Z. Anorg. Allg. Chem.* **1998**, *624*, 970-974.

13. Han, S. H.; Park, S.; Jeong, J. H. *Bull. Korean Chem. Soc.* **1999**, *20*, 741-743.

14. Han, S. H.; Roh, S.-G.; Jeong, J. H. *Polyhedron* **1999**, *18*, 3027-3030.

15. Roh, S.-G.; Jeong, J. H. *Acta Crystallogr. Sect. C: Cryst. Struct. Commun.* **2000**, *56*, e120-e121.

16. Wedler, M.; Gilje, J. W.; Noltemeyer, M.; Edelmann, F. T. *J. Organomet. Chem.* **1991**, *411*, 271-280.

17. Baudry, D.; Ephritikhine, M.; Kläui, W.; Lance, M.; Nierlich, M.; Vigner, J. *Inorg. Chem.* **1991**, *30*, 2333-2336.

18. Mathur, J. N.; Murali, M. S.; Nash, K. L. *Solvent Extr. Ion Exch.* **2001**, *19*, 357-390.

19. Román E., E.; Tapia C., F.; Hernández M., S. *Polyhedron* **1986**, *5*, 917-920.

20. Horwitz, E. P; Dietz, M. L.; Nelson, D. M.; LaRosa, J. J.; Fairman, W. D. *Anal. Chim. Acta* **1990**, *238*, 263-271.

Downloaded by STANFORD UNIV GREEN LIBR on August 10, 2012 | http://pubs.acs.org
Publication Date: June 9, 2006 | doi: 10.1021/bk-2006-0933.ch013

21. **ADF 2004.01**, SCM, Theoretical Chemistry, Vrije Universiteit, Amsterdam, The Netherlands (http://www.scm.com).

22. te Velde, G.; Bickelhaupt, F. M.; van Gisbergen, S. J. A.; Fonseca Guerra, C.; Baerends, E. J.; Snijders, J. G.; Ziegler, T. *J. Comput. Chem.* **2001**, *22*, 931-967

23. Fonseca Guerra, C.; Snijders, J. G.; te Velde, G.; Baerends, E. J. *Theor. Chem. Acc.* **1998**, *99*, 391-403.

24. Vosko, S.H.; Wilk, L.; Nusair, M. *Can. J. Phys*, **1980**, *58*, 1200-1211.

25. Perdew, J. P.; Wang, Y. *Phys. Rev. B* **1992**, *45*, 13244-13249.

26. Perdew, J. P.; Chevary, J. A.; Vosko, S. H.; Jackson, K. A.; Pederson, M. R.; Singh, D. J.; Foilhais, C. *Phys. Rev. B* **1992**, *46*, 6671-6687.

27. van Lenthe, E.; Baerends, E. J.; Snijders, J.G. *J. Chem. Phys.* **1993**, *99*, 4597-4610.

28. van Lenthe, E.; Baerends, E. J. *J. Comp. Chem.* **2003**, *24*, 1142-1156.

29. Rice, C. E.; Robinson, W. R. *Acta Cryst.* **1976,** *B32*, 2232-2233.

30. Lumetta, G. J.; Wester, D. W., McNamara, B. K.; Hubler, T. L., Latesky, S. L.; Martyr, C. C.; Richards, K. N. *Solvent Extr. Ion Exch.* **2004**, *22*, 947-960.

31. Weigel, F. In *The Chemistry of the Actinide Elements*, 2nd Ed.; Katz, J. J.; Seaborg, G. T.; Morss, L. R.; Eds.; Chapman and Hall: New York, NY, 1986; pp. 351-368.

Downloaded by STANFORD UNIV GREEN LIBR on August 10, 2012 | http://pubs.acs.org
Publication Date: June 9, 2006 | doi: 10.1021/bk-2006-0933.ch013

Downloaded by PENNSYLVANIA STATE UNIV on August 9, 2012 | http://pubs.acs.org
Publication Date: June 9, 2006 | doi: 10.1021/bk-2006-0933.ch014

Chapter 14

Actinide, Lanthanide, and Fission Product Speciation and Electrochemistry in Ionic Melts

A. I. Bhatt[1], H. Kinoshita[1], A. L. Koster[1], I. May[1,*], C. Sharrad[1], H. M. Steele[1], V. A. Volkovich[2], O. D. Fox[3], C. J. Jones[3], B. G. Lewin[3], J. M. Charnock[4], and C. Hennig[5]

[1]Centre for Radiochemistry Research, Department of Chemistry, The University of Manchester, Oxford Road, Manchester M13 9PL, United Kingdom
[2]Department of Rare Metals, Ural State Technical University-UPI, Ekaterinburg, Russia
[3]Nexiasolutions, BNFL, Sellafield, Seascale, Cumbria CA20 1PG, United Kingdom
[4]CLRC Daresbury Laboratory, Warrington, Cheshire WA4 4AD, United Kingdom
[5]ESRF, ROBL-CRG, BP 220, Grenoble, Cedex, France
[*]Corresponding author: Iain.May@man.ac.uk

We report the results of recent research that we have undertaken to increase our understanding of key actinide and fission product speciation in a range of ionic melts. These results will be used to develop novel electrochemical methods of separation of uranium and plutonium from irradiated nuclear fuel. Our studies in high temperature alkali metal melts (including LiCl and the eutectics LiCl-KCl and CsCl-NaCl) have focussed on *in-situ* speciation of U, Tc and Ru using both Electronic Absorption Spectroscopy (EAS) and X-ray Absorption Spectroscopy (XAS). The XAS studies have included Extended X-Ray Absorption Fine Structure (EXAFS) and X-Ray Absorption Near Edge Structure (XANES) measurements. We report what could be unusual uranium speciation in high temperature melts and evaluate the

In Separations for the Nuclear Fuel Cycle in the 21st Century; Lumetta, G., et al.;
ACS Symposium Series; American Chemical Society: Washington, DC, 2006.

likelihood of Ru or Tc volatilisation during plant operation. Our studies in lower temperature melts, commonly known as ionic liquids, have focussed on salts containing tertiary alkyl group 15 cations and the bis(trifluoromethylsulphonyl)imide anion, melts which we know to have exceptionally wide electrochemical windows. We report Ln, Th, U and Np speciation (XAS, EAS and vibrational spectroscopy) and electrochemistry in these melts.

Downloaded by PENNSYLVANIA STATE UNIV on August 9, 2012 | http://pubs.acs.org
Publication Date: June 9, 2006 | doi: 10.1021/bk-2006-0933.ch014

Introduction

The development of novel methods for the safe processing of irradiated nuclear fuel is a key challenge that the nuclear industry must face. Current research is focussed on advancements to PUREX process technology, including actinide partitioning and subsequent transmutation, and the development of novel alternative fuel treatment technologies to an industrial scale. These technologies include supercritical fluids and pyrochemical processing.

Pyrochemical Processing

High temperature molten salt processing of irradiated nuclear fuel is not a novel concept and there are currently two operating plants at the Research Institute for Atomic Reactors (RIAR) in Russia and at the Argonne National Laboratory (ANL) in the US. The two facilities both operate electrochemical processes for irradiated nuclear fuel treatment using molten chloride melts – a NaCl-KCl eutectic at the RIAR and a LiCl-KCl eutectic at the ANL. Advanced molten salt technologies are currently being developed by both institutes and by other nuclear research laboratories in Japan, Europe and the US. (1-9)

The Application of Low Temperature Ionic Liquids in Nuclear Waste Management

Low Temperature Ionic liquids (LTILs) are relatively novel solvent systems which are currently receiving a lot of interest for a whole range of chemical processes. (10-11) These ionic melts are generally classed as salts with melting points less than 100° C and tend to comprise of inorganic anions and organic cations. With regards to specific nuclear applications there have been studies into the use of water immiscable ionic liquids for solvent extraction processes, with particular reference to $\{UO_2\}^{2+}$, Sr^{2+} and Cs^+ extraction. (12-14) The replacement of alkali metal chloride melts with lower temperature ionic liquids in an electrochemical process is also attractive, with the obvious decrease in operating temperature and the potential for greatly reduced corrosion issues. Previously studies focussed on chloroaluminate melts, (15-16) although the hygroscopic nature of such melts would probably inhibits large scale operation. More recent studies have focussed tertiary alkyl ammonium or pyrrolidinium cation and bis(trifluoromethylsulfonyl)imide anion (TFSI, $[N(SO_2CF_3)_2]^-$) based salts which are much less moisture sensitive and appear to have electrochemical windows wide enough to undertake the electrodeposition of uranium and plutonium. (17-21)

Downloaded by PENNSYLVANIA STATE UNIV on August 9, 2012 | http://pubs.acs.org
Publication Date: June 9, 2006 | doi: 10.1021/bk-2006-0933.ch014

Current BNFL/Nexiasolutions Research Programme

For the past decade BNFL (British Nuclear Fuels Ltd) have undertaken a research and development programme into the application of ionic melt technologies for the electrochemical separation of U and Pu from irradiated nuclear fuel. This work continues through the new organisation Nexiasolutions which supercedes the Research and Technology group of BNFL. Since 2000 the Centre for Radiochemistry Research (CRR) at the University of Manchester in the UK has undertaken basic chemical research as part of this programme. This paper summarises some of the key results from the past four years collaboration in which both high temperature melts and low temperature ionic liquid studies have been undertaken.

High Temperature Molten Salt Studies

Experimental

A detailed account of the experimental method used to undertake high temperature molten salt spectroscopic measurements is given elsewhere. (22-25) XAS measurements were recorded at the Daresbury Laboratory in absorbance mode on station 9.3 (U L_{III}-edge and Ru K-edge) and in fluorescence mode (Tc K-edge and Re L_{III}-edge) on station 16.5. EAS with other supporting analysis was undertaken at the CRR laboratories.

Uranium Speciation

Previous Research

Probing actinide speciation in high temperature melts is extremely challenging due to both the harsh chemical environment, limiting the spectroscopic techniques available, and the radiological hazards. Radiological limitations restrict most studies to low specific activity radionuclides such as ^{238}U. EAS has been our standard method for probing speciation and is an excellent method for determining oxidation state, but not so useful in determining coordination environment. (22) Recent studies into actinide speciation in ionic melts have given an indication that simple monomeric complexes may not dominate actinide speciation in all cases. A Raman spectroscopy study has indicated that $ThCl_4$:CsCl melts contain oligomeric Th species with bridging chlorides. (26) EAS has provided evidence for $\{NpO_2\}^+:\{UO_2\}^{2+}$ cation:cation complexes in a CsCl melt (27) and a peroxide bridged $\{UO_2\}^{2+}$ dimer in a NaCl:CsCl melt. (28) Novel actinide complexes may also be present in alkali metal chloride melts of relevance to the pyrochemical processing of irradiated nuclear fuel.

XAS spectroscopy is an element specific technique which may be applied to probing chemical speciation in a wide range of diverse chemical matrices. It has previously found a wide range of applications for the determination of metal speciation, including actinide cation speciation. (29) A recent XAS study probing the U^{III} chemical environment in in a LiCl-KCl melt at 550 °C has been undertaken. (30) In this study EXAFS data was collected to an E_{max} of 17.7 keV and information obtained on the first coordination sphere which was fitted with 7.3 chloride ligands at 2.82 Å. This group found no evidence of oligomerisation in the melt system chosen with simple monomeric species appearing to dominate speciation.

In situ XAS Measurements

The furnace set-up that we have previously used to record *in situ* EAS measurements (22) has recently adapted to allow us to undertake *in situ* XAS (XANES and EXAFS) measurements. (23, 25) Currently, we are only able to obtain data in absorbance mode and our salt systems are restricted to low absorbing alkali metal halides (i.e. LiCl, LiCl-KCl and LiCl-$BeCl_2$). Uranium could be introduced into the melt by either direct dissolution of UCl_3, UCl_4 or UO_2Cl_2 or by *in situ* chlorination (by HCl or Cl_2) of UO_2 or UO_3.

Downloaded by PENNSYLVANIA STATE UNIV on August 9, 2012 | http://pubs.acs.org
Publication Date: June 9, 2006 | doi: 10.1021/bk-2006-0933.ch014

Preliminary results obtained from probing the U L_{III} edge reveal that we can use the XANES spectrum to distinguish between uranium in the +III, +IV, +V and +VI oxidation states. (23) EXAFS data fitting is in good agreement for classical 6 coordinate uranium species (e.g. $[U^{III}Cl_6]^{3-}$, $[U^{IV}Cl_6]^{2-}$, $[U^{V}O_2Cl_4]^{3-}$ and $[U^{VI}O_2Cl_4]^{2-}$). An example EXAFS data fit is shown in Figure 1. However, there is also often evidence for longer range interactions which we believe represent U-alkali metal and U-U interactions indicating that oligomeric species may be present in these high temperature melts.

Downloaded by PENNSYLVANIA STATE UNIV on August 9, 2012 | http://pubs.acs.org
Publication Date: June 9, 2006 | doi: 10.1021/bk-2006-0933.ch014

Fission Product Speciation in Molten Salts

Most nuclear power plants around the world use UO_2 based fuel and we are thus interested in the electrochemical processing of irradiated oxide fuel types. One method for the dissolution of oxide fuel in a high temperature melt is chlorination (either by HCl or Cl_2). However, this has the potential to bring additional fission products into the molten solution, including ^{99}Tc and ^{103}Ru and ^{106}Ru. Our specific interest in the chemistry of these two elements lies in the fact that both merit specific consideration during conventional PUREX process operations, with $[TcO_4]^-$ coextraction through solvent extraction operations (31-32) and care required to avoid the formation of volatile RuO_4 during any high temperature waste treatment process. (33)

We have previously reported a detailed study into the speciation of Tc and Re in a range of high temperature melts which have shown that Re is not always a good non-radioactive analogue for Tc in these systems. (24) The reaction between Re metal, ReO_2, ReO_3 and TcO_2 with HCl and Cl_2 were studied in LiCl-KCl, NaCl-CsCl and NaCl-KCl melts using *in* situ EAS. Quenched melts were also probed by XAS. This work has shown that $[ReCl_6]^{2-}$ is the dominant species formed for Re for all experimental conditions with TcO_2 alo reacting with HCl in a range of melts to form only $[TcCl_6]^{2-}$. However, the reaction between TcO_2 and Cl_2 leads to the formation of volatile chlorides and/or oxychlorides with $[TcO_4]^-$ remaining behind in the melt. In the design of any new molten salt fuel processing plant care should thus be taken to avoid any Tc volatility issues.

We have now turned our attention to Ru, studying Ru and RuO_2 dissolution by HCl and Cl_2 in NaCl-KCl, LiCl-KCl, NaCl-CsCl and LiCl. *In situ* EAS is potentially very informative but we have not yet conclusively been able to assign the broad absorbance bands that are observed. However, *in situ* EXAFS measurement in LiCl and LiCl-KCl have yielded more information and the data fit is consistent with the formation of $[Ru^{III}Cl_6]^{3-}$ as the major species irrespective of initial Ru starting material, ionic melt or chlorination method. Typical EXAFS data is given in Figure 2. We cannot, however, rule out the possibility that the major Ru oxidation state in these melts is Ru^{IV} and more detailed experimental studies are currently being undertaken.

Downloaded by PENNSYLVANIA STATE UNIV on August 9, 2012 | http://pubs.acs.org
Publication Date: June 9, 2006 | doi: 10.1021/bk-2006-0933.ch014

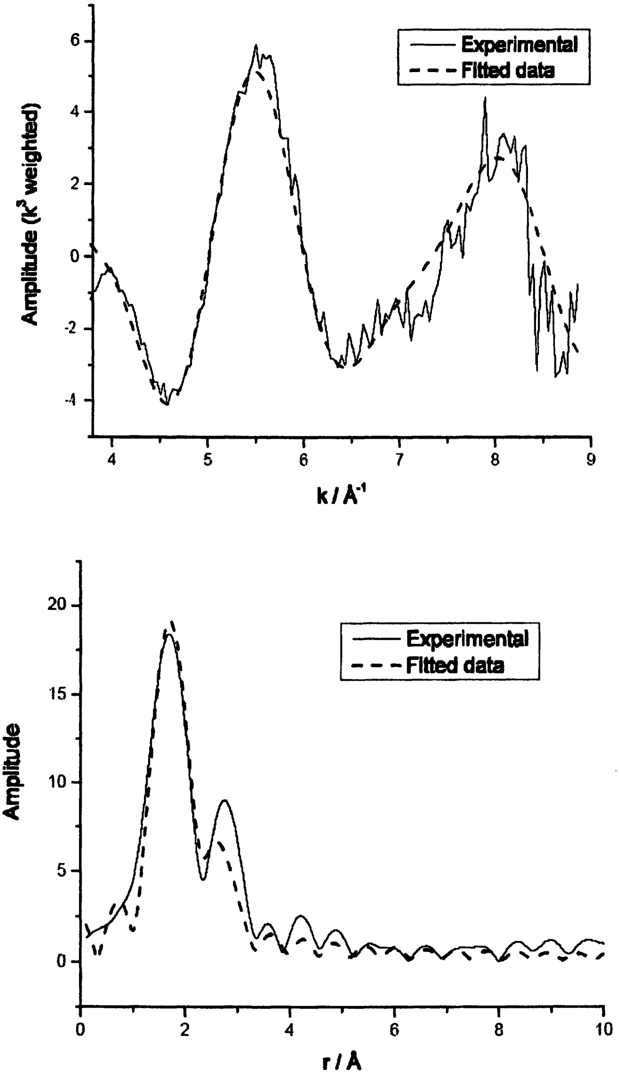

Figure 1. U L_{III}-edge EXAFS spectrum and fourier transform of UO_3 exposed to HCl in LiCl/KCl eutectic at 700 °C (experimental – solid line; theory – dashed line). Data can be fitted with the following model: 2×O – 1.75 Å; 4×Cl – 2.62 Å. %U = 1.56 %, k_{min} = 3.8, k_{max} = 9.0, R = 28.5

Downloaded by PENNSYLVANIA STATE UNIV on August 9, 2012 | http://pubs.acs.org
Publication Date: June 9, 2006 | doi: 10.1021/bk-2006-0933.ch014

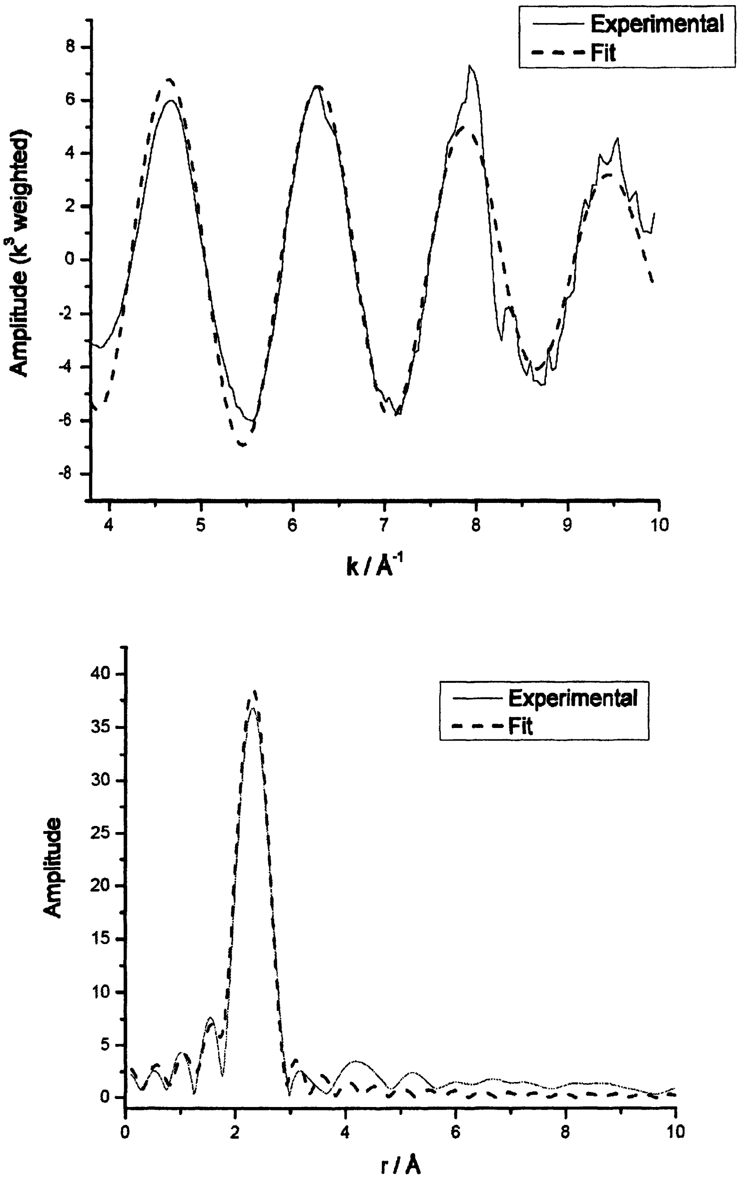

Figure 2. Ru K-edge EXAFS spectrum and fourier transform of RuO_2 chlorination with HCl in LiCl-KCl eutectic at 500°C (experimental – solid line; theory – dashed line). Data can be fitted with the following model: 6×Cl – 2.39 Å. %Ru = 0.60 %,

Low Temperature Ionic Liquid Studies

Experimental

More detailed experimental methods are described elsewhere. (34) XAS measurements were undertaken on station 16.5 at the CLRC Daresbury Laboratory and at the ROBL-CRG beamline at the ESRF. Synthetic chemistry, spectroscopic characterisation, X-ray crystallography and electrochemical measurements were all undertaken at the CRR laboratories.

Downloaded by PENNSYLVANIA STATE UNIV on August 9, 2012 | http://pubs.acs.org
Publication Date: June 9, 2006 | doi: 10.1021/bk-2006-0933.ch014

Electrochemical window measurements

Our initial aim was focused on evaluating novel LTIL systems with wide enough electrochemical windows to undertake the electrochemical deposition of U and Pu metal. Initial studies focused on the Group 15 quaternary alkyl salts of general formula $[Me_4X][TFSI]$, where X = N, P and As. Their electrochemical windows were measured both in the molten state (at 160 °C) and as supporting electrolytes in MeCN. (34) All had electrochemical windows wide enough to potentially undertake U and Pu metal deposition, as observed by through the observation of the Li^+/Li^0 couple. (34) We have since extended this study to ionic liquids with lower symmetry cations, including $[^nBuNMe_3][TFSI]$, which is a liquid at room temperature. All the ionic liquids were synthesized by metathesis reactions between Group 15 based alkyl cation halides and Li[TFSI]. For all the room temperature measurements the ferrocenium/ferrocene couple was used as an internal standard. (35).

F-element Speciation

Due to the presence of electron withdrawing CF_3 groups it would be expected that TFSI would be a weakly coordinating anion (Figure 3). This may explain why, until recently, the only X-ray structural study of coordinated TFSI is in the Cu complex, [Cu(CO)(TFSI)], where the ligand coordinates through the central nitrogen. (36) There have, however, been more recent reports indicating that TFSI is a flexible ligand, with several possible coordination modes. (37-38)

We have recently structurally characterized $[La(TFSI)_3(H_2O)_3]$ as a benchmark trivalent f-element complex. The three TFSI ligands coordinate to the La^{III} centre through bidentate sulfonyl oxygens (Figure 4). We have also been able to prepare a range of additional solid state TFSI complexes with other f-element cations, including Eu^{III}, Sm^{III}, Th^{IV}, U^{IV} and $\{UO_2\}^{2+}$, all characterised by a range of analytical and spectroscopic techniques.

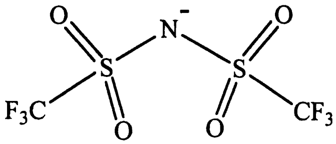
O
N
O
S
S
F3C
CF3
O
O

Figure 3. The TFSI anion

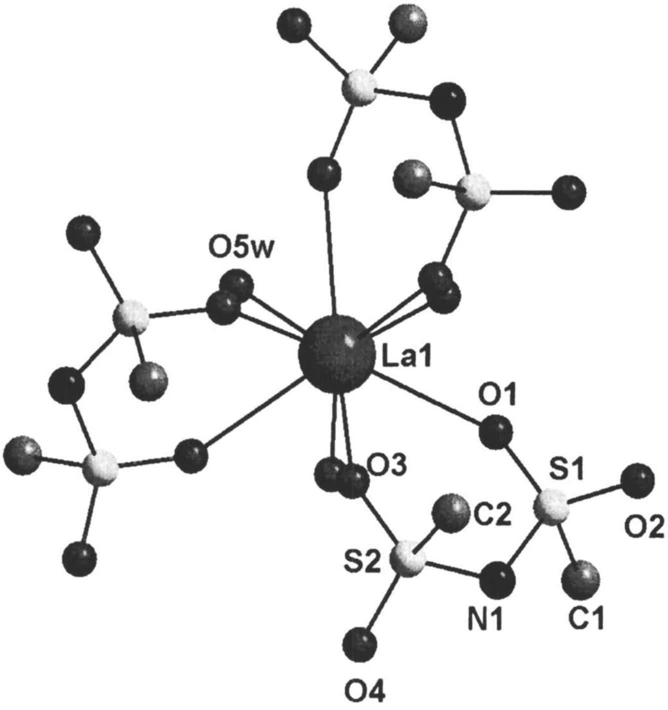
O5w
La1
O1
S1
O2
O3
C2
S2
N1
C1
O4

Figure 4. The structure of La(TFSI)$_3$(H$_2$O)$_3$

Downloaded by PENNSYLVANIA STATE UNIV on August 9, 2012 | http://pubs.acs.org
Publication Date: June 9, 2006 | doi: 10.1021/bk-2006-0933.ch014

Studying in situ speciation of f-element cations in TFSI based LTILs have been limited to EAS and XAS measurements. We have undertaken extensive XANES and EXAFS measurements on a range of uranium complexes in TFSI based melts. EAS has been used to confirm oxidation state purity in solution. The results confirm that TFSI is a weak ligand, for example it unable to displace coordinated chloride anions from UCl_4. Interestingly, a recent EXAFS study into $\{UO_2\}^{2+}$ solvent extraction into a TFSI based LTIL with nitrate and CMPO gave no evidence for the coordinated TFSI. [12] However, we have found evidence for TFSI remaining coordinated to U^{VI} with $[UO_2(TFSI)_2]$ appearing to remain intact when dissolved into $[BuNMe_3][TFSI]$, as might be expected.

We attempted to prepare a Np^{IV}-TFSI complex by reacting Np^{IV} hydroxide with 4 molar equivalents of HTFSI, removing H_2O *in vacuo*. However, on dissolution of the resultant solid in $[BuNMe_3][TFSI]$ oxidation to $\{NpO_2\}^+$ was indicated by EAS (39) despite our best attempts to eliminate oxygen and moisture from the system. This tends to suggest that TFSI is not effective at stabilizing the lower oxidation state. Two major bands are observed around the region for the major $\{NpO_2\}^+$ f-f transition suggesting the presence of more than one species in solution.

F-element Electrochemistry

Electrochemical studies have been undertaken in several of ionic liquids with a series of f-element cations, including La^{III}, Eu^{III}, Sm^{III}, Th^{IV}, U^{IV}, $\{UO_2\}^{2+}$ and $\{NpO_2\}^+$. In most cases reduction of Ln^{III} (or Ln^{II}) to Ln^0 or An^{III} to An^O was observed although often plating and stripping behaviour was not observed, probably due to the presence of moisture in the solvent system leading to the immediate formation of oxide on reduction to the metallic state. In addition, electrochemical features attributed to higher oxidation state processes (*e.g.* $U^{VI/IV}$, $Np^{V/IV}$) were also observed at more positive potentials. Typical cyclic voltammagrams showing the $Th^{IV/0}$ couples for $[^nBuNMe_3][TFSI]$ is shown in Figure 5.

Conclusions

Chemical research is required to support the development of novel ionic melt technologies for the electrochemical separation of U and Pu from irradiated nuclear fuel. Higher temperature melt studies have focused on *in situ* speciation of uranium and key fission products with XAS spectroscopy yielding information on U, Tc and Ru speciation which compliments EAS measurements. Currently we are looking into the application of NMR and Raman spectroscopy to probe f-element speciation in these melt systems further.

Downloaded by PENNSYLVANIA STATE UNIV on August 9, 2012 | http://pubs.acs.org
Publication Date: June 9, 2006 | doi: 10.1021/bk-2006-0933.ch014

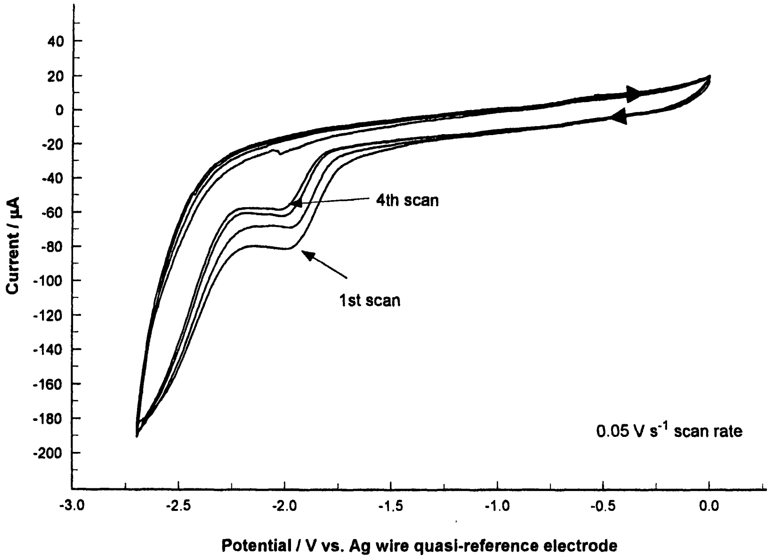

Figure. 5. Cyclic voltammograms of a Th^{IV}-TFSI complex in [BuNMe$_3$][TFSI], showing reduction to Th^0.

Our ionic liquid research has focused on group 15 quaternary alkyl bistriflimide salts which have electrochemical windows wide enough to potentially see the electrodeposition of U and Pu. Electrochemical and solution speciation studies indicate that it may be possible to electrochemical separate out actinides using this technology. Further studies are required to develop novel ionic liquid solvents that can be used for bulk electrodeposition of U and Pu.

References

1. Finch, R.J.; Miller, W.; Runge, J.; Hafenrichter, L.D.; Fletcher, G.; Williamson, M. *Abstracts of Papers of the American Chemical Society*, **2004**, *227*, IEC-249.
2. Li, S.X.; Vaden, D.; Westphal, B.R. *Abstracts of Papers of the American Chemical Society*, **2004**, *227*, IEC-249.
3. Benedict, R.W.; McFarlane, H.F. *Radwaste Magazine*, **1998**, *5*, 23.
4. Ossipenko, A.G.; Bychov, A.V.; Bovet, A.L.; Smolenski, V.V.; Mityaev, V.S.; Borodina, N.P. *J. Nucl. Sci. Tech.*, **2002**, *3*, 592.

Downloaded by PENNSYLVANIA STATE UNIV on August 9, 2012 | http://pubs.acs.org
Publication Date: June 9, 2006 | doi: 10.1021/bk-2006-0933.ch014

5. Serp, J.; Konnings, R.J.M.; Malmbeck, R.; Rebizant, J.; Scheppler, C.; Glatz, J.P. *J. Electroanal. Chem.*, **2004**, *561*, 143.
6. Hayashi, H.; Kobayashi, F.; Ogawa, T.; Minato, K. *J. Nucl. Sci. Tech.*, **2002**, *3*, 624.
7. Lambertin, D.; Sanchev, S.; Picard, G.S.; Lacquement, J. *Radiochim. Acta*, **2003**, *91*, 449.
8. Lambertin, D.; Lacquement, J.; Sanchev, S.; Picard, G. *Electrochem. Commun.*, **2002**, *4*, 447.
9. Koyama, T.; Kinoshita, H.; Inoue, T.; Ougier, M.; Malmbreck, R.; Glatz, J. –P.; Koch, L. *J. Nucl. Sci. Tech.*, **2002**, *3*, 765.
10. Wasserchied, P.; Keim, W. *Angew. Chem. Int. Ed.*, **2002**, *39*, 3772.
11. Welton, T. *Chem. Rev.*, **1999**, *99*, 2071.
12. Visser, A.E.; Jensen, M.P.; Laszak, I.; Nash, K.L.; Choppin, G.R.; Rogers, R.D. *Inorg. Chem.* **2003**, *42*, 2197.
13. Jensen, M.P.; Dzielawa, J.A.; Richert, P.; Dietz, M.L. *J. Amer. Chem. Soc.*, **2002**, *124*, 10665.
14. Dai, S.; Ju, Y.H.; Barnes, C.E. *Dalton Trans.*, **1999**, 1201.
15. Anderson,C.J.; Deakin, M.R.; Choppin, G.R.; Dolieslager, W.; Heerman, L.; Pruett, D.J. *Inorg. Chem.*, **1991**, *30*, 4013.
16. Hopkins, T.A.; Berg, J.M.; Costa, D.A.; Smith, W.H.; Dewey, H.J. *Inorg. Chem.*, **2001**, *40*, 1820.
17. MacFarlane, D.R.; Meakin, P.; Sun, J.; Forsyth, M. *J. Phys. Chem. B.* **1999**, *103*, 4164.
18. McFarlane, D.R.; Sun, J.; Golding, J.; Meakin, P.; Forsyth, M. *Electrochim. Acta*, **2000**, *45*, 1271.
19. Quin, B.M.; Ding, Z.; Moulton, R.; Bard, A.J. *Langmuir*, **2002**, *18*, 1734.
20. Murase, K.; Nitta, K.; Hirato, T.; Awakura, Y.J. *J. Applied Electrochem.*, **2001**, *31*, 1089.
21. Oldham Jr., W.J.; Costa, D.A.; Smith, W.H. *Los Alomos Internal Report* **2001**.
22. Volkovich, V.A.; Bhatt, A.I.; May, I.; Griffiths, T.R.; Thied, R.C. *J. Nucl. Sci. Tech.*, **2002**, *3*, 595.
23. Volkovich, V.A.; May, I.; Bhatt, A.I.; Griffiths, T.R.; Charnock, J.M.; Lewin, B. *International Symposium on ionic liquids in honour of Marcelle Gaune-Escard, Carry le Rouet, France, June 27-28,* **2003**.
24. Volkovich, V.A.; May, I.; Charnock, J.M; Lewin, B. *Phys. Chem. Chem. Phys.*, **2002**, *4*, 5753.
25. Volkovich, V.A.; May, I.; Charnock, J.M. *Rasplavy*, **2004**, *2*, 76.
26. G.M. Photiadis, G.N. Papatheodorou, *Dalton Trans.*, **1999**, 3541.
27. Yu.A. Barbanel, R.B. Dushin, V.V. Kolin, L.G. Mashirov, S.N. Nekhoroshkov, *Radiokhimiya*, **2003**, **45**, 253.
28. S.K. Vavilov, P.T. Porodnov, O.V. Skiba, *Rasplavy*, **1996**, **5**, 45.

Downloaded by PENNSYLVANIA STATE UNIV on August 9, 2012 | http://pubs.acs.org
Publication Date: June 9, 2006 | doi: 10.1021/bk-2006-0933.ch014

29. S.D. Conradson, K.D. Abney, B.D. Begg, E.D. Brady, D.L. Clark, C. Den Auwer, M. Ding, P.K. Dorhout, F.J. Espinosa-Faller, P.L. Gordon, R.G. Haire, N.J. Hess, R.F. Hess, D.W. Keogh, G.H. Lander, A.J. Lupinetti, L.A. Morales, M.P. Neu, P.D. Palmer, P. Paviet-Hartmann, S.D. Reilly, W.H. Runde, C.D. Tait, D.K. Viers, F. Wastin, *Inorg. Chem.*, **2004**, *43*, 116. (and references therein).
30. Y. Okamato, M. Akabori, A. Itoh, T. Ogawa, *J. Nucl. Sci. Tech.*, **2002**, *3*, 638.
31. T.J. Kemp, A.M. Thyer, P.D. Wilson, *Dalton Trans.*, **1993**, 2601.
32. T.J. Kemp, A.M. Thyer, P.D. Wilson, *Dalton Trans.*, **1993**, 2607.
33. E. Blasius, J.-P. Glatz, W. Neumann, *Radiochim. Acta*, **1981**, *29*, 159.
34. I. Bhatt, I. May, V.A. Volkovich, M.E. Hetherington, B. Lewin, *Dalton Trans.*, **2002**, 4532.
35. R.R. Gagné, C.A. Koval, G.C. Lisensky, *Inorg. Chem.*, **1980**, *19*, 2854.
36. O.G. Polyakov, S.M. Ivanova, C.M. Gaundinski, S.M. Miller, O.P. Anderson, S.H. Strauss, *Organomet.*, **1999**, *18*, 3769.
37. Oldham, W. J.; Williams, D. B. *Proc. Electrochem. Soc.,* **2002**, *2002-19,* 983.
38. M.E. Stoll, D.A. Costa, B.L. Scott, W.J. Oldham, *Abstracts of papers of the American Chemical Society*, **2004**, *227*, 159-NUCL.
39. *The Chemistry of the Actinide Elements Vol. 2, 2nd Ed.* Katz, J.J.; Seaborg, G.T.; Morss, L.R., Chapman & Hall, London, **1986**, 1266

Downloaded by PENNSYLVANIA STATE UNIV on August 9, 2012 | http://pubs.acs.org
Publication Date: June 9, 2006 | doi: 10.1021/bk-2006-0933.ch014

Downloaded by UNIV OF ARIZONA on August 10, 2012 | http://pubs.acs.org
Publication Date: June 9, 2006 | doi: 10.1021/bk-2006-0933.ch015

Chapter 15

Application of Ionic Liquids in Actinide and Fission Product Separations: Progress and Prospects

Dominique C. Stepinski, Blake A. Young, Mark P. Jensen, Paul G. Rickert, Julie A. Dzielawa, Andrew A. Dilger, David J. Rausch, and Mark L. Dietz*

Chemistry Division, Argonne National Laboratory, Argonne, IL 60439

Ionic liquids (ILs), particularly those that are liquid at room temperature, have attracted intense interest as alternatives to conventional organic solvents in a host of synthetic, catalytic, and electrochemical applications. Recently, growing attention has been devoted to their use in separations, typically as replacements for the organic diluents employed in traditional liquid-liquid extraction or membrane-based separations of organic solutes or metal ions. Although studies of the extraction of metal ions into various ILs indicate that these solvents frequently provide extraction efficiencies far greater than those obtained with conventional solvents, other work suggests that they suffer from various drawbacks that could limit their utility as extraction solvents. In this chapter, we examine the viability of ionic liquids as the basis for extraction systems for the separation of actinides and fission products from acidic media and consider approaches by which their limitations may be overcome.

In Separations for the Nuclear Fuel Cycle in the 21st Century; Lumetta, G., et al.;
ACS Symposium Series; American Chemical Society: Washington, DC, 2006.

Introduction

Growing world demand for energy, coupled with the prospect of the eventual exhaustion of readily accessible reserves of oil (*1*) and the poor economics, inconvenience, or adverse environmental impact associated with other energy sources (*2*), has recently led to a revival of interest in the possibilities afforded by nuclear energy. Public perceptions notwithstanding, nuclear energy is among the least hazardous approaches to the large-scale generation of power. Moreover, unlike fossil fuels, its use produces no emissions of carbon dioxide. Nuclear power remains one of the few large energy sources that has yet to be fully exploited. In fact, it is the only energy source whose use could be significantly increased as world energy needs rise (*2*).

The disposition of high-level radioactive wastes (in particular, spent nuclear fuel) remains a significant obstacle to the more widespread acceptance of nuclear energy. Unlike other countries, the United States does not currently reprocess spent nuclear fuel, a result of proliferation concerns and an ongoing glut in the supply of uranium that makes reprocessing uneconomical (*2, 3*). Instead, wastes containing long half-life radioactive contaminants are currently destined for incorporation into a stable waste form (e.g., vitrification in a glass matrix) and storage in a dry, stable, and remote location (e.g., the Yucca Mountain repository). Given likely future U.S. energy consumption and the accompanying need for repository space, the difficulty in licensing new repositories, and the millennia required for the waste generated from nuclear power production to decay, vitrification and storage are unlikely to remain viable in the long term. Thus, it seems reasonable to expect that spent fuel reprocessing will resume in the U.S. at some point. In the alternative, transmutation of the long-lived isotopes into shorter-lived ones using reactor- or accelerator-produced neutrons could be carried out. In either case, chemical separations are certain to play an important role (*2*).

Among separation methods, none has played a more significant part in the progress of nuclear technology than has solvent extraction (SX). The PUREX Process, in which a solution of tri-*n*-butyl phosphate (TBP) in a paraffinic hydrocarbon is used to extract plutonium and uranium from nitric acid solution (*4*), is the most well-established SX process for nuclear separations and is, in fact, used in all spent fuel reprocessing facilities now in operation (*2*). This process is thus likely to play a role (at least in the near term) in any efforts to design a sustainable nuclear fuel cycle. The removal of the major heat generators (Sr-90 and Cs-137) from spent fuel would greatly simplify its handling and treatment, and aqueous-based SX processes by which this might be achieved have also been described. The SREX Process, for example, which employs a solution of a macrocyclic polyether in any of various oxygenated aliphatic solvents (*5*) or in a paraffinic hydrocarbon-TBP mixture (*6*) to extract strontium from acidic nitrate media, has been shown to provide excellent decontamination factors for radiostrontium. In addition, it has been shown to be

Downloaded by UNIV OF ARIZONA on August 10, 2012 | http://pubs.acs.org
Publication Date: June 9, 2006 | doi: 10.1021/bk-2006-0933.ch015

fully compatible (*7*) with the PUREX and TRUEX (*8*) processes (the latter a process for the extraction of transuranium elements in which the PUREX process solvent is modified by addition of octyl(phenyl)-*N*, *N*-diisobutylcarbamoylmethylphosphine oxide (CMPO) to boost extraction of trivalent actinides such as Am(III)). Despite the many virtues of these "classical" SX processes, each of them involves the use of volatile or semivolatile organic compounds (VOCs) as solvents, thus raising both environmental (*e.g.*, fugative emissions) and health and safety (*e.g.*, solvent toxicity and flammability) concerns.

Increasing recognition of the need to develop more environmentally benign chemical processes and to extend the concepts and practices of "green chemistry" to the nuclear fuel cycle has recently led to interest in ionic liquids (ILs), particularly those that are liquid at room temperature (RTILs), as alternatives to conventional organic solvents in SX processes for nuclear materials (*9-13*). Many of these solvents exhibit a number of unique properties that make them attractive candidates for such an application, among them a near absence of vapor pressure, high thermal stability, and low flammability. In addition, ILs are extraordinarily tunable solvents, for which only minor changes in the nature of the cationic or anionic constituent can lead to significant changes in physicochemical properties. Initial reports would seem to suggest that ionic liquids offer great promise as extraction solvents in nuclear applications. Work by Dai *et al.* (*9*), for example, showed that the unique solvation environment offered by ionic liquids can make them especially efficient as solvents for the extraction of metal complexes from aqueous solution. Specifically, remarkably large strontium extraction coefficients, far exceeding those obtainable with any conventional organic solvent, were observed for the extraction of strontium from water into solutions of dicyclohexano-18-crown-6 (DCH18C6) in any of several *N,N'*-dialkylimidazolium-based RTILs (Figure 1). In a subsequent study by Visser *et al.* (*12*) investigating ionic liquids as solvents for the TRUEX process, the extraction of Pu^{4+}, Th^{4+} and UO_2^{2+} into 1-butyl-3-methylimidazolium hexafluorophosphate ($C_4mim^+PF_6^-$) by 0.1 M CMPO-1 M TBP was found to be at least an order of magnitude higher than that obtained for the same extractant concentrations in dodecane. In addition, distribution ratios for Am^{3+}, which is weakly extracted from, for example, 1 M HNO_3 by 0.1 M CMPO in the TBP/dodecane system (*8, 12, 14*), were at least two orders of magnitude higher when $C_4mim^+PF_6^-$ was substituted for dodecane. Work by Allen *et al.* (*13*), in which the radiation stability of dialkylimidazolium-based ionic liquids containing nitrate and chloride anions to α, β and γ radiation was assessed, indicates that ILs are relatively radiation resistant and that irradiation causes no significant decomposition of the organic (*i.e.*, cationic) component. In fact, ionic liquids were found to be more stable than TBP/kerosene mixtures, an observation attributed to the presence of an aromatic ring system that can dissipate energy and serve as a protective agent for the other reagents present.

Downloaded by UNIV OF ARIZONA on August 10, 2012 | http://pubs.acs.org
Publication Date: June 9, 2006 | doi: 10.1021/bk-2006-0933.ch015

In contrast to these encouraging results, work in this and other laboratories has shown that various ionic liquids exhibit certain characteristics that could adversely impact their utility in nuclear separations. For example, the use of imidazolium-based ionic liquids appears limited to systems in which the aqueous phase nitric acid concentration is relatively low (≤ 1 M). At higher HNO_3 concentrations, significant loss of the imidazolium cation to the aqueous phase can occur, eventually leading to degradation of the biphasic system (*10, 11, 15*). Similarly, in studies of hexafluorophosphate-based ILs, conversion of the PF_6^- anion to aqueous-soluble PO_4^{3-} and degradation of the organic phase is frequently observed at high acidity (*12*). Next, although extraction of metal complexes into ionic liquids is highly efficient at low aqueous acidity (*9*), it often decreases with an increasing acid concentration (*10, 11, 16*). The high distribution ratios typically observed at low acidity complicate stripping of extracted metal ions from the organic phase and thus, represent a significant potential limitation of ILs as extraction solvents in nuclear applications. Finally, and perhaps most important, EXAFS data and solvent extraction results indicate that the predominant mode of partitioning of, for example, UO_2^{2+} into IL systems is cation exchange (*11, 15*). Ionic liquid-based extraction systems for which the predominant mode of ion transfer involves concomitant loss of the cationic constituent of the ionic liquid to the aqueous phase clearly cannot be considered for use on the process scale. Such drawbacks represent major challenges to the incorporation of ionic liquid-based separation processes into the nuclear fuel cycle.

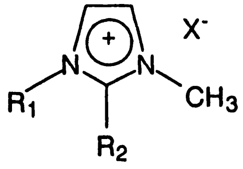

$X = PF_6^-, Tf_2N^-$

R_1 = ethyl, propyl, or butyl; R_2 = H or methyl

Figure 1. Representative hydrophobic methylimidazolium-based ILs (9, 17)

In this work, several of these concerns are considered in more detail and means by which they might be addressed are described. At the same time, a systematic comparison of ionic liquid-based and traditional separation processes for strontium and uranium is presented, thus providing an indication of the feasibility (and desirability) of the implementation of IL-based separations. In making this comparison, it must be noted, only the efficiency of extraction, the ease of recovery of extracted metal ions, and the extraction selectivity have been

Downloaded by UNIV OF ARIZONA on August 10, 2012 | http://pubs.acs.org
Publication Date: June 9, 2006 | doi: 10.1021/bk-2006-0933.ch015

considered. Other issues, such as the physicochemical properties of the solvents (*e.g.*, viscosity) and their relative cost and toxicity, while important enough to require eventual consideration, are beyond the scope of the present report.

Discussion

Extraction of strontium from acidic nitrate media by crown ethers: 1-octanol *vs.* **"short-chain" ILs.** Any evaluation of the suitability of ionic liquids as replacements for molecular solvents in a liquid-liquid extraction system must begin with a consideration of the strengths and limitations associated with the conventional system. In the conventional SREX Process, strontium partitioning between nitric acid and 1-octanol in the presence of the crown ether (either DCH18C6 or a dialkyl-substituted analog, such as the di-*t*-butyl- compound, DtBuCH18C6) proceeds *via* formation of a neutral strontium nitrato-crown ether complex (Equation 1), as indicated by D_{Sr} nitric acid dependency measurements such as are depicted in Figure 2 for a solution of DCH18C6 in octanol. As can

$$Sr^{2+} + 2\ NO_3^- + Crown_{org} \leftrightarrow Sr(NO_3)_2 \bullet Crown_{org} \qquad (1)$$

be seen, strontium extraction (here, determined radiometrically according to established procedures (*18*) increases essentially linearly over the acid concentration range examined. Thus, efficient extraction of strontium is readily achievable at high acidities, while at low acidities, D_{Sr} is sufficiently small as to permit efficient stripping of strontium from the organic phase. The ability to obtain both satisfactory strontium partitioning from aqueous phases containing appreciable concentrations of nitric acid and facile strontium recovery using only dilute acid or water for stripping represents a major advantage of this chemistry over alternative systems (*5*). The selectivity of the DCH18C6-octanol system is also impressive. Measurements of distribution ratios (*via* ICP-AES) for more than two dozen metallic elements (inert constituents and fission products) between a "dissolved sludge waste" (*19*) (acidified to 3 M HNO3) and a solution of DCH18C6 (0.1 M; mixed *cis-syn-cis* (A) and *cis-anti-cis* (B) isomers) in 1-octanol indicate that only Sr and Ba (D_M = 5.4 and 2.4 respectively) are appreciably extracted (although extraction of Ca, Mo, Ru and Pd, for which D_M values range from 0.2 to 0.7, is not insignificant). Thus, to be considered viable as a replacement for 1-octanol, an ionic liquid must yield a system that provides high strontium extraction efficiency (particularly at high acidity), facile recovery of extracted strontium (preferably at low acidity), and excellent strontium extraction selectivity.

As noted earlier, work by Dai *et al.* (*9*) has established that the extraction of strontium by DCH18C6 into a variety of ionic liquids from water is far more efficient than extraction into molecular organic solvents under the same conditions. As shown in Figure 2, however, the superior performance of the IL is significantly diminished by increasing aqueous nitric acid concentration. That is, in contrast to extraction into 1-octanol and other conventional solvents, the

Downloaded by UNIV OF ARIZONA on August 10, 2012 | http://pubs.acs.org
Publication Date: June 9, 2006 | doi: 10.1021/bk-2006-0933.ch015

D_{Sr} acid dependency in 1-pentyl-3-methylimidazolium *bis*[(trifluoromethyl) sulfonyl]imide (abbreviated henceforth as $C_5mim^+Tf_2N^-$), is seen to exhibit a

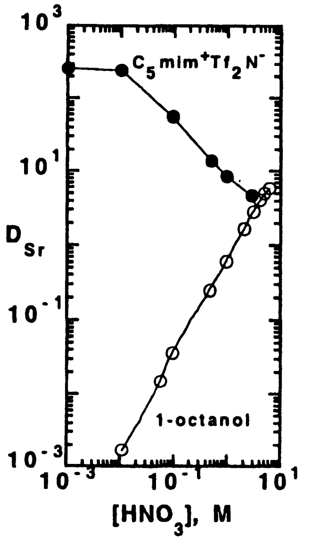

Figure 2. Strontium extraction by DCH18C6 crown ether in 1-octanol and $C_5mim^+Tf_2N^-$ from nitric acid solutions.

negative slope. (Note that $C_5mim^+Tf_2N^-$ comprises a representative "short chain" ionic liquid, so named to distinguish it from other ILs bearing longer, more hydrophobic alkyl substituents in the 1-position such as its 1-decyl analog, $C_{10}mim^+Tf_2N^-$.) In addition to its obvious fundamental interest, this difference in the shape of the acid dependency of D_{Sr} has significant implications for the potential utility of ILs as replacements for 1-octanol in the SREX Process. That is, given that nuclear waste solutions are often strongly acidic (≥ 3 M nitric acid), decline in extraction efficiency with acidity clearly poses a problem. This problem is compounded by the fact that extracted strontium must be recovered. Specifically, the high extraction efficiency at low acidity precludes the use of a dilute nitric acid solution or water for stripping, while the instability of imidazolium-based ILs to extensive contact with aqueous phases containing higher acid concentrations makes stripping with such solutions impractical. Taken together with studies of the extraction of various metal ions into $C_5mim^+Tf_2N^-$ containing DCH18C6 indicating that the selectivity of the system is no better (and in some cases, such as $\alpha_{Sr/Ba}$, is actually poorer) than for DCH18C6 in octanol, these results make it clear that $C_5mim^+Tf_2N^-$ (and by

Downloaded by UNIV OF ARIZONA on August 10, 2012 | http://pubs.acs.org
Publication Date: June 9, 2006 | doi: 10.1021/bk-2006-0933.ch015

Downloaded by UNIV OF ARIZONA on August 10, 2012 | http://pubs.acs.org
Publication Date: June 9, 2006 | doi: 10.1021/bk-2006-0933.ch015

analogy, other "short-chain" imidazolium-based ionic liquids) offers no advantage over a conventional organic solvent in this application.

Effect of phase modifier addition on the extraction behavior of "short-chain" imidazolium-based ionic liquids. In a pair of earlier reports (11, 20), we demonstrated that the differences in the behavior of ILs such as $C_5mim^+Tf_2N^-$ *vs.* 1-octanol as extraction solvents with neutral extractants such as crown ethers (most notably, the dramatic difference in the shape of the acid dependencies of D_{Sr} such as that depicted in Figure 2) have their origins in differences in the mechanism of cation partitioning, with extraction into the ILs proceeding *via* an ion-exchange mechanism in which the cationic metal-crown ether complex is exchanged for the cationic constituent of the ionic liquid. Such a mechanism has obvious negative implications for the utility of ILs in process-scale nuclear separations. In an effort to devise IL-based extraction systems for which ion exchange does not represent the dominant mode of metal ion partitioning, we have recently begun an investigation of the effect of phase modifier addition upon the mechanism of strontium extraction by DCH18C6. We anticipated that IL modification employing a conventional organic co-solvent for which ion exchange does not represent a viable extraction pathway might lead to a change in the mechanism of partitioning into the IL to extraction of a neutral metal nitrato-crown ether complex. With this in mind, the partitioning of strontium and nitrate ions between water and a series of TBP/$C_5mim^+Tf_2N^-$ mixtures in the presence of DCH18C6 was measured (Table I). (TBP was selected as a cosolvent for these experiments because of its well established usefulness as a phase modifier in conventional solvent systems (*21, 22*) and its reported solubility in imidazolium-based ILs (*15*).) Unexpectedly, for all of the mixtures,

Table I. Strontium[a] and nitrate[b] ion partitioning between water[c] and solutions of DCH18C6[d] in $C_5mim^+Tf_2N^-$/TBP

Solvent	*%E$_{Sr}$*	*%E$_{NO3-}$*	
		Observed	*Expected*[e]
25% TBP / $C_5mim^+Tf2N^-$	> 94	5.3	> 94
50% TBP / $C_5mim^+Tf2N^-$	> 94	2.0	> 94
60% TBP / $C_5mim^+Tf2N^-$	> 94	4.4	> 94
90% TBP / $C_5mim^+Tf2N^-$	> 90	4.5	> 90

[a] Determined radiometrically.
[b] Determined by ion chromatography.
[c] Containing 0.0310 M $Sr(NO_3)_2$.
[d] 0.202 M DCH18C6-A in the indicated ionic liquid.
[e] Assuming extraction of the neutral strontium nitrato-crown ether complex. For partitioning *via* cation exchange, no nitrate co-extraction ($\%E_{NO3-}=0$) is expected.

the amount of nitrate ion extracted was found to be far less than that anticipated assuming the extraction of a neutral strontium nitrato-crown ether complex. These results indicate that the presence of TBP, even at high concentrations, has no effect on the partitioning mechanism.

The absence of an effect is at least partly explained by the results of an EXAFS investigation of the effect of TBP on the coordination environment of the strontium-crown ether complex in $C_5mim^+Tf_2N^-$. In these experiments, the number of oxygen atoms coordinated to strontium following its extraction by DCH18C6 into a series of $TBP/C_5mim^+Tf_2N^-$ mixtures was determined, and the results compared to those obtained for TBP alone and for 1-octanol (Table II).

Table II. Average number of oxygen atoms in Sr coordination environment derived from EXAFs measurements

Solvent	N_O	*Axial* N_O[a]	*Distal* N_O[a]
1-Octanol[b]	10.2	4.2	2.1 ± 0.4
100% $C_5mim^+Tf_2N^-$[b]	8.7 ± 0.8	2.0	
60% TBP / $C_5mim^+Tf_2N^-$	7.3 ± 0.8	1.9	
90% TBP / $C_5mim^+Tf_2N^-$	7.9 ± 0.8	2.0	
100% TBP	8.6 ± 0.8	3.4	1.7 ± 0.8

[a] Assuming a hexacoordinate crown ether
[b] From reference 20.

As shown previously (*20*), when strontium is extracted into 1-octanol, a peak corresponding to 10 oxygen atoms at 2.7 Å, a second peak corresponding to 12 crown ether carbon atoms at 3.5 Å, and a third peak for the two distal (uncoordinated) oxygen atoms of NO_3^- at 4.3 Å are evident in the EXAFS. Thus, the extracted strontium complex is 10-coordinate (*i.e.*, $Sr(NO_3)_2(DCH18C6)$); six O atoms from the crown ether and four O atoms from two axially-coordinated bidentate nitrate groups are present in the inner coordination sphere (*20*). (Figure 3). Much the same coordination environment is observed when strontium is extracted into TBP. In contrast, no distal oxygen peak is observed in the EXAFS for any of the samples containing $C_5mim^+Tf_2N^-$ regardless of TBP concentration, indicating that no detectable nitrate is directly coordinated to the strontium-crown ether complex. Instead, the poor coordinating ability of the Tf_2N^- anion (*23*) and the amount of water present in $C_5mim^+Tf_2N^-$ make it likely that the axial sites are occupied by water molecules (Figure 3) (*20*). Thus, the inability of TBP addition to alter the predominant form of the metal complex in the ionic liquid underlies its lack of effect on the mechanism of strontium partitioning. Although these results do not entirely rule

Downloaded by UNIV OF ARIZONA on August 10, 2012 | http://pubs.acs.org
Publication Date: June 9, 2006 | doi: 10.1021/bk-2006-0933.ch015

out the possibility of employing a phase modifier to influence the mode of metal ion extraction into an ionic liquid, they are not especially encouraging, particularly given that the presence of as little as 10% (v/v) $C_5mim^+Tf_2N^-$ in TBP is sufficient to lead to partitioning *via* ion exchange.

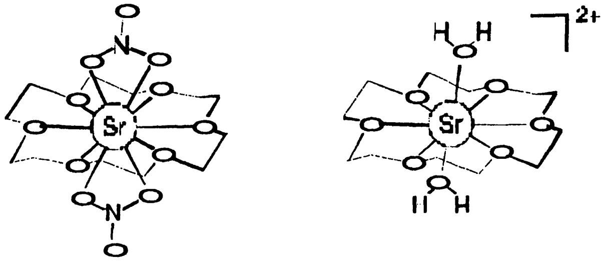

Figure 3. Coordination environments of $Sr(NO_3)_2(DCH18C6)$ in 1-octanol and the $Sr(DCH18C6)(H_2O)_2{}^{2+}$ cation present in $C_5mim^+Tf_2N^-$.

Downloaded by UNIV OF ARIZONA on August 10, 2012 | http://pubs.acs.org
Publication Date: June 9, 2006 | doi: 10.1021/bk-2006-0933.ch015

Effect of IL cation hydrophobicity on the viability of ionic liquids as replacements for 1-octanol in the SREX Process. More satisfactory results are obtained by increasing the chain length of one of the alkyl substituents on the imidazolium cation. That is, implicit in an ion-exchange mechanism for metal ion partitioning is the fact that as the hydrophobicity of the IL cation is increased, cation exchange will become increasingly difficult (*16*). In fact, a decrease in strontium partitioning with alkyl chain length has been reported for the extraction of strontium by DCH18C6 into a series of 1-alkyl-3-methylimidazolium bis[(trifluoromethyl)sulfonyl]imides (*11*). A sufficiently hydrophobic cation, therefore, might be expected to diminish or even eliminate cation exchange as a mode of strontium partitioning. Recently, this possibility has been examined by simultaneously measuring the partitioning of both strontium and nitrate ions between water and series of $C_nmim^+Tf_2N^-$ ionic liquids in the presence of DCH18C6 (*16*). As shown in Table III, the amount of nitrate extracted into the $C_5mim^+Tf_2N^-$ ionic liquid is vastly insufficient to produce a neutral strontium nitrato-crown ether complex. As the alkyl chain length is increased, however, nitrate extraction becomes increasingly significant, indicating that, as expected, the extraction mechanism shifts from cation exchange to extraction of a neutral complex with increasing IL cation hydrophobicity. For the $C_{10}mim^+Tf_2N^-$ ionic liquid, in fact, the amount of nitrate extracted is that expected for partitioning of a neutral nitrato complex.

Additional evidence of a shift in the mechanism of partitioning for strontium is provided by the dependency of D_{Sr} on nitric acid concentration for

$C_{10}mim^{+}Tf_2N^{-}$ (*16*). In contrast to the plot obtained in $C_5mim^{+}Tf_2N^{-}$, in $C_{10}mim^{+}Tf_2N^{-}$, increasing acidity is accompanied by an increase in the extraction of strontium (Figure 4), an observation consistent with partitioning *via* neutral

Table III. Strontium[a] and nitrate[b] ion partitioning between water[c] and solutions of DCH18C6[d] in $C_nmim^{+}Tf_2N^{-}$ ionic liquids

Organic phase	*$\%E_{Sr}$*	*$\%E_{NO_3^-}$*		*Partitioning mode*
		Observed	*Anticipated[e]*	
$C_5mim^{+}Tf_2N^{-}$	96.5	9 ± 7	96.5	Cation exchange
$C_6mim^{+}Tf_2N^{-}$	82.6	16.1 ± 0.8	82.6	Cation exchange
$C_8mim^{+}Tf_2N^{-}$	39.0	20.9 ± 1.0	39.0	Mixed
$C_{10}mim^{+}Tf_2N^{-}$	20.2	20.0 ± 1.0	20.2	Neutral complex

[a] Determined radiometrically.

[b] Determined by ion chromatography.

[c] Containing 0.0310 M $Sr(NO_3)_2$.

[d] 0.202 M DCH18C6-A in the indicated ionic liquid.

[e] Assuming extraction of the neutral strontium nitrato-crown ether complex. For partitioning *via* cation exchange, no nitrate co-extraction ($\%E_{NO_3^-}$=0) is anticipated.

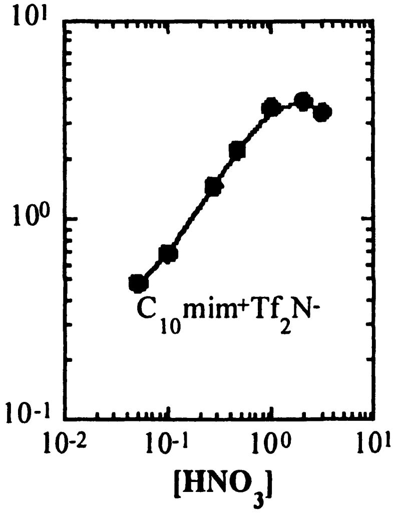

Figure 4. Nitric acid dependency of D_{Sr} for 0.1 M DCH18C6 in $C_{10}mim^{+}Tf_2N^{-}$.

Downloaded by UNIV OF ARIZONA on August 10, 2012 | http://pubs.acs.org
Publication Date: June 9, 2006 | doi: 10.1021/bk-2006-0933.ch015

complex extraction. Comparison of this acid dependency to that observed in 1-octanol (Figure 2) indicates that both the extraction efficiency at high acidity and the ease of recovery of extracted strontium will be comparable for the two systems. Measurements of the extraction of a variety of inert and fission product constituents between a dissolved sludge waste (acidified to 3 M in HNO_3) and a solution of DCH18C6-A/B in this same ionic liquid indicate that the selectivity of a modified SREX process in which the 1-octanol is replaced by $C_{10}mim^+Tf_2N^-$ will also be comparable to that of the conventional process, for which (as noted above) DM values greater than one are observed only for strontium and barium. Thus, the hoped for orders-of-magnitude improvement in strontium extraction efficiency and selectivity *vs.* the conventional extraction system is not observed, rendering it difficult to make a compelling case that replacement of 1-octanol by a "long-chain" ionic liquid such as $C_{10}mim^+Tf_2N^-$ is desirable.

Downloaded by UNIV OF ARIZONA on August 10, 2012 | http://pubs.acs.org
Publication Date: June 9, 2006 | doi: 10.1021/bk-2006-0933.ch015

Uranium extraction by an ionic liquid-based PUREX process solvent. As noted earlier, work by Visser *et al.* (*12*) has shown that uranium is extracted more than an order of magnitude more efficiently by a 0.1 M CMPO-1 M TBP mixture in $C_4mim^+PF_6^-$ than by the same pair of extractants in dodecane. Given this, the results obtained in the extraction of uranium by TBP alone (1.2 M) in dodecane and in a pair of $C_nmim^+Tf_2N^-$ (n = 5 or 10) ionic liquids (Figure 5) are completely unexpected. That is, as can be seen from a plot of the dependence of the uranium distribution ratio, DU, on TBP concentration, extraction of uranium from 3 M HNO_3 into dodecane is *more* efficient (by *ca.* a factor of 5) than extraction into either $C_5mim^+Tf_2N^-$ or $C_{10}mim^+Tf_2N^-$. A look at the nitric acid dependency of D_U at constant TBP concentration (1.2 M) in dodecane (Figure 5, right panel), shows that the extraction of uranium increases roughly linearly over the concentration range examined, as expected for the partitioning of a neutral uranium nitrato-TBP complex. In contrast, uranium partitioning into $C_5mim^+Tf_2N^-$ shows a complex dependency on nitric acid concentration consistent with a shift in mechanism from cation exchange to neutral complex extraction as the acidity increases. While interesting from a fundamental perspective, such behavior poses practical problems. That is, in dodecane, efficient uranium extraction can be achieved from aqueous phases containing high concentrations of acid and extracted uranium can be readily recovered using dilute nitric acid or water. For $C_5mim^+Tf_2N^-$, however, D_U exceeds 1 (*i.e.*, more than 50% of the U is present in the IL phase at equilibrium) over the entire range of acidities examined. Moreover, uranium is extracted equally well from either weakly or strongly acidic solutions. Although the acid dependency of D_U for $C_{10}mim^+Tf_2N^-$ conforms more closely to the desired shape (*i.e.*, increasing uranium partitioning with increasing acidity) uranium distribution ratios are generally lower than for dodecane. At the same time, the uranium selectivity of a 1.2 M solution of TBP in $C_{10}mim^+Tf_2N^-$ is no better than that obtained in dodecane. (Measurements of the partitioning of a number of inert components and fission products between dissolved sludge waste acidified to 3 M nitric acid and a 1.2 M solution of TBP in $C_{10}mim^+Tf_2N^-$ indicate that only U and Zr exhibit distribution ratios exceeding unity: 15.3 and 2.2, respectively. In dodecane, U

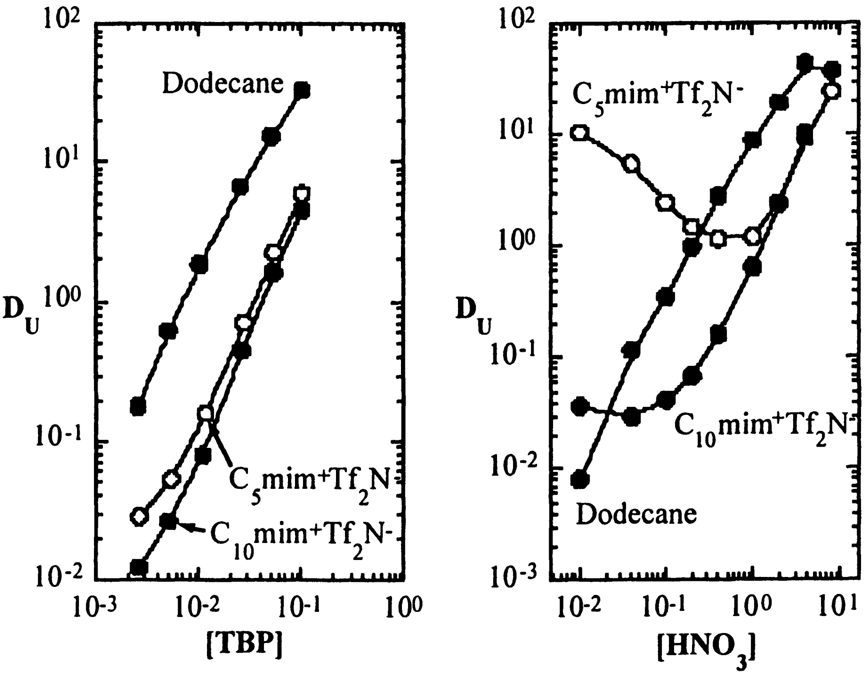

Figure 5. Uranium extraction by TBP in dodecane, $C_5mim^+Tf_2N^-$ or $C_{10}mim^+Tf_2N^-$ from nitric acid solutions. (Left panel: $[HNO_3] = 3$ M; Right panel: $[TBP] = 1.2$ M).

and Zr exhibit distribution ratios of 54.4 and 0.48, respectively.) Thus, from the perspective of extraction efficiency, selectivity, and ease of recovery of extracted uranium, the use of a TBP solution in either $C_5mim^+Tf_2N^-$ or $C_{10}mim^+Tf_2N^-$ offers no discernible advantages over a conventional PUREX process solvent based on dodecane.

Conclusions

The results presented here raise concerns regarding the viability of C_nmim^+-based ionic liquids as replacements for conventional organic solvents such as 1-octanol and dodecane in established processes employing neutral extractants for

Downloaded by UNIV OF ARIZONA on August 10, 2012 | http://pubs.acs.org
Publication Date: June 9, 2006 | doi: 10.1021/bk-2006-0933.ch015

actinide and fission product separations. "Short-chain" ILs such as $C_5mim^+Tf_2N^-$, which exhibit either decreasing extraction efficiency with increasing acidity (Sr with DCH18C6) or a complex dependence of D_M on $[HNO_3]$ (U with TBP), seem particularly ill-suited for this application. Although increasing the IL cation hydrophobicity leads to acid dependencies that exhibit the desired shape (*i.e.*, increasing extraction with rising acidity), the metal ion distribution ratios obtained are either comparable to or lower than those obtained in 1-octanol (for Sr) and dodecane (for U), respectively. Moreover, in neither case is an improvement in the extraction selectivity for the target metal ion observed. If our results prove to be representative of those generally achievable in the partitioning of actinides and fission products into RTILs, there may be less incentive to substitute ionic liquids for conventional solvents in nuclear fuel reprocessing applications.

Downloaded by UNIV OF ARIZONA on August 10, 2012 | http://pubs.acs.org
Publication Date: June 9, 2006 | doi: 10.1021/bk-2006-0933.ch015

Acknowledgments

The authors thank the Analytical Services Laboratory (ANL-CMT) for determination of the partitioning of dissolved sludge waste constituents (ICP/AES) and nitrate ion (ion chromatography). This work was performed under the auspices of the Office of Basic Energy Sciences, U.S. Department of Energy, under contract number W-31-ENG-109-38.

References

1. Roberts, P. *The End of Oil: On the Edge of a Perilous New World*; Houghton Mifflin: New York, 2004.
2. Watson, J. S. In *Chemical Separations in Nuclear Waste Management: The State of the Art and a Look to the Future*; Choppin, G. R.; Khankhasayev, M. K.; Plendl, H. S., Eds.; Battelle Press: Columbus, Ohio, 2002, pp. xii-ixix.
3. Saling, J. H.; Fentiman, A. W.; Tang, Y. S. *Radioactive Waste Management*; Taylor & Francis: New York, 2001.
4. Nash, K. L.; Barrans, R. E.; Chiarizia, R.; Dietz, M. L.; Jensen, M. P.; Rickert, P.; Moyer, B. A.; Bonnesen, P. V.; Bryan, J. C.; Sachleben, R. A. Fundamental Investigations of Separations Science for Radioactive Materials. *Solv. Extr. Ion Exch.* **2000**, *18,* 605-631.
5. Horwitz, E. P.; Dietz, M. L.; Fisher, D. E. SREX: A New Process for the Extraction and Recovery of Strontium from Acidic Nuclear Waste Streams. *Solv. Extr. Ion Exch.* **1991**, *9,* 1-25.
6. Dietz, M. L.; Horwitz, E. P.; Rogers, R. D. Extraction of Strontium from Acidic Nitrate Media Using a Modified PUREX Solvent *Solv. Extr. Ion Exch.* **1995**, *13,* 1-17.

7. Dietz, M. L.; Horwitz, E. P. In *Science and Technology for Disposal of Radioactive Tank Wastes*;Schulz, W.W.; Lombardo, N.J., Eds.; Plenum Press: New York, 1998, pp. 231-243.
8. Horwitz, E. P.; Kalina, D. G.; Diamond, H.; Vandegrift, G. F. The Truex Process - a Process for the Extraction of the Transuranic Elements from Nitric Acid Wastes Utilizing Modified Purex Process. *Solv. Extr. Ion Exch.* **1985,** *3,* 75-109.
9. Dai, S.; Ju, Y. H.; Barnes, C. E. Solvent Extraction of Strontium Nitrate by a Crown Ether Using Room-Temperature Ionic Liquids. *J. Chem. Soc., Dalton Trans.* **1999**, 1201-1202.
10. Visser, A. E.; Swatloski, R. P.; Hartman, D. H.; Huddleston, J. G.; Rogers, R. D. Traditional Extractants in Nontraditional Solvents: Groups 1 and 2 Extraction by Crown Ethers in Room-Temperature Ionic Liquids. *Ind. Eng. Chem. Res.* **2000,** *39,* 3596-3604.
11. Dietz, M. L.; Dzielawa, J. A. Ion-Exchange as a Mode of Cation Transfer into Room-Temperature Ionic Liquids Containing Crown Ethers: Implications for the 'Greenness' of Ionic Liquids as Diluents in Liquid-Liquid Extraction. *Chem. Commun.* **2001,** 2124-2125.
12. Visser, A. E.; Rogers, R. D. Room-Temperature Ionic Liquids: New Solvents for *f*-Element Separations and Associated Solution Chemistry. *J. Solid State Chem.* **2003,** *171,* 109-113.
13. Allen, D.; Baston, G.; Bradley, A. E.; Gorman, T.; Haile, A.; Hamblett, I.; Hatter, J. E.; Healey, J. F.; Hodgson, B.; Lewin, R.; Lovell, K. V.; Newton, B.; Pitner, W. R.; Rooney, D. W.; Sanders, D.; Seddon, K. R.; Sims, H. E.; Thied, R. C. An Investigation of the Radiochemical Stability of Ionic Liquids. *Green Chem.* **2002,** *4,* 152-158.
14. Schulz, W. W.; Horwitz, E. P. The Truex Process and the Management of Liquid TRU Waste. *Sep. Sci Technol.* **1988,** *23,* 1191-1210.
15. Visser, A. E.; Jensen, M. P.; Laszak, I.; Nash, K. L.; Choppin, G. R.; Rogers, R. D. Uranyl Coordination Environment in Hydrophobic Ionic Liquids: An in Situ Investigation. *Inorg. Chem.* **2003,** *42,* 2197-2199.
16. Dietz, M. L.; Dzielawa, J. A.; Laszak, I.; Jensen, M. P. Influence of Solvent Structural Variations on the Mechanism of Facilitated Ion Transfer into Room-Temperature Ionic Liquids. *Green Chem.* **2003,** *5,* 682-685.
17. Bonhote, P.; Dias, A. P.; Papageorgiou, N.; Kalyanasundaram, K.; Gratzel, M. Hydrophobic, Highly Conductive Ambient-Temperature Molten Salts. *Inorg. Chem.* **1996,** *35,* 1168-1178.
18. Horwitz, E. P.; Kalina, D. G.; Muscatello, A. C. The Extraction of Th(IV) and U(VI) by Dihexyl-*N,N*-diethylcarbamoylmethylphosphonate from Aqueous Nitrate Media. *Sep. Sci Technol.* **1981,** *16,* 403-416.
19. Vandegrift, G. F.; Leonard, R. A.; Steindler, M. J.; Horwitz, E. P.; Basile, L. J.; Diamond, H.; Kalina, D. G.; Kaplan, L. *Transuranic Decontamination of Nitric Acid Solutions by the Truex Solvent Extraction Process - Preliminary Development Studies;* Report No. ANL-84-45; U.S. DOE: Argonne, IL, 1984.

Downloaded by UNIV OF ARIZONA on August 10, 2012 | http://pubs.acs.org
Publication Date: June 9, 2006 | doi: 10.1021/bk-2006-0933.ch015

20. Jensen, M. P.; Dzielawa, J. A.; Rickert, P.; Dietz, M. L. EXAFS Investigation of the Mechanism of Facilitated Ion Transfer into a Room-Temperature Ionic Liquid. *J. Am. Chem. Soc.* **2002**, *124,* 10664-10665.
21. Kalina, D. G.; Horwitz, E.P. Variations in the Solvent Extraction Behavior of Bifunctional Phosphorus-Based Compounds with TBP. *Solv. Extr. Ion Exch.* **1985**, *3*, 235-250.
22. Chiarizia, R.; Horwitz, E. P. The Influence of TBP on Americium Extraction by Octyl(phenyl)-N,N-diisobutylcarbamoylmethylphosphine Oxide. *Inorg. Chim. Acta* **1987**, *140*, 261-263.
23. Haas, A.; Klare, C.; Betz, P.; Bruckmann, J.; Kruger, C.; Tsay, Y. H.; Aubke, F. Acyclic Sulfur-Nitrogen Compounds. Syntheses and Crystal and Molecular Structures of Bis((trifluoromethyl)sulfonyl)amine ($(CF_3SO_2)_2NH$), Magnesium Hexaaquo Bis((trifluoromethyl)sulfonyl)amide Dihydrate ($[Mg(H_2O)_6][(CF_3SO_2)2N]_2{\cdot}2H_2O$), and Bis(bis(fluorosulfonyl)-amino)sulfur ($(FSO_2)_2NSN(SO_2F)_2$). *Inorg. Chem.* **1996**, *35,* 1918-1925.

Downloaded by UNIV OF ARIZONA on August 10, 2012 | http://pubs.acs.org
Publication Date: June 9, 2006 | doi: 10.1021/bk-2006-0933.ch015

Downloaded by NORTH CAROLINA STATE UNIV on August 9, 2012 | http://pubs.acs.org
Publication Date: June 9, 2006 | doi: 10.1021/bk-2006-0933.ch016

Chapter 16

Use of Cyanex-301 for Separation of Am/Cm from Lanthanides in an Advanced Nuclear Fuel Cycle

Dean R. Peterman, Jack D. Law, Terry A. Todd, and Richard D. Tillotson

**Idaho National Engineering and Environmental Laboratory,
P.O. Box 1625, Idaho Falls, ID 83415**

As part of the Advanced Fuel Cycle Initiative (AFCI), technologies for advanced aqueous processing of spent LWR fuel are being developed. Included in this program is the separation of Am and Cm from the lanthanides. This separation would allow the Am/Cm to be fabricated into a target and recycled to a reactor and the lanthanides to be disposed of with the raffinates from the process. A Laboratory Directed Research and Development (LDRD) Project at the INEEL is investigating the use of the active extractant in the Cyanex-301 reagent, bis(2,4,4-trimethylpentyl)dithiophosphinic acid, as a potential method to accomplish this separation. Specifically, the extractant is being developed based on an ammonium acetate/acetic acid buffered feed to the process which can be used to strip the actinides and lanthanides from a preceding transuranic separation process. The extraction and scrub distribution coefficients of Am and Eu with this extractant, as a function of total acetate concentration and pH, have been measured. Additionally, the extraction behavior of several additional lanthanides are compared. The potential for developing a Cyanex-301 process for the separation of Am/Cm from lanthanides to support an advanced nuclear fuel cycle is discussed.

In Separations for the Nuclear Fuel Cycle in the 21st Century; Lumetta, G., et al.;
ACS Symposium Series; American Chemical Society: Washington, DC, 2006.

Introduction

The Advanced Fuel Cycle Initiative (AFCI) is funded by the U.S. Department of Energy's Office of Nuclear Energy, Science and Technology to develop advanced separation technologies to safely and economically reduce the volume and heat generation of spent nuclear fuel requiring geologic disposition, thereby extending the capacity of the Yucca Mountain repository and delaying or avoiding the need for a second repository. To accomplish this, the AFCI is developing advanced fuel reprocessing systems to separate key radionuclides from spent light water reactor (LWR) fuel. An advanced aqueous process that is being developed is the UREX+ process.

The UREX+ process consists of a series of solvent extraction processes that separate the following radionuclides: a) Tc and U using the Uranium Extraction (UREX) process, b) Cs and Sr using a cobalt dicarbollide/polyethylene glycol (CCD-PEG) process, c) Pu, Np, Am, Cm, and rare-earth fission products using the Plutonium Uranium Refining by Extraction (PUREX) based processes and/or the transuranic extraction (TRUEX) processes , and d) Am and Cm from the rare earths using a selective actinide extraction (SANEX) process.

Limited research is being performed as part of the AFCI program to support development of the UREX+ process relative to the separation of Am and Cm from the lanthanides. Separation of the Am and Cm from the lanthanides will allow the Am/Cm to be fabricated into a target and recycled to a reactor and the lanthanides to be disposed of with the final raffinate from the UREX+ process. Several extractants have been previously identified as promising technologies for the separation of Am/Cm from the lanthanides but have not been developed specifically to support the UREX+ process *(1)*. One such technology is the use of the active extractant in the Cyanex-301 reagent - bis(2,4,4-trimethylpentyl)dithiophosphinic acid *(1-3)*. As part of a laboratory Directed Research and Development (LDRD) project at the INEEL, the use of bis(2,4,4-trimethylpentyl)dithiophosphinic acid is being investigated as a potential method to accomplish this separation.

One of the limitations of using the active extractant in the Cyanex-301 reagent is that efficient separation of Am/Cm from the lanthanides can only be accomplished at a pH greater than approximately 3. Many acidic waste streams, including dissolved spent nuclear fuel, which could benefit from this separation have a pH much lower than 3. However, it is possible to design the flowsheets in the UREX+ process to provide a feed stream to the Cyanex-301 process with a pH greater than 3. This can be accomplished by extracting the Am/Cm and lanthanides from the dissolved spent LWR fuel using the TRUEX process and stripping these radionuclides with an ammonium acetate/acetic acid buffered strip solution. This strip product is at a favorable pH for separation of Am/Cm

Downloaded by NORTH CAROLINA STATE UNIV on August 9, 2012 | http://pubs.acs.org
Publication Date: June 9, 2006 | doi: 10.1021/bk-2006-0933.ch016

from the lanthanides. The separation of Am/Cm from the lanthanides in this buffered feed solution is the primary focus of the LDRD work performed at the INEEL.

Scope

The primary scope of this research was to experimentally evaluate the conditions required to effectively separate Am/Cm from the lanthanides in an ammonium acetate/acetic acid buffered solution using the purified Cyanex-301 reagent. Buffered solutions ranging from 0.2 *M* to 1.0 *M* total acetate concentration and a pH ranging from 3.7 to 5.7, obtained by varying the concentration ratio of acetic acid and ammonium acetate, were used. Distribution coefficients and the resulting separation factors were determined for ^{241}Am and ^{154}Eu. Additionally, the separation factors for ^{241}Am from ^{154}Eu were determined as a function of pH in a simulant (1.0 *M* total acetate) containing approximately 6 g/L total lanthanides, which is a typical lanthanide concentration which is expected to be present in dissolved spent LWR fuel. Differences in the separation factors of various lanthanides (La, Ce, Pr, Nd, Sm, Eu) were also evaluated.

Experimental

The Cyanex-301 reagent was obtained from Cytec Industries, Canada. As received, the Cyanex-301 is a mixture of approximately 77% of the active extractant, bis(2,4,4-trimethylpentyl)dithiophosphinic acid, with the balance being synthetic by-products. Purification of the Cyanex-301 reagent was performed using the method developed by Zhu et al. *(4)* and detailed by Modolo and Odoj *(2)*. This purification resulted in a >99.9% pure product. Due to degradation of the purified solvent, the Cyanex-301 was converted to the ammonium salt and refrigerated until ready for use. At this time the ammonium salt was converted to the acid form. The purified Cyanex-301 was then diluted by TBP and n-dodecane based on the results of Hill et al. *(3)*. A solvent composition of 0.25 *M* Cyanex-301 and 0.37 *M* TBP in n-dodecane was used for all testing. All experiments were conducted at ambient temperature.

A combination pH electrode and meter (Accumet) were used to measure the pH of the aqueous phases before and after contact with the organic solvent. The combination pH electrode was calibrated by acid-base titration in the appropriate ionic strength electrolyte solution. The measured pH of the aqueous phases before and after contact with the organic solvent agreed to within the experimental error.

Downloaded by NORTH CAROLINA STATE UNIV on August 9, 2012 | http://pubs.acs.org
Publication Date: June 9, 2006 | doi: 10.1021/bk-2006-0933.ch016

Results

pH and Total Acetate Dependency

Distribution coefficients for ^{154}Eu and ^{241}Am, as a function of pH and total acetate concentration, are given in Figures 1 and 2, respectively. For ^{154}Eu with a 0.2 *M* total acetate concentration, distribution coefficients increase from 14 to 371 as the pH is increased from 4.2 to 5.7. At a total acetate concentration of 0.5 *M*, the ^{154}Eu distribution coefficients increase from 0.8 at a pH of 3.7 to a high of 21.4 at a pH of 4.8 then decrease to 6.9 at a pH of 5.8. At a total acetate concentration of 1.0 *M*, the ^{154}Eu distribution coefficients increase from 0.4 at a pH of 3.7 to a high of 1.4 at a pH of 4.8 then decrease to 0.22 at a pH of 5.8. These data indicate that operating at a 1.0 *M* total acetate concentration will minimize the extraction of Eu. Additionally, for a total acetate concentration of 1.0 *M*, the lowest Eu distribution coefficients are obtained at a pH >5.

For total acetate concentrations of 0.2 *M* and 0.5 *M*, the measured ^{241}Am distribution coefficients increase with increasing pH. However, detection limits were reached in the aqueous phase at pH values ranging from 4.8 to 5.8. These data are indicated by the open symbols in Figure 2. As a result, actual distribution coefficients for ^{241}Am at these pH values are unknown. At a total acetate concentration of 1.0 *M*, distribution coefficients for ^{241}Am increase from 72 at a pH of 3.7 to a maximum of 500 at 4.8, then decrease to 82 at a pH of 5.8.

The separation factor for Am from Eu is defined as D_{Am}/D_{Eu}. The higher the separation factor, the more efficient the resulting separation. Separation factors for Am from Eu are summarized in Table I. The separation factor for the extraction of Am from Eu by Cyanex-301 in the absence of TBP was not measured. Separation factors increase as the total acetate concentration is increased. In general, separation factors are also higher at the higher pH values. Based on these data, the best separation of Am from Eu is obtained at a total acetetate concentration of 1.0 *M* and a pH in the range of 5.2 to 5.8.

Table I. Separation Factors (D_{Am}/D_{Eu}).

PH	*0.2 M Acetate*	*0.5 M Acetate*	*1.0 M Acetate*
3.8	5.9	155	171
4.2	75.6	139	257
4.8	>33.0	>93	353
5.2	14.1	>127	372
5.5	>28.6	>157	383
5.8	13.8	>185	365

Downloaded by NORTH CAROLINA STATE UNIV on August 9, 2012 | http://pubs.acs.org
Publication Date: June 9, 2006 | doi: 10.1021/bk-2006-0933.ch016

Downloaded by NORTH CAROLINA STATE UNIV on August 9, 2012 | http://pubs.acs.org
Publication Date: June 9, 2006 | doi: 10.1021/bk-2006-0933.ch016

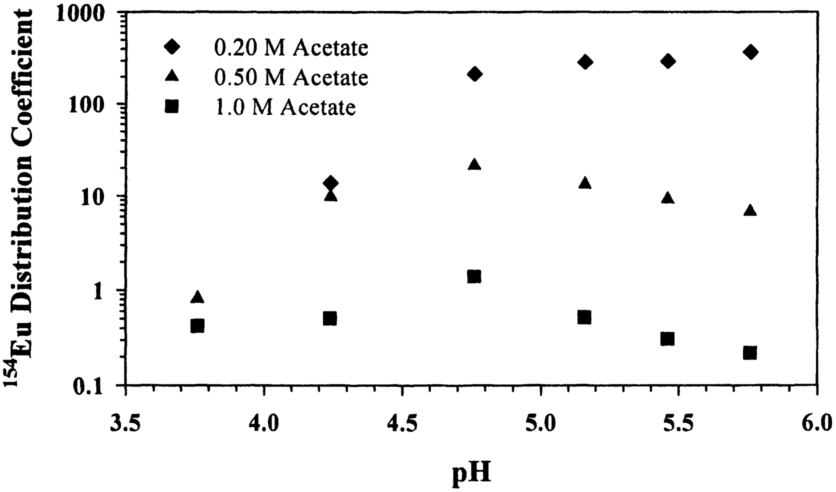

Figure 1. Distribution coefficients of ^{154}Eu as a function of pH at total acetate concentrations of 0.2 M, 0.5 M, and 1.0 M and a Cyanex-301 solvent composition of 0.25 M Cyanex, 0.37 M TBP in n-dodecane.

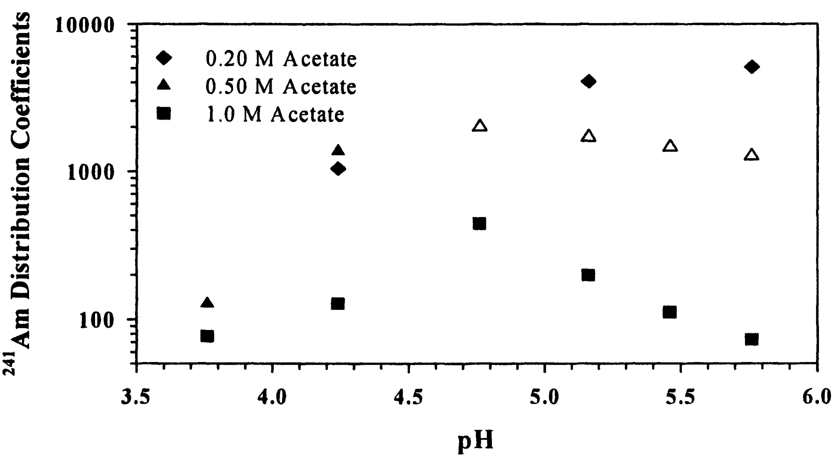

Figure 2. Distribution coefficient of ^{241}Am as a function of pH at total acetate concentrations of 0.2 M, 0.5 M, and 1.0 M and a Cyanex-301 solvent composition of 0.25 M Cyanex, 0.37 M TBP in n-dodecane. The open symbols represent minimum values as the aqueous phase concentrations were below the analytical detection limit.

The goal with the Cyanex-301 process is to separate the Am and Cm from the lanthanides. Typically, when the Cyanex-301 extractant has been studied for the separation of Am/Cm from lanthanides, the separation of Eu from Am was used to evaluate the effectiveness of the extractant *(2,3,5)*. However, recent results from flowsheet testing at Argonne National Laboratory (ANL) using the Cyanex-301 extractant indicate that all of the lanthanides do not behave similarily to Eu and a fractionation among the lanthanides may result *(6)*. Therefore, further testing was performed at the INEEL in which distribution coefficients were mesasured for many of the lanthanides.

Downloaded by NORTH CAROLINA STATE UNIV on August 9, 2012 | http://pubs.acs.org
Publication Date: June 9, 2006 | doi: 10.1021/bk-2006-0933.ch016

Evaluation of the Separation of Actinides from Lanthanides with Simulated Feed Solution

Extraction and scrub distribution coefficients for the lanthanides were measured using the non-radioactive feed simulant composition given in Table II. Three successive extraction contacts, using fresh simulant and the solvent from the previous contact, were performed. The solvent from the extraction contacts was then scrubbed using 1.0 *M* acetic acid. Additionally, identical tests were performed in which the simulant was spiked with ^{241}Am and ^{154}Eu so separation factors could be determined. Extraction distribution coefficients (first extraction contact, E1) for the lanthanides from the feed simulant as a function of pH at 1.0 *M* total acetate concentration are presented in Figure 3. The distribution coefficients were calculated from the results of inductively coupled mass spectrometry analysis of metals concentration in the aqueous and organic phases following mixing and separation. Additionally, the extraction distribution coefficients for each of the three extraction contacts at each pH, as well as the scrub distribution coefficients, are given in Table III.

The separation factors calculated using the data presented in Figure 3 and Table III increase across (to europium) the lanthanides series. At the lower pH of 3.8, the distribution coefficients of all of the lanthanides were less than 1.0. At pH's of 4.8 and 5.5, the distribution coefficients of the lighter lanthanides (La, Ce, Pr) are greater than 1.0 while the heavier lanthanides are less than 1.0. This is likely due to weaker complexation of the lighter lanthanides by acetate at higher solution pH values. These results indicate that good separation of all of the lanthanides from Am can only be obtained at the lower pH (less than ~ 4.0) when using a 1 *M* total acetate buffer. Additionally, the scrub distrbution coefficients for the lanthanides at a pH of 3.8 are below 1.0 and the Am scrub distribution coefficient is 15. This will allow for the extracted lanthanides to be effectively scrubbed from the Cyanex-301 solvent.

Table II. Feed Simulant to Cyanex-301 Process.

Component	*Concentration*
Total Acetate (*M*)	1.0
pH	3.8 to 5.5
Am *(g/L)*	trace
La *(g/L)*	0.8
Ce *(g/L)*	1.6
Pr *(g/L)*	0.7
Nd *(g/L)*	2.7
Pm *(g/L)*	0.012
Sm *(g/L)*	0.5
Eu *(g/L)*	0.1

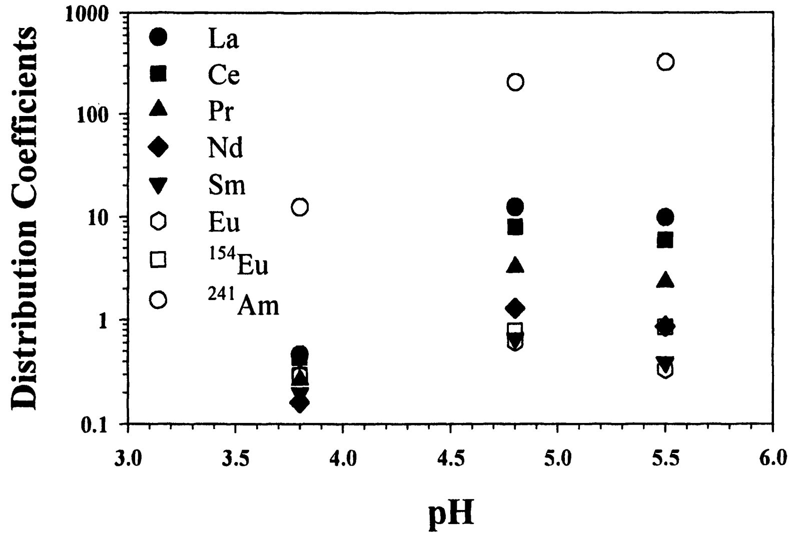

Figure 3. Lanthanide and Am distribution coefficients as a function of pH at a total acetate concentration of 1.0 M and a Cyanex-301 solvent composition of 0.25 M Cyanex, 0.37 M TBP in n-dodecane.

Downloaded by NORTH CAROLINA STATE UNIV on August 9, 2012 | http://pubs.acs.org
Publication Date: June 9, 2006 | doi: 10.1021/bk-2006-0933.ch016

Table III. Lanthanide extraction and scrub (1.0 *M* acetic acid) distribution coefficients from simulant (1 *M* total acetate) with the Cyanex-301 solvent as a function of pH.

pH	*Contact*	*La*	*Ce*	*Pr*	*Nd*	*Sm*	*Eu*	^{154}Eu	^{241}Am
3.8	E1	0.46	0.44	0.27	0.16	0.20	0.30	0.29	12.44
	E2	0.57	0.47	0.26	0.14	0.11	0.14	0.15	15.62
	E3	0.66	0.52	0.28	0.13	0.09	0.10	0.12	17.11
	Sc1	0.51	0.42	0.21	0.10	0.07	0.07	0.09	14.93
4.8	E1	12.41	7.97	3.25	1.30	0.65	0.61	0.78	206.2
	E2	6.23	4.10	1.61	0.60	0.26	0.23	0.30	100.3
	E3	4.49	2.98	1.16	0.43	0.19	0.17	0.21	68.13
	Sc1	1.81	1.35	0.61	0.25	0.15	0.13	0.18	37.68
5.5	E1	9.78	5.92	2.32	0.86	0.39	0.34	0.85	325.7
	E2	4.99	3.04	1.15	0.40	0.16	0.14	0.17	67.18
	E3	4.18	2.67	1.00	0.35	0.14	0.11	0.14	56.73
	Sc1	3.57	2.61	1.14	0.45	0.24	0.24	0.30	66.27

Conclusions

The Cyanex-301 extractant will effectively separate Am from Eu in an ammonium acetate/acetic acid buffered feed solution. Separation factors greater than 300 were obtained for a pH range of 4.8 to 5.8 with a 1.0 *M* total acetate buffer solution. The Eu distribution coefficient ranged from 1.4 at a pH of 4.8 to 0.22 at a pH of 5.8.

In an ammonium acetate/acetic acid buffered feed simulant, containing approximately 6.4 g/L lanthanides, separation factors increased along the lanthanide series at a total acetate concentration of 1.0 *M* and pH values ranging from 3.8 to 5.5, resulting in significant extraction of the lighter lanthanides (La, Ce, and Pr) at a pH of 4.8 and 5.5. However, at a pH of 3.8, the separation factors of the lanthanides ranged from 13 to 78 and lanthanide distribution coefficients were all low, ranging from 0.16 to 0.46. The increase in separation factors that was observed across the lanthanide series is likely due to weaker complexation of the lighter lanthanides by acetate, particularily at the higher pH values.

Downloaded by NORTH CAROLINA STATE UNIV on August 9, 2012 | http://pubs.acs.org
Publication Date: June 9, 2006 | doi: 10.1021/bk-2006-0933.ch016

The data indicate that a Cyanex-301 flowsheet can be developed which will efficiently separate the lanthanides from Am and Cm. The use of an acetic acid scrub will increase the separation of actinides from the lanthanides. The primary issue in developing a large scale process for the separation of Am and Cm from dissolved spent LWR fuel is the stability of the Cyanex-301 extractant, bis(2,4,4-trimethylpentyl)dithiophosphinic acid. The extractant is known to oxidize and decompose in the presence of acid, with the resulting by-products diminishing the selectivity of the solvent *(2)*. A method for removal of these degradation products is needed in order to develop a viable large scale Cyanex-301 process.

Downloaded by NORTH CAROLINA STATE UNIV on August 9, 2012 | http://pubs.acs.org
Publication Date: June 9, 2006 | doi: 10.1021/bk-2006-0933.ch016

Acknowledgments

The authors wish to acknowledge the assistance of George F. Vandegrift and Lætitia H. Delmau during the performance of this work. In addition, the authors would like to thank William F. Bauer and Byron M. White for providing excellent analytical support. This work was performed for the U.S. Department of Energy under Contract No. DE-AC07-99ID13727.

References

1. Swanson, J. L., Pierra, C., and Vandegrift, G. F., "Preliminary Evaluation of Solvent-Extraction and/or Ion-Exchange Process for Meeting AAA Program Multi-Tier Systems Recovery and Purification Goals," Argonne National Laboratory Report ANL-02/29, May 30, 2002.
2. Modolo, G. and Odoj, R. *J. Rad. Nucl. Chem.* **1998**, *228*, 83-88.
3. Hill, C., Madic, C., Baron, P. Ozawa, M. Tanaka, Y. *J. Alloys Comp.* **1998**, *271-273*, 159-162.
4. Zhu, Y., Chen, J. Jiao, R. *Solvent Extr. Ion Exch,* **1996**, *14(1),* 61-68.
5. Chen, J., Zhu, Y., Jiao, R. *Sep. Sci. & Technol.* **1996**, *31(19)*, 2723-2731
6. Vandegrift, G. F., et.al., "Lab-Scale Demonstration of the UREX+ Process," *Proceedings from Waste Management 2004*, Tucson, AZ, April 2004.

Downloaded by PENNSYLVANIA STATE UNIV on August 10, 2012 | http://pubs.acs.org
Publication Date: June 9, 2006 | doi: 10.1021/bk-2006-0933.ch017

Chapter 17

Extraction Separation of Am(III) and Eu(III) with TPEN Isomers and Decanoic Acid

T. Matsumura[1] and K. Takeshita[2,*]

[1]**Department of Materials Science, Japan Atomic Energy Research Institute, Tokai-mura 319–1195, Japan**
[2]**Chemical Resources Laboratory, Tokyo Institute of Technology, Yokohama 226–8503, Japan**

TPEN isomers with different positions of nitrogen donors in pyridyl groups, t2pen, t3pen and t4pen, were synthesized and the extraction separation of Am(III) and Eu(III) with these ligands and a fatty acid, decanoic acid, was investigated. All isomers were similar in the complexation in the aqueous phase, such as the protonation and the complex formation of Eu, however, the extraction behavior of Am and Eu was quite different. The synergistic extraction effect for Am was observed for t2pen and the high separation factor of about 100 was measured under the condition that the initial molar ratio of t2pen to decanoic acid in the organic phase is kept at 1:2. The value is comparable to that for the extraction system with BTP. On the other hand, the extractability of other isomers, t3pen and t4pen, was very low and no separation of Am and Eu was observed. Only t2pen, in which nitrogen donors in four pyridyl groups are positioned in the vicinity of the skeletal structure (N-C-C-N structure), is available for the extraction separation of Am.

In Separations for the Nuclear Fuel Cycle in the 21st Century; Lumetta, G., et al.;
ACS Symposium Series; American Chemical Society: Washington, DC, 2006.

Introduction

Transmutation is recently noted as an advanced fuel-cycle technology, in which long-lived radioactive nuclides are converted to short-lived ones by a fast reactor or an accelerator with high energy neutrons. By introducing the transmutation technology into the HLW (high level radioactive wastes) treatment process, the quantity of radioactive wastes requiring geologic disposal is decreased to about one-fifth that without transmutation and the radioactivity of wastes is attenuated faster. The increase of environmental risk by geologic disposal of nuclear wastes can be suppressed considerably. About 50 kg HLW is present in 1 ton spent nuclear fuel and the weight fraction of minor actinides (MA) is evaluated as only 2% in the HLW. However, the minor actinides contain many long-lived nuclides such as ^{241}Am ($t_{1/2}$=433 yr), ^{243}Am ($t_{1/2}$=7000 yr), ^{245}Cm ($t_{1/2}$=8500 yr) and ^{246}Cm ($t_{1/2}$=4730 yr). Therefore, the development of a separation process of MA, especially trivalent actinides (An(III)) such as Am and Cm, from HLW is indispensable to success of transmutation technology.

Lanthanides (Ln(III)), which corresponds to up to 30 times the total amount of actinides, are present in HLW.[1] These nuclides adversely affect the efficiency of the transmutation of actinides, because of large neutron absorption cross-sections. The separation of An(III) from Ln(III) is one of the important needs in successfully establishing the transmutation technology. One approach for the separation of An(III) is to develop soft-donor extractants, with which the softer An(III) is coordinated in preference to Ln(III). In the EU, U.S.A. and Japan, many soft-donor extractants with nitrogen donors have been developed for the extraction separation of An(III).[2] Since these extractants consist of carbon, hydrogen, oxygen and nitrogen, no secondary waste is generated by the combustion of spent extractants.[3] One successful example is 2,6-di(5,6-dipropyl-1,2,4-triazin-3-yl)-pyridine (BTP) and its analogues which have high selectivity between Am and Ln(III) without any co-extractant.[4] However, the chemical instability of BTP and its analogues is still a matter of concern.

Jensen et al. reported that N,N,N',N'-tetrakis(2-methylpyridyl)ethylenediamine (t2pen)* forms preferentially complexes with Am rather than Eu in the aqueous solution and the stability constant for the formation of Am-t2pen complex corresponds to 100-fold that of Eu-t2pen complex.[5] This compound is a podand-type ligand with six nitrogen donors and encapsulates a metal ion. The authors found that Am was extracted selectively from the aqueous phase containing Eu by using t2pen diluted with nitrobenzene as an organic phase.[6] Then, the separation factor of Am was evaluated as 80 at the maximum. Next,

---

* This compound is called generally "TPEN", however, is abbreviated as t2pen in this study, because of the distinction from other TPEN isomers.

Downloaded by PENNSYLVANIA STATE UNIV on August 10, 2012 | http://pubs.acs.org
Publication Date: June 9, 2006 | doi: 10.1021/bk-2006-0933.ch017

Downloaded by PENNSYLVANIA STATE UNIV on August 10, 2012 | http://pubs.acs.org
Publication Date: June 9, 2006 | doi: 10.1021/bk-2006-0933.ch017

we explored a more preferable solvent with low toxicity and high solubility to t2pen. Recently, a synergistic extraction of Am with t2pen and D2EHPA (di(2-ethylhexyl)phosphoric acid) diluted with 1-octanol was tested.[7] Am was extracted selectively from Eu and the maximum separation factor of Am was 100, which corresponds to the ratio of stability constant of t2pen-Am complex to that of t2pen-Eu complex in the aqueous phase.[7]

However, from the viewpoint of the establishment of waste-free process, the use of D2EHPA containing phosphorus is not preferable. In this study, a higher fatty acid, decanoic acid, is used instead of D2EHPA. Furthermore, TPEN isomers with different positions of nitrogen donors in the pyridyl groups, t2pen (TPEN), t3pen and t4pen, are synthesized and the extraction separation of Am and Eu by a synergistic extraction system with these ligands and decanoic acid diluted with 1-octanol is investigated. The chemical structures of TPEN isomers are shown in Fig.1. Firstly, the protonation of TPEN isomers and the complexation of TPEN isomers and Eu in the aqueous phase is evaluated quantitatively by potentiometric titration. Then, Eu is used as a substitute of Am. Next, the extraction of the metal-TPEN isomer complex with decanoic acid is examined and the stoichiometric relation for the extraction reaction is evaluated by slope analysis technique. From these results, the applicability of the synergistic extraction with TPEN isomers and decanoic acid to the separation process of An(III) and Ln(III) is discussed.

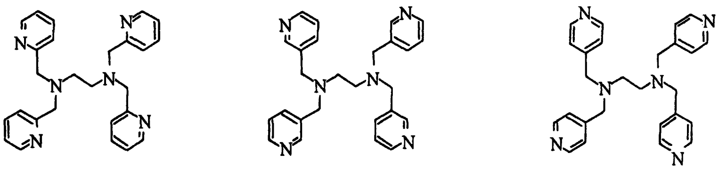

N,N,N',N'-tetrakis-
(2-pyridylmethyl)ethylenediamine
(t2pen)

N,N,N',N'-tetrakis-
(3-pyridylmethyl)ethylenediamine
(t3pen)

N,N,N',N'-tetrakis-
(4-pyridylmethyl)ethylenediamine
(t4pen)

Figure 1. Chemical structure of TPEN isomers.

Experimental

Chemicals

Main reagents used for the synthesis of TPEN isomers and the extraction tests, 1-octanol, decanoic acid, ethylenediamine, 2-(chloromethyl)pyridine hydrochloride, 3-(chloromethyl)pyridine hydrochloride and 4-(chloromethyl)-pyridine hydrochloride, were purchased from Wako Pure Chemical Industeries

Ltd. and used without further purification. Other chemicals were reagent grade. The radiotracers supplied by FRAMATOME, ^{241}Am (800 kBq in 1mL 1M HNO_3) and ^{152}Eu (3.0MBq in 5mL 1M HCl), were dried under an infrared lamp and diluted by 10^{-3} M HNO_3. The radioactivities of ^{241}Am and ^{152}Eu in the stock solutions were 200 and 1250 kBq/mL, respectively.

Downloaded by PENNSYLVANIA STATE UNIV on August 10, 2012 | http://pubs.acs.org
Publication Date: June 9, 2006 | doi: 10.1021/bk-2006-0933.ch017

Synthesis of TPEN isomers

A TPEN isomer, t2pen, was synthesized as reported previously.[8, 9] 2-(chloromethyl)pyridine hydrochloride (6.56g, 0.040 mol.) was dissolved in 5.0 mL of water and the resulting solution was neutralized by adding 7.4 mL of 5.4 mol/L NaOH solution. Ethylenediamine (0.67 mL, 0.010 mol.) was added dropwise in the solution. The pH value was kept in the range of 8.0 ± 0.1 by a pH-stat (COMTITE-900, Hiranuma Ltd.) using 1 mol/L NaOH solution. The reaction mixture was stirred at room temperature (25±0.1°C) for 4 days. The white precipitate formed in the mixture was filtered off, washed with pure water and dried in vacuo for 1 day. The dried precipitate was analyzed by FT-IR (SPECTRUM2000, PerkinElmer, Inc.), elemental analysis (EA1110CHN, CE Instruments Ltd.) and mass spectroscopy (ZQ2000, Waters Co. Ltd.). It was ascertained that the precipitate obtained was t2pen. In the FT-IR spectrum, the stretching vibrations of pyridine rings were observed in the range of 1400 to 1600 cm^{-1}. The results of elemental analysis were as follows; C: H: N = 73.4 (73.6): 6.31 (6.60): 20.0 (19.8), where the numbers in parenthesis denote the weight ratio of carbon, hydrogen and nitrogen calculated from the chemical formula of t2pen, $C_{26}H_{28}N_6$. In the mass spectrum, two peaks of $[H(t2pen)]^+$ and $[Na(t2pen)]^+$ were observed at the mass numbers of 425 and 447, respectively. Then, sodium ion in $[Na(t2pen)]^+$ came from NaOH added for the neutralization of 2-(chloromethyl)pyridine. The yield of t2pen was 30%.

Synthesis methods of other TPEN isomers, t3pen and t4pen, are analogous to TPEN. 3-(chloromethyl)pyridine hydrochloride or 4-(chloromethyl)pyridine hydrochloride (6.56g, 0.040 mol.) was dissolved in 5.0 mL of water and the solution obtained was neutralized by the NaOH solution. Ethylenediamine (0.67 mL, 0.010 mol.) was added dropwise in the solution. The pH value was kept in the range of 10.0 ± 0.1 by the pH-stat. The reaction mixtures were stirred at room temperature for 3 weeks for t3pen and 2 weeks for t4pen, respectively. The t3pen was extracted from the reaction mixture by diethyl ether. After removal of the diethyl ether with a rotary evaporator, a yellow oily residue was obtained. The residue was refined by recrystallization from mixed solvent of acetone and hexane. Finally, a white precipitate of the desired agent was formed, filtered off, washed with hexane, and dried in vacuo. The t4pen was extracted from the reaction mixture by diethyl ether and was chromatographed over silica gel column. The final residue was yellow oily agent. These synthesized compounds were also analyzed by FT-IR, elemental analysis and mass spectroscopy and were identified as t3pen and t4pen. In the FT-IR spectra of these compounds, the stretching vibrations of pyridine rings were observed in the range of 1400 to 1600cm^{-1}. The results of elemental analysis were as follows; C: H: N= 73.4: 6.88: 19.5 for t3pen and C: H: N= 74.0: 6.69: 19.3 for t4pen. These values are similar to the theoretical ones calculated from the chemical fomula of t3pen and t4pen, C: H: N = 73.6: 6.60: 19.8. The mass spectra of t3pen and t4pen were shown in Figure 2. Two typical peaks at 425 and 447 were observed. These results indicate the presence of tpen isomers with H^+ and Na^+. The yields of t3pen and t4pen were 5% and 12%, respectively.

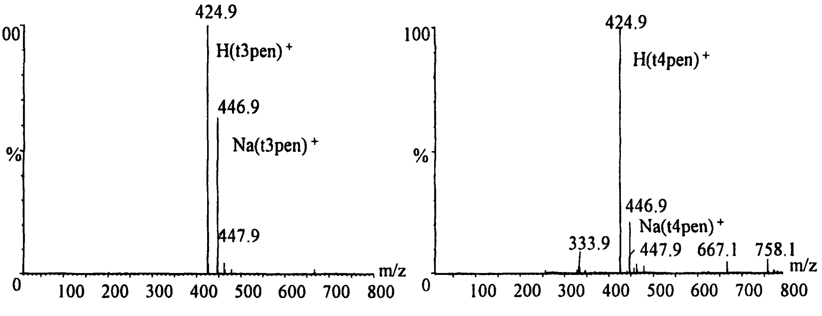

(a) t3pen (b) t4pen

Figure 2. Mass spectra of t3pen and t4pen.

Evaluation of complexation of TPEN isomers in aqueous solution

The complexation of TPEN isomers in aqueous solution, such as the protonation of TPEN isomers and the complex formation of TPEN isomers with Eu(III) were measured by the potentiomeric titration technique. Aqueous solutions with 8.9×10^{-4} mol/L TPEN isomers were prepared for the evaluation of protonation. The ionic strength and initial pH were adjusted to 0.1 and 2.0, respectively, by adding HNO_3 and $NaNO_3$. Titration data were measured by adding dropwise a mixture of 0.02 M NaOH and 0.09 M $NaNO_3$ as a titrant in the aqueous solutions by an automatic titrator (COM980Win Hiranuma). Titration curve can be calculated by solving simultaneously the mass balance of TPEN isomer and the charge balance in the aqueous solution.[10] The protonation constants of TPEN isomers were determined by fitting the calculated titration curve to the experimental data. The complexation of TPEN isomers with Eu(III) can be also evaluated by the potentiometric titration technique. Aqueous solutions with 8.9×10^{-4} mol/L $Eu(NO_3)_3$ and TPEN isomers in amounts equimolar with Eu(III) were prepared. The formation constant for Eu-TPEN isomer complex was determined by the same manner as the measurement of protonation constants.

Downloaded by PENNSYLVANIA STATE UNIV on August 10, 2012 | http://pubs.acs.org
Publication Date: June 9, 2006 | doi: 10.1021/bk-2006-0933.ch017

Downloaded by PENNSYLVANIA STATE UNIV on August 10, 2012 | http://pubs.acs.org
Publication Date: June 9, 2006 | doi: 10.1021/bk-2006-0933.ch017

Extraction Tests of Am(III) and Eu(III)

Mixtures of TPEN isomers and decanoic acid diluted with 1-octanol were prepared as the organic phase. Each 2.5 mL of 0.1 M NH_4NO_3 aqueous solution and organic solution was placed in a glass centrifugal tube with stopper and shaken for 15 minutes at room temperature (25±0.1°C). The mixture was centrifuged for 5 minutes at 2500 rpm. The pH of the aqueous phase was measured by a pH meter (F-23, Horiba) and adjusted to aimed pH value by ammonia and nitric acid. The procedure was repeated until the pH of the aqueous phase attained equilibrium with the organic phase. After the pre-equilibrium of pH, each 2 μL of ^{241}Am and ^{152}Eu stock solutions was added and the tube was shaken vigorously for 15 minutes. The resulting mixture was then centrifuged for 5 minutes at 2500 rpm. After centrifuging, each 2 mL of aqueous and organic phases was sampled and the radioactivities of ^{241}Am and ^{152}Eu were analyzed with a high-purity germanium gamma-spectrometer system (EG&G Ortec). The energy lines at 59.54 keV and 121.78 keV were used for evaluating the concentrations of ^{241}Am and ^{152}Eu, respectively. Care was taken during measurements to ensure that net counts were at least 10000 counts in order to maintain the statistical error of individual measurements in the order of 1 %. From these results, the concentrations of Am(III) and Eu(III) in the organic phase and the aqueous phase were determined. The distribution ratio and the separation factor of Am, defined as D=[metal concentration in organic phase]/[metal concentration in aqueous phase] and $SF_{Am/Eu}=D_{Am}/D_{Eu}$, respectively, were calculated from the concentrations of Am and Eu in the aqueous and organic phases.

Results and Discussion

Complexation of TPEN isomers in aqueous solution

Information on the complexation of TPEN isomers in aqueous solution, namely the protonation of TPEN isomers and the complex formation of metal and TPEN isomers, is very useful for the analysis of extraction mechanisms. The formation constants of these complexes with TPEN isomers were evaluated quantitatively by UV and potentiometric titration methods. Figure 3 shows the titration curve for an aqueous solution containing a TPEN isomer, t4pen. Two equivalent points were observed in the titration curve. These results indicate that following four-steps of protonation reactions,

$$\mathrm{H(t4pen)^+ \leftrightarrows H^+ + t4pen} \qquad K_1 \qquad (1)$$

$$\mathrm{H_2(t4pen)^{2+} \leftrightarrows H^+ + H(t4pen)^+} \qquad K_2 \qquad (2)$$

Downloaded by PENNSYLVANIA STATE UNIV on August 10, 2012 | http://pubs.acs.org
Publication Date: June 9, 2006 | doi: 10.1021/bk-2006-0933.ch017

$$H_3(t4pen)^{3+} \leftrightarrows H^+ + H_2(t4pen)^{2+} \qquad K_3 \qquad (3)$$

$$H_4(t4pen)^{4+} \leftrightarrows H^+ + H_3(t4pen)^{3+} \qquad K_4 \qquad (4)$$

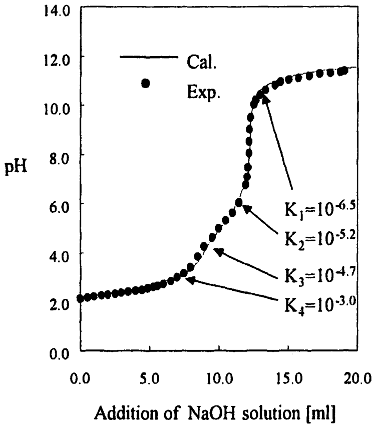

Figure 3. Titration curve for aqueous solution of t4pen.

where K_1, K_2, K_3 and K_4 denote the dissociation constants of protonated t4pen molecules, $H(t4pen)^+$, $H_2(t4pen)^{2+}$, $H_3(t4pen)^{3+}$ and $H_4(t4pen)^{4+}$, respectively. The similar titration curves were obtained for t2pen and t3pen. As shown in the previous paper[10], a titration curve can be calculated by solving simultaneously both the mass balance of t4pen and the charge balance. Then, these dissociation constants can be determined successfully by fitting the calculated titration curve to the experimental data. The appropriate dissociation constants for t2pen, t3pen and t4pen, which were determined under the experimental conditions of 25°C and the ionic strength of 0.1, were summarized in Table 1. These values are comparable to those for t2pen measured by Jensen.[5] These results indicate that the protonation of TPEN isomers is little affected by the position of nitrogen donors in the pyridyl groups of TPEN isomers.

Table I. Comparison of dissociation constants.

	pK_1	pK_2	pK_3	pK_4
t2pen	7.2	4.8	3.3	3.0
t3pen	6.2	5.2	4.2	3.8
t4pen	6.5	5.2	4.7	3.0

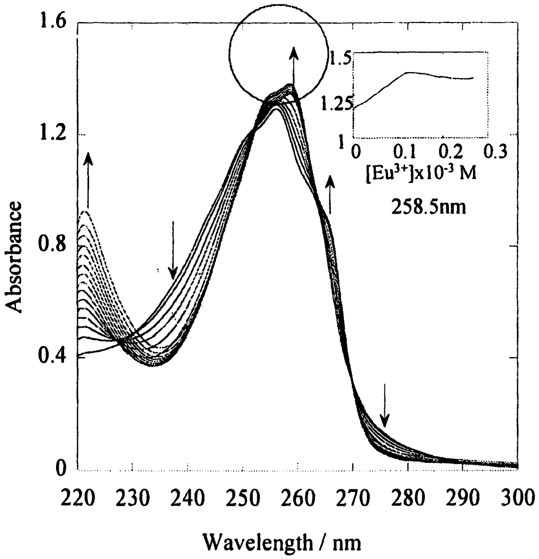

Figure 4. Results of UV titration. Aqueous solution containing 1x10^{-4} M t2pen was titrated with that containing 1x10^{-5} M Eu.

Next, the complex formation of Eu and TPEN isomers is discussed. Figure 4 shows the results of UV titration for t2pen.[7] Then, the aqueous solution dissolving 1x10^{-4} M t2pen was titrated with an aqueous solution with 1x10^{-5} M Eu. The peak at 260 nm is assigned as t2pen-Eu complex. The small figure in Fig.3 shows the change of peak height with increasing the concentration of Eu. The peak height is increased until the molar ratio of Eu ion to t2pen reaches to 1:1 and after that remained constant. This means that the formation of Eu-t2pen complex can be described as a 1:1 complex,

$$\mathrm{Eu^{3+} + t2pen \leftrightarrows Eu(t2pen)^{3+}} \qquad (5)$$

The same results were also observed for other TPEN isomers. The formation constants of complexes with Eu and TPEN isomers can be determined by the potentiometric titration method. Figure 5 shows the results of potentiometric titration tests for t4pen. All protonation constants, K_1 to K_4, have been already determined and the equilibrium constants for hydrolysis and nitrato complex formation of Eu were given previously.[11] Titration curves were calculated from the mass balance of TPEN isomer and the charge balance in the aqueous solution. The solid lines show the calculated titration curves. When the complex formation is given as 10^4, the calculated titration curve is well agreed with the experimental data in the acidic pH range. The same titration curves were obtained for t2pen and t3pen. The Eu complex formation of these isomers can be evaluated as about 10^4. The tpen isomers show similar behavior for the complex

Downloaded by PENNSYLVANIA STATE UNIV on August 10, 2012 | http://pubs.acs.org
Publication Date: June 9, 2006 | doi: 10.1021/bk-2006-0933.ch017

formation with Eu. It should be noted that the formation constant obtained is similar to that for La-t2pen complex measured by Jensen, $K_{La\text{-}t2pen} = 10^{3.5}$ [5]

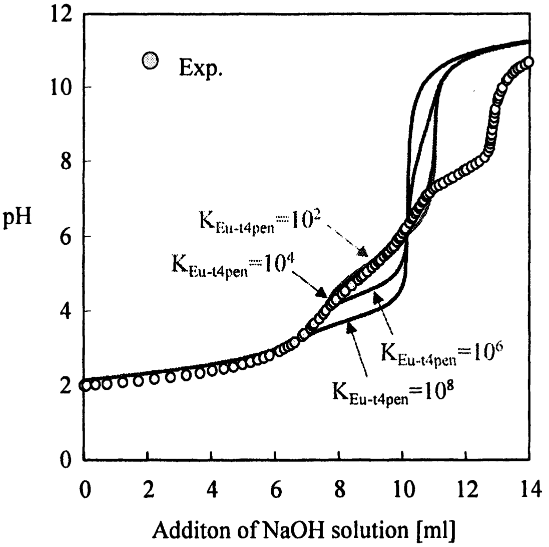

Figure 5. Titration curve for aqueous solution with t4pen and Eu.

Synergistic Extraction of Am with decanoic acid and TPEN isomers

The synergistic extraction of Am with decanoic acid (main extractant) and TPEN isomers (synergist) was studied. Generally, a fatty acid, decanoic acid, is not useful for the metal extraction, because of low extractability. In this synergistic system, decanoic acid plays a role as a hydrophobic anion to receive the metal-TPEN complex from the aqueous phase. The initial concentrations of Am and Eu were very small (the order of 10^{-8} mol/L). TPEN isomers that corresponded to 10^5 times those of Am and Eu, were added in the organic phase. In this condition, it should be noted that most of Am and Eu forms complexes with TPEN isomers.

Figure 6 shows the comparison of distribution ratios between Am and Eu for t2pen, t3pen and t4pen. Only t2pen showed higher extractability and selectivity of Am. The maximum separation factor of Am was evaluated as about 70. However, the other TPEN isomers, t3pen and t4pen, showed low extractability of Am and no separation of Am and Eu. Especially, the extractability of t4pen was very weak and similar to that for the direct extraction of decanoic acid (solid line in Fig.6(c)). These results suggest that the position of nitrogen donor in the pyridyl group is very important for the extraction

Downloaded by PENNSYLVANIA STATE UNIV on August 10, 2012 | http://pubs.acs.org
Publication Date: June 9, 2006 | doi: 10.1021/bk-2006-0933.ch017

separation of Am. The nitrogen donors in the pyridyl groups should be positioned in the vicinity of the skeletal structure of ligand (N-C-C-N structure).

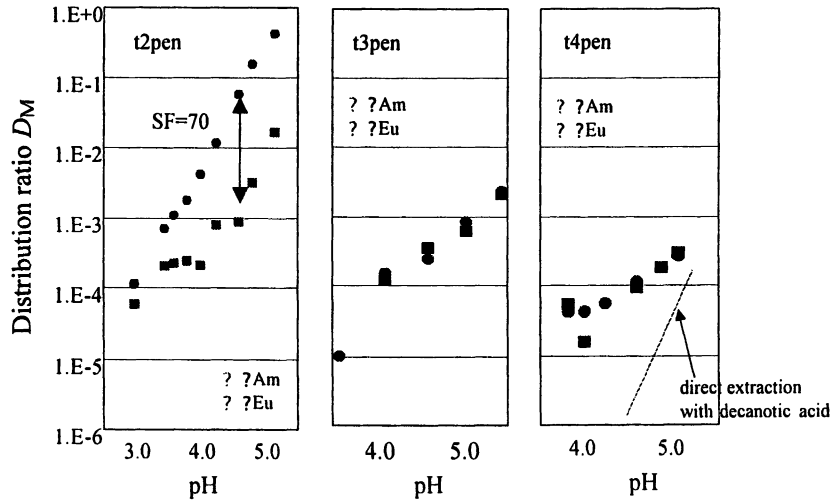

(a) t2pen (b) t3pen (c) t4pen

Figure 6. Comparison of distribution ratios between Am and Eu for TPEN isomers.

Figure 7 shows the comparison of extractability of TPEN isomers. As seen in the extraction system with t2pen, the slope for the extraction of Am is given as about 2. These results indicate that two decanoic acid molecules are coordinated with an Am-t2pen complex. The stoichiometric relation for the extraction of Am is represented apparently as follows,

$$Am^{3+} + t2pen + 2HR \leftrightharpoons Am(t2pen)R_2^{+} + 2H^{+} \qquad (6)$$

Then, the coordination of one nitrate ion to $Am(t2pen)R_2^{+}$ is required for the neutralization of complex. Am(III) may be extracted as $Am(t2pen)R_2(NO_3)$. However, the extraction mechanism should be discussed carefully. The dissolution of t2pen to the aqueous phases, the protonation of t2pen and the formation Am-t2pen complex in the aqueous phase has to be considered for the evaluation of extraction mechanism.

On the other hand, the distribution ratios for the extraction systems with t3pen and t4pen were very low and the slopes were evaluated as less than 1. This may be because the complexation of Am with t3pen and t4pen in the aqueous phase is weaker than that with t2pen. The formation constants of Am-t3pen and Am-t4pen complexes should be measured. From these results, the

Downloaded by PENNSYLVANIA STATE UNIV on August 10, 2012 | http://pubs.acs.org
Publication Date: June 9, 2006 | doi: 10.1021/bk-2006-0933.ch017

Downloaded by PENNSYLVANIA STATE UNIV on August 10, 2012 | http://pubs.acs.org
Publication Date: June 9, 2006 | doi: 10.1021/bk-2006-0933.ch017

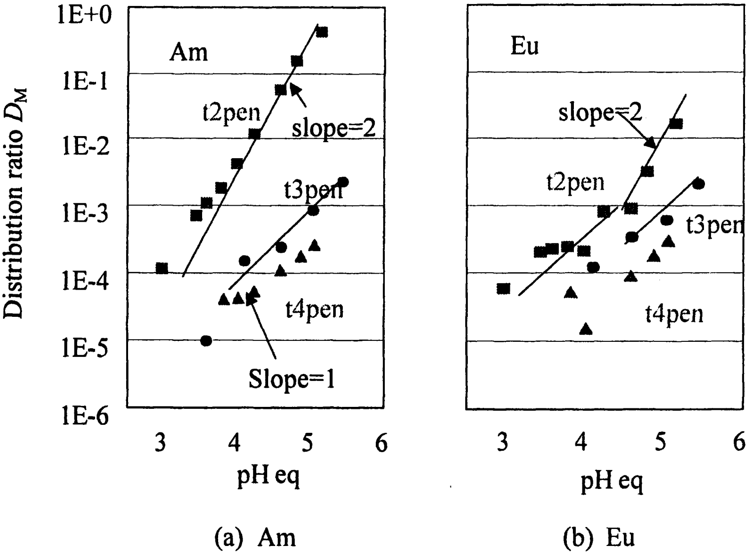

Figure 7. Comparison of slopes between log D and pH.

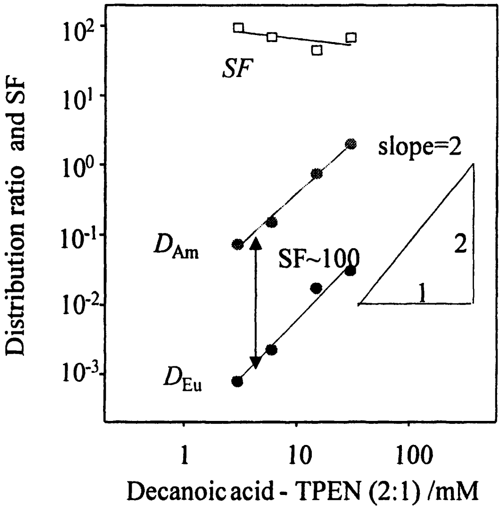

Figure 8. Change in the distribution ratios (D_{Am} and D_{Eu}) and separation factor of Am (SF) with the concentration of decanoic acid.

relation between the extractability of Am and the position of nitirogen donor in the pyridyl group will be clarified. The results of Fig.7 suggest that the molar ratio of decanoic acid and t2pen should be kept at 2:1 for the synergistic extraction of Am. Figure 8 shows the change in the separation factors of Am with the concentration of decanoic acid under the condition that the initial molar ratio of decanoic acid to t2pen is kept at 2:1. The high separation factor of about 100 was observed in the wide concentration range of decanoic acid. This value is comparable to that for the extraction system with BTP.

Downloaded by PENNSYLVANIA STATE UNIV on August 10, 2012 | http://pubs.acs.org
Publication Date: June 9, 2006 | doi: 10.1021/bk-2006-0933.ch017

Conclusions

(1) TPEN isomers, t2pen, t3pen and t4pen, show similar behavior for the complexation in the aqueous phase, such as the protonation of these isomers and the complex formation with Eu.

(2) The extraction separation of Am over Eu is affected strongly by the position of nitrogen donors in pyridyl groups. The high extractability and selectivity of Am are observed only for t2pen, in which the nitrogen donors are positioned in the vicinity of skeletal structure (N-C-C-N structure).

(3) Am forms a complex with t2pen, $Am(t2pen)^{3+}$, in the aqueous phase and is extracted to the organic phase by the coordination of two decanoic acid molecules. When the molar ratio of deanoic acid to t2pen in the organic phase is kept at 2:1, the high separation factor of about 100 is observed. This value is comparable to that for the extraction system with BTP. The synergistic extraction system with t2pen and decanoic acid is applicable for the group separation of trivalent actinides from lanthanides.

Acknowledgement

The authors are grateful to Prof. Kenneth L. Nash, Washington State University, for valuable discussions on the synthesis and complexation of TPEN isomers.

References

1 Ando, Y., Takano, H., Estimation of LWR Spent Fuel Composition, JAERI-Research 99-004(1999)

2 Karmazin, L.; Mazzanti, M.; Gateau, C., Hill, C., and Pécaut, J. The Important Effect of Ligand Architecture on the Selectivity of Metal Ion

Recognition in An(III)/Ln(III) Separation with N-donor Extractants. *Chem. Commun.*, **2002**, 2892-2893

3 Musikas, C. Completely Incinerable Extractants for the Nuclear Industry – A Review. *Min. Pro. Ext. Met. Rev.*, **1997**, 17, 109-142.

4 Kolarik, Z.; Mullich, U. and Grassner F. Selective Extraction of Am(III) over Eu(III) by 2,6-Ditriazolyl- and 2,6-Ditriazinylpyridines. *Solv. Extr. Ion Exch.*, **1999**, 17, 23-32.

5 Jensen, M. P.; Morss, L. R.; Beitz, J. V.; Ensor, D. D. Aqueous Complexation of Trivalent Lanthanide and Actinide Cations by N,N,N',N'-Tetrakis(2-pyridylmethyl)ethylenediamine. *J. Alloys. Comp.*, **2000**, 303-304, 137-141.

6 Watanabe. M., Mirvaliev R., Tachimori, S., Takeshita, K., Nakano, Y., Morikawa, K., Mori, R., Separation of Americium(III) from lanthanide by Encapsulating Hexadentate-ligand. *Chem. Lett.,* **2002**, 31, 1230-1231.

7 Watanabe, M., Mirvaliev, R., Tachimori, S., Takeshita, K., Nakano, Y., Morikawa, K., Chikazawa, T., Mori, R.. Sective Extraction of Americium(III) over Macroscopic Concentration of Lanthanides(III) by Synergistic System of TPEN and D2EHPA in 1-Octanol, *Solv. Extr. Ion Exch.,* **2004**, 22, 377-390; Mirvaliev, R., Watanabe, M., Matsumura, T., Tachimori, S., Takeshita, K., Selective Separation of Am(III) from Ln(III) with a Novel Synergistic Extraction System, N, N, N', N'-tetrakis(2-methylpyridyl)ethylenediamine (TPEN) and Decanoic Acid in 1-Octanol. *J. Nucl. Sci. Technol.,* , **2004**, 41, 1122-1124.

8 Chang, H. -R.; McCusker, J. K.; Toftlund, H.; Wilson, S. R.; Trautwein, A. X.; Winker, H. D.; Hendrickson, N., [Tetrakis(2-pyridylmethyl)ethylenediamine]iron(II) Perchlorate, the First Rapidly Interconverting Ferrous Spin-crossover Complex. *J. Am. Chem. Soc.* **1990**, 112, 6814-6827.

9 Morss, L. R.; Rogers, R. D., Synthesis and Crystal Structures of $[M(NO_3)_2(tpen)][NO_3]\cdot 3H_2O$ (M=La, Tb), Rare Earth Complexes with Strong M-N Bonds. *Inorg. Chim. Acta,* **1997**, 255, 193-197.

10 Takeshita, K., K.Watanabe, Y.Nakano and M.Watanabe, Solvent extraction separation of Cd(II) and Zn(II) with the organophosphorus extractant D2EHPA and the aqueous nitrogen-donor ligand TPEN, *Hydrometallurgy*, **2003**, 70 , 63-71

11 Martell, A. E.; Smith, R. M., Critical stability constants; Plenum Press, New York 1989.

Downloaded by PENNSYLVANIA STATE UNIV on August 10, 2012 | http://pubs.acs.org
Publication Date: June 9, 2006 | doi: 10.1021/bk-2006-0933.ch017

Downloaded by COLUMBIA UNIV on August 9, 2012 | http://pubs.acs.org
Publication Date: June 9, 2006 | doi: 10.1021/bk-2006-0933.ch018

Chapter 18

The Influence of Simple Organic Ligands on the Partitioning Mechanism of Trivalent Lanthanum to Goethite

Sarah E. Pepper[1], Brienne N. Bottenus[1], Larry C. Hull[1,2], Carrie G. Shepler[1], and Sue B. Clark[1]

[1]Department of Chemistry, Washington State University, Pullman, WA 99164–4630
[2]On sabbatical from: Idaho National Laboratory, Idaho Falls, ID 83415

The sorption of trivalent lanthanum (La^{3+}) by goethite was investigated in the absence and presence of gluconate as a function of metal concentration and ionic strength at two pH values. A single site Langmuir model was fit to the data. Surface complexation appears to be responsible for the removal of La^{3+} from solution in the absence of gluconate. In the presence of gluconate, La^{3+} dominates the sorption at low concentrations. As the gluconate concentration is increased, the La-gluconate complexes, $La(GH_4)^{2+}$ and $La(GH_3)^{+}$ begin to dominate the aqueous speciation of La. These species are believed to be responsible for the adsorption of La^{3+} from solution at higher gluconate concentrations. At pH 7, the number of surface sorption sites appears to increase by a factor of two in the presence of gluconate, compared to pH 5.5, possibly through the formation of ternary surface complexes between the metal:ligand complex and La adsorbed to the goethite surface. Ionic strength appears to have little effect on the sorption of La^{3+} regardless of the presence or absence of gluconate.

In Separations for the Nuclear Fuel Cycle in the 21st Century; Lumetta, G., et al.;
ACS Symposium Series; American Chemical Society: Washington, DC, 2006.

Introduction

The sorption of metal ions from aqueous solution has received considerable attention over the last few decades. Fission products and actinides are of particular concern since the longevity of many of these species can pose risks to humans and ecological health for many years. Hence, removal prior to disposal or limiting their mobility in the environment can be advantageous.

Iron oxides, hydroxides and oxyhydroxides (termed iron oxides for convenience) are widespread in nature. One of the main characteristics of all iron oxides is that they have large surface areas that can influence the chemistry of a system. In many cases, iron oxides are responsible for regulating the concentration and distribution of pollutants. It is, therefore, essential that they be considered in descriptions of the distribution of contaminants in the near-surface environment (*1*). Goethite is one of the most abundant iron oxides in nature and has been shown to adsorb trace metals more strongly than most other adsorbents (*2*). In particular, goethite, along with humic acid and clay minerals, is one of the most important sinks for exogenous rare earth elements (*3*).

The polyhydroxycarboxylate anion, gluconate ($CH_2OH(CHOH)_4COO^-$), has been shown to form stable complexes with radionuclides and other metal cations such as the lanthanides (*4-9*). The structure and composition of the complexes depend on a number of experimental conditions, including pH, concentration of gluconate and the ratio of lanthanide to acid (*10-15*). Over the pH range 3 to 10, ^{13}C NMR suggests that a 1:1 complex forms in solution between the gluconate anion and La (*16*).

Gluconic acid is a close structural analogue for α-isosaccharinic acid (ISA), (*5*) an important cellulose degradation product found in nuclear fuel repositories. Little is reported on the effect of gluconate on the sorption of trivalent f-elements by goethite. In the present study, a batch methodology was therefore employed to explore La partitioning in the absence and in the presence of the gluconate anion as a function of metal concentration and ionic strength at two pH values. Powder X-ray Diffraction (XRD), Scanning Electron Microscopy (SEM) and Energy Dispersive X-ray (EDAX) Spectroscopy were utilized to investigate any changes in the solid during the sorption experiments. As goethite can be assumed to contain a certain number of surface sites (*17*), a single site Langmuir model was fit to the data.

Sorption processes on oxide surfaces

The goethite surface is amphoteric; at low pH values the surface hydroxyl groups tend to protonate and at higher pH values, they are deprotonated. This leads to a variability of charge at the mineral surface (*18*). The point of zero charge (PZC) is the pH value at which the surface is neutrally charged; below

Downloaded by COLUMBIA UNIV on August 9, 2012 | http://pubs.acs.org
Publication Date: June 9, 2006 | doi: 10.1021/bk-2006-0933.ch018

this value, the surface will be predominantly positively charged, whereas above this value, the surface will be negatively charged (*17*). In the case of goethite, the PZC is reported in the region of 7.80 to 8.90 (*19-20,* respectively).

The uptake of metals by a goethite surface is generally considered to involve one of two types of sorption; surface complexation or surface precipitation. Surface complexation involves metal cation coordination with surface oxygen atoms and is usually accompanied by the release of protons. There are two types of surface complexation, inner sphere and outer sphere. Inner sphere complexation involves direct coordination between the metal and the surface. Outer sphere complexation involves the adsorbates retaining some or all of their solvating water molecules. Surface precipitation involves the formation of a multilayer phase on the oxide surface (*17*). At high sorbate/sorbent ratios, surface precipitation may participate in the total apparent sorption of cations and anions and may even become the dominant sorption mechanism (*21, 22*).

The presence of ligands in solution may enhance or reduce the sorption of cations to a mineral surface. Enhanced sorption has been suggested to occur via one of three different mechanisms (*23*):

- Surface precipitation
- Cooperative electrostatics
- Ternary surface complexation

In this case, surface precipitation involves the formation of a phase similar to that formed during metal ion uptake, though the phase contains both the metal ion and the ligand (*24*).

The mechanism of cooperative electrostatics involves the sorption of both the metal and the ligand. For example, at pH values above the PZC, metal ion adsorption increases the net surface charge, which in turn favors the sorption of the anionic ligand. Conversely, at pH values below the PZC, the sorption of the ligand lowers the surface charge thus making metal ion adsorption more favorable (*25, 26*).

The formation of a ternary surface complex involves interaction between the metal complex and the surface. As with metal ion surface complexation, two types exist, outer sphere and inner sphere (*27, 28*). Outer sphere complexation arises through the electrostatic interaction between the complex in solution and the surface without displacement of surface water molecules. Inner sphere complexation arises from the formation of bonds between the solution species and the surface with the displacement of surface bound water molecules. Outer sphere and inner sphere complexes have been further categorized according to the position of the ligand and the metal in relation to the surface. In Type A complexes, the metal ion is bound to the surface and the ligand is bound only to the metal and in Type B complexes, the ligand is bound to the surface and the metal is bound to the ligand only (*29, 23*).

Downloaded by COLUMBIA UNIV on August 9, 2012 | http://pubs.acs.org
Publication Date: June 9, 2006 | doi: 10.1021/bk-2006-0933.ch018

Reduction of cation sorption in the presence of ligands occurs when the ligand binds the metal strongly but is poorly sorbed by the surface. Ligands that form strong complexes with metals tend to stabilize the cation in solution thus reducing metal sorption. It is also possible that the ligand will preferentially compete for surface sites, thus reducing the sorption of the cation (*29*).

Experimental

Solid goethite was prepared using a modified version of the method described by Schwertmann and Cornell (*1*). A solution of ferric chloride was hydrolyzed using potassium hydroxide and then heated for 60 hours at 70 °C. After washing the product three times with deionized water, it was freeze-dried. Analysis of the product by powder XRD showed sharp goethite peaks only, with no broadening to indicate the presence of amorphous material and no unidentified peaks to suggest other crystalline material was present.

Suspensions of goethite were prepared by dispersing the mineral in 9 ml of background electrolyte, which were then allowed to hydrate overnight. Background electrolyte concentrations were either 1.0, 0.1 or 0.01 M KNO_3. Samples were prepared in triplicate at each concentration. The reaction was initiated by adding either La^{3+} (prepared from lanthanum chloride) or a 1:1 solution of La^{3+} and gluconate (prepared from sodium gluconate), giving a final solid to solution ratio of 0.1 g to 10 mL (which corresponds to 10 g goethite per L). Previous experiments had shown that the tube walls did not sorb La^{3+}.

A range of metal concentrations, either with or without an equivalent concentration of gluconate, from 10^{-4} to 10^{-2} M were studied. The solution pH was either 5.5 or 7. In all cases, NaOH or HCl (1.0 or 0.1 M) was used to adjust the solution pH. The pH was not controlled during the period of the experiment, but the initial and final pH were monitored. In most cases, the pH deviated by less than 0.5 pH units over the course of the experiment.

The suspensions were placed on a shaker for 24 hours at 20 °C. Early experiments had shown that this period of time was sufficient to allow equilibrium. The supernatant was filtered through a 0.2 μm nylon filter, which had been shown not to sorb La, and analyzed for La and Fe by a Perkin Elmer Optima ICP-OES. Partitioning to the surface was determined by difference from the amount of La observed in the solution.

$$La^{3+} \text{ inital (mole/L)} - La^{3+} \text{ final (mole/L)} = La^{3+} \text{ sorbed (mole/L)}$$

At the conclusion of the experiment, the solid material was washed several times with deionized water and allowed to air dry before analysis by powder XRD and

Downloaded by COLUMBIA UNIV on August 9, 2012 | http://pubs.acs.org
Publication Date: June 9, 2006 | doi: 10.1021/bk-2006-0933.ch018

SEM. This was to verify if any changes had occurred in the crystal structure or morphology of the solid during the course of the experiment.

Results and Discussion

Figure 1 shows the speciation of La^{3+} in the absence and in the presence of gluconate, calculated from the values given in Table I. In the absence of gluconate, the hydrolysis of La^{3+} is not important in solution until above pH 8.5 (Figure 1a). It would, therefore, appear that at the pH values investigated in this study, i.e. 5.5 and 7, that free La^{3+} dominates the system at all concentrations of La. When gluconate complexes to La^{3+} (Figure 1b) the activity of the free La^{3+} is lowered in solution, which raises the pH of hydrolysis to above 9. NMR spectroscopy has suggested that poly-gluconate complexes are not formed in solution under similar reaction conditions to those used in this study (*16*). Therefore, the poly-gluconate species, as reported by Giroux et al. (*9*), have not been considered. It would appear that the La gluconate complexes of $La(GH_4)^{2+}$ and $La(GH_3)^{+}$ are the important complexed species in solution, under the conditions employed in this study.

As the concentration of La and gluconate are increased, the contribution of the La-gluconate complexes increases. At the lower concentrations, La^{3+} dominates the speciation (Figure 2). The curves presented in Figure 2 arise due to the following relationship. For example, the complexation reaction of La^{3+} and gluconate can be described as:

$$La^{3+} + GH_4^{-} \leftrightarrow La(GH_4)^{2+}$$

Gluconate is abbreviated to GH_4^{-}, which represents the four hydrogen ions on the alcohol groups that can be released when the anion coordinates with a metal ion. The equilibrium constant for the above reaction is given by the following expression, where γ represents the activity coefficient:

$$K = \frac{[La(GH_4)^{2+}]\gamma_2}{[La^{3+}]\gamma_3[GH_4^-]\gamma_1}$$

However, under the experimental conditions used in this study, La^{3+} and gluconate are present at a 1:1 mole ratio and therefore at equal concentrations. Consequently at constant ionic strength, the concentration of the complex is proportional to the square of the La concentration multiplied by a constant:

Downloaded by COLUMBIA UNIV on August 9, 2012 | http://pubs.acs.org
Publication Date: June 9, 2006 | doi: 10.1021/bk-2006-0933.ch018

Downloaded by COLUMBIA UNIV on August 9, 2012 | http://pubs.acs.org
Publication Date: June 9, 2006 | doi: 10.1021/bk-2006-0933.ch018

Table I. Equilibrium constants for lanthanum and gluconate used in the aqueous speciation model

Reaction	*Log K @ 25 °C (I = 0)*	*Reference*
$La^{3+} + H_2O = LaOH^{2+} + H^+$	-8.64	30
$La^{3+} + 2H_2O = La(OH)_2^+ + 2H^+$	-18.17	30
$La^{3+} + 3H_2O = La(OH)_{3(aq)} + 3H^+$	-27.91	30
$La^{3+} + 4H_2O = La(OH)_4^- + 4H^+$	-40.81	30
$La^{3+} + 3H_2O = La(OH)_{3(s)} + 3H^+$	-20.29	31
$La^{3+} + 3H_2O = La(OH)_{3(am)} + 3H^+$	-23.49	31
$H^+ + GH_4^- = HGH_4$	3.8	6
$La^{3+} + GH_4^- = LaGH_4^{2+}$	2.6	6
$La^{3+} + GH_4^- = LaGH_3^+ + H^+$	4.0	6
$La^{3+} + GH_4^- = LaGH_2 + 2H^+$	11.3	6

Note: The formation of poly-gluconate complexes, as reported by Giroux et al. (*9*), are not important at the concentrations and metal to ligand ratios considered in this study and therefore have been omitted.

Downloaded by COLUMBIA UNIV on August 9, 2012 | http://pubs.acs.org
Publication Date: June 9, 2006 | doi: 10.1021/bk-2006-0933.ch018

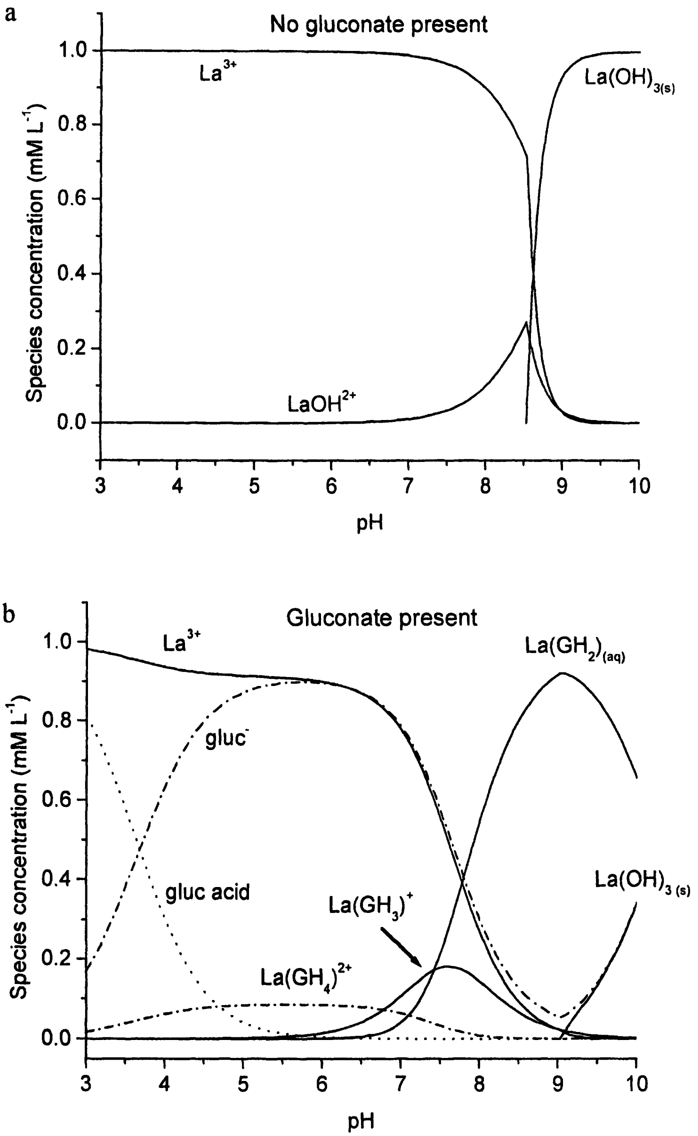

Figure 1: Speciation diagrams for La (a) in the absence of gluconate and (b) in the presence of gluconate, produced from the values given in Table 1. [La^{3+}] = [gluc] = 1 x 10^{-3} M. Species present at very low concentrations have been omitted for clarity, for example La(OH)$_2^+$, La(OH)$_{3\,(aq)}$, and La(OH)$_4^-$.

$$mLa(GH_4)^{2+} \propto (mLa^{3+})^2.[\log K \frac{\gamma_2}{\gamma_1\gamma_3}]$$

The ratio of the complex to free metal in solution is a nonlinear function of the concentration of the metal. Therefore, at the mid concentration range, between 10 and 30% of the La^{3+} is complexed to gluconate and at the higher concentrations investigated, this percentage rises to around 60%.

At the two pH values investigated, as the initial concentration of La^{3+} is increased, the amount of La^{3+} sorbed to the surface also increases (Figure 3). The sorption increases rapidly at first but then generally tends towards a constant value, except for the last data point at pH 7 in the absence of gluconate. At this pH, no constant value appeared to be reached at the highest La^{3+} concentration used in this study. This is discussed in more detail below. With the exception of the last data point at pH 7, this suggests that there is progressive filling of a limited number of sites with the most energetically favorable sites being occupied first (*32*). As described above, hydrolysis does not appear to be an important process in solution and therefore a proposed reaction mechanism that describes the surface complexation of La^{3+} to goethite, where S- represents the mineral surface, is (*3*):

$$\text{S-OH} + La^{3+} \leftrightarrow \text{S-OLa}^{2+} + H^+$$

The presence of gluconate markedly influences the system at pH 7, but it does not seem to have as much of an effect at pH 5.5 (Figure 3). At pH 7, the data suggest that gluconate increases the total amount of La^{3+} sorbed by the goethite surface. This is contrary to other studies that have reported that organic complexants generally enhance lanthanide sorption at low pH but reduce sorption at intermediate to high pH values (*3, 33*). Despite this difference, the overall shape of the uptake curves, at both pH values, are comparable to those in the absence of gluconate. This suggests that a similar reaction mechanism, i.e. surface complexation, is responsible for the sorption of La^{3+}, regardless of the presence or absence of gluconate. By extending the reaction mechanism proposed for La^{3+} sorption, the sorption of the two La-gluconate complexes believed to form in solution to goethite may be considered as:

$$\text{S-OH} + La(GH_4)^{2+} \leftrightarrow \text{S-OLa}(GH_4)^{+} + H^+$$
$$\text{S-OH} + La(GH_3)^{+} \leftrightarrow \text{S-OLa}(GH_3) + H^+$$

It has been reported that iron oxides, such as goethite, have a finite number of adsorption sites per unit surface area (*18, 34*). The number of sites per unit surface area is generally in the range of 2.5×10^{-6} to 3.5×10^{-6} moles of sites per m^2 of mineral (*18, 34, 35*). With the amount of goethite used in these

Downloaded by COLUMBIA UNIV on August 9, 2012 | http://pubs.acs.org
Publication Date: June 9, 2006 | doi: 10.1021/bk-2006-0933.ch018

Downloaded by COLUMBIA UNIV on August 9, 2012 | http://pubs.acs.org
Publication Date: June 9, 2006 | doi: 10.1021/bk-2006-0933.ch018

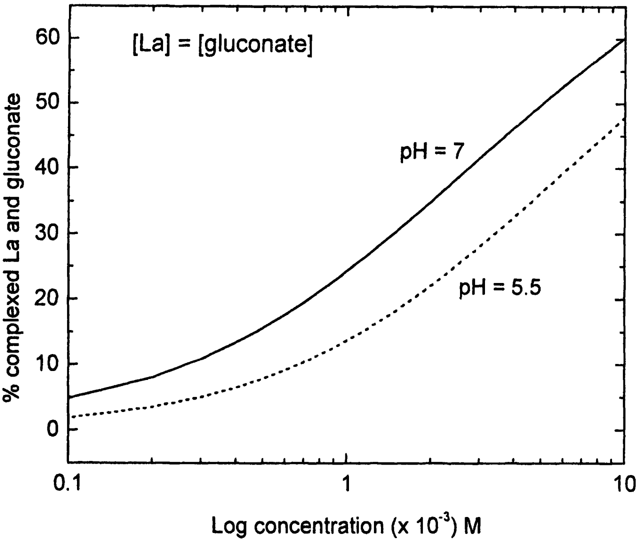

Figure 2: Percentage of lanthanum complexed by gluconate over the range of concentrations used in this study (1 x 10^{-4} to 1 x 10^{-2} M).

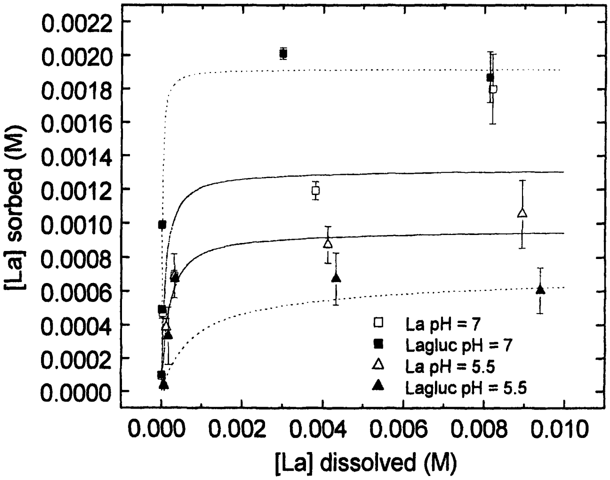

Figure 3: Amount of La^{3+} sorbed by goethite at pH 7 and pH 5.5 at a background electrolyte concentration of 0.1 M. Solid lines represent Langmuir isotherms fit in the absence of gluconate and dashed lines represent fits in the presence of gluconate. Error bars represent ± 2 sigma deviations.

experiments (10 g L^{-1}) and assuming a goethite surface area of 50 m^2 g^{-1} (*34*), the calculated number of surface sites is on the order of 1 x 10^{-3} to 2 x 10^{-3} M of adsorption sites. The Langmuir isotherm has been used to describe adsorption to a surface with a finite number of sites and is given by the equation:

$$C_{ads} = \frac{KN_{max}C_{dis}}{1 + KC_{dis}}$$

where:			
	C_{ads}	=	concentration on a solid phase (mol L^{-1})
	C_{dis}	=	concentration in dissolved phase (mol L^{-1})
	K	=	binding constant (L mol^{-1})
	N_{max}	=	number of adsorption sites (mol L^{-1})

Using the equation above, a single-site Langmuir isotherm was fitted to the experimental data and the values of K and N_{max} were determined that best described the measured adsorption data. The parameters are shown in Table II with 95% confidence limit uncertainties (2σ). The Langmuir model appears to fit the data reasonably well (Figure 3). The use of the Langmuir model is not unreasonable given that goethite contains a finite number of surface sites (*18, 34*). The model suggests that sorption of La^{3+} to the goethite surface should tend towards a constant value. Each data set reaches a maximum adsorption concentration, with the exception of the last data point at pH 7 in the absence of gluconate. This concentration is too low for precipitation of solid $La(OH)_3$, therefore no explanation can be given for this result at this time. The calculated number of adsorption sites (N_{max}) varies from 5 x 10^{-4} to 2 x 10^{-3} M, which is consistent with the number of sites calculated from the amount of goethite and the estimated site density. In general, the calculated number of sites (N_{max}) is higher for the systems in the presence of gluconate, particularly at pH 7. This increase in the number of sites may account for the observation that more La^{3+} is sorbed at pH 7 in the presence of gluconate compared to that in the absence of gluconate. It suggests that gluconate increases the number of sites available to La^{3+} possibly through the creation of new sites. It may be that new sites are created through the formation of a ternary surface complex, where a La^{3+} or La-gluconate complex binds to the surface and a subsequent La^{3+} or La-gluconate complex binds to that. Lackovic et al. (*36*) proposed a similar idea for the uptake of cadmium to goethite in the presence of the citrate anion, where a [$SOCd^{+}$-$LCdOH^{2-}$] species was an important species (where L represents the citrate anion). Further support for this hypothesis comes from the lack of alteration of the goethite morphology observed in the SEM data (data not shown).

Downloaded by COLUMBIA UNIV on August 9, 2012 | http://pubs.acs.org
Publication Date: June 9, 2006 | doi: 10.1021/bk-2006-0933.ch018

The relatively large amount of uncertainty in the binding constant values is the result of scatter in the experimental data. Despite this uncertainty, it appears as though the binding constants are larger at pH 7 as compared to pH 5.5. There appears to be statistically little effect to the K values in the presence of gluconate however, the calculated N_{max} values were affected. This seems to imply that pH is the most important control on the adsorption constant while gluconate affects N_{max}.

Figure 4 shows the effect of changing ionic strength on the partitioning of La in the absence of gluconate at pH 5.5. It appears as though no definite trend in sorption with increasing ionic strength exists. This lack of trend is observed in the presence of gluconate and at pH 7, for both systems (data not shown). It has been reported that below the PZC, increasing the ionic strength causes the electric double layer to contract. This in turn causes shielding of the positive surface charge, which results in an increase in the sorption of a positive species (*18*). The lack of trend with ionic strength suggests that it is not an important control on the uptake of La^{3+}. However, the shapes of the curves at the three ionic strengths investigated indicate that a similar reaction mechanism is responsible for the removal of La^{3+} from solution. The Langmuir parameters calculated from the experimental data (Table II) support this observation that ionic strength plays little role in the removal of lanthanum from solution.

Table II. Binding constant (K) and maximum number of sites (N_{max}) calculated from Langmuir isotherms fitted to the experimental data.

System	*Ionic strength (M)*	*pH*	*K (L mol^{-1}) (x 10^3)*	*K error (x 10^3)*	*N_{max} (mol L^{-1}) (x 10^{-3})*	*N_{max} error (x 10^{-3})*
La	0.01	5.5	6.412	4.344	0.7833	0.06640
La	0.1	5.5	6.731	3.530	0.9620	0.2145
La	1	5.5	0.4438	1.211	0.7291	0.1173
La	0.01	7	1023	1520	1.208	0.7048
La	0.1	7	13550	8.897	1.318	0.7241
La	1	7	18.57	11.84	0.9720	0.5346
La/gluc	0.01	5.5	7.516	8.654	0.5435	0.5408
La/gluc	0.1	5.5	1.291	2.970	0.6752	1.264
La/gluc	1	5.5	0.4480	1.571	1.405	2.695
La/gluc	0.01	7	30.32	17.04	1.067	0.05670
La/gluc	0.1	7	83.58	849.7	1.921	4.313
La/gluc	1	7	5.946	25.28	1.938	0.6428

Downloaded by COLUMBIA UNIV on August 9, 2012 | http://pubs.acs.org
Publication Date: June 9, 2006 | doi: 10.1021/bk-2006-0933.ch018

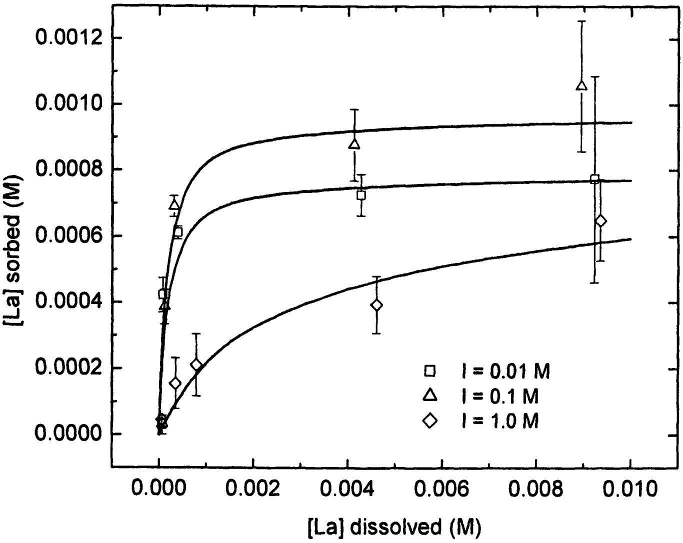

Figure 4: Effect of ionic strength on sorption at pH 5.5 in the absence of gluconate. Lines represent Langmuir isotherms fit to the data. Error bars represent ± 2 sigma deviations.

Downloaded by COLUMBIA UNIV on August 9, 2012 | http://pubs.acs.org
Publication Date: June 9, 2006 | doi: 10.1021/bk-2006-0933.ch018

Conclusions

The results of this study suggest that surface complexation is responsible for the removal of La^{3+} from solution in contact with goethite. The presence of gluconate does not appear to affect the sorption mechanism, *i.e.* surface complexation, which suggests that Type A metal complexes sorb to the goethite surface (metal bound to the surface and the ligand attached to the metal center).

At the pH values investigated and over the range of metal concentrations used in this study, hydrolysis does not appear to play a part in the sorption of La^{3+} to goethite, regardless of the presence or absence of gluconate. In the absence of gluconate, La^{3+} is sorbed to goethite. In the presence of gluconate, at low metal concentrations La^{3+} is the principal species responsible for La sorption. As the metal (and gluconate) concentration increases, the La-gluconate complexes, $La(GH_4)^{2+}$ and $La(GH_3)^{+}$, begin to dominate the aqueous speciation of La. At pH 7, in the presence of gluconate, the amount of La^{3+} adsorbed to the goethite surface is approximately double that adsorbed in the absence of gluconate. This suggests that gluconate participates in the surface adsorption reaction possibly through the formation of ternary surface complexes. However, spectroscopic studies, such as EXAFS, need to be performed to confirm the presence of this complex on the goethite surface. Ionic strength has very little effect on the sorption of La^{3+} regardless of the presence or absence of gluconate. We suggest that the surface complexation of La^{3+} is represented by the following reactions:

$$\text{S-OH} + La^{3+} \leftrightarrow \text{S-OLa}^{2+} + H^{+}$$

$$\text{S-OH} + La(GH_4)^{2+} \leftrightarrow \text{S-OLa}(GH_4)^{+} + H^{+}$$

$$\text{S-OH} + La(GH_3)^{+} \leftrightarrow \text{S-OLa}(GH_3) + H^{+}$$

The presence of gluconate seems to increase the amount of La^{3+} sorbed to goethite at pH 7. This implies that gluconate may inhibit the migration of La^{3+} through the environment.

Downloaded by COLUMBIA UNIV on August 9, 2012 | http://pubs.acs.org
Publication Date: June 9, 2006 | doi: 10.1021/bk-2006-0933.ch018

Acknowledgements

We are grateful to the Electron Microscopy Center at Washington State University for the use of their facilities. Comments by members of the Radiochemistry Center helped improve this manuscript.

This research was funded by the DOE Environmental Management Sciences Program and the Office of Science. Funding for Larry Hull during his sabbatical was provided by the Inland Northwest Research Alliance.

References

1. Schwertmann, U.; Cornell, R. M. *Iron Oxides in the Laboratory;* VCH: Weinheim, Germany, 1991; pp 5-71.
2. Borggaard, O. K. *J. Soil Sci.* **1987,** *38,* 229-238.
3. Zhenghua, W.; Jun, L.; Hongyan, G.; Xiaorong, W.; Chunsheng, Y. *Chem. Spec. Bioavail.* **2001,** *13,* 75-81.
4. Escander, G. M.; Peregrin, J. M. S.; Sierra, M. G.; Martino, D.; Santoro, M.; Frutos, A. A.; Garcia, S. I.; Labadie, G.; Sala, L. F. *Polyhedron* **1996,** *15,* 2251-2261.
5. Sawyer, D. T. *Chem. Rev.* **1964,** *64,* 633-643.
6. Sawyer, D. T.; Brannan, J. R. *Inorg. Chem.* **1966,** *5,* 65-70.
7. Tajmir-Riahi, H.; Agbebavi, J. T. *Carbohydr. Res.* **1993,** *241,* 25-35.
8. Giroux, S.; Rubini, P.; Henry, B.; Aury, S. *Polyhedron* **2000,** *19,* 1567-1574.
9. Warwick, P.; Evans, N.; Hall, T.; Vines, S. *Radiochim. Acta* **2003,** *91,* 233-240.
10. Giroux, S.; Aury, S.; Henry, B.; Rubini, P. *Eur. J. Inorg. Chem.* **2002,** 1162-1168.
11. Fialkov, Y. A.; Kostromina, N. A. *Russ. J. Inorg. Chem. (Engl. Transl.)* **1959,** *4,* 678-683.
12. Kostromina, N. A. *Russ. J. Inorg. Chem. (Engl. Transl.)* **1960,** *5,* 46-49.
13. Katzin, L. I. *Inorg. Chem.* **1968,** *7,* 1183-1191.
14. Panda, C.; Patnaik, R. K. *J. Indian Chem. Soc.* **1979,** *56,* 951-953.
15. Zhernosekov, K. P.; Mauerhofer, E.; Getahun, G.; Warwick, P.; Rosch, F. *Radiochim. Acta* **2003,** *91,* 599-602.
16. Clark, S. B.; Zhang, Z.; Pepper, S. E. The complexation of trivalent rare earths with gluconate, This Publication, ACS, 2004.
17. Robertson, A. P.; Leckie, J.O. *J. Colloid Interface Sci.* **1997,** *188,* 444-472.
18. Dzombak, D. A.; Morel, F. M. M. *Surface Complexation Modeling;* John Wiley and Sons: New York, 1990; pp 1-87.
19. Fendorf, S.; Fendorf, M. *Clays Clay Miner.* **1996,** *44,* 220-227.
20. Weerasooriya, R.; Tobschall, H. J. *Toxicol. Environ. Chem.* **1999,** *68,* 169-177.
21. Farley, K. J.; Dzombak, D. A.; Morel, F. M. M. *J. Colloid Interface Sci.* **1985,** *106,* 226-242.
22. Dzombak, D. D.; Morel, F. M. M. *J. Colloid Interface Sci.* **1986,** *112,* 588-598.
23. Sheals, J.; Granstrom, M.; Sjoberg, S.; Persson, P. *J. Colloid Interface Sci.* **2003,** *262,* 38-47.
24. Hawke, D.; Carpenter, P. D.; Hunter, K. A. *Environ. Sci. Technol.* **1989,** *23,* 187-191.

Downloaded by COLUMBIA UNIV on August 9, 2012 | http://pubs.acs.org
Publication Date: June 9, 2006 | doi: 10.1021/bk-2006-0933.ch018

25. Bargar, J. R.; Persson, P.; Brown, G. E. *Geochim. Cosmochim. Acta* **1999,** *63,* 2957-2969.
26. Venema, P.; Hiemstra, T., van Riemsdijk, W. H. *J. Colloid Interface Sci.* **1997,** *192,* 94-103.
27. Davis, J. A.; Leckie, J. O. *Environ. Sci. Technol.* **1978,** *12,* 1309-1315.
28. Benjamin, M. M.; Leckie, J. O. *Environ. Sci. Technol.* **1981,** *15,* 1050-1057.
29. Benjamin, M. M.; Leckie, J. O *Environ. Sci. Technol.* **1982,** *16,* 162-170.
30. Haas, J. R.; Shock, E. L.; Sassani, D. C. *Geochim. Cosmochim. Acta* **1995,** *59,* 4329-4350.
31. Spahiu, K.; Bruno, J. *A Selected Thermodynamic Database for Rare Earth Elements to be used in HLNW Performance Assessment Exercises;* SKB-95-35, Svensk Karnbranslehantering AB: Stockholm, Sweden, 1995; pp 1-80.
32. Parkman, R. H.; Charnock, J. M.; Bryan, N. D.; Livens, F. R.; Vaughan, D. J. *Am. Mineral.* **1999,** *84,* 407-419.
33. Fairhurst, A. J.; Warwick, P. *Colloids Surf., A* **1998,** *145,* 229-234.
34. Turner, D. R.; Sassman, S. A. *J. Contam. Hydrol.* **1996,** *21,* 311-332.
35. Koretsky, C. *J. Hydrol.,* **2000,** *230,* 127-171.
36. Lackovic, K.; Angove, M. J.; Wells, J. D.; Johnson, B. B. *J. Colloid Interface Sci.* **2004,** *269,* 37-45.

Downloaded by COLUMBIA UNIV on August 9, 2012 | http://pubs.acs.org
Publication Date: June 9, 2006 | doi: 10.1021/bk-2006-0933.ch018

Downloaded by NORTH CAROLINA STATE UNIV on August 10, 2012 | http://pubs.acs.org
Publication Date: June 9, 2006 | doi: 10.1021/bk-2006-0933.ch019

Chapter 19

Neptunium Association with Selected Uranyl Phases Anticipated in the Yucca Mountain Repository

Judah I. Friese[1], Matthew Douglas[1], and James L. Jerden, Jr.[2]

[1]**Pacific Northwest National Laboratory, P.O. Box 999, Richland, WA 99352**
[2]**Argonne National Laboratory, 9700 South Cass Avenue, Argonne, IL 60439**

Spent nuclear fuel (SNF) in the United States is planned to be permanently stored in a geological respository located at Yucca Mountain. Under the anticipated moist, oxidizing environment, a suite of secondary uranium solids is expected to form, which will likely impact the release and potential mobility of other radionuclides contained in the SNF. This chapter provides a summary of selected studies of neptunium (Np) with three phases suggested likely to form under the anticipated respository conditions: metaschoepite ($[(UO_2)_8O_2(OH)_{12}]\cdot10H_2O$), α-uranophane ($Ca[(UO_2)(SiO_3OH)]_2\cdot5H_2O$), and studtite ($UO_4\cdot4H_2O$). Results suggest that uranophane and studtite have a higher capacity for neptunium association than metaschoepite, although uptake of Np by metaschoepite increases proportionally to the quantity of Na included in the synthesis. The release of Np into solution from batch dissolution studies exceeded congruent release with uranium for the uranophane and studtite solid phases. Ultimately, the mechanism of Np association with these phases is inconclusive and further studies will need to be conducted to answer this important question.

In Separations for the Nuclear Fuel Cycle in the 21st Century; Lumetta, G., et al.;
ACS Symposium Series; American Chemical Society: Washington, DC, 2006.

The quantity of high-level radioactive waste in the United States requiring permanent disposal continues to increase at a steady rate. The Yucca Mountain site in southwestern Nevada is currently the subject of an ongoing technical evaluation of its suitability to host the nation's first repository for high-level radioactive waste. Approximately 70,000 metric tons of spent nuclear fuel (SNF) from commercial power plants (as UO_2) is planned to be emplaced in the repository at Yucca Mountain (1). Of interest is the capability of the repository to retain the vast array of radionuclides with different chemical properties for the lifetime of the repository, currently debated to be between 10,000 to greater than 270,000 years. Under the conditions anticipated at Yucca Mountain, the interaction of SNF with the local environment is expected to form a suite of secondary U solids. Natural analog studies as well as work with SNF have shown that UO_2 undergoes oxidative corrosion in the presence of oxidizing water to form hexavalent U phases that reflect the composition of the water. One issue under consideration is the fate of long-lived isotopes present in the waste, particularly their interaction with the predominant hexavalent U solids expected to form at the repository.

Neptunium-237 (^{237}Np) is present in SNF at 400–600 ppm and will be one of the major contributors to dose after 50,000 years because of its long half-life of 2.14×10^6 years (2). Under the conditions expected at Yucca Mountain, Np will likely exist in the pentavalent oxidation state as the neptunyl ion, NpO_2^+, resulting in a relatively high mobility. Burns et al. (3) suggested some time ago that radionuclides such as Np may be incorporated into the predominant uranium (U) solids present in the repository, forming solid solutions and thereby reducing its potential mobility in the environment. This chapter summarizes the results of work done to investigate the interaction of dissolved Np with three uranyl solids, each of differing structural type and deemed likely to form in a repository for SNF at Yucca Mountain.

Phases Used in Synthesis Experiments

The uranyl oxide hydrate metaschoepite, $[(UO_2)_8O_2(OH)_{12}]\cdot 10H_2O$, has been identified as an initial precipitate on the surface of natural U ore deposits and on SNF following corrosion studies using an oxidizing groundwater (4, 5, 6, 7). Its presence at the boundaries of exposed U ores indicates its potential stability, and it has been shown to persist for hundreds of thousands of years in the environment (8). The α-uranophane phase is a layered uranyl silicate with formula $Ca[(UO_2)(SiO_3OH)]_2\cdot 5H_2O$. It contains calcium cations in the interlayer to balance the structural charge and waters of hydration that provide a hydrogen-bonding network between layers. Studtite, $UO_4\cdot 4H_2O$, and metastudtite, $UO_4\cdot 2H_2O$, are uranyl peroxide hydrates and have received increased attention recently (9, 10, 11, 12). These phases are composed of chains of uranyl

Downloaded by NORTH CAROLINA STATE UNIV on August 10, 2012 | http://pubs.acs.org
Publication Date: June 9, 2006 | doi: 10.1021/bk-2006-0933.ch019

polyhedra linked by peroxide units. Because of the high radiation field surrounding a geologic repository of SNF, the production of peroxide in sufficient quantity to precipitate uranyl peroxide solid phases is possible (10). Studtite has been observed on the surface of SNF following its immersion in deionized water for 2 years (9) and as a component of SNF stored at the Hanford site in the United States (13).

Evaluation of the Crystal Chemistry of U(VI) Minerals

Burns et al. (14, 3, 15) have evaluated the crystal chemistry of the U(VI) minerals and predicted the incorporation of transuranium elements into their structures. As trace-level actinides are released during corrosion and alteration of SNF, partitioning into predominant uranyl phases has been suggested to result in decreased mobility. Using bond-valence arguments, likely mechanisms of incorporation were hypothesized depending on the ionic radius and valence state of the non-U cation. Because it adopts a similar dioxo cation geometry, Np(V) could substitute for U(VI) in the structures of various U solids, provided that a charge-balance mechanism exists to compensate for the difference in cationic charge. Two proposed mechanisms for charge balance are the substitution of O^{2-} by OH^- and/or incorporation of additional low-valence cations, such as Na^+, into the interlayer (15).

Experimentally, there is conflicting evidence for the incorporation of Np into metaschoepite. Buck et al. (16) reported that dehydrated schoepite, a uranyl oxide hydrate phase favored above 90°C with formula $(UO_2)O_{0.25-x}(OH)_{1.5+2x}$, $(0<x<0.25)$ (17, 18), retained Np at ~550 ppm concentration during SNF corrosion studies. In contrast, another study characterized alteration products from SNF by X-ray absorption spectrometry to establish an upper limit for Np in dehydrated schoepite of 200 to 333 ppm (19). Finch et al. (20) defined an upper limit of 2 mol% Np incorporation into dehydrated schoepite following analyses of solids generated during aqueous corrosion of unirradiated Np-bearing U-oxides. A recent study by Burns et al. (12) suggests that very little Np(V) is partitioned into synthetic metaschoepite. A small fraction of the Np in solution was removed during the formation of metaschoepite; however, a 30-second rinse with 0.5 M acetic acid removed virtually all Np from the bulk solid, suggesting it had been surface sorbed.

Synthesis of Two Different Sets of Metaschoepite Samples

In studies conducted by Friese et al. (21, 22), two different sets of metaschoepite samples were synthesized. Precipitation of the uranyl hydrolysis product metaschoepite was accomplished by increasing the pH of a uranyl

Downloaded by NORTH CAROLINA STATE UNIV on August 10, 2012 | http://pubs.acs.org
Publication Date: June 9, 2006 | doi: 10.1021/bk-2006-0933.ch019

Downloaded by NORTH CAROLINA STATE UNIV on August 10, 2012 | http://pubs.acs.org
Publication Date: June 9, 2006 | doi: 10.1021/bk-2006-0933.ch019

Table 1. First Set of Radiochemical Data from Initial Metaschoepite Tests at Various Neptunium Concentrations

Sample ID:	2 mol% Np	1 mol% Np	0.5 mol% Np	0 mol% Np
pH	4.6	10.4	4.6	4.5
[U] sol'n	0.785 mM	3.68E–4 mM	0.826 mM	1.058 mM
[Np] solid[a]	48 ppm	3400 ppm	<3.6 ppm	N/A
[Np] sol'n[b]	2.045E-4 M	2.0E-7 M	5.8E-5 M	N/A
% Np in sol'n	68	0.1	77	N/A

[a] Concentration in solid after wash steps.

[b] Concentration in solution before wash steps. Most of the neptunium is in the wash of the solid.

Table 2. Radiochemical Data from Metaschoepite Tests for Transformation to Studtite

Sample ID:	4-30-03C	4-30-03D	4-30-03E	4-30-03F
pH	5.5	5.5	5.5	5.5
Initial Mol % Np	2	2	0	0
[Np] solid[a]	<10 ppm	6500 ppm	N/A	N/A
[Np] sol'n[b]	1.47E-4 M[a]	<1.3E-7 M	N/A	N/A

[a] Concentration in solid after wash steps.

[b] Concentration in solution before wash steps. Most of the neptunium is in the wash of the solid.

Table 3. Second Set Test Matrix, Meta-Schoepite

Initial mol % Np	2	1	0.5	0	1	1	1
mol Np added	6.00E-06	3.00E-06	1.50E-06	0	3.00E-06	3.00E-06	3.00E-06
Final pH	5.5	5.5	5.5	5.5	4.5	6.5	8.5

Reproduced with permission from reference 22. Copyright 2004, Material Research Society.

Downloaded by NORTH CAROLINA STATE UNIV on August 10, 2012 | http://pubs.acs.org
Publication Date: June 9, 2006 | doi: 10.1021/bk-2006-0933.ch019

acetate solution to 5.5 with NaOH. The first set contained eight samples of metaschoepite doped with varying quantities of Np. The second set varied two parameters: the quantity of Np and the pH used in the synthesis. The data from the first set of tests are presented in Table 1 and Table 2. The data for the second set are presented in Table 3.

Several important trends can be seen in these data. At low pH (5.5 or lower), there was very little Np associated with the solid. For two samples, the amount of Np associated with the solid was below the detection limit of the method. The amount of Np in solution in contact with the metaschoepite was high (approximately the amount added), and its solubility was not controlled by the solid phase. The mole-percent of Np did not seem to affect the solution concentration, which is further indication that all the Np was in solution rather than associated with the solid.

One of the metaschoepite samples was synthesized at pH 10.4. Virtually all of the Np was associated with the solid phase, with less than 0.1% still in solution. Direct measurement of Np in the solid by gamma energy analysis (GEA) indicated 3400 ppm Np. However, X-ray powder diffraction (XRD) suggested that the structure was somewhat different from metaschoepite, and the phase was not unambiguously identified, but was likely a sodium uranyl oxyhydroxide phase. There are three main possibilities for the mechanism of association of Np with this sample:

1. The Np may have precipitated as a separate hydroxide phase and aggregated with the U solid following centrifugation.
2. The Np could have sorbed to the surface of the metaschoepite (or sodium uranyl oxyhydroxide phase).
3. The Np may be incorporated/co-precipitated into/with the structure of the metaschoepite (or sodium uranyl oxyhydroxide phase).

There was an attempt to identify a discrete Np solid phase, and to accomplish this, 137 energy dispersive X-ray spectra (EDS) were obtained of many different particles. Only peaks resulting from U and a small peak attributed to Na were observed in the EDS spectra, indicating that Np did not precipitate as separate detectable particles.

In another set of metaschoepite syntheses, the quantity of Np was maintained at a constant level while the pH range was varied from 4.5 to 8.5 in an attempt to probe the pH dependence of Np partitioning. Including solids an attempt to probe the pH dependence of Np partitioning. Including solids previously synthesized, the complete range of pH's investigated thus ranged from 4.5 to 10.4. As the pH of the synthesis was increased, the amount of Np in solution decreased such that it was undetectable by GEA at pH 10.4, consistent with the hydrolysis of neptunium(V). At pH 8.5, about 6% of the neptunium was associated with the solid (Figure 1), whereas almost 0% and 100% was associated with the solid at a pH of 4.5 and 10.4, respectively. Although hydrolysis is expected for Np(V), the measured concentration of Np in solution was an order of magnitude lower (~10^{-7}M) than that expected for a pure Np hydrolysis phase. The exact chemical form of the Np in the solid cannot be determined by these data. This trend would indicate that pH may play an important role in Np association with the meta-schoepite solids. It is also possible that the presence of Na plays a role in Np association with the metaschoepite solids. A series of experiments designed to investigate this possibility are described later in this chapter.

The studies with metaschoepite suggest that Np generally has a very small affinity for the phase; the only evidence for significant association with Np occurred at the highest pH examined, 10.4. XRD indicates that the structure of the solid phase changed at this high pH, and the speciation of the dissolved Np is also expected to differ in this pH regime, making the nature of the association unclear. These results are consistent with those of Burns et al. (12), who observed little Np association with metaschoepite.

Investigation of the Roles of pH and Sodium

Other U(VI) mineral synthesis experiments investigating the role that pH and Na play in the incorporation of Np into U(VI) minerals were performed by Jerden. In these experiments, uranyl oxide hydrates (i.e., dehydrated schoepite or a structurally similar Na-bearing U(VI) mineral) were precipitated from solutions containing U, Ni, and a range of Np concentrations by base titration. Nickel (as Ni^{2+}) was included in these experiments because it is anticipated to be one of the dominant ions in solutions resulting from the corrosion of alloys that make up the waste package containing the SNF (23).

In these co-precipitation experiments, two different bases were used to bring the experimental solutions to supersaturation: (1) sodium hydroxide (NaOH), and (2) tris(hydroxymethyl) aminomethane (referred to as tris). The tris buffer was used because it contains no Na. Comparing results from experiments using these two bases, therefore, helped distinguish between the role that Na played vs. the role that the hydrogen ion activity (i.e., pH) played in Np incorporation. After precipitation of the U(VI) minerals, the samples were allowed to stand in their mother solutions for 9 days at 90°C. The supernatant was centrifuge-filtered (50 nanometer nominal filter pore diameter), acidified, and analyzed for U, Np, and Ni by inductively coupled plasma mass spectroscopy. Results are presented in Tables 4 and 5.

Downloaded by NORTH CAROLINA STATE UNIV on August 10, 2012 | http://pubs.acs.org
Publication Date: June 9, 2006 | doi: 10.1021/bk-2006-0933.ch019

Downloaded by NORTH CAROLINA STATE UNIV on August 10, 2012 | http://pubs.acs.org
Publication Date: June 9, 2006 | doi: 10.1021/bk-2006-0933.ch019

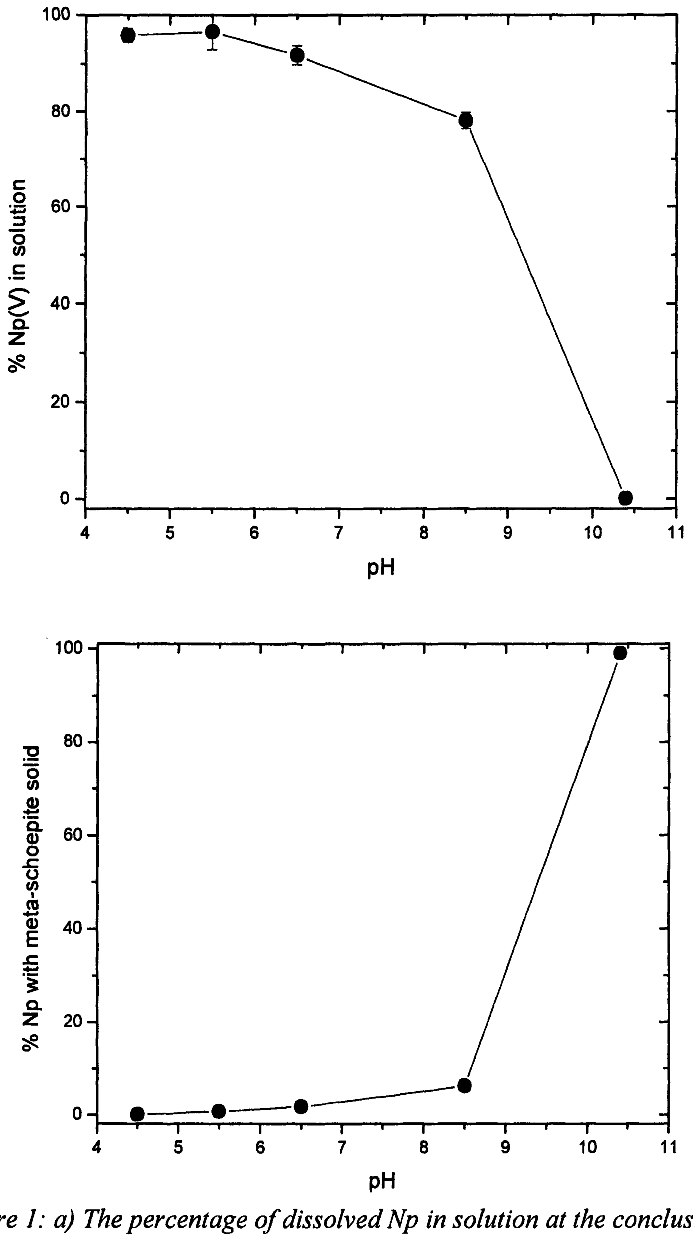

Figure 1: a) The percentage of dissolved Np in solution at the conclusion of metaschoepite precipitation as a function of pH. b) The percentage of Np associated with the metaschoepite solid as a function of pH, as determined by GEA. Figure published by permission (22). (Reproduced with permission from reference 22. Copyright 2004, Material Research Society.)

Downloaded by NORTH CAROLINA STATE UNIV on August 10, 2012 | http://pubs.acs.org
Publication Date: June 9, 2006 | doi: 10.1021/bk-2006-0933.ch019

Table 4. Results from 90°C Co-Precipitation Experiments Using Sodium Hydroxide to Set the pH.

U(VI) oxide hydrate	*NaOH (1)*	*NaOH (2)*	*NaOH (3)*	*NaOH (4)*	*NaOH (5)*	*NaOH (6)*	*NaOH (7)*	*NaOH (8)*
pH	5.2	7.2	8	6.2	6	7.2	5	8.2
mol % Np[a]	0	0	8	6	4	3	1	1
Initial U Sol'n (molar)	4.5E-03	4.7E-03	3.9E-03	3.2E-03	4.3E-03	4.7E-03	4.7E-03	4.8E-03
Initial Np Sol'n	----	----	2.8E-04	2.1E-04	1.8E-04	1.6E-04	5.6E-05	5.3E-05
Initial Ni Sol'n (molar)	4.3E-03	5.1E-03	4.7E-03	3.8E-03	4.7E-03	4.7E-03	4.6E-03	4.7E-03
Final[b] U Sol'n (molar)	2.1E-05	7.8E-07	7.7E-05	3.3E-06	6.8E-06	1.2E-06	6.2E-05	2.2E-06
Final Np Sol'n (molar)	----	----	2.0E-05	2.1E-04	1.3E-04	3.3E-05	5.0E-05	2.9E-06
Final Ni Sol'n (molar)	2.9E-03	4.6E-05	2.7E-03	2.0E-03	2.0E-03	7.1E-05	2.8E-03	6.5E-06
% Uptake Np by precipitates[c]	----	----	93	2	28	80	11	94

[a] Mol % of actinides = Np/(U+Np)x100.

[b] Final refers to after precipitation of U(VI) oxide hydrate.

[c] %Uptake = $[(Np)_{initial}\text{-}(Np)_{final}/(Np)_{initial}]x100$.

Downloaded by NORTH CAROLINA STATE UNIV on August 10, 2012 | http://pubs.acs.org
Publication Date: June 9, 2006 | doi: 10.1021/bk-2006-0933.ch019

Table 5. Results from 90°C Co-Precipitation Experiments Using Tris Buffer to Set the pH.

U(VI) Oxide Hydrate	*Tris (1)*	*Tris (2)*	*Tris (3)*	*Tris (4)*	*Tris (5)*	*Tris (6)*	*Tris (7)*	*Tris (8)*
pH	7.8	4.4	6.6	7.8	4.4	7.6	4.4	7.8
mol % Np[a]	0	0	7	6	4	4	1	1
Initial U Sol'n (molar)	4.5 E-03	4.9 E-03	4.1 E-03	4.1 E-03	4.8 E-03	4.4 E-03	4.8 E-03	4.9 E-03
Initial Np Sol'n (molar)	----	----	3.0 E-04	2.9 E-04	1.7 E-04	1.6 E-04	5.8 E-05	5.9 E-05
Initial Ni Sol'n (molar)	4.5 E-03	4.9 E-03	4.9 E-03	4.9 E-03	4.5 E-03	4.6 E-03	5.0 E-03	5.1 E-03
Final[b] U Sol'n (molar)	8.7 E-05	1.4 E-03	1.7 E-06	6.9 E-05	1.4 E-03	5.4 E-05	1.8 E-03	6.7 E-05
Final Np Sol'n (molar)	----	----	2.1 E-04	2.3 E-04	1.4 E-04	1.2 E-04	4.8 E-05	3.9 E-05
Final Ni Sol'n (molar)	2.5 E-03	2.8 E-03	1.6 E-03	2.7 E-03	2.6 E-03	2.4 E-03	2.9 E-03	2.7 E-03
% Uptake Np by precipitates[c]	----	----	31	19	18	29	17	34

[a] Mol % of actinides = Np/(U+Np)x100.

[b] Final refers to after precipitation of U(VI) oxide hydrate.

[c] %Uptake = $[(Np)_{initial}-(Np)_{final}/(Np)_{initial}]$x100.

The mass of Np that was removed from solution by precipitation of the uranyl oxide hydrate is reported as Np "uptake," which was calculated as a percent Np in the final solution relative to the initial solution. The starting solutions contained a U to Ni ratio of approximately 1, and U to Np ratios of ~15, ~25, and ~85, in addition to four samples with no Np (Tables 4 and 5). The initial concentrations of U and Ni varied from $10^{-2.3}$ to $10^{-2.5}$ molar. The initial concentration of Np (in Np bearing samples) varied from $10^{-3.5}$ to $10^{-4.3}$ molar. Na concentrations (following precipitation by NaOH titration) varied from 10^{-4} to $10^{-1.5}$ molar.

The percentage of Np removed from solution due to precipitation was greater than 90% for samples titrated with NaOH to pH values greater than 7 (Figure 2). Samples titrated with tris to similar pH values show Np uptake of less than 35%. This suggests that Na, which is not present in the tris titrated samples, plays an important role in the Np uptake process.

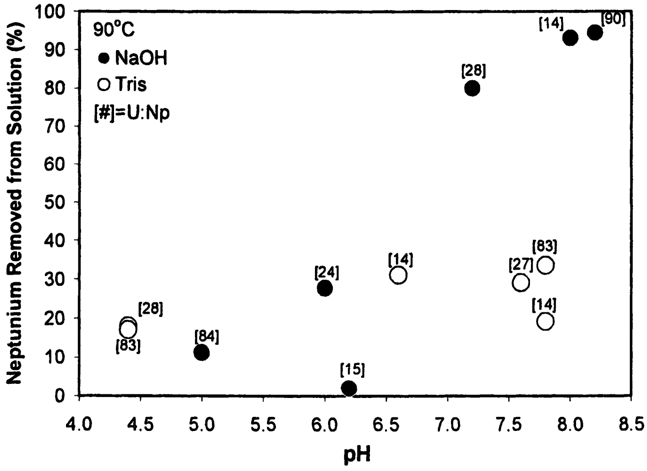

Figure 2. Neptunium uptake as a function of pH for U-Np-Ni co-precipitation tests. Bracketed numbers indicate U:Np ratio in starting solution.

It is likely, based on crystal chemical arguments, that Np is incorporated into the precipitating phase by substituting for U in the crystal structure. In oxygen saturated fluids with pH >2 (such as those used in these experiments and expected to be present in the repository), Np will be present as Np(V), which is predicted to substitute for U(VI) due to molecular structural similarities. For example, Np(V) forms the nearly linear $[NpO_2]^+$ ion with axial bond lengths of approximately 0.18 nm, which is nearly the same as axial bond lengths of the linear uranyl ion $[UO_2]^{2+}$. Furthermore, in a number of minerals, $[NpO_2]^+$ is known to coordinate to five equatorial oxygen atoms (oxygens perpendicular to the linear $[NpO_2]^+$ ion), thus forming pentagonal bipyrimidal coordination polyhedra with bond lengths and geometries very similar to U(VI) pentagonal bipyrimidal coordination polyhedra that form the uranyl oxide hydrate structures (3, 12). However, the substitution of Np(V) for U(VI) will require some crystal chemical rearrangement because of the lower bond-valence contributions to the oxygen atoms of the $[NpO_2]^+$ ion. The coupled substitution (U(VI), O_2^-) ↔ (Np(V), OH^-) has been suggested as a local structural charge balance mechanism but has not been demonstrated.

These U(VI) mineral synthesis experiments suggest that the structural charge balance for Np(V) substituting for U(VI) in uranyl oxide hydrates may be accomplished in the presence of cations such as Na. If this Na charge compensation mechanism limits the amount of Np that can be incorporated into the precipitating phases, this would explain why our lower pH samples (those less than 7) show relatively lower Np uptakes. As more Na is made available

Downloaded by NORTH CAROLINA STATE UNIV on August 10, 2012 | http://pubs.acs.org
Publication Date: June 9, 2006 | doi: 10.1021/bk-2006-0933.ch019

during titration, the precipitating phases would be able to incorporate more Np. The uptake process was found to be insensitive to the ratio of U to Np in the starting solution.

The mechanism of Np uptake could include incorporation into the uranyl mineral lattice or adsorption of Np to uranyl mineral surfaces. The precipitation of a separate Np phase is considered unlikely in these tests based on optical microscopic and scanning electron microscopy (SEM)/EDS characterization of solids from experiments showing higher Np uptake. The measured uptake of Np by U(VI) solids precipitated in the tris base is believed to be largely due to sorption based on the nearly 100% removal of Np from these solids by a 30-second rinse in dilute acetic acid. Acetic acid rinses of the solids produced by NaOH titration removed less than 50% of the Np associated with the solids. Following the acid rinse, two solid samples from tests NaOH 8 and Tris 8 (Tables 4 and 5, respectively) were dissolved and analyzed by ICPMS. Results indicate that the precipitates formed by NaOH titration contained approximately 1.2 Wt% Np while the precipitates formed by tris titration were below detection for Np (<100 ppm in solid). The results of these experiments are therefore consistent with the hypothesis that Np may be incorporated into uranyl oxide hydrate precipitates if Na is present to provide charge balance in the precipitating phase.

Downloaded by NORTH CAROLINA STATE UNIV on August 10, 2012 | http://pubs.acs.org
Publication Date: June 9, 2006 | doi: 10.1021/bk-2006-0933.ch019

Controlled Corrosion Studies of Uranium Oxides Doped with Neptunium

Another approach to investigating Np incorporation into U(VI) minerals was taken by Finch et al. (24). These tests involved controlled corrosion studies of U oxides (U_3O_8) doped with Np. The Np-doped U_3O_8 tests involved first synthesizing U_3O_8 powders containing 9.4% and 1.0 wt% Np. Synthesis and characterization of the starting powders are described elsewhere (25). Characterization of these starting materials by powder XRD, SEM/EDS, and X-ray absorption spectroscopy indicated that Np was incorporated into the U_3O_8 structure (lattice parameters change with different Np:U ratios) and was initially present as Np(IV). The corrosion tests involved placing approximately 20 mg of Np-doped U_3O_8 powder in a crucible located inside a stainless-steel Parr vessel. Approximately 30 mL of deionized water was added to the Parr vessel so that water contacted the U_3O_8 by vapor condensation (i.e., the water was not placed in direct contact with the Np-doped U_3O_8 powder). The steel vessels were sealed and placed into temperature-controlled ovens for the duration of the tests.

Results from the Np-doped U_3O_8 corrosion tests are summarized in Table 6. Sample Np-U_3O_8(1) containing 9.4 wt% Np was reacted at 90°C for 14 days after which the reacted solids were examined by optical microscopy, and no evidence of reaction was observed. The sample was therefore placed back into the steel reaction vessel and reacted at 150°C for 10 days. Examination of these reacted powders by SEM revealed that, in addition to bladed dehydrated schoepite crystals (mineral identification confirmed by XRD), the reacted powders also contained spherical particles containing only Np and O. Powder XRD of this reacted sample confirmed that that Np-bearing particles were NpO_2. Comparison of the powder XRD patterns of the unreacted Np-U_3O_8 and reacted solids clearly demonstrate the absence of NpO_2 in the unreacted samples. No Np was detectable (by EDS) in the dehydrated schoepite crystals near the NpO_2 spheres. Sample Np-U_3O_8(2) containing 1 wt% Np was reacted at 150°C for 17 days. The SEM and XRD analyses of reacted solids from this test show evidence for only two phases: U_3O_8 and dehydrated schoepite. Again, Np was not detected in EDS analyses of the dehydrated schoepite crystals (EDS detection limit estimated to be 0.5 wt%).

Table 6. Results from Np-Doped U_3O_8 Corrosion Tests.

	Np-U_3O_8(1)	*Np-U_3O_8(2)*	*Np-U_3O_8(3)*	*Np-U_3O_8(4)*
Wt% Np in U_3O_8	9.4%	9.4%	1%	1%
Reaction Temp. (°C)	90 & 150	90	90	150
Reaction Duration (days)	14 @ 90 10 @ 150	112 days	112 days	17 days
Reaction Products	DSch NpO_2	DSch MSch NpO_2 Np_2O_5(?)	DSch	DSch
ID of React. Products by	SEM-EDS, XRD	SEM-EDS, XRD	XRD	SEM-EDS, XRD

Sample Np-U_3O_8(3) containing 9.4 wt% Np was reacted at 90°C for 112 days. Characterization of the reacted solids (SEM/EDS, XRD) indicated the presence of dehydrated schoepite and metaschoepite and unreacted U_3O_8. Analyses of the dehydrated schoepite and metaschoepite crystals (by EDS) revealed no evidence for Np. The NpO_2 spheres noted in the higher temperature test were not noted in this 90°C reacted sample; however, sub-micron regions enriched in Np (but not morphologically distinct from the U_3O_8 powder) were observed. X-ray powder diffraction data of sample Np-U_3O_8(3) revealed a relatively complex, multi-phase pattern. Clearly identifiable diffraction peaks in

Downloaded by NORTH CAROLINA STATE UNIV on August 10, 2012 | http://pubs.acs.org
Publication Date: June 9, 2006 | doi: 10.1021/bk-2006-0933.ch019

the data can be assigned unambiguously to dehydrated schoepite, metaschoepite, and U_3O_8. Several peaks can be assigned to NpO_2 (based in part on similar assignments in the 150°C sample). Following assignment of all diffraction peaks to the above four phases, several additional peaks were tentatively identified as corresponding to Np_2O_5. Sample Np-U_3O_8(4) with 1 wt% Np was also reacted for 112 days at 90°C; however, the only minerals identified by XRD in the reacted powder were dehydrated schoepite (most abundant) and metaschoepite, along with minor U_3O_8 (presumably residual starting material). Neptunium was not detectable (by EDS) in the dehydrated schoepite or metaschoepite crystals, and there was no evidence for NpO_2 or Np_2O_5 in the XRD pattern.

Downloaded by NORTH CAROLINA STATE UNIV on August 10, 2012 | http://pubs.acs.org
Publication Date: June 9, 2006 | doi: 10.1021/bk-2006-0933.ch019

Summary of Neptunium-Doped Uranium Oxide Corrosion Tests

In summary, the Np-doped U_3O_8 corrosion tests revealed no evidence for the incorporation of Np into dehydrated schoepite or metaschoepite that formed from fluids containing no other ions besides Np and U. This observation is based on SEM/EDS analyses of these alteration minerals from all samples and is supported by results of full-pattern Rietveld refinements performed on the XRD results by Dr. Robert Finch of Argonne National Laboratory. The Rietveld refinements yielded information on the unit cell parameters of dehydrated schoepite formed from the corrosion of the Np-doped U_3O_8. It was anticipated that Np-substitution into the lattice of this alteration phase would shift the lattice parameters relative to a Np-free dehydrated schoepite pattern (perhaps similar to what has been shown for Np-doped U_3O_8) (25). The Rietveld refinements indicated that the lattice parameters for dehydrated schoepite (the most abundant mineral in reacted powders) formed in these tests did not vary from those expected from a Np-free sample. This analysis indicated that the dehydrated schoepite formed from the corrosion of Np-doped U_3O_8 in water vapor did not incorporate Np in quantities high enough to influence its lattice parameters. The Np-doped U_3O_8 corrosion tests are consistent with previous observations (12) that, in the absence of low valence ions to provide charge balance, uranyl oxide hydrates such as dehydrated schoepite do not incorporate significant amounts of Np.

Uranophane Formation in the Presence of Np(V)

Experiments examining the interaction of Np with uranophane (26) showed a different trend than the metaschoepite synthesis experiments. As described previously, uranophane contains interlayer Ca^{2+} cations and may also accommodate monovalent cations, which could provide a mechanism for the

Downloaded by NORTH CAROLINA STATE UNIV on August 10, 2012 | http://pubs.acs.org
Publication Date: June 9, 2006 | doi: 10.1021/bk-2006-0933.ch019

Table 7. Results of Uranophane Syntheses in the Presence of Np.

Uranophane	*2 mol% Np*	*1 mol% Np*	*0.5 mol% Np*	*0 mol% Np*
Initial pH	10	10	10	10
Final pH	9.8	9.3	9.2	9.4
Initial [Np] (M)	(2.0 ± 0.1) × 10^{-4}	(1.0 ± 0.1) × 10^{-4}	(5.0 ± 0.3) × 10^{-5}	N/A
Final [Np] (M)	(2.6 ± 0.5) × 10^{-7}	(2.6 ± 0.5) × 10^{-7}	(1.3 ± 0.2) × 10^{-7}	N/A
Solid phase [Np] (μg/g)	15,800 ± 700	10,200 ± 400	4,700 ± 200	N/A

maintenance of charge balance following substitution of U(VI) by Np(V). Friese et al. (21) conducted a series of Parr-bomb synthesis experiments in which varying quantities of Np(V) were included in the system. Following isolation and washing of the solids, the quantity of Np associated with each sample was measured by GEA, with the results shown in Table 7. These results demonstrate that as the quantity of Np(V) in the synthesis solution was increased, the Np associated with solid also increased.

Characterization of these solids by XRD did not show significant structural changes between solids synthesized in the presence of Np and those without Np. This was not surprising because of the small amount of Np used in the syntheses, which was only 2 mol% at the highest level. Scanning electron microscopy images showed that in at least one case, crystallites of solids synthesized in the presence of Np were smaller than those formed in its absence, following reaction under otherwise identical conditions. While it can be speculated that the smaller crystallite size is a result of disruption in the structural lattice caused by the incorporation of Np, no further supporting evidence is available.

Downloaded by NORTH CAROLINA STATE UNIV on August 10, 2012 | http://pubs.acs.org
Publication Date: June 9, 2006 | doi: 10.1021/bk-2006-0933.ch019

Np-uranophane Batch Dissolution Study

A Np-doped uranophane sample (780 ppm Np) and a uranophane sample prepared in the absence of Np were subjected to a batch dissolution study. Solids (in duplicate) were weighed and placed into polyethylene vials containing 50 mL of 0.010 M $NaNO_3$ and 0.005 M 2-(N-morpholino)ethanesulfonic acid buffer at pH 6.0. The vials were maintained at 30°C in a waterbath for the 4-month duration of the study and were only removed for the brief periods required for sampling. Aliquots of the suspension were withdrawn at periodic time intervals such that the solid:solution ratio remained constant throughout the experiment. The supernatant was filtered using 0.2-μm membrane filters and acidified with 2% HNO_3 before subsequent analysis of dissolved concentrations of U and Np by inductively coupled plasma-mass spectrometry.

Measured dissolved U and Np concentrations are shown in Figure 3. The U concentration increased for the first two days of the study and then decreased at a high rate before leveling off to a more moderate rate of decrease in solution. The observed behavior is consistent with the precipitation of a new U controlling solid. No differences were noted between the U concentrations for the solid that contained Np and that which did not contain Np. The dissolved Np concentration exhibited a different behavior than U; it increased consistently over the first 2000 hours before reaching a constant level over the final two sampling times. At the conclusion of the study, the ratio of Np:U in solution far exceeded that in the initial solid, demonstrating that release of Np and U into solution was not congruent. XRD analysis of the solid at the conclusion of the study showed that a second phase, likely the uranyl oxide hydrate metaschoepite, precipitated (Figure 4). It is possible that the sample contained some amorphous U solid

Downloaded by NORTH CAROLINA STATE UNIV on August 10, 2012 | http://pubs.acs.org
Publication Date: June 9, 2006 | doi: 10.1021/bk-2006-0933.ch019

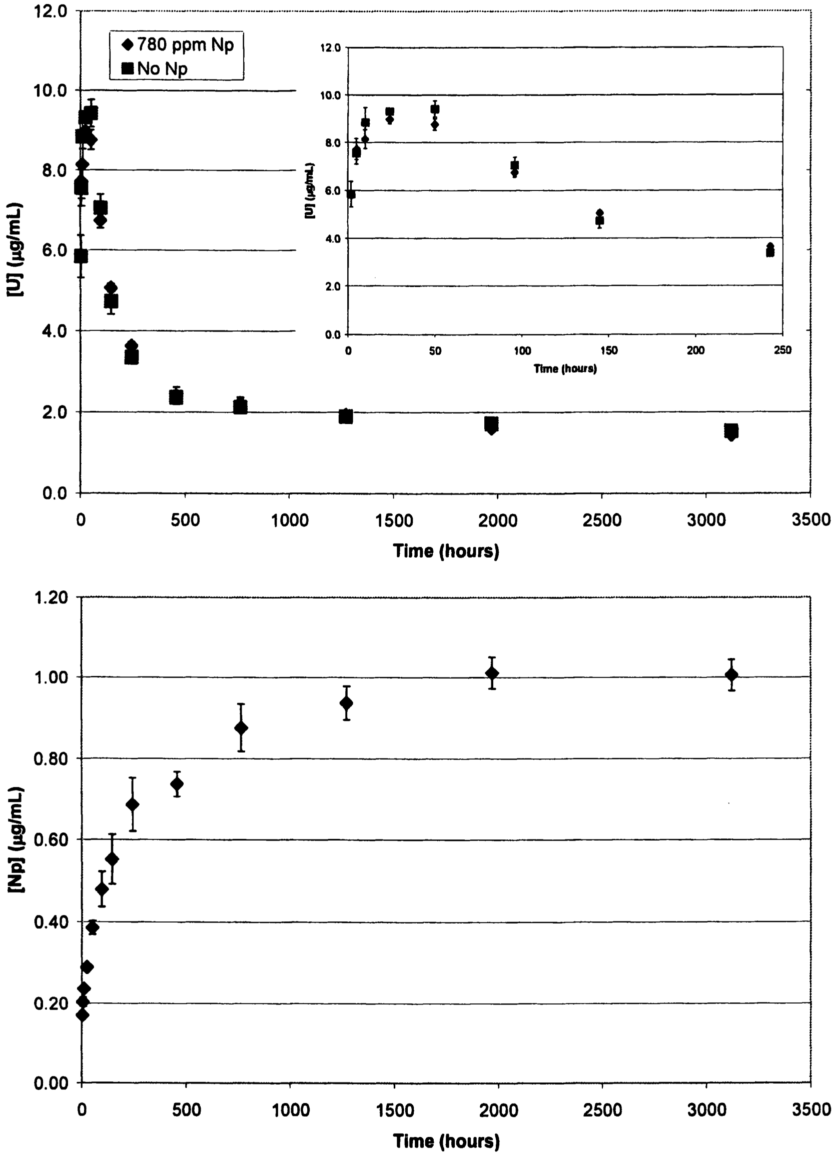

Figure 3: a) Dissolved U concentration over time of batch dissolution study of uranophane with 780 ppm Np in the bulk solid and uranophane without Np. The inset is an expansion of the first 10 days of the study. b) Dissolved Np concentration. The data points reflect the mean of duplicate samples, while the error bars show the range measured.

Downloaded by NORTH CAROLINA STATE UNIV on August 10, 2012 | http://pubs.acs.org
Publication Date: June 9, 2006 | doi: 10.1021/bk-2006-0933.ch019

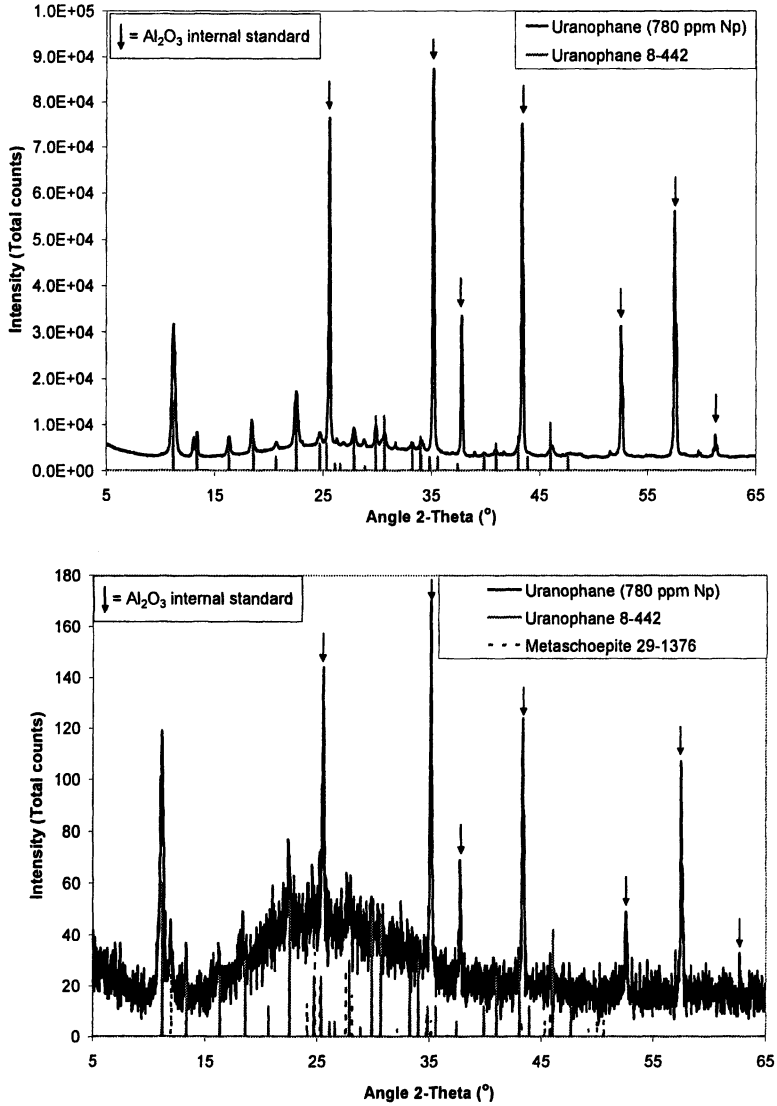

Figure 4: a) The XRD pattern of the solid synthesized in the presence of Np was consistent with the α-uranophane International Centre for Diffraction Data-Powder Diffraction File reference pattern. b) The XRD pattern of the Np-containing uranophane at the conclusion of the dissolution study suggested metaschoepite formed as an additional secondary phase.

initially, which rapidly dissolved, resulting in a U concentration that exceeded the solubility product for metaschoepite. Although the mechanism of Np association with this phase remained uncertain, it did not result in a lower solution concentration than predicted for a Np(V) oxide phase—mass balance calculations suggested that virtually all Np was released to solution.

Studtite Formation in the Presence of Neptunium

Experiments involving studtite formation in the presence of Np have also been conducted (27). These experiments began with the precipitation of metaschoepite in the presence of dissolved Np(V), which was then transformed to studtite by the addition of excess hydrogen peroxide. Although similar to metaschoepite in the sense that studtite lacks a structural charge deficit, unlike metaschoepite, it was shown to have a high affinity for Np. While the XRD pattern for studtite with 6500 ppm Np was virtually identical to studtite precipitated in the absence of Np, the solids differed in their physical appearance. The mechanisms of association could not be unequivocally determined by available characterization means.

It is possible that the addition of hydrogen peroxide altered the oxidation state of the Np(V); however, this was not monitored. A batch dissolution experiment of the Np-containing studtite and a control sample prepared in the absence of Np was conducted under the identical conditions as for uranophane, described above. The U concentration increased initially to a maximum value and slowly decreased with time, consistent with the ripening and coarsening of the metastudtite solid. The Np concentration, however, increased throughout the experiment, suggesting it was being excluded from the reprecipitated uranyl solid. Again, the ratio of Np:U in solution exceeded that in the solid phase. One reason for incongruent release of Np may have been a result of the small particle sizes of the crystallites. Once again, the solubility of Np does not appear to have been significantly reduced following its association with a hexavalent U phase.

Issue of Incorporation Versus Sorption of Neptunium

Despite the efforts of these studies to elucidate interaction of Np with uranyl solids, the issue of incorporation versus sorption of the Np has not been resolved. Characterization techniques including XRD and transmission electron microscopy-electron energy loss spectroscopy have provided information on the structure of solid precipitates and have shown that Np is associated with individual crystallites. However, they have not unequivocally demonstrated its incorporation into the structure of uranyl solid phases. Extended X-ray absorption fine structure may provide the best means for determining the nature of the association mechanism by providing information on the chemical environment of any Np associated with the uranyl solids.

Downloaded by NORTH CAROLINA STATE UNIV on August 10, 2012 | http://pubs.acs.org
Publication Date: June 9, 2006 | doi: 10.1021/bk-2006-0933.ch019

In addition to the mechanism of Np association with the U solid phases, an important issue is the extent to which the Np will be released from the solid phase back into solution. In the case of synthetically prepared uranophane and studtite, the Np is released into solution at a higher rate than the U, which is not consistent with the idea of retardation of radionuclide mobility following interaction with uranyl solids.

References

(1) Ewing, R.C., Macfarlane, A. Science, **2002**, Vol 296 659-660

(2) U.S. Department of Energy, Office of Civilian Radioactive Waste Management: Final Report Total System Performance Assessment Peer Review Panel, (February 1999).

(3) Burns, P. C.; Hawthorne, F. C.; Ewing, R. C. *Can. Mineral.* **1997**, 35, 1551-1570.

(4) Finch, R. J.; Ewing, R. C. *J. Nucl. Mater.* **1992**, 190, 133-156.

(5) Wronkiewicz, D. J.; Bates, J. K.; Wolf, S. F.; Buck, E. C. *J. Nucl. Mater.* **1992**, 238, 78-95.

(6) Finn, P. A.; Finch, R. J.; Buck, E. C.; Bates, J. K. *Mater. Res. Soc. Symp. Proc.* **1998**, 506, 123-131.

(7) Finch, R. J.; Buck, E. C.; Finn, P. A.; Bates, J. K. (1999). Oxidative corrosion of spent UO2 fuel in vapor and dripping groundwater at 90°C. *Materials Research Society Symposium Proceedings*, **556**, 431-438.

(8) Finch, R. J.; Suksi, J.; Rasilainen, K.; Ewing, R. C. *Mat. Res. Soc. Symp. Proc.* **1996**, 412, 823-830.

(9) McNamara, B.; Buck, E. C.; Hanson, B. D. *Mat. Res. Soc. Symp. Proc.* **2003**, 757, 401-406.

(10) Burns, P. C.; Hughes, K. A.. *Am. Mineral.* **2003**, 88, 1165-1168.

(11) Hughes Kubatko, K. A.; Helean, K. B.; Navrotsky, A.; Burns, P. C. *Science* **2003**, 302, 1191-1193.

(12) Burns, P. C.; Deely, K. M.; Skanthakumar, S. *Radiochim. Acta* **2004**, 151-159.

(13) Abrefah, J. A.; Siciliano, E. R. *Am. Nucl. Soc. Symp. Proc.* **2002**, 9, 522-529.

(14) Burns, P. C.; Miller, M. L.; Ewing, R. C. *Can. Mineral.* **1996**, 34, 845-880.

(15) Burns, P. C.; Ewing, R. C.; Miller, M. L. *J. Nucl. Mater.* **1997**, 245, 1-9.

(16) Buck, E. C.; Finch, R. J.; Finn, P. A.; Bates, J. K. *Mater. Res. Soc. Symp. Proc.* **1998**, 506, 83-91.

(17) Sowder, A. G.; Clark, S. B.; Fjeld, R. A. *Environ. Sci. Technol.* **1999**, 33, 3552-3557.

(18) Finch, R. J. et al. *Can. Mineral.* **1998**, 36, 831-845.

Downloaded by NORTH CAROLINA STATE UNIV on August 10, 2012 | http://pubs.acs.org
Publication Date: June 9, 2006 | doi: 10.1021/bk-2006-0933.ch019

(20) Finch, R. J.; Fortner, J. A.; Buck, E. C.; Wolf, S. F. *Mater. Res. Soc. Symp. Proc.* **2002**, 713, 647-654.

(21) Friese, J. I.; Hanson, B. D.; Douglas, M.; Clark, S. B.; Abrefah, J. *PNNL 14856,* **2004**.

(22) Friese, J. I.; Douglas, M.; Buck, E. C.; Clark, S. B.; Hanson, B. D. Mater. Res. Soc. Symp. Proc. 2004, **824**, CC9.2.1-CC9.2.6.

(23) Yucca Mountain In-Package Chemistry Model Report

(24) Finch, R.J. Mater. Res. Soc. Symp Proc. **2002**, 713, 639-646.

(25) Finch, R.J., Kropf, A.J. Mater. Res. Soc. Symp Proc. 2003, **775**, 455-462.

(26) Douglas, M., Clark, S. B., Friese, J. I., Arey, B. W., Buck, E. C., Hanson, B. D., Utsunomiya, S., Ewing, R. C. *Radiochim. Acta* **2005**, 93, 265-272.

(27) Douglas, M., Clark, S. B., Friese, J. I., Arey, B. W., Buck, E. C., Hanson, B. D. *Environ. Sci. Technol.* (accepted).

Downloaded by NORTH CAROLINA STATE UNIV on August 10, 2012 | http://pubs.acs.org
Publication Date: June 9, 2006 | doi: 10.1021/bk-2006-0933.ch019

Downloaded by UNIV MASSACHUSETTS AMHERST on August 9, 2012 | http://pubs.acs.org
Publication Date: June 9, 2006 | doi: 10.1021/bk-2006-0933.ch020

Chapter 20

Speciation and Solubility Modeling of Actinides in the Waste Isolation Pilot Plant

Donald E. Wall, Nathalie A. Wall, and Laurence H. Brush

Carlsbad Programs Group, Sandia National Laboratories, Carlsbad, NM 88220

The WIPP geochemical model uses the Pitzer equations coupled to a thermodynamic database to carry out speciation and solubility calculations for the actinides in the +III, +IV, and +V oxidation states in aqueous systems composed of Na^+–K^+–Mg^{2+}–Ca^{2+}–SO_4^{2-}–OH^-–CO_3^{2-}–HCO_3^-–H_2O–acetate–citrate–oxalate–EDTA. The WIPP database incorporates results for actinide speciation and complexation work carried out primarily at Pacific Northwest National Laboratory, Forschungszentrum Karlsruhe (Germany) and Florida State University. Calculations are performed at Sandia National Laboratories with the code FMT, using the Harvie-Møller-Weare database, and parameters that were developed specifically for actinides in high ionic strength aqueous solutions. This paper describes derivation of the thermodynamic database, and provides normalized standard chemical potentials and Pitzer parameters for modeling An(III, IV, and V) speciation and solubility in brines.

In Separations for the Nuclear Fuel Cycle in the 21st Century; Lumetta, G., et al.;
ACS Symposium Series; American Chemical Society: Washington, DC, 2006.

Introduction

The Waste Isolation Pilot Plant, located 42 km east of Carlsbad, New Mexico has been accepting defense related transuranic waste since March 1999. The repository is located approximately 655 meters below the surface in the Salado Formation, a bedded salt formation. The salt formation is primarily halite (NaCl), but also contains clay seams, anhydrite ($CaSO_4$), gypsum ($CaSO_4 \cdot 2H_2O$), polyhalite ($K_2MgCa_2(SO_4)_4 \cdot 2H_2O$) and magnesite ($MgCO_3$). In the undisturbed state, reconsolidation of the host rock will establish a post-closure environment that will prevent the movement of radionuclides due to the low porosity and permeability of the halite of the Salado Formation. Brine from the Salado enters the repository through dewatering of the disturbed rock zone whereas brine may also enter from the Castile Formation if exploratory drilling for natural resources intersects a disposal area and an underlying brine pocket. Radionuclides may, under certain conditions, move to the accessible environment as dissolved, suspended, or colloidal material, with the magnitude of a direct brine release (DBR) proportional to the radionuclide solubility. Brine solution chemistry will be controlled by emplacement of MgO, which will buffer the brines at mildly basic pH about 9 and act as a sink for CO_3^{2-} that could form as a result of CO_2 production by microbes that act upon the cellulosic, plastic, and rubber materials in the waste.

The radionuclides of greatest concern in the WIPP are $^{239,240}Pu$ and ^{241}Am, which account for more than 99% of the total radioactivity for most of the 10,000 year regulatory period. Iron will be emplaced within the repository as part of the waste and waste drums, and will maintain a chemically reducing condition. As a result, Pu is expected to exist as Pu(III) or Pu(IV) and Am as Am(III). U is modeled as U(IV) in half of the performance assessment vectors and as U(VI) in the other half; likewise, Np is modeled as Np(IV) in half of the vectors and as Np(V) in the other half. Speciation and solubility calculations are carried out for three oxidation states, An(III, IV, and V) but not for An(VI) due to the propensity of U(VI) to form polynuclear species, for which the thermodynamic database for modeling at high ionic strengths is inadequate. The solubility values for U(VI) have been determined based upon a literature survey of the most relevant solubility studies (*1*).

Ions of importance in Salado and Castile brines are H^+, Na^+, K^+, Mg^{2+}, Ca^{2+}, OH^-, Cl^-, CO_3^{2-}, and SO_4^{2-}. Representative compositions of the Salado and Castile brines are given in Table I (*2,3*). Actinide solubilities may also be influenced by the predominant organic ligands present in the waste: acetate, citrate, oxalate, and EDTA.

The semi-empirical Pitzer equations are used to calculate the ionic activity coefficients for the actinides, and inorganic and organic complexing agents in the WIPP inventory. Solubilities are calculated with the Fracture Matrix Transport (FMT) code, which determines the minimum Gibbs free

Downloaded by UNIV MASSACHUSETTS AMHERST on August 9, 2012 | http://pubs.acs.org
Publication Date: June 9, 2006 | doi: 10.1021/bk-2006-0933.ch020

Table I. Composition of the WIPP Brines

Component	*Castile Fm. (mM)*[b]	*Salado Fm.(mM)*[c]
B(III)[a]	63	156
Br^-	11	27
Ca^{2+}	12	14
Cl^-	4800	5610
K^+	97	467
Mg^{2+}	19	1020
Na^+	4870	3570
SO_4^{2-}	170	178

[a] B is added to the synthetic brines as $Na_2B_4O_7\bullet 10H_2O$

[b] Described by Popielak et al. (*3*)

[c] Described by Snider (*2*)

energy for an input array of possible system components. The speciation and solubility of each oxidation state are determined separately, without accounting for redox interchanges among the available oxidation states. The Pitzer parameters that describe the ionic activity coefficients were either taken directly from the literature or calculated with the code NONLIN, which was developed by A. Felmy at PNNL. The NONLIN calculations were applied to results of studies of the variation of stability constants of actinides with organic ligands as functions of ionic strength.

Much of the FMT database, including standard chemical potentials and Pitzer parameters, was developed during the 1990's to carry out speciation and solubility calculations for actinides in high NaCl content brines. Most of the early work focused on the influence of inorganic ligands, such as CO_3^{2-}, OH^-, and SO_4^{2-}, with additional focus on organic ligands as more data became available on the composition of the wastes destined for the WIPP. Compilation of the database is described in a series of SNL memoranda written by C.F. Novak and E.R. Giambalvo; the memoranda are available from the WIPP records center (*4-10*). This paper lists the normalized standard chemical potentials (μ^0/RT) and the Pitzer parameters for the species used in speciation and solubility calculations for the WIPP. The μ^0/RT values for the WIPP modeling were based upon a review of relevant literature reports, and research programs funded by the WIPP project. Some values from the NEA database were incorporated in the WIPP calculations, and are also included in the present data tables (*11*).

The symbols used to denote binary Pitzer parameters are very similar to those commonly used to represent stability constants. The binary Pitzer parameters are indicated by $\beta^{(0)}$, $\beta^{(1)}$, $\beta^{(2)}$ and C^{Φ} with superscript numerals in parentheses for the β terms. Stability constants that use the β symbol may include a superscript zero without parentheses when standard state conditions

Downloaded by UNIV MASSACHUSETTS AMHERST on August 9, 2012 | http://pubs.acs.org
Publication Date: June 9, 2006 | doi: 10.1021/bk-2006-0933.ch020

are indicated, and may include a subscript index of the form β_{pqr}; the indices p,q,r respectively indicate the number of metal ions, protons, and ligands involved in complex formation. The subscript index is omitted if the context is clear. The β terms for Pitzer parameters *always* use superscript numbers in parentheses, the β terms for stability constants *never* use the parentheses either in superscript or subscript.

Downloaded by UNIV MASSACHUSETTS AMHERST on August 9, 2012 | http://pubs.acs.org
Publication Date: June 9, 2006 | doi: 10.1021/bk-2006-0933.ch020

The An(III) Model

Most of the work on An(III) complexation has been performed with Am(III) or Cm(III). These data have been used to generate a model for An(III) speciation and solubility. Due to the similarity of the chemical behavior of Pu(III), Am(III), and Cm(III), the chemical potentials, stability constants, and Pitzer parameters that were determined for Am(III) and Cm(III) have been applied to modeling of the Pu(III) solution behavior. The reactions with inorganic species that are used to model the speciation and solubility for Am(III) and Pu(III) are given below.

$$An^{3+} + CO_3^{2-} \rightleftharpoons AnCO_3^{+}$$

$$An^{3+} + 2CO_3^{2-} \rightleftharpoons An(CO_3)_2^{-}$$

$$An^{3+} + 3CO_3^{2-} \rightleftharpoons An(CO_3)_3^{3-}$$

$$An^{3+} + 4CO_3^{2-} \rightleftharpoons An(CO_3)_4^{5-}$$

$$An^{3+} + OH^{-} \rightleftharpoons AnOH^{2+}$$

$$An^{3+} + 2OH^{-} \rightleftharpoons An(OH)_2^{+}$$

$$An^{3+} + 3OH^{-} \rightleftharpoons An(OH)_3(aq)$$

$$An^{3+} + 3OH^{-} \rightleftharpoons An(OH)_3(s)$$

$$An^{3+} + Cl^{-} \rightleftharpoons AnCl^{2+}$$

$$An^{3+} + 2Cl^{-} \rightleftharpoons AnCl_2^{+}$$

$$An^{3+} + SO_4^{2-} \rightleftharpoons An(SO_4)^{+}$$

$$An^{3+} + 2SO_4^{2-} \rightleftharpoons An(SO_4)_2^{-}$$

$$An^{3+} + OH^{-} + CO_3^{2-} \rightleftharpoons AnCO_3OH(s)$$

$$Na^{+} + An^{3+} + 2CO_3^{2-} + 6H_2O \rightleftharpoons NaAn(CO_3)_2{\bullet}6H_2O(s)$$

$$An^{3+} + PO_4^{3-} \rightleftharpoons AnPO_4(cr)$$

Fanghänel et al. (*12*) used peak deconvolution of time resolved laser fluorescence spectra (TRLFS) to measure the stability constants of formation of the carbonate complexes $Cm(CO_3)_n^{3-2n}$ in 0-6 m NaCl solution at 25 °C. The

Downloaded by UNIV MASSACHUSETTS AMHERST on August 9, 2012 | http://pubs.acs.org
Publication Date: June 9, 2006 | doi: 10.1021/bk-2006-0933.ch020

Table II. Normalized Standard Chemical Potentials for An(III)

Species	μ^0/RT^a	μ^0/RT^b	*Ref.*
An^{3+}	-241.511 ± 1.918	-241.694	32
$AnCO_3^+$	-472.882 ± 2.134	-473.29 ± 0.69	12
$An(CO_3)_2^-$	-697.116 ± 2.384	-697.52 ± 1.38	12
$An(CO_3)_3^{3-}$	-914.903 ± 3.034	-915.53 ± 0.92	12
$An(CO_3)_4^{5-}$	Not available	-1123.40 ± 1.15	12
$AnSO_4^+$	-549.235 ± 1.956	-549.56^c	16
$An(SO_4)_2^-$	-850.282 ± 1.978	-850.99^c	16
$AnOH^{2+}$	-320.593 ±2.237	-319.96 ± 0.21	17
$An(OH)_2^+$	-398.063 ± 2.505	-396.89 ± 0.46	17
$An(OH)_3(aq)$	-468.165 ± 2.238	-469.53	19, 34
$AnCl^{2+}$	-294.995 ± 1.920	-295.20 ± 0.07	19
$AnCl_2^+$	-345.671 ± 1.924	-345.90 ± 0.12	19
$AnCO_3OH(cr)$	Not available	-570.34	12, 13
$AnCO_3OH\bullet 0.5H_2O(cr)$	-617.291 ± 5.560		
$AnCO_3OH(am,hyd)$	-564.396		
$An(OH)_3(s)$	-492.572 ± 2.364	-495.32	19, 33
$NaAn(CO_3)_2\bullet 6H_2O$	Not available	-1396.468	35
$AnPO_4(cr)$	Not available	-709.75	21
$AnPO_4(am, hyd)$	-712.268 ± 1.382		

[a] NEA database values; uncertainties are the 95% confidence limit (*11*)

[b] WIPP values based on referenced work, derivation of the uncertainties are not described in some of the references

[c] based on non-published work that was cited in the reference

standard chemical potentials for the carbonate complexes are listed in Table II; the Pitzer parameters are given in Tables III through V. Fanghänel et al. (*12*) reported standard state complexation constants for $Cm(CO_3)_n^{3-2n}$ at zero ionic strength of log β^0_{101} = 8.1 ± 0.3, log β^0_{102} = 13.0 ± 0.6, log β^0_{103} = 15.2 ± 0.4, log β^0_{104} = 13.0 ± 0.5; a description of the derivation of error limits was not provided. The authors also noted that there was no indication of formation of mixed hydroxide-carbonate complexes. Finally, the authors compared published solubility data to model predictions using their stability constant values, Pitzer parameters, and a log K^0_{sp} = -22.7 for $AmCO_3OH(s)$. The fit of the model to the experimental data of Felmy et al. (*13*), Bernhopf (*14*) and Giffaut (*15*) was good, especially in the log $[CO_3^{2-}]$ range of 10^{-6} to 10^{-7} M, which is particularly relevant for WIPP conditions.

Fanghänel and Kim (*16*) published a review of Cm(III) complexation with Cl^-, SO_4^{2-}, CO_3^{2-} and OH^-. The authors describe examination of the fluorescence of Cm(III) with various SO_4^{2-} concentrations, and plot the variation

Downloaded by UNIV MASSACHUSETTS AMHERST on August 9, 2012 | http://pubs.acs.org
Publication Date: June 9, 2006 | doi: 10.1021/bk-2006-0933.ch020

Table III. Binary Pitzer Parameters for An(III)

Cation	*Anion*	$\beta^{(0)}$	$\beta^{(1)}$	$\beta^{(2)}$	C^{Φ}	*Ref.*
Na^+	$An(CO_3)^{2-}$	-0.24	0.224	0	0.0284	12
Na^+	$An(CO_3)_3^{3-}$	0.125	4.73	0	0.0007	12
Na^+	$An(CO_3)_4^{5-}$	2.022	19.22	0	-0.305	12
$AnCO_3^+$	Cl^-	-0.072	0.403	0	0.0388	12
An^{3+}	SO_4^{2-}	1.792	15.04	0	0.600	16
$AnSO_4^+$	Cl^-	-0.091	-0.39	0	0.048	16
Na^+	$An(SO_4)^{2-}$	-0.354	0.4	0	0.051	16
An^{3+}	$H_2PO_4^{2-}$	0	0	-93	0	36
An^{3+}	ClO_4^-	0.8	5.35	0	-0.0048	13
An^{3+}	Cl^-	0.5856	5.60	0	-0.016	19
$AnOH^{2+}$	Cl^-	-0.055	1.60	0	0.050	19
$An(OH)_2^+$	Cl^-	-0.616	-0.45	0	0.050	19
$AnCl^{2+}$	Cl^-	0.593	3.15	0	-0.006	19
$AnCl_2^+$	Cl^-	0.516	1.75	0	0.010	19

Table IV. Neutral Ion Interaction Parameters for An(III)

Species	*Ion*	λ	*Ref.*
$An(OH)_3(aq)$	Na^+	-0.2	19
$An(OH)_3(aq)$	Cl^-	-0.2	19

Table V. Ternary Interaction Parameters (θ,ψ) for An(III)

Ion i	*Ion j*	*Ion k*	θ_{ij}	ψ_{ijk}	*Ref.*
Ca^{2+}	An^{3+}	Cl^-	0.2	0	19
Ca^{2+}	$AnCl^{2+}$	Cl^-	-0.014	0	19
Ca^{2+}	$AnCl_2^+$	Cl^-	-0.196	0	19
Na^+	An^{3+}	Cl^-	0.1	0	19
Cl^-	$An(CO_3)_3^{3-}$	Na^+	0	0	12
SO_4^{2-}	ClO_4^-	Na^+	0	0	36

in the log β_{101} and log β_{102} values as a function of NaCl concentration over a range of 0 to 6 m. The authors state that the data were used to develop parameters for the SIT model. The An(III)–SO_4^{2-} stability constant and Pitzer parameters used in WIPP modeling are based on work with Cm(III), presented in Table 1 of a report by Fanghänel and Kim (*16*), which references unpublished data from their laboratory as the source of the parameter values. As of the date of this writing, detailed results of the study describing the measurement of the Cm(III)–SO_4^{2-} stability constants and Pitzer parameter data have not been published. As a result, we have not attempted to evaluate the uncertainty associated with the An(III)–SO_4^{2-} parameters.

Pitzer parameters and stability constants of formation for the An(III) hydroxides were reported by Fanghänel et al. (*17*). The stability constants were determined in 1, 2, and 4 m NaCl solutions by examination of the Cm spectra using TRLFS. Varying the pH from 4 to 10, the investigators report the existence of three Cm species: Cm^{3+}, $Cm(OH)^{2+}$, and $Cm(OH)_2^{+}$. The authors used the data to determine the binary Pitzer parameters $\beta^{(0)}$, $\beta^{(1)}$ and C^{Φ} for the Cm(III) hydrolysis species, and using the Pitzer equations, they extrapolated the stability constants to zero ionic strength, and determined $\log \beta^0_{101} = 6.44 \pm 0.09$ and $\log \beta^0_{102} = 12.3 \pm 0.2$; a description of the derivation of error limits was not provided. As a test of the suitability of the parameters, the authors compared the predicted values with experimental solubilities of $Am(OH)_3$ in 5.61 m NaCl solution over a pH range of 5 to 12, and found good agreement. Additionally, the authors note that the thermodynamic model predicts a solubility for $Am(OH)_3$ at pH = 9 to be about four orders of magnitude greater in saturated NaCl solution than in deionized water. The reported stability constants were used to calculate the standard chemical potentials of formation of the hydroxide complexes.

Fanghänel et al. (*18*) reported results of a study of inner sphere Cl^- complexation of Cm(III) in a pH ≅ 2 solution, varying the Cl^- concentration from $2 < [CaCl_2] < 6.5$ m by addition of $CaCl_2$. The authors reported difficulty extrapolating to zero ionic strength due to a lack of data at lower Cl^- concentrations, although a further analysis reported later by the same research group (*19*) provides the Pitzer parameters and values of $\log \beta^0_{101} = 0.24 \pm 0.03$ and $\beta^0_{102} = -0.74 \pm 0.05$, for 25 °C and zero ionic strength; a description of the derivation of error limits was not provided. Harvie et al. (*20*) stated that the behavior of complexes of the metal ion of interest with the anion in the bulk electrolyte is sufficiently described in the $\beta^{(0)}$, $\beta^{(1)}$, and C^{Φ} parameters as ionic strength effects when complexation constants are less than $\log \beta \cong 1.3$ in dilute solution. Complexation by Cl^- of An(III) has much less effect on the solubility under WIPP conditions than the ionic strength effect exerted by the presence of large amounts of Cl^-.

The anions PO_4^{3-} and ClO_4^- are not important components in the WIPP inventory, but were included in the database to accommodate possible future changes. Neither component is currently included in the WIPP geochemical model. The NEA database (*11*) provides a chemical potential for $AmPO_4$(am,hyd), while a similar value is quoted by Rai et al. (*21*) for a crystalline phase. Both values are reproduced in Table II. The solubility-limiting solid phase that is used in WIPP speciation and solubility calculations for trivalent actinides is $Am(OH)_3$ with a $\log K^0_{sp} = -27.5$ at 25 °C and zero ionic strength. Consequently, $Am(OH)_3$ is less soluble under WIPP conditions (pH ≅ 9 and $[CO_3^{2-}] \cong 10^{-5}$ m) than $AmCO_3OH$(cr), as described by Fanghänel et al. (*12*), based on work of Felmy et al. (*13*). The $\log K^0_{sp}$ and standard

Downloaded by UNIV MASSACHUSETTS AMHERST on August 9, 2012 | http://pubs.acs.org
Publication Date: June 9, 2006 | doi: 10.1021/bk-2006-0933.ch020

chemical potential values for $AmCO_3OH(cr)$ are -22.7 and -570.34, respectively. The NEA database (*11*) does not provide data for $AmCO_3OH(cr)$, but includes values for $AmCO_3OH{\bullet}0.5H_2O(cr)$ and $AmCO_3OH(am,hyd)$.

The An(IV) Model

The actinides that can exist in the +IV oxidation state that are also in the WIPP inventory include Th(IV), U(IV), Np(IV) and Pu(IV). Much of the data used as input into the An(IV) model was developed using Th as the An(IV) analog, with application of the results to U(IV), Np(IV) and Pu(IV). Th is considered to be a conservative analog in WIPP solubility calculations because the solubility-limiting solid phases of Th(IV) are more soluble than the analogous U(IV), Np(IV) or Pu(IV) phases (*22*). Th(IV) forms weaker complexes with ligands than the other An(IV) ions, however performance assessment calculations seek to establish boundary conditions of solubility rather than more accurately representative but less easily defensible sets of speciation conditions. The reactions that are used in the modeling of Th(IV), U(IV), Np(IV) and Pu(IV) with inorganic species are given below:

$$AnO_2(am) + 2H_2O \rightleftharpoons An(OH)_4(aq)$$

$$An^{4+} + 4OH^- \rightleftharpoons An(OH)_4(aq)$$

$$An^{4+} + 3OH^- + CO_3^{2-} \rightleftharpoons AnCO_3(OH)_3^-$$

$$An^{4+} + 5CO_3^{2-} \rightleftharpoons An(CO_3)_5^{6-}$$

$$An^{4+} + 2SO_4^{2-} \rightleftharpoons An(SO_4)_2(aq)$$

$$An^{4+} + 3SO_4^{2-} \rightleftharpoons An(SO_4)_3^{2-}$$

$$An^{4+} + 2SO_4^{2-} + 9H_2O \rightleftharpoons An(SO_4)_2{\bullet}9H_2O(s)$$

$$An^{4+} + 2SO_4^{2-} + 8H_2O \rightleftharpoons An(SO_4)_2{\bullet}8H_2O(s)$$

$$An^{4+} + 2Na^+ + 3SO_4^{2-} + 6H_2O \rightleftharpoons An(SO_4)_2{\bullet}Na_2SO_4{\bullet}6H_2O(s)$$

$$An^{4+} + 2K^+ + 3SO_4^{2-} + 4H_2O \rightleftharpoons An(SO_4)_2{\bullet}K_2SO_4{\bullet}4H_2O(s)$$

$$An^{4+} + 4K^+ + 4SO_4^{2-} + 6H_2O \rightleftharpoons An(SO_4)_2{\bullet}2K_2SO_4{\bullet}6H_2O(s)$$

$$An^{4+} + 7K^+ + 5.5SO_4^{2-} \rightleftharpoons An(SO_4)_2{\bullet}3.5K_2SO_4(s)$$

The hydrolysis species, $An(OH)_{4n-1}$ (n=1,2,3) are not considered because they will not be important species at the pH ≅ 9 expected to exist within the repository. The chemical potentials and Pitzer parameters for the complexes of An(IV) with inorganic anions are given in Tables VI through IX.

Downloaded by UNIV MASSACHUSETTS AMHERST on August 9, 2012 | http://pubs.acs.org
Publication Date: June 9, 2006 | doi: 10.1021/bk-2006-0933.ch020

Table VI. Normalized Standard Chemical Potentials for An(IV)

Species	μ^0/RT	*Ref.*
Th^{4+}	-284.227	32
$Th(CO_3)_5^{6-}$	-1411.378	25
$ThCO_3(OH)_3^-$	-775.627	25
$Th(OH)_4(aq)$	-622.47	37
$Th(SO_4)_2(aq)$	-911.69	26
$Th(SO_4)_3^{2-}$	-1214	26
$ThO_2(am)$	-451.408	28
$Th(SO_4)_2{\bullet}9H_2O(s)$	-1775.9	26
$Th(SO_4)_2{\bullet}8H_2O(s)$	-1680	26
$Th(SO_4)_2{\bullet}Na_2SO_4{\bullet}6H_2O(s)$	-2011.29	26
$Th(SO_4)_2{\bullet}K_2SO_4{\bullet}4H_2O(s)$	-1837.57	26
$Th(SO_4)_2{\bullet}2K_2SO_4{\bullet}2H_2O(s)$	-2181.81	26
$Th(SO_4)_2{\bullet}3.5K_2SO_4(s)$	-2790.83	26

Table VII. Binary Pitzer Parameters for An(IV)

Cation	*Anion*	$\beta^{(0)}$	$\beta^{(1)}$	$\beta^{(2)}$	C^{Φ}	*Ref.*
Na^+	$Th(SO_4)_3^{2-}$	0.12	0	0	0	26
Na^+	$ThCO_3(OH)_3^-$	0	0	0	0	25
Na^+	$Th(CO_3)_5^{6-}$	1.31	30	0	0	25
K^+	$Th(SO_4)_3^{2-}$	0.9	0	0	0	26
H^+	$Th(SO_4)_3^{2-}$	0.84	0	0	0	26
Th^{4+}	Cl^-	1.092	13.7	-160	-0.112	27
Th^{4+}	SO_4^{2-}	1.56	0	0	0	26
Th^{4+}	HSO_4^-	1.44	0	0	0	26

Table VIII. Neutral Ion Interaction Parameters (λ) for An(IV)

Neutral	*Ion*	λ	*Ref.*
$Th(SO_4)_2(aq)$	Cl^-	0.29	26
$Th(SO_4)_2(aq)$	HSO_4^-	0.68	26

Table IX. Ternary Ion Interaction Parameters (θ,ψ) for An(IV)

ion i	*ion j*	*ion k*	θ_{ij}	ψ_{ijk}	*Ref.*
Na^+	Th^{4+}	Cl^-	0.42	0.21	38
Mg^{2+}	Th^{4+}	Cl^-	0.60	0.21	38
H^+	Th^{4+}	Cl^-	0.60	0.37	27
$Th(CO_3)_5^{6-}$	Cl^-	Na^+	2.0	-0.08	39
$Th(CO_3)_5^{6-}$	ClO_4^-	Na^+	5.5	0	25

Downloaded by UNIV MASSACHUSETTS AMHERST on August 9, 2012 | http://pubs.acs.org
Publication Date: June 9, 2006 | doi: 10.1021/bk-2006-0933.ch020

Osthols et al. (*23*) reported stability constants for the reactions

$$ThO_2(cr) + H^+ + H_2O + CO_3^{2-} \rightleftharpoons ThCO_3(OH)_3^-$$
$$ThO_2 + 4H^+ + 5CO_3^{2-} \rightleftharpoons Th(CO_3)_5^{6-} + 4H_2O$$

The log β values for $ThCO_3(OH)_3^-$ and $Th(CO_3)_5^{6-}$ are 6.11 ± 0.19 and 42.12 ± 0.32 in 0.5 M $NaClO_4$ at 25 °C; the uncertainties are given at 3σ. The authors used the SIT approach to calculate the standard state stability constants at zero ionic strength, resulting in log $\beta \pm 3\sigma$ values of 6.78 ± 0.3 and 39.64 ± 0.4, respectively. Rai et al. (*24*) reported results of a study of the solubility of Th(IV) and U(IV) hydrous oxides in concentrated $NaHCO_3$ and Na_2CO_3 solutions. The study was not carried out with either $NaClO_4$ or NaCl background electrolytes. The data reported by Osthols et al. (*23*) and Rai et al. (*24*) were later interpreted by Felmy et al. (*25*), who calculated the standard state log β^0 of 6.78 for $ThCO_3(OH)_3^-$ and 37.6 for $Th(CO_3)_5^{6-}$. Felmy et al. (*25*) also reported binary Pitzer parameters for the interaction of the $ThCO_3(OH)_3^-$ and $Th(CO_3)_5^{6-}$ complexes with Na^+, although this was based on the data published by Osthols et al. for a single ionic strength, 0.5 M $NaClO_4$ solution. Felmy et al. (*25*) state that, due to the high charge on the $Th(CO_3)_5^{6-}$ anion, stability constants may exhibit large variations depending upon the identity of the electrolyte, and that it is impossible to extrapolate unambiguous standard-state thermodynamic quantities for such highly charged species from solution data in different electrolyte media. The WIPP model for carbonate complexation of tetravalent actinides is based on the work of Felmy et al. (*25*).

The thermodynamic and Pitzer parameters for the An(IV)–SO_4^{2-} species that have been incorporated into the WIPP PA database are for $An(SO_4)_2(aq)$ and $An(SO_4)_3^{2-}$, based on a study of the thermodynamics of Th^{4+}–SO_4^{2-} interactions in the Na^+–K^+–Li^+–NH_4^+–Th^{4+}–SO_4^{2-}–HSO_4^-–H_2O system, published by Felmy and Rai (*26*).

Formation of complexes of An(IV) with chloride is not specifically modeled with values of μ^0/RT, although it is known that ion pairing occurs in concentrated chloride systems. Chloride complexation is accounted for as an ionic strength effect by the inclusion of a large negative value for $\beta^{(2)}$ in the binary interaction parameters for Th^{4+} with Cl^- as described by Roy et al. (*27*). The $\beta^{(2)}$ parameter is given in Table VII.

The solubility-limiting solid phase for the tetravalent actinides in the WIPP geochemical model is $AnO_2(am)$, with $ThO_2(am)$ used as the model for $UO_2(am)$, $NpO_2(am)$, and $PuO_2(am)$. Felmy et al. (*28*) measured the solubility of $ThO_2(am)$ in NaCl solutions from 0.6 to 3.0 M and in 0.6 M KCl over a pcH range of 3 to 11, using equilibration times extending beyond one year. The authors reported solubilities of $ThO_2(am)$ that were up to three orders of magnitude greater in NaCl than in $NaClO_4$ solutions, with solubilities increasing with NaCl ionic strength, illustrating the large chemical behavior differences of

Downloaded by UNIV MASSACHUSETTS AMHERST on August 9, 2012 | http://pubs.acs.org
Publication Date: June 9, 2006 | doi: 10.1021/bk-2006-0933.ch020

actinides in chloride and perchlorate solutions, and the impossibility of adequately accounting for the differences without experimental data. The authors found that, under carefully controlled conditions, Th exhibited a solubility of approximately 3 × 10^{-8} M at pH = 9 in 3 M NaCl solution in the absence of carbonate and other complexing ligands, thus, since the presence of sulfate, carbonate, and other ligands may be expected to increase solubility, this may be regarded as an approximate lower limit of solubility when using Th as a model for An(IV) behavior in mildly basic NaCl brines.

Downloaded by UNIV MASSACHUSETTS AMHERST on August 9, 2012 | http://pubs.acs.org
Publication Date: June 9, 2006 | doi: 10.1021/bk-2006-0933.ch020

The An(V) Model

The pentavalent actinide solubility model for WIPP includes only Np(V). Pu(V) is not a thermodynamically stable oxidation state at pH ≅ 9 under the reducing conditions that will prevail within the WIPP; the DOE has proposed and the EPA has accepted exclusion of Pu(V) from the WIPP geochemical model. The oxidation state distribution of Np is modeled by assigning a probability equal to 0.5 for occurrence of either Np(IV) or Np(V). The decision to assign a 0.5 probability for the oxidation state distribution model of Np has very little impact upon WIPP performance due to the small amount of Np in the inventory. The inorganic complexation and precipitation reactions that are included in the WIPP geochemical model are given below:

$$NpO_2^+ + OH^- \rightleftharpoons NpO_2OH(aq)$$

$$NpO_2^+ + OH^- \rightleftharpoons NpO_2OH(s, aged)$$

$$NpO_2^+ + OH^- \rightleftharpoons NpO_2OH(s, am)$$

$$NpO_2^+ + 2OH^- \rightleftharpoons NpO_2(OH)_2^-$$

$$NpO_2^+ + CO_3^{2-} \rightleftharpoons NpO_2CO_3^-$$

$$NpO_2^+ + 2CO_3^{2-} \rightleftharpoons NpO_2(CO_3)_2^{3-}$$

$$NpO_2^+ + 3CO_3^{2-} \rightleftharpoons NpO_2(CO_3)_3^{5-}$$

$$Na^+ + NpO_2^+ + CO_3^{2-} + 3.5H_2O \rightleftharpoons NaNpO_2CO_3{\bullet}3.5H_2O(s)$$

$$3Na^+ + NpO_2^+ + 2CO_3^{2-} \rightleftharpoons Na_3NpO_2(CO_3)_2(s)$$

$$K^+ + NpO_2^+ + CO_3^{2-} \rightleftharpoons KNpO_2CO_3(s)$$

$$3K^+ + NpO_2^+ + 2CO_3^{2-} + 0.5H_2O \rightleftharpoons K_3NpO_2(CO_3)_2{\bullet}0.5H_2O(s)$$

Fanghänel et al. (*29* and references therein) reported Pitzer parameters for OH^- and CO_3^{2-} complexes of NpO_2^+ in $NaClO_4$ and NaCl solutions, based upon an evaluation of previously published experimental data for solubility studies on

NpO_2^+ in 0.1–3 M $NaClO_4$ and 5 M NaCl. In the cases of the interaction of Na^+ with $NpO_2CO_3^-$ and $NpO_2(OH)_2^-$, insufficient data was available at low ionic strengths to calculate the $\beta^{(1)}$ Pitzer parameter. The authors estimated the value of $\beta^{(1)} = 0.34$ for $Na^+/NpO_2CO_3^-$, and set $\beta^{(1)} = 0$ for $Na^+/NpO_2(OH)_2^-$. A subsequent report by Novak et al. (*30*), describing thermodynamic modeling of Np(V) in K_2CO_3 solutions, features the adoption of the Pitzer parameters that characterize the interaction of Na^+ with $NpO_2(OH)_n^{1-n}$, $NpO_2CO_3^-$ and $NpO_2(CO_3)_2^{3-}$ as reasonable estimates for the interaction of K^+ with the same species. As a result, the DOE has elected to adopt the same approach, assigning the interaction parameters for K^+ with the neptunyl hydroxides and carbonates (except $NpO_2(CO_3)_3^{5-}$) to be the same as the respective parameters for Na^+. The data for interaction of K^+ with $NpO_2(CO_3)_3^{5-}$ were judged sufficient for parameter determination without resort to analogy. Likewise, the interaction parameters for Mg^{2+} with $NpO_2(OH)_n^{1-n}$, $NpO_2CO_3^-$ and $NpO_2(CO_3)_2^{3-}$ have been set equal to those used for Na^+. Novak et al. (*30*) describe derivation of the binary parameters for Mg^{2+} with $NpO_2(CO_3)_3^{5-}$ as the average value of the respective Na^+ and K^+ parameters, giving a reasonable approximation in the absence of additional data. The $NpO_2(OH)_2^-$ moiety will not exist at pH ≅ 9, therefore the interaction parameters have been set to zero. Further experimental work would be required if it becomes necessary to extend WIPP geochemical modeling to pH > 10 values. The normalized standard chemical potentials and Pitzer parameters used for modeling speciation and solubility of Np(V) are provided in Tables X through XIII.

Additional Modeling Considerations

Normalized standard chemical potentials for the WIPP brine components H_2O, H^+, Na^+, K^+, Mg^{2+}, Ca^{2+}, Cl^-, SO_4^{2-}, HSO_4^-, OH^-, HCO_3^- and CO_3^{2-} are provided in Table XIV. During the course of a speciation and solubility calculation, the FMT code adjusts brine composition to account for changes in chemistry, such as depletion of Mg^{2+} content in Salado brine as a result of increasing pH due to reaction of MgO with water. Binary and ternary ion interaction parameters for Mg^{2+} with actinide complexes are not included in the WIPP geochemical model. In general, the impact of the ternary parameters is small, but not negligible. Omission of the binary and ternary parameters for Mg^{2+} has not been viewed as a significant issue due to precipitation of Mg^{2+} at the mildly basic pH of the repository brines. The experimental work of measuring stability constants for actinide-organic ligand interactions at various ionic strengths was carried out at Florida State University by Choppin and coworkers (*31*). Stability constants of acetate, citrate, oxalate, and EDTA with

Downloaded by UNIV MASSACHUSETTS AMHERST on August 9, 2012 | http://pubs.acs.org
Publication Date: June 9, 2006 | doi: 10.1021/bk-2006-0933.ch020

Table X. Normalized Standard Chemical Potentials for Np(V)

Species	*μ^0/RT* [a]	*μ^0/RT* [b]	*Ref.*
NpO_2^+	-366.186 ± 2.270	-369.105	32
$NpO_2CO_3^-$	-590.563 ± 2.280	-593.601	29
$NpO_2(CO_3)_2^{3-}$	-807.134 ± 2.293	-809.832	29
$NpO_2(CO_3)_3^{5-}$	-1017.704 ± 2.313	-1020.214	29
$NpO_2OH(aq)$	-435.828 ± 2.784	-438.730	29
$NpO_2(OH)_2^-$	-503.167 ± 2.546	-506.238	29
NpO_2OH(am,aged)	-451.025 ± 2.545	-454.369	40
NpO_2OH(am)	-449.643 ± 2.317	-452.757	40
$NaNpO_2CO_3 \bullet 3.5H_2O$	-1044.948 ± 2.343	-1048.058	40
$Na_3NpO_2(CO_3)_2(s)$	-1141.841 ± 2.568	-1144.597	40
$KNpO_2CO_3(s)$	-723.379 ± 2.318	-727.330	30
$K_3NpO_2(CO_3)_2(s)$	-1169.574 ± 2.326	-1173.546	30

[a] NEA database values; uncertainties are at 95% confidence limit (*11*)

[b] WIPP values based on referenced work

Table XI. Binary Pitzer Parameters for Np(V)

Cation	*Anion*	*$\beta^{(0)}$*	*$\beta^{(1)}$*	*$\beta^{(2)}$*	*C^{Φ}*	*Ref.*
Na^+	$NpO_2(OH)_2^-$	0	0	0	0	29
Na^+	$NpO_2CO_3^-$	0.1	0.34	0	0	29
Na^+	$NpO_2(CO_3)_2^{3-}$	0.48	4.4	0	0	29
Na^+	$NpO_2(CO_3)_3^{5-}$	1.8	22.7	0	0	29
K^+	$NpO_2(OH)_2^-$	0	0	0	0	
K^+	$NpO_2CO_3^-$	0.1	0.34	0	0	30
K^+	$NpO_2(CO_3)_2^{3-}$	0.48	4.4	0	0	30
K^+	$NpO_2(CO_3)_3^{5-}$	2.34	22.7	-96	-0.22	30
Mg^{2+}	$NpO_2(OH)_2^-$	0	0	0	0	
Mg^{2+}	$NpO_2CO_3^-$	0.1	0.34	0	0	41
Mg^{2+}	$NpO_2(CO_3)_2^{3-}$	0.48	4.4	0	0	41
Mg^{2+}	$NpO_2(CO_3)_3^{5-}$	2.07	22.7	-48	-0.11	41
NpO_2^+	Cl^-	0.1415	0.281	0	0	40
NpO_2^+	ClO_4^-	0.257	0.18	0	0.0081	40

Table XII. Neutral Ion Interaction Parameter (λ) for Np(V)

Neutral Species	*Ion*	*λ*	*Ref.*
$NpO_2OH(aq)$	Na^+	0	29
$NpO_2OH(aq)$	ClO_4^-	0	29
$NpO_2OH(aq)$	Cl^-	-0.19	29

Downloaded by UNIV MASSACHUSETTS AMHERST on August 9, 2012 | http://pubs.acs.org
Publication Date: June 9, 2006 | doi: 10.1021/bk-2006-0933.ch020

Table XIII. Ternary Interaction Parameters for Np(V)

ion i	*ion j*	*ion k*	θ_{ij}	ψ_{ijk}	*Ref.*
Cl^-	$NpO_2(OH)_2^-$	Na^+	-0.24	0	29
Cl^-	$NpO_2CO_3^-$	Na^+	-0.21	0	29
Cl^-	$NpO_2(CO_3)_2^{3-}$	Na^+	-0.26	0	29
Cl^-	$NpO_2(CO_3)_3^{5-}$	Na^+	-0.26	0	29
CO_3^{2-}	$NpO_2(CO_3)_3^{5-}$	K^+	-1.9	0	41

Table XIV. Normalized Standard Chemical Potentials of WIPP Brine Components

Species	μ^0/RT [a]	$\Delta_f G_m^0$ [b]	μ^0/RT [b]
H_2O	-95.6635	-237.140 ± 0.041	-95.6606 ± 0.017
H^+	0	0	0
Na^+	-105.651	-261.953 ± 0.096	-105.670 ± 0.039
K^+	-113.957	-282.510 ± 0.116	-113.963 ± 0.047
Mg^{2+}	-183.468	-455.375 ± 1.335	-183.695 ± 0.539
Ca^{2+}	-223.30	-552.806 ± 1.050	-222.998 ± 0.424
Cl^-	-52.955	-131.217 ± 0.117	-52.932 ± 0.047
SO_4^{2-}	-300.386	-744.004 ± 0.418	-300.126 ± 0.169
HSO_4^-	-304.942	-755.315 ± 1.342	-304.689 ± 0.541
OH^-	-63.435	-157.220 ± 0.072	-63.422 ± 0.029
HCO_3^-	-236.751	-586.845 ± 0.251	-236.729 ± 0.101
CO_3^{2-}	-212.944	-527.900 ± 0.390	-212.951 ± 0.157

[a] *R*eference 19

[b] Reference 11. NEA database values; the uncertainties are at the 95% confidence limit

Th(IV), Np(V) and Am(III) were determined by solvent extraction; Mg^{2+} stability constants with the same ligands were measured by potentiometric titration. Interactions of the organic ligands with Mg^{2+} were added to the database to account for the competitive effect of Mg^{2+} in WIPP brines, especially the Salado brine. The normalized standard chemical potentials for the species that are included in the WIPP geochemical model are reproduced in Tables XV through XVIII. The Pitzer parameters are presented in Tables XIX to XXI. The inclusion of organic ligands does not have a significant effect on the solubility of An(III) and An(IV) under WIPP conditions due to the extensive competition with hydrolysis and carbonate complexation. However, due to the absence of hydrolysis of Np(V) and Pu(V) at pH ≅ 9, it may be anticipated that organic ligand complexation will both enhance the solubility of these species, and enlarge the stability field for the An(V) oxidation state with respect to both pH and Eh.

Downloaded by UNIV MASSACHUSETTS AMHERST on August 9, 2012 | http://pubs.acs.org
Publication Date: June 9, 2006 | doi: 10.1021/bk-2006-0933.ch020

Downloaded by UNIV MASSACHUSETTS AMHERST on August 9, 2012 | http://pubs.acs.org
Publication Date: June 9, 2006 | doi: 10.1021/bk-2006-0933.ch020

Table XV. Normalized Standard Chemical Potentials for Acetate Complexes

Species	μ^0/RT	*Ref.*
HAc(aq)	-158.300	31
Ac^-	-147.347	31
$AmAc^{2+}$	-395.356	9
$ThAc^{3+}$	-448.525	31
$ThAc_2^{2+}$	-604.800	42
NpO_2Ac(aq)	-519.615	10
$MgAc^+$	-333.346	9

Table XVI. Normalized Standard Chemical Potentials for Citrate Complexes

Species	μ^0/RT	*Ref.*
H_3Cit(aq)	0	31, 43
H_2Cit^-	7.476	31, 43
$HCit^{2-}$	18.620	31, 43
Cit^{3-}	33.410	31, 43
AmCit(aq)	-228.687	31
$ThCit^+$	-285.898	31
NpO_2Cit^{2-}	-343.747	31
$MgCit^-$	-162.261	9

Table XVII. Normalized Standard Chemical Potentials for Oxalate Complexes

Species	μ^0/RT	*Ref.*
H_2Ox(aq)	0	31, 43
HOx^-	3.209	31, 43
Ox^{2-}	13.017	31, 43
$AmOx^-$	-242.853	31, 44
$ThOx^{2+}$	-297.428	31, 44
NpO_2Ox^-	-365.851	31, 44
MgOx(aq)	-179.185	9

Downloaded by UNIV MASSACHUSETTS AMHERST on August 9, 2012 | http://pubs.acs.org
Publication Date: June 9, 2006 | doi: 10.1021/bk-2006-0933.ch020

Table XVIII. Normalized Standard Chemical Potentials for EDTA Complexes

Species	μ^0/RT	*Ref.*
$H_4EDTA(aq)$	0	31, 43
H_3EDTA^-	5.761	31, 43
H_2EDTA^{2-}	12.870	31, 43
$HEDTA^{3-}$	28.710	31, 43
$EDTA^{4-}$	53.050	31, 43
$AmEDTA^-$	-232.977	31
$ThEDTA(aq)$	-285.419	9
NpO_2EDTA^{3-}	-335.708	31, 45
$MgEDTA^{2-}$	-153.734	9
$NpO_2H(EDTA)^{2-}$	-351.852	31, 45
$NpO_2H_2(EDTA)^-$	-364.098	31, 45

Table XIX. Neutral-Ion Interaction Parameter (λ)

Neutral Species[a]	*Ion*	λ	*Ref.*
HAc	Cl^-	0	31, 46
H_3Cit	Cl^-	0	31, 43
H_4EDTA	Cl^-	0	31, 43
H_2Ox	Cl^-	0	31, 43
AmCit	Cl^-	-0.406	31
ThEDTA	Cl^-	0.1111	9
NpO_2Ac	Cl^-	-0.104	10
MgOx	Cl^-	0.0189	9

[a] all species are aqueous solution species

A speciation and solubility model for An(VI) has not been explicitly developed as it has for An(III), An(IV) and An(V). The only two radionuclides that could reasonably be expected to exist in the hexavalent oxidation state are U and Pu. The current solubility model for U(VI) is based upon a literature survey by Hobart and Moore (*1*). Studies designed to elucidate thermodynamics of interactions between U(VI) and both inorganic and organic ligands are considerably complicated by the tendency of U(VI) to form polynuclear species. Fortunately, the radioactive inventory of U in the WIPP is small, and U is not an important component in calculating releases from the repository. Additionally, Pu is not expected to persist as Pu(V) or Pu(VI) due to the large amount of metallic Fe that will be present within the WIPP, mitigating the necessity to develop a speciation and solubility model for Pu(VI).

Table XX. Ternary Pitzer Parameters

Anion i	*Anion j*	*Cation k*	$\theta_{i,j}$	$\Psi_{i,j,k}$	*Ref.*
Ac^-	Cl^-	Na^+	-0.09	0.01029	42, 46

Table XXI. Binary Pitzer Parameters for Actinides and Organic Ligands

Cation	*Anion*	$\beta^{(0)}$	$\beta^{(1)}$	$\beta^{(2)}$	C^{Φ}	*Ref.*
Na^+	Ac^-	0.1426	0.22	0	-0.00629	29, 46
K^+	Ac^-	0.1587	0.3251	0	-0.0066	47
H^+	Ac^-	0	0	0	0	46
$MgAc^+$	Cl^-	-0.0833	0.29	0	0.0987	9
$ThAc_2^{2+}$	Cl^-	0.4671	1.74	0	0.143	42
$AmAc^{2+}$	Cl^-	0.309	1.74	0	-0.132	9
Na^+	H_2Cit^-	-0.1296	0.29	0	0.013	31, 43
Na^+	$HCit^{2-}$	-0.0989	1.74	0	0.027	31, 43
Na^+	Cit^{3-}	0.0887	5.22	0	0.047	31, 43
Na^+	$MgCit^-$	0.1742	0.29	0	-0.06923	9
$ThCit^+$	Cl^-	-0.7467	0.29	0	0.319	31
Na^+	NpO_2Cit^{2-}	-0.4226	1.75	0	0.142	31
Na^+	HOx^-	-0.2448	0.29	0	0.068	31, 43
Na^+	Ox^{2-}	-0.2176	1.74	0	0.122	31, 43
$ThOx^{2+}$	Cl^-	-0.343	1.74	0	0.5	31, 44
$AmOx^+$	Cl^-	-0.9374	0.29	0	0.248	31, 44
Na^+	NpO_2Ox^-	-0.5418	0.29	0	0.095	31, 44
Na^+	H_3EDTA-	-0.2345	0.29	0	0.059	31, 43
Na^+	H_2EDTA^{2-}	-0.1262	1.74	0	0.054	31, 43
Na^+	$HEDTA^{3-}$	0.5458	5.22	0	-0.048	31, 43
Na^+	$EDTA^{4-}$	1.016	11.6	0	0.001	31, 43
Na^+	$MgEDTA^{2-}$	0.2134	1.74	0	0.00869	9
Na^+	NpO_2EDTA^{3-}	0.683	5.911	0	0	31, 45
Na^+	$NpO_2H(EDTA)^{2-}$	0.4733	-1.504	0	0	45
Na^+	$NpO_2H_2(EDTA)^-$	-0.8285	0.2575	0	0.256	45
Na^+	$AmEDTA^-$	-0.2239	0.29	0	0.002	31

Conclusions

Normalized standard chemical potentials and Pitzer parameters for the FMT database used in the WIPP geochemical model have been taken from a literature review or programs funded by the WIPP project. The database used in An(III,IV, and V) speciation and solubility calculations have been reproduced in the present work.

Downloaded by UNIV MASSACHUSETTS AMHERST on August 9, 2012 | http://pubs.acs.org
Publication Date: June 9, 2006 | doi: 10.1021/bk-2006-0933.ch020

Acknowledgments

Compilation of the WIPP thermodynamic database is the result of a long term effort with the involvement of numerous individuals; however, three people deserve special recognition: Craig Novak and Emily Giambalvo, both formerly of Sandia National Laboratories and Robert Moore, currently with SNL, carried out a great deal of the work on the database compilation. This research is funded by WIPP programs administered by the U.S. Department of Energy. Sandia National Laboratories is a multiprogram laboratory operated by Sandia Corporation, a Lockheed Martin Company, for the United States Department of Energy supported this research under contract DE-AC04-94AL85000.

Downloaded by UNIV MASSACHUSETTS AMHERST on August 9, 2012 | http://pubs.acs.org
Publication Date: June 9, 2006 | doi: 10.1021/bk-2006-0933.ch020

References

1. Hobart, D.E.; Moore, R.C. *Analysis of Uranium(VI) Solubility Data for WIPP Performance Assessment: Implementation of Analysis Plan AP-028*; Sandia National Laboratories: Albuquerque, NM, Unpublished report on file in the Sandia WIPP Records Center, Carlsbad, NM, as WPO#36488, 1996.
2. Snider, A.C. *Verification of the Definition of Generic Weep Brine and the Development of a Recipe for This Brine.* Sandia National Laboratories: Carlsbad, NM, Unpublished report on file in the Sandia WIPP Records Center, Carlsbad, NM, as ERMS# 527505, 2003.
3. Popielak, R.S.; Beauheim, R.L.; Black, S.R.; Coons, W.E.; Ellingson, C.T.; Olsen, R.L. *Brine Reservoirs in the Castile Formation, Waste Isolation Pilot Plant Project (WIPP), Southeastern New Mexico.* TME 3153. U.S. Department of Energy, Waste Isolation Pilot Plant: Carlsbad, NM, 1983.
4. Novak, C.F. 1996. *Predictions of +III, +IV, and +V Actinide Solubilities in WIPP Salado and Castile Brine Using the Revised Thermodynamic Database HMW_Am3Pu3Th4Np5_960823.CHEMDAT.* Sandia National Laboratories: Albuquerque, NM, Unpublished memorandum to R.V. Bynum, November 04, 1996. Copy on file in the Sandia WIPP Records Center, Carlsbad, NM, as ERMS# 537331.
5. Novak, C.F.; Moore, R.C. *Estimates of Dissolved Concentrations for +III, +IV, +V, and +VI Actinides in a Salado and a Castile Brine under Anticipated Repository Conditions.* Sandia National Laboratories: Albuquerque, NM. Unpublished memorandum to M.D. Siegel, March 28, 1996. Copy on file in the Sandia WIPP Records Center, Carlsbad, NM, as ERMS# 236207.
6. Giambalvo, E.R. *Recommended Parameter Values for Modeling An(III) Solubility in WIPP Brines.* Sandia National Laboratories: Carlsbad, NM.

Unpublished memorandum to L.H. Brush, July 25, 2002. Copy on file in the Sandia WIPP Records Center, Carlsbad, NM as ERMS# 522982.

7. Giambalvo, E.R. *Recommended Parameter Values for Modeling An(IV) Solubility in WIPP Brines.* Sandia National Laboratories: Carlsbad, NM. Unpublished memorandum to L.H. Brush, July 26, 2002. Copy on file in the Sandia WIPP Records Center, Carlsbad, NM, as ERMS# 522986.
8. Giambalvo, E.R. *Recommended Parameter Values for Modeling An(V) Solubility in WIPP Brines.* Sandia National Laboratories: Carlsbad, NM, Unpublished memorandum to L.H. Brush, July 26, 2002. Copy on file in the Sandia WIPP Records Center, Carlsbad, NM as ERMS# 522990.
9. Giambalvo, E.R. *Recommended Parameter Values for Modeling Organic Ligands in WIPP Brines.* Sandia National Laboratories: Carlsbad, NM, Unpublished memorandum to L.H. Brush, July 25, 2002. Copy on file in the Sandia WIPP Records Center, Carlsbad, NM, as ERMS# 522981.
10. Giambalvo, E.R. *Release of FMT Database FMT_021120.CHEMDAT.* Unpublished memorandum to L.H. Brush, March 10, 2003. Sandia National Laboratories, Carlsbad, NM. Copy on file in the Sandia WIPP Records Center, Carlsbad, NM, as ERMS# 526372.
11. *Update on the Chemical Thermodynamics of Uranium, Neptunium, Plutonium, Americium, and Technetium*; Mompean, F., Illemassene, M., Domenech-Orti, C., Ben Said, K., Eds. Chemical Thermodynamics Series; Vol. 5, Elsevier: Amsterdam, Netherlands, 2003.
12. Fanghänel, T.; Könnecke, T.; Weger, H.T.; Paviet-Hartmann, P.; Neck, V.; Kim, J.I. Thermodynamics of Cm(III) in Concentrated Salt Solutions: Carbonate Complexation in NaCl Solutions at 25 °C. *J. Solution Chem.* **1999,** *28* (4), 447-462.
13. Felmy, A.R.; Rai, D.; Fulton, R.W. The Solubility of $AmOHCO_3(c)$ and the Aqueous Thermodynamics of the System Na^+-Am^{3+}-HCO_3^--CO_3^{2-}-OH^--H_2O. *Radiochim. Acta.* **1990,** *50* (4), 193-204.
14. Bernkopf, M.F.; Kim, J.I. *Hydrolysereaktionen und Karbonatkomplexierung von Dreiwertigem Americium im Naturlichen Aquatischen System*; Report RCM-02884; München, Germany, Institut für Radiochemie Technischen Universitat München, 1984.
15. Giffaut, E. Influence des Ions Chlorure sur la Chimie des Actinides. Effets de la Radiolyse et de la Température. PhD Thesis. Université de Paris-Sud U.F.R. Scientifique D'Orsay, Paris, France, 1994.
16. Fanghänel, T.; Kim, J.I. Spectroscopic Evaluation of Thermodynamics of Trivalent Actinides in Brines. *J. Alloys Compd.* **1998,** *271*, 728-737.
17. Fanghänel, T.; Kim, J.I.; Paviet, P.; Klenze, R.; Hauser, W. Thermodynamics of Radioactive Trace Elements in Concentrated Electrolyte Solutions: Hydrolysis of Cm^{3+} in NaCl Solutions. *Radiochim. Acta.* **1994,** *66/67*, 81-87.

Downloaded by UNIV MASSACHUSETTS AMHERST on August 9, 2012 | http://pubs.acs.org
Publication Date: June 9, 2006 | doi: 10.1021/bk-2006-0933.ch020

18. Fanghänel, T.; Kim, J.I.; Klenze, R.; Kato, Y. Formation of Cm(III) Chloride Complexes in $CaCl_2$ Solutions. *J. Alloys Compd.* **1995,** *225*, 308-311.
19. Könnecke, T.; Fanghänel, T.; Kim, J.I. Thermodynamics of Trivalent Actinides in Concentrated Electrolyte Solutions: Modeling the Chloride Complexation of Cm(III). *Radiochim. Acta.* **1997,***76* (3), 131-135.
20. Harvie, C.E.; Moller, N.; Weare, J.H. The Prediction of Mineral Solubilities in Natural Waters: The Na-K-Mg-Ca-H-Cl-SO_4-OH-HCO_3-CO_3-CO_2-H_2O System to High Ionic Strengths at 25 °C. *Geochim. Cosmochim. Acta.* **1984,** *48* (4), 723-751.
21. Rai, D.; Felmy, A.R.; Fulton, R.W. Solubility and Ion Activity Product of $AmPO_4 \cdot xH_2O(am)$. *Radiochim. Acta.* **1992,** *56* (1), 7-14.
22. Neck, V.; Kim, J.I. Solubility and Hydrolysis of Tetravalent Actinides. *Radiochim. Acta.* **2001,** *89* (1), 1-16.
23. Östhols, E.; Bruno, J.; Grenthe, I. On the Influence of Carbonate on Mineral Dissolution: III. The Solubility of Microcrystalline ThO_2 in CO_2–H_2O Media. *Geochim. Cosmochim. Acta.* **1994,** *58* (2), 613-623.
24. Rai, D.; Felmy, A.R.; Moore, D.A.; Mason, M.J. The Solubility of Th(IV) and U(IV) Hydrous Oxides in Concentrated $NaHCO_3$ and Na_2CO_3 Solutions. *Scientific Basis for Nuclear Waste Management XVIII, Materials Research Society Symposium, Vol. 353, October 23-27, 1994, Kyoto, Japan.* Eds. T. Murakami and R.C. Ewing. 1143-1150. 1995
25. Felmy, A.R.; Rai, D.; Sterner, S.M.; Mason, M.J.; Hess, N.J.; Conradson S.D. Thermodynamic Models for Highly Charged Aqueous Species: Solubility of Th(IV) Hydrous Oxide in Concentrated $NaHCO_3$ and Na_2CO_3 Solutions. *J. Solution Chem.* **1997,** *26* (3), 233-248.
26. Felmy, A.R.; Rai, D. An Aqueous Thermodynamic Model for a High Valence 4:2 Electrolyte Th^{4+}-SO_4^{2-} in the System Na^+-K^+-Li^+-NH_4^+-Th^{4+}-SO_4^{2-}-HSO_4^--H_2O. *J. Solution Chem.* **1992,** *21* (5), 407-423.
27. Roy, R.N.; Vogel, K.M.; Good, C.E.; Davis, W.B.; Roy, L.N.; Johnson, D.A.; Felmy, A.R.; Pitzer, K.S. Activity Coefficients in Electrolyte Mixtures: HCl + $ThCl_4$ + H_2O for 5-55 °C. *J. Phys. Chem.* **1992,** *96* (26), 11065-11072
28. Felmy, A.R.; Rai, D.; Mason, M.J. The Solubility of Hydrous Thorium(IV) Oxide in Chloride Media: Development of an Aqueous Ion-Interaction Model. *Radiochim. Acta.* **1991,** *55* (4), 177-185.
29. Fanghänel, T.; Neck, V.; Kim, J.I. Thermodynamics of Neptunium(V) in Concentrated Salt Solutions: II. Ion Interaction (Pitzer) Parameters for Np(V) Hydrolysis Species and Carbonate Complexes. *Radiochim. Acta.* **1995,** *69* (3), 169-176.
30. Novak, C.F.; Al Mahamid, I.; Becraft, K.A.; Carpenter, S.A.; Hakem, N.; Prussin, T. Measurement and Thermodynamic Modeling of Np(V)

Downloaded by UNIV MASSACHUSETTS AMHERST on August 9, 2012 | http://pubs.acs.org
Publication Date: June 9, 2006 | doi: 10.1021/bk-2006-0933.ch020

Solubility in Aqueous K_2CO_3 Solutions to High Concentrations. *J. Solution Chem.* **1997**, *26* (7), 681-697.

31. Choppin, G.R.; Bond, A.H.; Borkowski, M.; Bronikowski, M.G.; Chen, J.F.; Wall, N.A.; Lis, S.; Mizera, J.; Moore, R.C. Pokrovsky, O.; Xia, Y.X. *Waste Isolation Pilot Plant Actinide Source Term Test Program: Solubility Studies and Development of Modeling Parameters*; SAND99-0943; Sandia National Laboratories: Albuquerque, NM, 2001.
32. Fuger, J.; Oetting, F.L. *The Chemical Thermodynamics of Actinide Elements and Compounds. Part 2. The Actinide Aqueous Ions.* International Atomic Energy Agency, Vienna, Austria, 1976.
33. Morss, L.R.; Williams, C.W. Synthesis of Crystalline Americium Hydroxide, $Am(OH)_3$, and Determination of its Enthalpy of Formation; Estimation of the Solubility-Product Constants of Actinide(III) Hydroxides. *Radiochim. Acta.* **1994,** *66/67*, 89-93.
34. *Chemical Thermodynamics of Americium.* Silva, R.J., Bidoglio, G., Rand, M.H., Robouch, P.B., Wanner, H., Puigdomenech, I., Eds. Chemical Thermodynamics Series, Vol. 2, Elsevier: Amsterdam, Netherlands, 1995.
35. Rao, L.; Rai, D.; Felmy, A.R.; Fulton, R.W.; Novak, C.F. Solubility of $NaNd(CO_3)_2{\bullet}6H_2O$ in Concentrated Na_2CO_3 and $NaHCO_3$ Solutions. *Radiochim. Acta.* **1996,** *75* (3), 141-147.
36. Rai, D.; Felmy, A.; Fulton, R. Nd^{3+} and Am^{3+} Ion Interactions with Sulfate Ion and Their Influence on $NdPO_4(c)$ Solubility. *J. Solution Chem.* **1995,** *24* (9), 879-895.
37. Ryan, J.L.; Rai, D. Thorium(IV) Hydrous Oxide Solubility. *Inorg. Chem.* **1987,** *26* (24), 4140-4142.
38. Rai, D.; Felmy, A.R.; Sterner, M.S.; Moore, D.A.; Mason, M.J.; Novak, C.F. The Solubility of Th(IV) and U(IV) Hydrous Oxides in Concentrated NaCl and $MgCl_2$ Solutions. *Radiochim. Acta.* **1997,** *79* (4), 239-247.
39. Felmy, A.R.; Rai; D. Application of Pitzer's Equations for Modeling the Aqueous Thermodynamics of Actinide Species in Natural Waters: A Review. *J. Solution Chem.* **1999,** *28* (5), 533-553.
40. Neck, V.; Fanghänel, T.; Rudolph, G.; Kim, J.I. Thermodynamics of Neptunium(V) in Concentrated Salt Solutions: Chloride Complexation and Ion Interaction (Pitzer) Parameters for the NpO_2^+ Ion. *Radiochim. Acta.* **1995,** *69* (1), 39-47.
41. Al Mahamid, I.; Novak, C.F.; Becraft, K.A.; Carpenter, S.A.; Hakem, N. Solubility of Np(V) in K-Cl-CO_3 and Na-K-Cl-CO_3 Solutions to High Concentrations: Measurements and Thermodynamic Model Predictions. *Radiochim. Acta.* **1998,** *81* (2), 93-101.
42. Moore, R.C.; Borkowski, M.; Bronikowski, M.G.; Chen, J.; Pokrovsky, O.S.; Xia, Y.; Choppin, G.R. Thermodynamic Modeling of Actinide Complexation with Acetate and Lactate at High Ionic Strength. *J. Solution Chem.* **1999,** *28* (5), 521-531

Downloaded by UNIV MASSACHUSETTS AMHERST on August 9, 2012 | http://pubs.acs.org
Publication Date: June 9, 2006 | doi: 10.1021/bk-2006-0933.ch020

43. Mizera, J.; Bond, A.H.; Choppin, G.R.; Moore, R.C. Dissociation Constants of Carboxylic Acids at High Ionic Strengths. In *Actinide Speciation in High Ionic Strength Medi*; Reed, D.T., Ed.; Kluwer Academic/Plenum Publishers: New York, NY, 1999;113-124.
44. Borkowski, M.; Moore, R.C.; Bronikowski, M.; Chen, J.F.; Pokrovsky, O.S.; Xia, Y.X.; Choppin, G.R. Thermodynamic Modeling of Actinide Complexation with Oxalate at High Ionic Strength. *J. Radioanal. Nucl. Chem.* **2001**, *248* (2), 467-471.
45. Pokrovsky, O.S.; Bronikowski, M.; Moore, R.C.; Choppin, G.R. Interaction of Neptunyl(V) and Uranyl(VI) with EDTA in NaCl Media: Experimental Study and Pitzer Modeling. *Radiochim. Acta.* **1998,** *80* (1), 23-29.
46. Novak, C.; Borkowski, M.; Choppin, G. Thermodynamic Modeling of Neptunium(V)-Acetate Complexation in Concentrated NaCl Media. *Radiochim. Acta.* **1996,** *74,* 111-116.
47. Pitzer, K. Ion Interaction Approach: Theory and Data Correlation. In *Activity Coefficients in Electrolyte Solutions, 2nd Edition*; Pitzer, K., Ed.; CRC Press: Boca Raton, FL, 1991; pp 75-153

Downloaded by UNIV MASSACHUSETTS AMHERST on August 9, 2012 | http://pubs.acs.org
Publication Date: June 9, 2006 | doi: 10.1021/bk-2006-0933.ch020

Downloaded by 89.163.35.42 on August 9, 2012 | http://pubs.acs.org
Publication Date: June 9, 2006 | doi: 10.1021/bk-2006-0933.ix001

Author Index

Arm, Stuart T., 103
Bakel, Allen J., 71
Bhatt, A. I., 219
Birkett, J. E., 89
Borkowski, M., 135
Bottenus, Brienne N., 277
Bowers, Delbert L., 71
Brush, Laurence H., 313
Carrott, M. J., 89
Charnock, J. M., 219
Chiarizia, R., 135
Clark, Sue B., 3, 277
Crooks, G., 89
Czerwinski, K., 119
Dietz, Mark L., 233
Dilger, Andrew A., 233
Douglas, Matthew, 293
Draye, M., 119
Dzielawa, Julie A., 233
Foos, J., 119
Ford, Doris, 183
Fox, O. D., 89, 219
Friese, Judah I., 3, 293
Fugate, Glenn A., 167
Goeury, S., 119
Gordon, Pamela, 183
Hennig, C., 219
Hubler, Timothy L., 201
Hull, Larry C., 277
Jarvinen, Gordon, 183
Jenkins, Jon A., 103
Jensen, Mark P., 135, 233
Jerden, James L., Jr., 293
Jiang, Jun, 151
Jones, C. J., 89, 219
Keogh, D. Webster, 183
Kinoshita, H., 219
Koster, A. L., 219
Latesky, Stan L., 201
Law, Jack D., 251
Lewin, B. G., 219
Li, Jun, 201
Long, Kristy, 183
Lumetta, Gregg J., 3, 201
Maher, C. J., 89
Matsumura, T., 261
May, Iain, 151, 219
Mayhew, Phil, 151
Mayne, Michael, 183
McNamara, Bruce K., 201
Mullins, Don, 183
Nash, Kenneth L., 3, 21, 135
Navratil, James D., 167
Ogden, Mark D., 151
Palmer, Phillip, 183
Pepper, Sarah E., 277
Petchsaiprasert, J., 119
Peterman, Dean R., 251
Plaue, J., 119
Quigley, Kevin J., 71
Rausch, David J., 233
Regalbuto, Monica C., 71
Reichert, Heidi, 183
Rickert, Paul G., 233
Roube, C. V., 89
Sarsfield, Mark J., 151
Sharrad, C., 219
Shepler, Carrie G., 277
Steele, H. M., 219
Stepinski, Dominique C., 233
Stillman, John A., 71
Tait, C. Drew, 183

Takeshita, K., 261
Taylor, R. J., 89
Tillotson, Richard D., 251
Todd, Terry A., 41, 251
Vandegrift, George F., 71
Volkovich, V. A., 219
Wai, Chien M., 57
Wall, Donald E., 313
Wall, Nathalie A., 313
Wester, Dennis W., 201
Wigeland, R. A., 41
Young, Blake A., 233

Downloaded by 89.163.35.42 on August 9, 2012 | http://pubs.acs.org
Publication Date: June 9, 2006 | doi: 10.1021/bk-2006-0933.ix001

Subject Index

A

Acetate and pH dependency, distribution coefficients, ^{154}Eu and ^{241}Am, 254–255*f*
Acetohydroxamic acid (AHA)
  neptunium and plutonium co-recovery, 99–101
  neptunium rejection trials, 94–99
  plutonium reduction, 43
Actinide Crystallization Process description, 189, 191–194
Actinide separations
  applications, Kläui ligands, 201–218
  by crystallization, 185–196
  from lanthanides using simulated feed solution, 256–258
  processes in design and pilot stages, 26–30
  transuranium element extraction, 47–50
  See also Actinides; F-elements; Lanthanides; *specific elements*
Actinides
  ionic activity coefficients, Pitzer equations, calculations, 314–316
  partitioning, future, 21–40
  speciation and solubility modeling, Waste Isolation Pilot Plant, 313–334
  third phase formation in solvent extraction by tri-*n*-butylphosphate, 135–150
  See also Actinide separations; F-elements; Lanthanides; *specific elements*
Advanced Fuel Cycle Initiative, developing technologies, 41–52, 72, 184, 252
AHA. *See* Acetohydroxamic acid
Americium and curium, separation from the lanthanides with Cyanex-301, 251–259
Americium and europium
  distribution coefficients and separation factors, determination, 253–255*f*
  extraction separation with TPEN isomers and decanoic acid, 261–273
  separation factors with TPEN isomers, 262–263
Americium solution behavior model, chemical potentials, stability constants, Pitzer parameters, 316–320
Americium sorption in actinide separations using Kläui ligand resin, 209, 212
Americium synergistic extraction with decanoic acid and TPEN isomers, 269–274
Aminopolycarboxylates in subsurface waste storage tanks, 31
Ammonium acetate/acetic acid feed solution, americium separation from europium with Cyanex-301, 253–258
Ammonium carbamate
  aqueous solution interactions, 151–166
  dissociation in water, equilibria, 152
AMUSE. *See* Argonne Model for Universal Solvent Extraction
An(III) model, chemical potentials, stability constants, Pitzer parameters (WIPP database), 316–320
An(IV) model, chemical potentials, stability constants, Pitzer parameters (WIPP database), 320–323

Downloaded by 89.163.35.42 on August 9, 2012 | http://pubs.acs.org
Publication Date: June 9, 2006 | doi: 10.1021/bk-2006-0933.ix002

An(V) model, chemical potentials, stability constants, Pitzer parameters (WIPP database), 323–324, 325*t*–326*t*
Anionic half-sandwich chelates. *See* Kläui ligands
Aqueous biphasic extraction, 34–35
Aqueous hazes. *See Haze entries*
Argonne Model for Universal Solvent Extraction, 76, 123
Arsenazo III in aqueous biphasic extraction, 34–35

B

Batch dissolution study, neptunium(V)-uranophane, 307–310
Batch equilibrium measurements, separations with Kläui ligand resins, 209, 212–213*f*
Batch-sorption coefficients (K_d), calculations, separations with Kläui ligand resins, 204–205
Baxter's model for hard-spheres with surface adhesion. *See* Particle interaction model
Bench-scale batch crystallizer, uranyl nitrate crystallization, 186–187*f*
Big Rock Point Reactor, irradiated nuclear fuel, dissolution, 71–88
Binding constants, lanthanum sorption onto goethite, 286–287*t*
2,7-Bis(2,2'-arsonophenylazo)-1,8-dihydroxynaphthalene-3,6-disulfonic acid. *See* Arsenazo III
Bis(trifluoromethylsulphonyl)imide f-element complexes, 226–228
Bis(2,4,4-trimethylpentyl)dithiophosphinic acid. *See* Cyanex-301
Bond lengths and structures, lanthanum(III) Kläui ligand complexes, 208–211*f*
Brine components (WIPP database)
  chemical potentials (normalized standard), 324, 326–328
  Pitzer parameters, 326, 328*t*–329*t*
1-Butyl-3-methylimidazolium hexafluorophosphate, TRUEX process solvent, 235

C

^{13}C NMR uranyl ion with aqueous ^{15}N labeled ammonium carbamate, 155, 157*f*–158, 160
Calix[4]arene-bis-(tert-octylbenzo-crown-6) structure, 47*f*
Carbamoylmethyl phosphine oxides as extractants, 26–28
Carbon dioxide release by fossil fuel consumption, 4–5, 234
Carbon dioxide supercritical
  actinide extractions, 35–36
  spent nuclear fuel reprocessing, 57–67
Carlsbad, New Mexico (US), Waste Isolation Pilot Plant, 314
Castile Formation brine, 314, 315*t*
CCD/PEG process. *See* Chlorinated cobalt dicarbollide/polyethylene glycol process
Centrifugal contactor
  haze formation, 113, 115*f*–116, 117*f*
  process equipment, liquid-liquid extraction, 104–105*f*, 110
Cesium phosphomolybdate, ammonium carbamate interactions, 154–155, 160–164
Cesium/strontium extraction from raffinate, UREX or codecontamination process, 44–47*f*
Chemical potentials (normalized standard) (WIPP database)
  An(III) complexes, 316–317
  An(IV) complexes, 320–321*t*
  An(V) complexes, 323–325*t*
  brine components, 324, 326– 328

Downloaded by 89.163.35.42 on August 9, 2012 | http://pubs.acs.org
Publication Date: June 9, 2006 | doi: 10.1021/bk-2006-0933.ix002

Chemical separations benefiting geologic repositories, 50–52
Chlorinated cobalt dicarbollide/polyethylene glycol (CCD/PEG) process, 44–46*f*
CHON principle in extractant design, 29–30
Cladding dissolution and analysis, 82–83
Cladding selection for fuel dissolution, 74–76
CMPO. *See* Octyl(phenyl)-N,N-diisobutylcarbamoylmethylphosphine oxide
Codecontamination process, 44–45, 46*f*
Column experiments, actinide separations using Kläui ligand resin, 213–215
Continuous crystallization, optimization, 185, 189
Coordination complexes between plutonium and hydrogen peroxide, 169–176
Corrosion studies, uranium oxides doped with neptunium, 303–305
Cost reductions in future PUREX technology, 90–91
CPM. *See* Cesium phosphomolybdate
Crown ether/calixarene solvent in
    cesium and strontium separations, 45, 47*f*
    See also Dicyclohexano-18-crown-6, strontium extraction
Crystal structures, mixed plutonium peroxide precipitates, 175–176
Crystallization, uranium complexes, 183–197
Crystallizer unit operation, 188–190*f*
Curium/americium separation from the lanthanides with Cyanex-301, 251–259
Cyanex-301
    americium/curium separation from lanthanides, 251–259
    americium separation from europium, 31–32

D

DDP process. *See* Dimitrovgrad Dry Process
Decanoic acid, synergistic extraction Am with TPEN isomers, 269–272
Decontamination factor (DF), neptunium decontamination of uranium product, 94, 96
Density functional theory (DFT) calculations, lanthanum–Kläui ligand complexes, 206, 208–211*f*
DF. *See* Decontamination factor
4',4',(5')-Di-(*t*-butyldicyclo-hexano)-18-crown-6, structure, 47*f*
Dialkylimidazolium-based ionic liquids, radiation stability, 235
DIAMEX (Diamide Extraction) process, 48–49
Diamides as extractants. *See specific compounds*
Dicyclohexano-18-crown-6, strontium
    extraction, 235
    imidazolium-based ionic liquids (short chain), phase modifier addition, 239–241*f*
    partitioning between nitric acid and ionic liquids; nitric acid and 1-octanol, 237–238
    See also Crown ether/calixarene solvent in cesium and strontium separations
Diethylene-triamine-N,N,N',N",N"-pentaacetic acid (DTPA), actinide-lanthanide separation processes, 31
Diisodecylphosphoric acid (DIDPA) in transuranium element separation, 29, 31
Dimethyl-dioctyl-hexaethoxymalonamide (DMDOHEMA), 49, 50*f*

Downloaded by 89.163.35.42 on August 9, 2012 | http://pubs.acs.org
Publication Date: June 9, 2006 | doi: 10.1021/bk-2006-0933.ix002

Dimitrovgrad Dry Process, 33
Direct Oxide Reduction (DOR) process, plutonium conversion and separation, 33
Discrete contactors, connection, process equipment, liquid-liquid extraction, 105–106*f*
Dissociation constants, protonated TPEN isomers in aqueous solution, 266–267
Distribution coefficients and separation factors for ^{154}Eu and ^{241}Am, 253–255*f*
DMDBTDMA. *See* N,N'-Dimethyl-N,N'-dibutyltetradecylmalonamide
DMDOHEMA. *See* Dimethyl-dioctyl-hexaethoxymalonamide
Dodecane
  uranyl extraction with SANS measurements, 138, 141
  uranyl third-phase formation, tri-*n*-butylphosphate/nitric acid system, 121–132
DOR process. *See* Direct Oxide Reduction process
DTPA. *See* Diethylene-triamine-N,N,N',N",N"-pentaacetic acid

E

EAS. *See* Electronic Absorption Spectroscopy
Eddy size in haze formation, 108–109
Electricity generation options, life cycle assessments, environmental impacts, 6–10
Electrochemical window measurements in low temperature ionic liquids, 226
Electrometallurgical processing schemes, advantages, 32–33
Electronic Absorption Spectroscopy (EAS)
  actinide speciation studies, 222
  uranium bis(trifluoromethyl-sulphonyl)imide complexes, 228
ElectroRefining (ER) process, plutonium purification, 33
Environmental impacts, energy production, life cycle assessments, 6–10
Equipment in irradiated nuclear fuel dissolution, 72–73*f*
ER process. *See* ElectroRefining process
Europium and americium
  distribution coefficients and separation factors, 253–255*f*
  extraction separation with TPEN isomers and decanoic acid, 261–273
  extraction tests, TPEN isomers and decanoic acid mixtures, 266
  separation factors with TPEN isomers, 262–263
Europium and TPEN isomers, complex formation, 268–269
Extended X-Ray Absorption Fine Structure (EXAFS)
  strontium coordination environments, determination, 240–241*f*
  uranium(III) in LiCl-KCl melt, 222
  See also X-Ray Absorption Spectroscopy (XAS)
Extractant design, CHON principle, 29
Extractants. *See specific extractants*
Extraction tests with TPEN isomers and decanoic acid, Am(III) and Eu(III), 266

F

F-elements
  electrochemistry in low temperature ionic liquids, 228–229

Downloaded by 89.163.35.42 on August 9, 2012 | http://pubs.acs.org
Publication Date: June 9, 2006 | doi: 10.1021/bk-2006-0933.ix002

  speciation in low temperature ionic liquids, 227–228
  See also Actinide separations; Actinides; Lanthanides; *specific elements*
Fission-based nuclear power, factors in expansion, summary, 10–11
Fission product speciation in molten salts, 223–225*f*
Flory-Huggins theory of polymer solutions, 137
Fluoride volatility process, 34
Fluorinated β–diketones in supercritical carbon dioxide extractions, 59–61
Fluorine substitution in chelates, solubility effects in SF-CO_2, 58
Fort St. Vrain gas cooled reactor, 25
Fossil fuel consumption and geopolitical situation, 4–6, 234
Fracture Matrix Transport code, actinide solubility calculations, 314–315
FTIR spectra, lanthanum–Kläui ligand complexes, 205–207*f*
Fuel (irradiated). *See* Nuclear irradiated fuel

G

Geologic repositories, 10, 50–52
  See also Yucca Mountain repository
Gluconate effect on lanthanum(III) speciation, 281–289
Goethite, partitioning mechanism for lanthanum sorption, 277–291
Gravity mixer-settler
  haze formation, 111, 112*f*, 114*f*
  process equipment, liquid-liquid extraction, 104, 105*f*, 110
Green chemistry, extension to nuclear fuel cycle, 235
Group transuranium element extraction, 47–50

H

Hamaker Constant, 108
Hanford Site, Washington (US), 295
Haze behavior, hypotheses, 109–110
Haze entrainment, implications for organic phase product purity, 116, 117
Haze formation, hypotheses, 108–109
Hazes in liquid-liquid extractions, formation and behavior, 103–118
Hexachlorocobaltdicarbolide anion in CCD/PEG process, 45, 46*f*
High Level Waste (HLW)
  radiotoxicity reduction possibilities, 91
  transmutation technology, 262
High temperature molten salts, 221–225*f*
  See also Low temperature ionic liquids
HLW. *See* High Level Waste
Hydrogen peroxide
  coordination complexes with plutonium, 169–176
  oxidation state chemistry, 168–169
Hydrogenated polypropylene tetramer, uranyl third phase formation in tri-*n*-butylphosphate/nitric acid, 121–132
Hydroxamic acids in neptunium and plutonium control, 94–101

I

ICP-MS. *See* Inductively-coupled plasma mass spectrometry
Imidazolium-based ionic liquids (short chain), phase modifier addition effects, 239–241*f*
Inductively-coupled plasma mass spectrometry (ICP-MS), dissolved fuel elemental concentrations, 77, 79*t*

Downloaded by 89.163.35.42 on August 9, 2012 | http://pubs.acs.org
Publication Date: June 9, 2006 | doi: 10.1021/bk-2006-0933.ix002

Downloaded by 89.163.35.42 on August 9, 2012 | http://pubs.acs.org
Publication Date: June 9, 2006 | doi: 10.1021/bk-2006-0933.ix002

Industrial experience with plutonium and uranium recovery, 24–26
Infrared assignments, uranyl nitrate with ^{15}N enriched ammonium carbamate, precipitate, 158–159
Ionic activity constants, actinides, calculations, 314–316
Ionic liquids
  actinide and fission product separations, 233–247
  cation hydrophobicity, viability of ionic liquids in SREX Process, 241–243
  limiting factors in nuclear separations, 236
  low temperature, in nuclear waste management, 220–221
Ionic melts, actinide, lanthanide and fission product speciation and electrochemistry, 219–231
Ionic strength, effect on lanthanum sorption on goethite, 287–288*f*
Iron oxides. *See* Goethite
Irradiated fuel. *See* Nuclear spent fuel

K

Kläui–lanthanum complexes
  density functional theory calculations, 206, 208–211*f*
  spectroscopy, 205–207*f*
Kläui ligand resins
  actinide separations, 209, 212–215
  preparation, 204–205
Kläui ligands, preparation and structure, 202–203

L

Langmuir isotherm model for lanthanum adsorption on goethite, 286–287*t*
Lanthanides
  actinide(III) and lanthanide(III) group separation, 30–32
  separation from actinides, group transuranium element extraction, 47–50
  separation from actinides using simulated feed solution, 256–258
  See also Actinide separations; Actinides; F-elements; *specific elements*
Lanthanum–bis(trifluoromethylsulphonyl)imide complex, 226–227*f*
Lanthanum coordination polyhedron by computational modeling, 208–211
Lanthanum–Kläui ligand complexes
  density functional theory calculations, 206, 208–211*f*
  preparation, resins, 203–205
  spectroscopic characterizations, 205–207*f*
Lanthanum sorption on goethite, partitioning mechanism, 277–291
Life cycle assessments, environmental impacts, electricity generation options, 6–10
Liquid-liquid extractions, haze formation and behavior, 103–118
Low temperature ionic liquids (LTILs)
  f-element electrochemistry, 228–229
  f-element speciation, 226–228
  nuclear waste management, 220–221
  See also High temperature molten salts

M

Mass balance, neptunium rejection trial, 96–97
Mass balance summary for irradiated fuel analyses, 83–86

Mathematical process models, actinide crystallization, 195
Metal diethyldithiocarbamates, solubility in SF-CO_2, 58
Metaschoepite, uranyl oxide hydrate
  environmental persistence, 294
  neptunium(V)-doped, corrosion studies, 303–305
  neptunium(V) incorporation, 295–303
Metastudtite, uranyl peroxide hydrate, 294–295
Microemulsion model, third phase formation, 137
Minor Actinide burning, 93
Molten Salt Extraction (MSE) process, ^{241}Am removal from weapon-grade plutonium, 33
Molten salts in plutonium conversion and separation, 32–33
Molybdate. *See* Cesium phosphomolybdate
Molybdenum, zirconium, plutonium, residue from dissolution, irradiated fuel, 81–85
MSE process. *See* Molten Salt Extraction process

N

N,N'-dialkylimidazolium-based LTILs, strontium extraction by dicyclohexano-18-crown-6, 235, 236*f*
N,N'-dimethyl-N,N'-dibutyltetradecylmalonamide (DMDBTDMA), 29–30, 48–49, 50*f*
N,N,N',N'-tetrakis(2-methylpyridyl)ethylenediamine. *See* TPEN
N,N,N',N'-tetraoctyldiglycolamide (TODGA), 48
Navier Stokes equations, 108
Neptunium and plutonium fuel cycles, PUREX-style flowsheets, 89–102
Neptunium control in advanced fuel cycles, 92–99
Neptunium-doped uranium oxides, corrosion studies, 303–305
^{237}Neptunium half life, 294
Neptunium/plutonium co-recovery with hydroxamic acid ligands, 99–101
Neptunium(V) at Yucca Mountain repository, association with uranyl phases, 293–312
  in studtite formation, 310
  in uranophane formation, 305–310
  incorporation into dehydrated schoepite, 298, 300–303
  incorporation into metaschoepite, 295–298, 299*f*
Nitric acid concentration, changes upon phase splitting, 123, 125*t*
NONLIN calculations, ionic activity coefficients, actinide stability constants, 315
Nuclear fuel cycle, future significance, overview, 3–20
Nuclear spent fuels
  Advanced Fuel Cycle Initiative, developing technologies, 41–52, 72, 184, 252
  management, 11–14
  partitioning, uranium complexes, crystallization, 183–197
  pyrochemical processing, 220
  radioactive components over time, 11–12, 22–23
  reprocessing with supercritical carbon dioxide, 57–67
Nuclear spent fuels from Big Rock Point Reactor
  dissolution, 74–76
  elemental composition results, 76–81
  mass balance summary, 83–86

Downloaded by 89.163.35.42 on August 9, 2012 | http://pubs.acs.org
Publication Date: June 9, 2006 | doi: 10.1021/bk-2006-0933.ix002

residue recovery and analysis, 81–82

O

Octane in thorium(IV) extraction, 141–148
Octyl(phenyl)-N,N-di-isobutylcarbamoylmethylphosphine oxide (CMPO), 26–28, 48, 49*f*
Organic acid phase concentration upon third phase formation, 122–126
Organic phase product purity, haze entrainment implications, 116, 117
Organic uranium phase concentration, 126–128
ORIGEN2 code in irradiated fuel composition, estimation, 76–81
Out of Gas: The End of the Age of Oil, 5
Oxidation state chemistry, hydrogen peroxide and plutonium, 168–169

P

P & T. *See* Partitioning and transmutation
^{31}P NMR spectra lanthanum–Kläui ligand complexes, 205–207*f*
Particle growth and interaction models, SANS measurement interpretation, 138–147
Partitioning and transmutation (P & T), 23
  transuranium elements segregation from high level waste, 91
Pentamethylcyclopentadienyl-containing ligands. *See* Kläui ligands
1-Pentyl-3-methylimidazolium bis[(trifluoromethyl)sulfonyl]imide
  in strontium extraction, 237–243
  in uranium extraction, 243–244
Perdeutero-*n*-dodecane. *See* Dodecane
Perdeutero-*n*-octane. *See* Octane
pH and sodium cation effects, neptunium(V) incorporation into dehydrated schoepite, 298, 300–303
pH and total acetate dependency, distribution coefficients, ^{154}Eu and ^{241}Am, 254–255*f*
Phase modifier addition effects, "short-chain" imidazolium-based ionic liquids, strontium extraction, 239–241*f*
Phase splitting, changes in nitric acid concentration, 123, 125*t*
Physical chemistry, crystallization, 186–188
Pitzer equations, actinide ionic activity coefficients, calculations, 314–316
Pitzer parameters (WIPP database)
  An(III) complexes, 316–320
  An(IV) complexes, 320, 321*t*
  An(V) complexes, 323–324, 326*t*
  brine components, 326, 328*t*–329*t*
Plutonium and hydrogen peroxide, coordination complexes, 169–176
Plutonium and neptunium fuel cycles, PUREX-style flowsheets, 89–102
Plutonium conversion and separation by molten salts, 32–33
Plutonium, molybdenum, zirconium, residue from dissolution, irradiated fuel, 81–85
Plutonium/neptunium co-recovery in advanced fuel cycles, hydroxamic acid ligands, 99–101
Plutonium peroxide precipitates, 173, 175–178
Plutonium processing, oxidation state adjustment, 178, 179*f*
Plutonium uranium recovery by extraction process. *See* PUREX process

Downloaded by 89.163.35.42 on August 9, 2012 | http://pubs.acs.org
Publication Date: June 9, 2006 | doi: 10.1021/bk-2006-0933.ix002

Plutonium/uranium recovery processes, industrial experience, 24–26
Plutonium(IV) peroxide complex (brown), 169–170, 171*f*, 172*f*
Plutonium(IV) peroxide complex (red), 170–172*f*
Plutonium(IV) sorption in actinide separations using Kläui ligand resin, 209, 212–215
Plutonium(V) peroxide complex, 173
Plutonium(VI) peroxide complex, 173, 174*f*
Polymeric species with bifunctional ligands and high metal concentrations, 136
Potentiometric titration technique, TPEN isomers and metal complexes, 265
Primary drop breakage in haze formation, 108–109
Process chemistry, plutonium peroxide role, 167–181
Process equipment, liquid-liquid extraction, 104–107*f*, 110
Process safety issues, uranyl third phase formation, 121
Protonation reactions, TPEN isomers in aqueous solution, 266–267
Pulsed column
  haze formation, 111, 113, 114*f*
  process equipment, liquid-liquid extraction, 106–107*f*, 110
PUREX process, 24–25, 234
  solid phases and solution,
    ammonium carbamate interactions, 151–166
  See also SF-PUREX (wet) process
PUREX-style flowsheets for neptunium and plutonium fuel cycles, 89–102
PUREX technology, drivers for development, 90–92
Pyrochemical processes, 32–33

R

Radiation stability, dialkylimidazolium-based ionic liquids, 235
Radioactive components over time, spent fuels, 11–12, 22–23
Raman spectra, cesium phosphomolybdate interaction with ammonium carbamate, 160–161, 162*f*
Residue formation factors, irradiated fuel, 85
Residue recovery and analysis, irradiated fuel, 81–82
Reynolds number, 109
Rhenium speciation in high temperature salts, technetium comparison, 223
Room-temperature ionic liquids, alternative solvents, actinide separations, 35
Ruthenium speciation in high temperature salts, 223, 225*f*

S

Safety. *See* Process safety
Salado Formation brine, 314, 325*t*
SANEX processes. *See* Selective actinide extraction processes
SANS. *See* Small-angle neutron scattering
Savannah River Site, South Carolina (US), plutonium peroxide precipitation process, 176–178
Scattered neutrons, intensity calculations, 138
Schoepite, dehydrated neptunium(V)-doped, corrosion
    studies, 303–305

Downloaded by 89.163.35.42 on August 9, 2012 | http://pubs.acs.org
Publication Date: June 9, 2006 | doi: 10.1021/bk-2006-0933.ix002

Downloaded by 89.163.35.42 on August 9, 2012 | http://pubs.acs.org
Publication Date: June 9, 2006 | doi: 10.1021/bk-2006-0933.ix002

- sodium cation and pH effects on neptunium(V) incorporation, 298, 300–303

Selective actinide extraction (SANEX) processes, 32

Separation factors and distribution coefficients, ^{154}Eu and ^{241}Am, 253–255*f*

Separations, future nuclear, attributes, 14–17

SF-CO_2. *See* Supercritical carbon dioxide

SF-PUREX (wet) process for nuclear waste treatment, 61–62*f*
- *See also* PUREX process

Simulated feed solution, actinide separation from lanthanides, 256–258

Sintered UO_2, process tests for dissolution, 73–74*t*

Small-angle neutron scattering (SANS) measurements and calculations, 137–141

Sodium cation and pH effects, neptunium(V) incorporation into dehydrated schoepite, 298, 300–303

Soft-donor extractants, 31–32

Sorption, lanthanum on goethite, partitioning mechanism, 277–291

Sorption processes on oxide surfaces, 279–280

Spectroscopic characterizations, lanthanum–Kläui ligand complexes, 205–207

Spent fuels. *See* Nuclear irradiated fuels

SREX process
- strontium extraction from acidic nitrate media, 234–235
- viability of ionic liquids dependence on ionic liquid cation hydrophobicity, 241–243

Stability constants
- An(III)-hydroxides, 319
- Eu(III) and Am(III) t2pen complexes, 262–263
- Th(IV)-carbonate reactions, 322

Stickiness parameters, critical values, 145, 147

Sticky spheres model. *See* Particle growth and interaction models

Strontium/cesium extraction from raffinate, UREX or codecontamination process, 44–47*f*

Strontium coordination environments by EXAFS, 240–241*f*

Strontium extraction
- by dicyclohexano-18-crown-6 in N,N'-dialkylimidazolium-based LTIL's, 235, 236*f*
- from nitrate media (acidic), 237–239
- in 1-pentyl-3-methylimidazolium bis[(trifluoromethyl)sulfonyl]-imide, 237–243
- phase modifier addition effects on "short-chain" imidazolium-based ionic liquids, 239–241*f*

Structures and bond lengths, lanthanum–Kläui ligand complexes, 208–211*f*

Studtite as uranyl peroxide hydrate, 294–295

Studtite formation in neptunium(V) presence, 310

Super-DIREX process in spent nuclear fuel reprocessing, 64–65*f*

Supercritical carbon dioxide (SF-CO_2) spent nuclear fuel reprocessing, 57–67

Supercritical fluid extraction, actinides, 35–36

Surface complexation reactions, lanthanum(III) to goethite, 284

T

TALSPEAK process, 31

TBP. *See* Tri-*n*-butyl phosphate
Technetium speciation in high temperature salts, compared to rhenium, 223
Technetium/uranium extraction, 43–44
Thenoyltrifluoroacetone (TTA) in SF-CO_2 extractions, 59–61
Thermal ionization mass spectrometry (TIMS) elemental composition in irradiated fuel, 77, 79–81
Third phase formation
  actinide extraction by tri-*n*-butyl phosphate, 135–150
  uranyl, tri-*n*-butylphosphate/nitric acid system, 119–134
THOREX process, 25–26
Thorium(IV) extraction, models for SANS data interpretation, 141–148
TIMS. *See* Thermal ionization mass spectrometry
TODGA extractant. *See* N,N,N',N'-tetraoctyldiglycolamide
TPEN isomers
  complexation in aqueous solution, 265, 266–268
  structures, 263
  synergistic extraction, Am(III) with decanoic acid, 269–272
  synthesis, 264–265
TRAMEX process, 30–31
Transmutation technology for high level waste, 262
Transuranium Extraction process. *See* TRUEX process
Tri-*n*-butyl phosphate (TBP)
  in odorless kerosene liquid-liquid system, 103–118
  in PUREX process, 24
  in SF-CO_2 extractions, 59–65
  in THOREX process, 26
  in UREX process, 43, 46
Tri-*n*-butyl phosphate/nitric acid system, uranyl third phase formation, 119–134, 135–150
Trialkylphosphine oxide (TRPO), 28
TRUEX process, 27–28, 48, 235
TTA. *See* Thenoyltrifluoroacetone
Turbulence characteristics, effects on haze manifestations, 103–118

U

UDBP. *See* Uranyl dibutylphosphate
Uranium complexes, crystallization, partitioning, spent nuclear fuel, 183–197
Uranium extraction
  by ionic liquid-based PUREX process solvent, 243–244
  by supercritical carbon dioxide, 59–61
  UREX process, 43–44, 46*f*
  UREX + process, irradiated nuclear fuel dissolution, 72–86, 252
Uranium ores. *See* Metaschoepite, Metastudtite, Schoepite; Studtite; Uranophane
Uranium oxides, neptunium-doped, corrosion studies, 303–305
Uranium plutonium recovery, industrial experience, 24–26
Uranium speciation in high temperature molten salts, 222–224*f*
Uranium/technetium extraction, 43–44, 46*f*
Uranium(VI) minerals, crystal chemistry evaluation, 295
Uranium(VI) sorption in actinide separations using Kläui ligand resin, 209, 212–213*f*
Uranophane formation in neptunium(V) presence, 305–310
α-Uranophane phase, layered uranyl silicate, description, 294
Uranyl dibutylphosphate (UDBP) with ammonium carbamate, 154, 159–160, 163–164

Downloaded by 89.163.35.42 on August 9, 2012 | http://pubs.acs.org
Publication Date: June 9, 2006 | doi: 10.1021/bk-2006-0933.ix002

Uranyl extraction models for SANS data interpretation, 141–148
Uranyl ion, stoichiometric reactions with ammonium carbamate, 154, 155–159, 163–164
Uranyl nitrate crystallization, process flow diagram, 192*f*–193*f*
Uranyl third phase formation in tri-*n*-butylphosphate/nitric acid system, 119–134, 135–150
UREX process, 43–44, 46*f*
UREX + process in irradiated nuclear fuel dissolution, 72–86, 252
UV-visible absorption spectra
  uranyl dibutylphosphate with ammonium carbamate, 155, 156*f*, 159–160
  uranyl third phase formation in TBP/nitric acid systems, 128–131*f*

V

Vibropacked fuel fabrication, 33
Volatility-based separations, 34

W

Waste isolation pilot plant (WIPP), brine components, chemical potentials, Pitzer parameters, 324, 326–329*t*
Waste isolation pilot plant (WIPP) thermodynamic database, chemical potentials, stability constants, Pitzer parameters, actinide speciation, solubility modeling, 315–329
Waters of hydration in uranyl nitrate, thermal gravimetric analysis, 186, 188
WIPP. *See* Waste isolation pilot plant

X

X-Ray Absorption Spectroscopy (XAS), uranium *in situ* studies, 222–224*f*, 228
  See also Extended X-Ray Absorption Fine Structure (EXAFS)
X-Ray Diffraction (XRD)
  mixed plutonium peroxide precipitates, 175
  neptunium(V)-containing α–uranophane, 307, 309*f*
  Rietveld refinements, unit cell parameters, dehydrated schoepite, 305

Y

Yucca Mountain repository, Nevada (US), 12–13, 293–294
  neptunium association with uranyl phases, 293–312
  statutory capacity, 184
  storage, 234, 252, 294
  thermal load contributors from spent fuel or waste, 50–52
  See also Geologic repositories

Z

Zirconium, molybdenum, plutonium, residue from dissolution, irradiated fuel, 81–85

Downloaded by 89.163.35.42 on August 9, 2012 | http://pubs.acs.org
Publication Date: June 9, 2006 | doi: 10.1021/bk-2006-0933.ix002